Title

200 BeV Accelerator: Studies on Experimental USE Volume II 1964 - 1965

Authors

Chinowsky, W
Dols, C
Hughes, E
et al.

Publication Date

1966-04-01

200 BEV ACCELERATOR: Studies on Experimental Use | 1964-5 Vol. 2

Equipment | Targeting Facilities

Lawrence Radiation Laboratory
Berkeley, California

DISCLAIMER

UCRL-16830
(UCID-10184)

UNIVERSITY OF CALIFORNIA

Lawrence Radiation Laboratory
Berkeley, California

AEC Contract No. W-7405-eng-48

200 BeV ACCELERATOR:
STUDIES ON EXPERIMENTAL USE
1964 - 1965

Volume II
Experimental Equipment
Targeting, Experimental Areas, and Facilities

April 1966

UCRL-16830
(UCID-10184)

200 BeV ACCELERATOR: STUDIES ON EXPERIMENTAL USE

Volume II

1964 - 1965

A. Experimental Equipment

B. Targeting, Experimental Areas, and Facilities

AUTHORS:

W. Chinowsky	LRL, Berkeley
C. Dols	LRL, Berkeley
E. Hughes	Winona Jr. College, Winona, Minnesota
D. Keefe	LRL, Berkeley
M. Longo	University of Michigan
R. B. Meuser	LRL, Berkeley
V. Perez-Mendez	LRL, Berkeley
M. Scolnick	LRL, Berkeley
M. L. Stevenson	LRL, Berkeley
T. E. Toohig	Woodstock College-Johns Hopkins University
G. H. Trilling	LRL, Berkeley
W. A. Wenzel	LRL, Berkeley
R. W. Williams	University of Washington

EDITORIAL NOTE

The reports in this volume are connected mainly with the experimental use of the proposed 200 BeV accelerator. These reports were largely for limited distribution (UCID series) and not intended for journal publication. They are therefore informally written and sometimes repetitious. Nevertheless, we felt it valuable to bind these papers together in their original form without the excessive labor of retyping, detailed proofreading, or redrawing of figures.

The papers are grouped roughly in four broad categories: A, High Energy Elementary Particle Reactions, and B, Experiments and Secondary Beams in Volume I; C, Experimental Equipment, and D, Targeting, Experimental Areas, and Facilities, in Volume II.

W. S. Gilbert
D. Keefe

April 1966

sb

Volume II

Contents

PRELIMINARY DRAFT

UCID-10168
AS/Experimental/01
January 22, 1965
D. Keefe
(Original - 1/15/65)

University of California
Lawrence Radiation Laboratory
Berkeley, California

MAJOR ITEMS OF SCIENTIFIC EQUIPMENT EXPECTED TO BE IN USE AT THE 200 GEV ACCELERATOR LABORATORY

D. Keefe
W. A. Wenzel
V. Perez-Mendez
M. L. Stevenson
W. Chinowsky
R. B. Mauser
G. H. Trilling

I. INTRODUCTION

The purpose of this note is to forecast the major items of experimental equipment, with rough cost figures, which will be needed at the 200 GeV accelerator laboratory. Included here are only the exceptionally large items which could not conceivably be financed out of the base R and D operating and equipment budget. For example, conventional experimental electronics and detectors and scanning equipment are not considered here.

It is necessary at the outset to state certain assumptions and qualifications associated with these predictions. Indeed, the degree of qualification is intimately related with the time-scale for a given project. If parameters need to be frozen within a year or so, as in the case of the accelerator structure, then the current set of parameters is likely to be very close to the final one; whereas in the case of transport equipment for secondary beams, which need not be ordered for about six years, our current estimate of specifications is bound to be much further from the ultimate choice. To repeat a well-worn idea: the field of elementary particle physics is a rapidly changing one and to predict what will be the most active frontiers a decade from now is impossible. Thus, the intrinsic purpose of some of the pieces of equipment visualized below may become diminished in importance. It is still more likely that in several cases, while their purpose remains the same, the details of the hardware will be quite different when the time for their purchase arrives. For instance, our present concept of all transport elements being constructed of copper and iron with conventional power supplies and water cooling could, in the space of a few years, be radically altered if superconducting elements were to be proved economically feasible on a large scale. Admitting this, we still prefer to base cost estimates on the established technology of today and regard the possible breakthroughs as providing a bonus we may hope for. If they should occur, we could buy the equivalent equipment for less money--or more likely, buy more equipment for the same money. Another example, which is probably further in the future, is the possibility of developing superconducting cavities for rf separated beams operating at lower power, higher frequency and longer spill times than anything envisaged at the moment.

The working picture for the 200 GeV laboratory assumes that about 25% of the accelerator experimental program will be absorbed by on-site physics groups and 75% by users. The ratio of the number of on-site to off-site experimenters is expected to be less than this ratio, since the on-site personnel will be those choosing to devote a large fraction of their time to physics research on the 200 GeV accelerator whereas the visiting groups will largely be from universities where they have teaching responsibilities in addition to their research activities and furthermore may conduct experiments at other accelerator laboratories. The apportionment of transport equipment would be determined by the exigencies of the current operating schedule and on the average be partitioned exactly as the time-ratio; likewise the number of photographs produced by the giant bubble chamber--here considered as much a national facility as the accelerator itself--would tend to divide in the same ratio. In this sense, the equipment and operating costs of such items are conceived to be largely devoted to the service of outside users. On the other hand, the central computing center and main data-reduction center are conceived to be predominantly devoted to fulfilling the needs of in-house groups. This is based on the present-day experience that most outside groups visit the accelerator laboratory only for the time necessary to set up the experiment and take data, and desire to retain a maximum of the effort in their particle physics program based at their home institution, e.g., data of reduction or construction of detection apparatus. Despite the high ratio of visitor-to-resident use of machine time, we feel that perhaps only 20% of the computer facilities may be required by outside visitors. Development of analysis, kinematics, beam-transport or other such programs will certainly be a common requirement of visitors, but we assume that the really time-consuming massive production runs on data analysis will be reserved for their home institutions.

II. SCIENTIFIC EQUIPMENT

The major items of equipment considered below are as follows:

1. A giant hydrogen/deuterium bubble chamber of approximately 100 m^3 volume (six tons of hydrogen).

2. A magnet providing a large volume of magnetic field (~ 120 m^3 at ~ 20 kG) suitable for large-scale spark chamber experiments on high energy interactions.
3. Computer facilities (a) On-line provision of small computers for experimenters, (b) Major computing center for physics research.
4. Bending and focusing magnets for routine transport of secondary beams.
5. Special beam facilities (a) 100 GeV/c rf separated beam
   (b) neutrino/μ-meson beam.
6. Special focusing devices.

In the following sections these items are discussed at more length as regards their visualized use, justification, approximate cost and desirable time-scale for construction. For the purposes of this note these descriptions are necessarily confined to summary form and no detailed defenses of certain choices of parameters are presented. As regards time-scales we favor, in all cases, delaying until the latest possible time the freezing of designs in order to take advantage of the latest technical advances and to minimize the projection of future demand in the field of elementary particle physics.

II. 1. A 100 Cubic Meter Liquid Hydrogen and Deuterium Bubble Chamber (6 tons of Hydrogen).

II. 1. 1 The Interesting Physics: A large liquid hydrogen (deuterium) chamber for use with the 200 GeV proton synchrotron is needed to further our understanding of weak, strong, and electromagnetic interactions. Notable among the experiments for which the bubble chamber is ideally suited are the following:

a. Neutrino interactions
b. Inelastic interactions of mesons, baryons and anti-baryons
c. Study of the production of resonant states.

II. 1. 2 The Experimental Difficulites of Bubble Chamber Physics at High Energy: The experimental difficulties to a great extent are overcome at present energies by analysis methods based on kinematical constraints. These will largel fail at the greater energies involved. The experimental difficulties can be summarized as follows:

a. The loss of vital information about a reaction because several out-going neutral particles escape detection in the chamber.

b. The difficulty of identifying outgoing charged particles as pions, kaons, protons, muons or electrons.

c. The limited momentum measurement accuracy of charged particles of high momentum.

d. The small cross section for neutrino interactions.

II. 1. 3 How the 100 Cubic Meter Chamber Can Solve These Difficulties: Considered in the order of Section II. 1. 2 the solutions are:

a. Neutrons, γ rays, and neutral strange particles can be detected provided sufficient path length exists between the primary interaction and the walls of the chamber. Keeping in mind that, i) the neutron-proton mean free path is 10 meters, ii) the γ-ray radiation length is 10 meters, iii) the mean decay length of a 15 GeV/c K_1^o meson is one meter, and iv) roughly one meter of high momentum measurement of the secondary tracks, one realizes that 3 meters from the primary interaction to the nearest wall would be very helpful. Twenty to thirty per cent of all neutrons and γ rays will convert in this distance. For those experiments that would require a larger γ conversion efficiency, there would be sufficient space to put lead plates.

b. The existence of lead plates surrounding the primary interaction volume would also aid in the identification of electrons. Additional plates, provided they were thick enough, would aid in the identification of muons. In practice the best way of identifying the leptons emerging from neutrino interactions is to use a beam known to consist of either neutrinos or antineutrinos. If lepton conservation is strictly obeyed, then in most reactions the negative (positive) particle emerging from a neutrino (antineutrino) interaction is a lepton. For this reason it is essential to produce the neutrino beams from momentum analyzed meson beams as described in Section II. 5.

c. The value of having long, unobstructed, tracks in liquid hydrogen for the purpose of determining both direction and magnitude of momentum hardly needs mentioning.

d. The need for large volume is usually considered to be required by the low neutrino cross-section. We place it last in importance because the reason we propose a chamber as large as 100 m^3 is because of topics a, b, and c of II. 1. 2 above. The 200 BeV accelerator will produce adequate neutrino fluxes to give reasonable counting rates in somewhat smaller chambers.

II. 1. 4 Estimated Construction Cost: Detailed proposals for 40 m^3 and 26.5 m^3 chambers have been made by the BNL and Argonne laboratories. The chamber configuration that we propose differs little from these proposals although the size is greater. A possible shape is that of a 6 meter diameter sphere with 1 meter sliced off both top and bottom to allow the pole tips of the magnet to be placed closer together. (See Fig. 1)

Preliminary estimates, aided by the more detailed cost estimates of BNL, suggest a total cost of $34.7 million distributed as follows:

1.	Chamber and Expansion	M$ 9.0
2.	Magnet* (20 kilogauss) and Power Supply	10.0
3.	Cryogenics	6.7
4.	Optics	2.4
5.	Electronic controls	2.6
6.	Building	6.0
	TOTAL	M$ 34.7

*Conventional magnet. Development of superconducting magnets for this purpose may alter this cost estimate.

II. 1. 5 Operation Costs: These costs are estimated assuming a full-time crew of operators working three shifts. It is further assumed that the chamber will be taking pictures approximately 40% of the operating time of the accelerator (≈ 3 million pictures/year).

1.	Magnet power + crew	$3.0 million
2.	Film (20 cm, 3 views/pulse)	3.0
	TOTAL	$6.0 million

II. 1. 6 Time Scale: The construction time will be 5 years. In order to have the chamber in operation a year after turn-on of the accelerator (December 1972), construction should be started in December 1968. Thus a one-year study program oriented towards submission of a proposal and detailed cost estimate should be initiated in calendar year 1966.

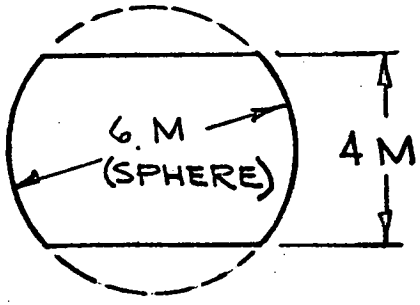

HYDROGEN
VOLUME

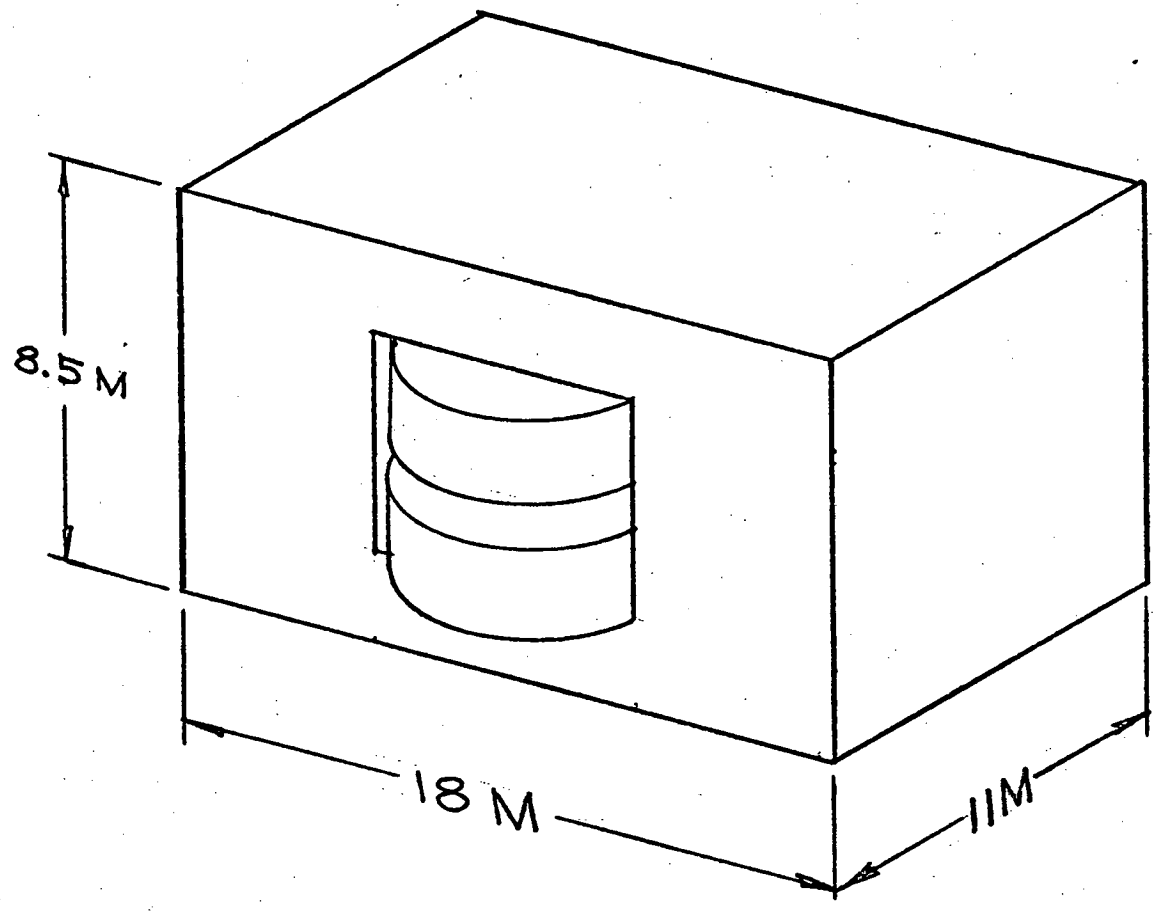

MAGNET

FIG. 1

II. 2. A Large Magnet for Spark Chamber Experiments

II. 2. 1. Physics Use: The need for large volumes of magnetic field in connection with spark chamber experiments has become apparent in the last few years, and relatively massive magnets designed mainly for this application have been constructed recently at ANL, BNL, and LRL. Spark chamber arrays with their dead spaces at the boundaries, stereo view mirrors, and associated electrical equipment inevitably tend to be bulky, and even the largest aperture conventional analyzing magnets are far too restricted in aperture to allow comfortable insertion of equipment inside the magnetic field. Experimenters instead have tended to restrict the placement of chambers to regions outside the magnetic field or to build magnets tailored to the specific needs of an experiment. Hence, the provision of a large volume of magnetic field is considered as the most direct and flexible solution to a wide variety of experimental problems--a volume in which hydrogen targets, a scintillator arrays and spark chambers of large solid angle acceptance can be assembled.

Experimental use of such a magnet should remain very flexible. The significant advantages of the device, properly instrumented with spark chambers and other electronics, will be:

1. The selectivity of spark chambers triggered by high resolution scintillation and cerenkov counters will be particularly useful at higher energies, where the multiplicity of kinematically possible final states is greater than at presently available energies.
2. Within the magnetic field the large distance in any direction to the nearest boundary permits the use of detectors with many attenuation or radiation lengths of material.
3. The active volume is large enough to permit flexible use of inhomogeneous detectors. For example, secondaries from a small hydrogen target can be accurately momentum-analyzed in low density spark chambers before interaction analysis in high density chambers, from which the secondaries can be momentum-analyzed, etc.
4. The total length of magnetic field is enough so that non-interacting particles and high energy secondaries can be accurately analyzed.

The magnet design studied has a rectangular aperture of 2 m x 4 m cross-section, and a length of 15 m. With one pole tip removed the field would be 16.7 kG. At 100 BeV, for example, this gives an angle of bend of 75 mr, providing for very accurage measurement of all high energy particles.

II. 2. 2. Parameters and Cost: The dimensions of the proposed magnetic volume are 2 m x 4 m x 15 m = 120 m^3. The magnet is illustrated in Fig. 2. The cost has been optimized including power costs, with the assumption of 50% utilization at full field for 10 years.

Yoke	M$ 2.0
Copper	1.5
Power Supply (4.8 MW)	0.25
Handling and Support Structure	0.25
Engineering	0.25
TOTAL	M$ 4.25

The design parameters need not be frozen until a year before turn-on of the 200 GeV accelerator.

II. 3. Computer Facilities

II. 3. 1. On-Line Data Processing in the Experimental Areas: It is clear from trendsat the major accelerator laboratories in the last two years that many non-bubble-chamber experiments will come to rely heavily on small local computers in the experimental area for fast data storage and partial real-time analysis. The advantage of instant feed-back of information, at command, to the experimenter is of great advantage in detecting errors in the experimental equipment and in judging the course of the experiment.

A total of six peripheral processors each located close to the particle detection equipment it serves should be adequate to meet the needs of experimenters. These will communicate on a time-sharing basis with a fast computer for partial on-line analysis. A convenient location for this fast computer is the main control room. The main function of a peripheral processor is to control the flow of data to the local fast storage (cores or discs) to reduce these data between beam pulses with the help of the high speed arithmetic processor in the main control room, and finally to store the partially reduced data on a local tape unit.

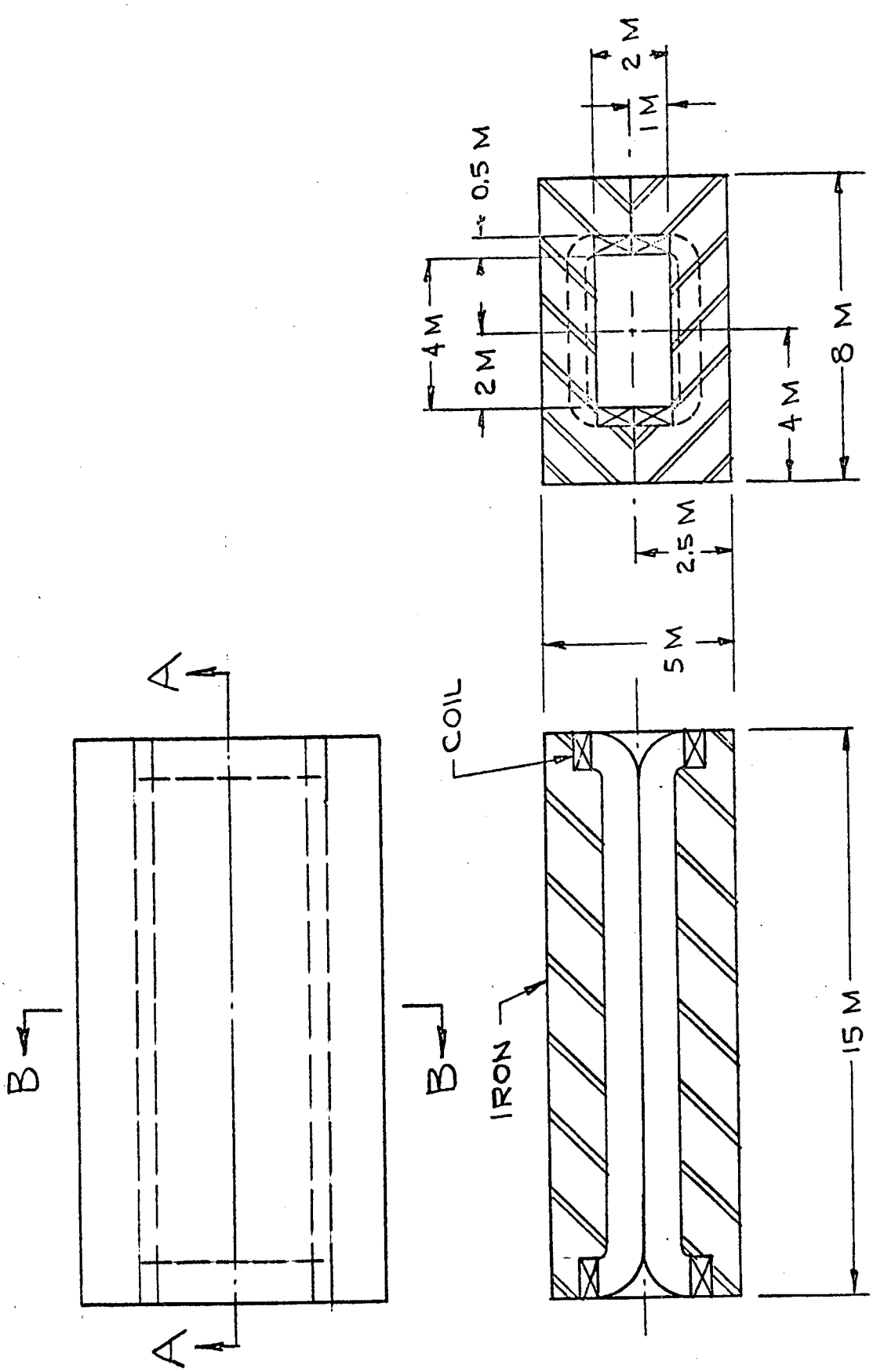
A
B
B
A
COIL
IRON
15 M
5 M
2.5 M
4 M
2 M
+ 0.5 M
2 M
1 M
4 M
8 M
SECTION A-A
SECTION B-B

FIG. 2

Apart from being convenient, from the standpoint of communication, to the experimental areas, the main control room is an attractive choice for locating the fast experimental computer for another reason. The accelerator design study calls for a computer in the main control room to monitor and control many devices in the accelerator and injector systems. This Accelerator-Control Computer, costing in the neighborhood of $300,000, is considered an integral part of the accelerator system and is included in the cost estimates for the construction project. In the event of an emergency, e.g., failure of the control computer, a priority interruption of the fast experimental computer could allow it to take over temporary control of the accelerator and keep the machine in operation at the cost of partial interruption of on-line service to experiments. Instead of being two separate pieces of hardware, the experimental computer and accelerator control computer could be two logically independent portions of a single machine.

The organization of these computers is illustrated in Fig. 3.

Cost:

Accelerator Control Requirements	$300,000
Experimental Peripheral Processors (total of six)	900,000
Fast Computer and Interconnections	800,000
TOTAL	$2,000,000

This does not include the cost of the interface electronics between the experimental detectors and the peripheral processors.

Time Scale: The Accelerator Control Computer should be installed and working two to three years before the completion of the accelerator to help in debugging the machine. The peripheral processors and fast experimental computer need not be installed until a few months before turn-on of the accelerator.

II. 3. 2. Central Computer Facility: The concept here is of a central computer with five or six major input-output areas and a larger number of input consoles to service the resident and visiting group needs. We are assuming for the present purpose that the major fraction of the data analysis is to be done at the home institutions of the visiting groups. With these qualifications we project that the costs of the computer center needed during the first few years of operation are as follows:

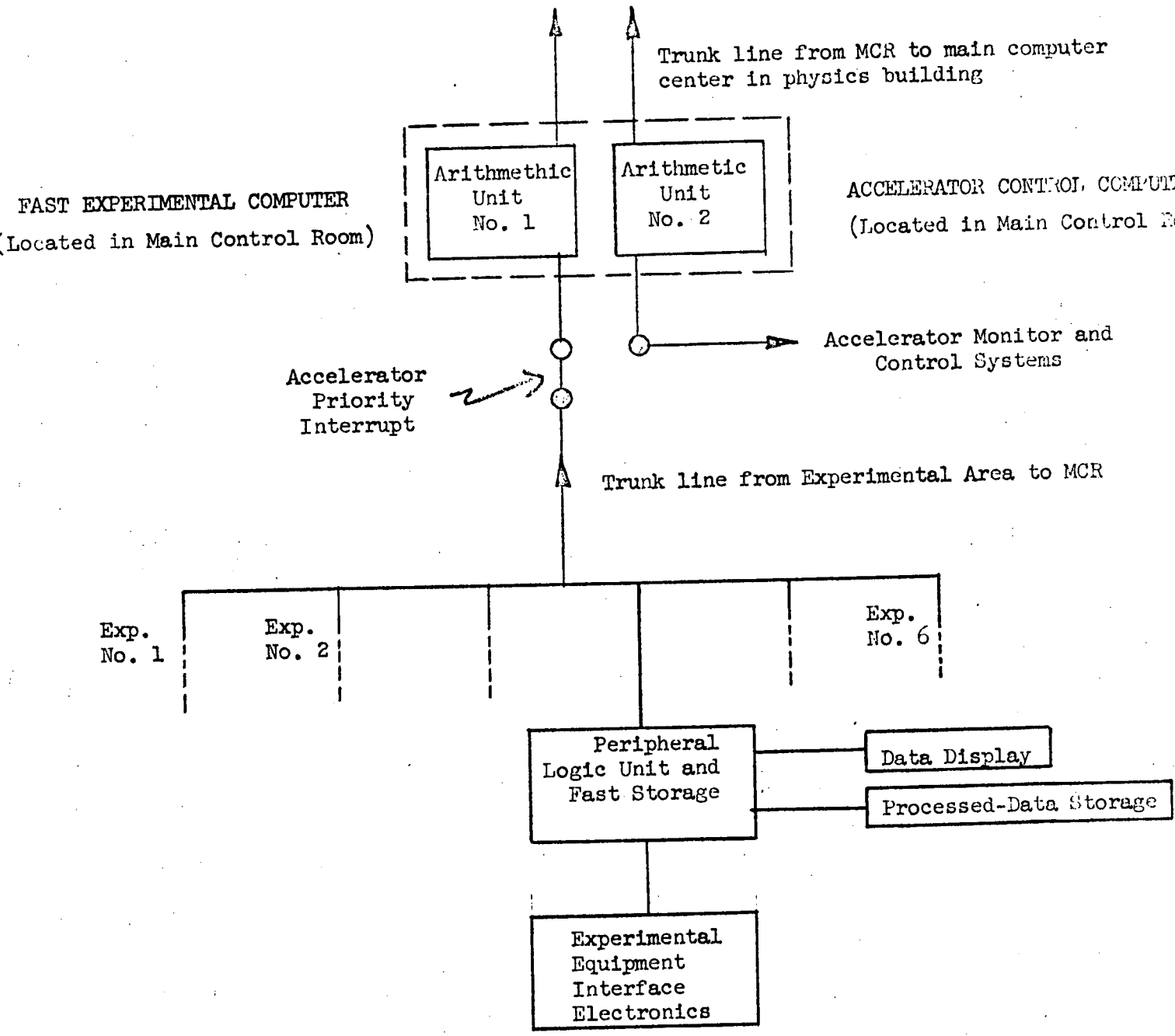
Trunk line from MCR to main computer center in physics building
FAST EXPERIMENTAL COMPUTER
(Located in Main Control Room)
Arithmethic Unit No. 1
Arithmetic Unit No. 2
ACCELERATOR CONTROL COMPUT
(Located in Main Control R
Accelerator Monitor and Control Systems
Accelerator Priority Interrupt
Trunk line from Experimental Area to MCR
Exp. No. 1
Exp. No. 2
Exp. No. 6
Peripheral Logic Unit and Fast Storage
Data Display
Processed-Data Storage
Experimental Equipment Interface Electronics

Figure 3.

Main Computer and Input-Output Processors	$7,000,000
Mass Storage ~ 10^{12} bits	1,000,000
Communications Facility	200,000
TOTAL	$8,200,000

The communications facility is to provide the read-in read-out devices which can be used to transmit data over telephone lines to the home computers of the users' groups, so that a large fraction of the data analysis can be done elsewhere.

Time Scale: Several years before turn-on of the 200 GeV accelerator, it will be necessary to establish resident experimental groups with part-time responsibility towards certain aspects of the construction project. For the remaining fraction of their time they will be occupied with experimental research at other major accelerators and therefore will need good computer facilities on-site for data analysis and miscellaneous computation. Therefore, it will be necessary to have about half the computer capacity described above installed some three years before turn-on and to schedule appropriately the expansion of facilities up to the full level in time to meet the needs of the experimental program at the new machine.

The practice of companies at present (and in the near future) is to produce "families" of machines, which is ideally suited to our need for a growth rate tailored to rather rapidly changing needs. Other solutions of an interim nature in the early pre-operating years, are to rent computers or to establish a communication link capable of handling tape-writing speeds with a nearby computer center. (For example, if the site were Camp Parks then either LRL Berkeley or LRL Livermore would be feasible centers upon which to parasite.)

II. 4. Conventional Transport Equipment - Bending and Focusing Magnets

For primary energies above about 20 GeV the angular distribution of high energy secondary particles produced from a target appears to be roughly described by the simple expression

$$\frac{dN(p)}{d\Omega} \qquad e^{-p\theta/p_o}$$

with p_o = 0.22 GeV/c.

This result has been established at energies available at the CPS and the approximate features of this so-called constant transverse momentum law ($\bar{p}_{transverse} \approx 2\ p_o$) have been verified in many cosmic ray experiments up to

TABLE I

Type	C or H	Aperture in.	Length in.	Field k-gauss	Per Magnet: Weight tons	Power kw	Magnet Cost $1000	Pwr.Sup. Cost $1000	Quant.	Magnet Cost $1000	Pwr.Sup. Cost $1000
Q(L.P.)	-	4 dia.	60	11*	3	180	11.	10	20	220	200
		4 dia.	120	11*	5	360	14.5	19	20	290	380
		8 dia.	60	11*	11	180	23.5	10	20	470	200
		8 dia.	120	11*	20	360	36.	19	20	720	380
Q(H.P.)		4 dia.	120	10*	1	750	11.	39	8	88	312
		8 dia.	120	10*	4	750	15.	39	8	120	312
Q(Septum)		8 dia.	160	10*	25	500	55.	26	8	440	208
BM	C	4 x 12	80	20	13	500	20.	26	5	100	130
	H	4 x 12	80	20	8	500	15.5	26	10	155	260
	H	4 x 12	160	20	15	900	24.5	46	15	368	690
	C	8 x 16	80	20	26	750	35.	39	5	175	195
	H	8 x 16	80	20	15	750	27.	39	10	270	390
	H	8 x 16	160	20	51	1100	57.	56	15	855	840
										4271 + 4497	
										= 8768	
										($8,768,000)	

KEY: Q(L. P.) = Low Power Quadrupole
Q(H. P.) = High Power Quadrupole
Q(Septum) = Quadrupole with Iron Septum
BM = Bending Magnet

* at center of pole

energies several orders of magnitude greater. Thus, we feel confident in assuming its approximate validity for secondary particles produced from targets at the 200 GeV accelerator. This leads to the conclusion that 70% of the secondary particles with energy E emerge within a cone of half angle

$$\theta_{rms} = 0.54/E$$

Thus, the higher the energy of the secondary particles selected, the more strongly collimated they are in the forward direction. In arriving at the dimensions of the transport elements in typical beams at the new accelerator facility, we have assumed that for a given secondary momentum the aim should be to capture a large fraction of the flux (say 10-50%), that access to production angles close to 0° is possible--by using external targets and appropriate target magnets--and that conditions should be optimized for high energy secondary beams. We define a high-energy secondary beam roughly as exceeding ~ 20 GeV, viz., beyond the reach (for high intensity) of the AGS. No doubt, there will be several experiments using particles in the overlap region 6-20 GeV and some at lower energies; these will certainly be possible with elements of the chosen dimensions, but the optimization of dimensions is based on high energy beams.

The choice of quadrupole apertures (10 cm and 20 cm) is based on a study of how close to the target the first elements in the transport systems may reasonably be expected to be located. The longest focussing magnets have been optimized for secondary momenta in the range 70-100 GeV/c. Lower momenta can be handled with the shorter elements or else by sacrificing some acceptance solid-angle. Higher momenta, up to the maximum of 200 GeV, can be transported either by bolting a number of elements together to create quadrupoles of greater effective length or by using separated elements to give greater focussing with some loss in acceptance solid angle. The bending magnets have been chosen to match in aperture the quadrupoles and their lengths have been arrived at assuming that beams with momentum widths in the neighborhood of 1% to 0.1% will be required. Transverse interferences between transport elements in adjacent beam channels or between a high energy secondary beam and the full energy proton beam can be minimized by the use of high-power "slim" quadrupoles, septum quadrupoles, and C-magnets. A small proportion of the elements listed below are of these types--a small number because only the first few elements in any secondary beam need to have these special properties.

L = 80", 160"

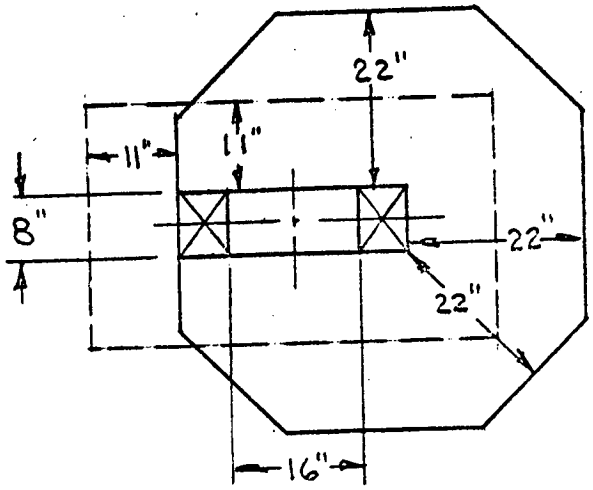

L = 80, 160"

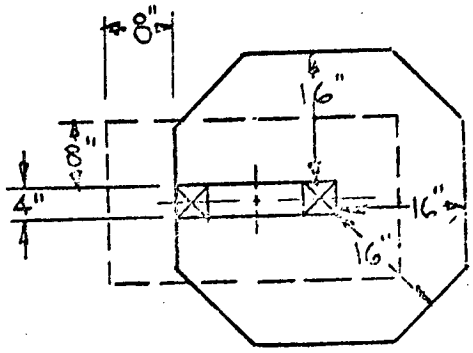

"C" TYPE ——
"H" TYPE ---

FIG. 4a BENDING MAGNETS

L = 60", 120"

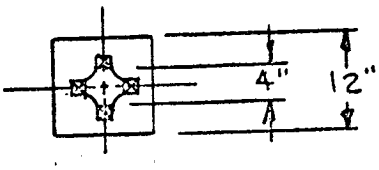

L = 60", 120"

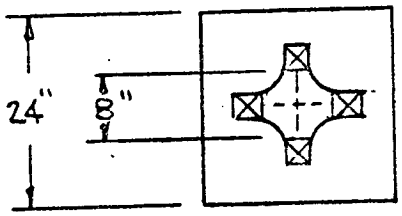

FIG. 4b LOW POWER QUADRUPOLES

L = 120"

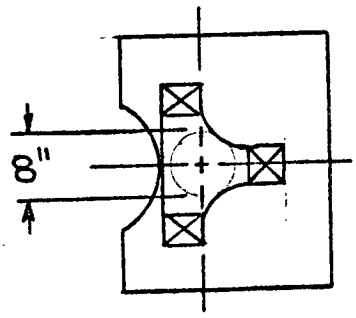

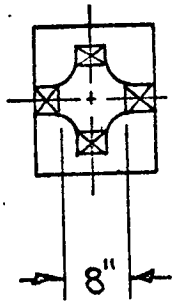

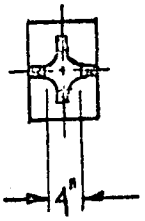

FIG. 4c SPECIAL QUADRUPOLES

Table I shows the properties and costs of the standard transport elements proposed. Figure 4 shows typical dimensions.

It is interesting to note for comparison that the total bending strength $\Sigma(BL)$ of the bending magnets proposed is 360 Tesla-meters, and the total focussing power $\Sigma(B'L)$ of the quadrupoles is 3000 Teslas. These can be compared with the corresponding values 118 T-m and 1020 T respectively for the CERN PS magnets. Thus, the dispersive and focussing powers of the proposed equipment are about three times more than at the CPS, although the energies of the accelerators differ by a factor of eight. Partly for the reason that the constant transverse-momentum law dominates particle production at CERN energies and higher, and partly for other reasons of a more detailed nature, the integrated strength of the transport equipment seem to scale roughly in proportion to the square root of the accelerator energy.

Time Scale: Half of the proposed equipment should be delivered and in the course of being tested at turn-on time. In less than a year after this some experiments will have been performed, and by then the validity of the choice of parameters checked, whereupon the remainder would be ordered. We note that CERN initially ordered roughly equal numbers of 2 m and 1 m quadrupoles and later found it desirable to add greatly to their stock of 1 m elements and also to acquire many elements 0.5 m long. Since the popularity of certain sizes of transport elements is tied so closely to the physics program at the time, some two-step approach such as that proposed seems justified and not over-cautious.

II. 5. Special Beam Facilities: Certain secondary beams contain such a large number of transport elements or such special devices that they should be considered as separate entities. Their cost exceeds what could reasonably be financed from a base annual equipment budget, and were one to draw on the regular pool of transport equipment the number of elements is great enough seriously to detract from the rest of the experimental program. The two examples we have in mind are:

(i) An rf separated beam with a design momentum of about 100 GeV/c for anti-protons.

(ii) A neutrino beam (also providing a μ-meson facility).

Every effort will be made to enable the giant bubble chamber to utilize both of these beams at a single location. Likewise, every effort will be made to ensure that these beams can also be used in other experiments. In

the case of the neutrino beam the solution is trivial since a second experiment can be located directly in front of or behind the giant bubble chamber without suffering loss in flux or geometry. In the case of the separated beam it seems feasible to install a switching magnet in the final clean-up stage after the last cavity, which could switch the beam between a channel leading to the bubble chamber and another leading to the second experimental detector. The second experiment could either involve counter or spark-chamber detectors or a small bubble chamber.

Finally, it should be noted that the 100 GeV/c rf separated beam referred to will permit a large number of physics experiments at other momenta to be performed. For example, there are certain pass-bands in the momentum scale below the design value, for which rf separation will work. Also, by installing a gas cerenkov counter and switching off the rf cavities, experiments with $\pi^{\pm}$- meson or proton primaries can be carried out, without spatial separation, simply by tagging the separate tracks in the chamber according to the cerenkov counter response. Intensity control using this mode is easily accomplished by means of a fast kicker to pass only the first few particles desired and deflect the remainder away from the chamber.

Figure 5 shows a schematic layout of one arrangement in the long EPB area whereby the separated beam could run using target area A and the neutrino beam could use target area C and both serve the giant bubble chamber. The pion beam (P ~ 10-30 GeV/c) from which the neutrinos arise would be deflected downwards shortly after the target and run close to the floor (within 1') to enable the transverse shielding to be minimized. The beam itself is simply a linear strong focussing channel to trap the π-mesons in a pencil beam and give them time to decay. Most of the product μ-mesons will also be trapped and can be used in a separate experiment at the end of the channel.

Cost:

(i) 100 GeV/c rf separated beam (Length ≈ 1.3 km)

Beam transport	Quadrupoles	M$ 0.84
	Bending Magnets	0.75
	Power Supplies	1.40
RF deflection	Cavities and rf equip.	1.25
	Beam pipe, collimators	0.15
	TOTAL	M$4.39

FIG. 5 DUAL BEAM FACILITY FOR BUBBLE CHAMBER IN "LONG E.P.B." AREA

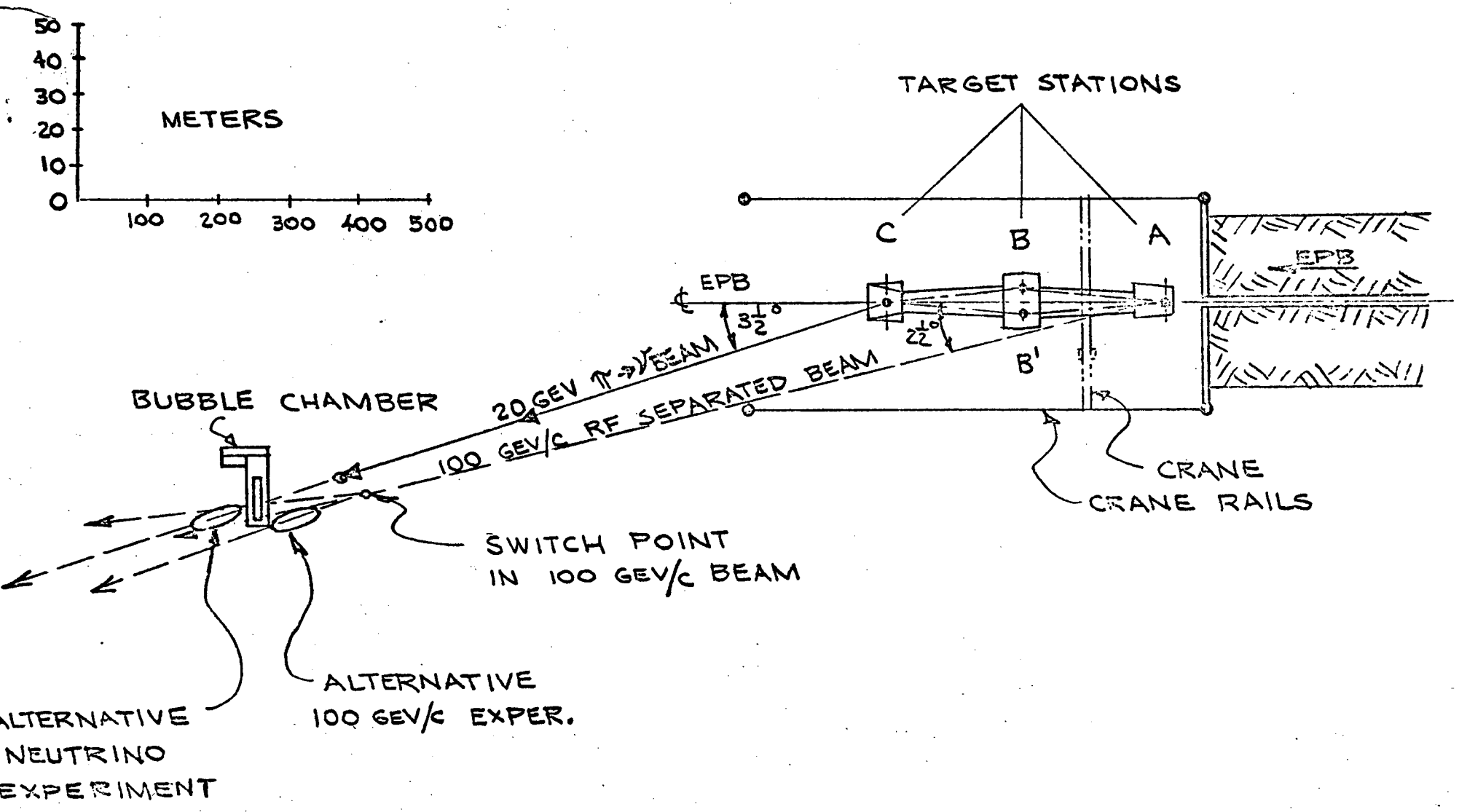

(ii) Neutrino Beam (Length = 0.9 km)

Quadrupoles	180 singlets (4" x 60")	M$1.98
	Power Supplies	1.80
Bending Magnets	6 H-type (4" x 12" x 160")	0.15
	Power Supplies	0.28
Shielding (Iron and Heavy Concrete)		1.00
	TOTAL	M$5.21

Time Scale: The neutrino beam should be completed when the large bubble chamber is ready for production running, viz., one year after turn-on. Part, at least, of the separated beam should be installed about 6 months earlier in order to deliver particles of a known momentum to the chamber during the pre-operating engineering runs.

II. 6. Special Beam Transport Equipment: We include this item in title only and can make no significant remarks about what might be invented or required in this field. The van-der-Meer horn of plenty and the AGS plasma lens are two generic examples at the present time. Both are broad-band focussing devices which were necessary to produce a parallel beam of π-mesons irrespective of secondary momentum for use in the CPS and AGS neutrino experiments. It seems very probable that some such highly-specialized device costing several million dollars will be called for, but that its nature and design will have to be dictated by the physics requirements at that time. The need to handle very high energy secondary beams implies that costs will be substantially larger than in the CPS and AGS examples.

III. SUMMARY

TABLE II

Item No.	Description	Cost (M$)
1.	Hydrogen/deuterium Bubble Chamber (96 m^3) (inc. magnet and power supply)	34.7
2.	Large Spark Chamber Magnet: (inc. Power Supply)	4.25
3.	Computers	
	1. Experimental area on-line facilities	2.0
	2. General-purpose computer center	8.2
4.	General Purpose Beam Transport Equipment (inc. power supplies)	8.77
5.	Special Beam Facilities	
	1. RF separated beam (100 GeV/c)	4.39
	2. Neutrino beam	5.21
	TOTAL	M$67.52

UCID 10123
AS/Experimental/01
July 23, 1964
Michael J. Longo

NOTE ON MAGNETS FOR USE IN HIGH-ENERGY BEAMS AT THE PROPOSED 200 GeV ACCELERATOR

In considering possible experiments for the proposed accelerator, one is soon led to a consideration of beam design. In order to design a beam, he must first make a guess as to what kinds of magnets will be available. This note presents the author's "guesses" based on a study of requirements for typical experimental situations. It is not meant to be a comprehensive study of magnet design, but rather to suggest what kind of magnets would be desirable for typical experiments involving beams with energies from 50 to 200 GeV.

It is clear from the outset that a major limitation on general-purpose magnets will be cost — both for fabrication and power. It is, therefore, not reasonable to just scale up the length of magnets currently in use at existing accelerators. It is also likely that large superconducting magnets will be either unavailable or economically unattractive during the first few years of accelerator operation so that we consider here only magnets of the conventional type. This means that the maximum field in bending magnets is approximately 20 kg and that the maximum field gradient in quadrupoles is approximately $12r^{-1}$ (kg/in) where r is the radius in inches.

Quadrupoles

At low beam energies, quadrupoles with a radius of 6 inches or more are often used. However, it is not clear that such quadrupoles would be practical at high energies due to the limitation on the maximum field gradient mentioned above.

In order to get a feeling for the problem, let us consider a typical situation shown in the figure:

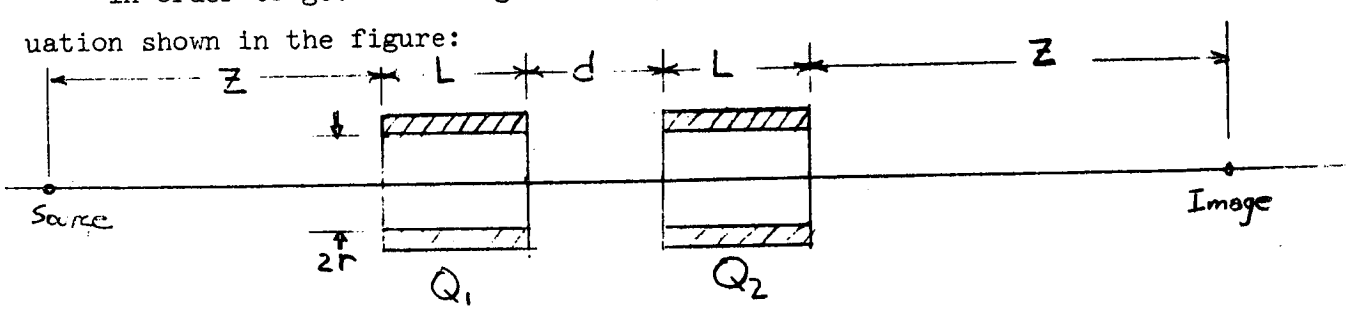

The image and object distances are taken to be equal for simplicity and "by symmetry" the field gradients in the two quadrupoles will be equal and opposite. We define a parameter

$$\theta = \left[\frac{L^2 G}{1312\ P} \right]^{\frac{1}{2}},$$

where L is the length of each quadrupole section (in inches), G is the gradient (kg/inch), and P is the beam momentum (GeV/c). If we replace the quadrupole doublet by an equivalent thin lens of focal length

$$f = \tfrac{1}{2} \left(Z + L + \frac{d}{2}\right),$$

then we find that for $\theta^2 \ll 1$,

$$\frac{1}{f} \approx \frac{\theta^4}{L} \left(\frac{d}{L} + \frac{2}{3}\right) = \frac{L^3 G^2}{(1312P)^2} \left(\frac{d}{L} + \frac{2}{3}\right) \qquad (1)$$

This formula turns out to be an excellent approximation for $\theta \lesssim 0.5$. The solid angle accepted by the quadrupole is approximately

$$\Delta\Omega \simeq \frac{\pi r^2}{(Z + L + \frac{d}{2})^2} = \frac{\pi r^2}{4f^2} = \frac{\pi r^2}{4} \cdot \frac{\theta^8}{L^2} \left(\frac{d}{L} + \frac{2}{3}\right)^2$$

If we take the maximum allowable gradient to be

$$G_{max} = \frac{12}{r} \left(\frac{kg}{in.}\right),$$

then

$$(\Delta\Omega)_{max} = \frac{\pi L^6}{4(1312P)^4} \cdot \frac{(12)^4}{r^2} \left(\frac{d}{L} + \frac{2}{3}\right)^2 \qquad (2)$$

This leads to the surprising result that the solid angle accepted varies <u>inversely</u> with the square of the radius. This result, however, is only correct for θ small, so eq. (2) is not valid for small <u>r</u>. We have also assumed that the quadrupole can be brought as close to the source as desired, an assumption that may not always be true in practice. It is also true that we can always get a larger solid angle by increasing r <u>provided</u> that we increase L appropriately at the same time. Eventually, however, as L is increased and the entrance of the quadrupole moves closer to the source the gain in useful solid angle with increasing L becomes very small. (See table IV and discussion below).

In order to investigate the problem more quantitatively the configuration shown below has been studied in detail, using the computer program "OPTIK".[1]

---

[1] Thomas J. Devlin, "Optik, a Computer Program for the Optics of High-Energy Beams." UCRL-9727, Sept. 15, 1961 (unpublished).

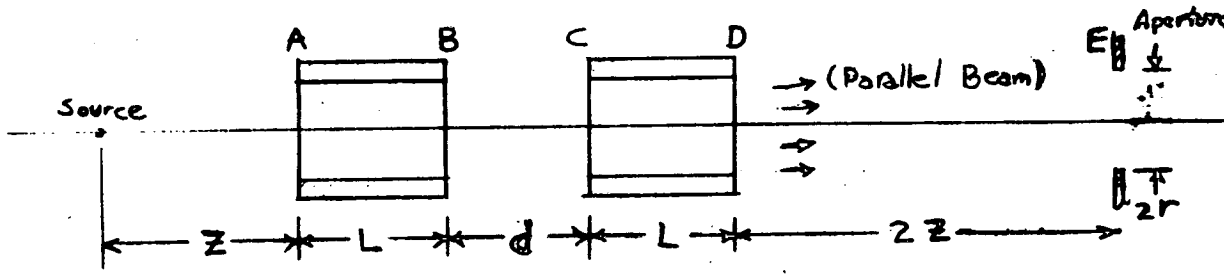

The gradients in the two quadrupoles were adjusted to give a parallel beam out of the second quadrupole. This represents a very common experimental situation. The object distance Z was chosen to give a gradient in the first quadrupole of $12r^{-1}$ (kg/inch). The effect of the various apertures in the system at positions A, B, C, D, and E was then determined using OPTIK. The radius of each aperture was taken as r, the radius of the quadrupole. The aperture at E represents, for example, the entrance to another quadrupole. The limitation imposed by the various apertures on the phase space accepted from the source for various values of r is shown in Fig. 1. The case illustrated is for L = 64", d = 64" and P = 100 GeV/c with quadrupoles of radii 0.5", 1.0", 2.0", and 4.0". In these plots each aperture projects into a line in phase space. Only those rays emanating from the source for which the corresponding points in phase space are closer to the origin than this line will be passed by the aperture. The results are summarized in Table 1.

TABLE 1

L = 64", d = 64", P = 100 GeV/c

					Maximum Source Dimensions			
					without Aperture E		with Aperture E	
r (inches)	G_1 (kg/in)	G_2 (kg/in)	Z (in.)	$\Delta\Omega$ (ster) x 10^6	CD	DC	CD	DC
0.5	23.9	12.4	114.	12.0	±0.5"	±0.19"	±0.14"	±0.19"
1.0	12.0	8.92	350.	11.0	1.0	0.57	0.37	0.57
2.0	6.00	5.42	1195.	5.7	2.0	1.46	0.99	1.46
4.0	3.00	2.92	4490.	2.1	4.0	3.50	2.59	3.50

For comparison, about 70% of the pion flux at 100 GeV/c is contained within a solid angle of 6.0×10^{-6} ster. according to the CKP formula. In this case the 0.5" quadrupole accepts the largest solid angle, but it would only be suitable for use with rather small sources (~ 0.25" diameter). It is expected that the external beam of the 200 GeV accelerator can be focussed to spot ~ 0.1" diameter or less[2] so in general this is not a severe limitation. It is interesting to note that if the beam is made convergent rather than parallel on leaving the second quadrupole, then the smaller-bore quadrupoles are favored even more over the larger ones.

In Table II we show the same quantities for L = 64", d = 128".

TABLE II

L = 64", d = 128", P = 100 GeV/c

					Maximum Source Dimensions			
					without Aperture E		with Aperture E	
r (inches)	G_1 (kg/in)	G_2 (kg/in)	Z (in.)	$\Delta\Omega$ (ster.) $\times 10^6$	CD	DC	CD	DC
0.5	24.0	9.05	93.	4.4	±0.34"	±0.14"	±0.12	±0.16
1.0	12.0	7.21	264.	10.1	1.0	0.46	0.31	0.46
2.0	6.00	4.39	821.	13.5	2.0	1.28	0.82	1.28
4.0	3.00	2.31	2902.	10.7	4.0	3.13	2.23	3.13

In this case the 1" quadrupole subtends a slightly larger solid angle than the others. Table III shows the effect of increasing L to 128" while keeping d = 128".

TABLE III

L = 128", d = 128", P = 100 GeV/c

					Maximum Source Dimensions			
					without Aperture E		with Aperture E	
r (inches)	G_1 (kg/in)	G_2 (kg/in)	Z (in.)	$\Delta\Omega$ (ster.) 10^6	CD	DC	CD	DC
0.5	24.0	4.24	1.5"	13.8	±0.12"	±0.05"	--	--
1.0	12.0	3.76	68.5	28.2	0.44	0.21	0.24	0.22
2.0	6.00	3.10	227.	47.0	2.0	0.77	0.57	0.77
4.0	3.00	2.23	700.	44.0	4.0	2.28	1.47	2.28

[2] Glen Lambertson, private communication.

Figure 1

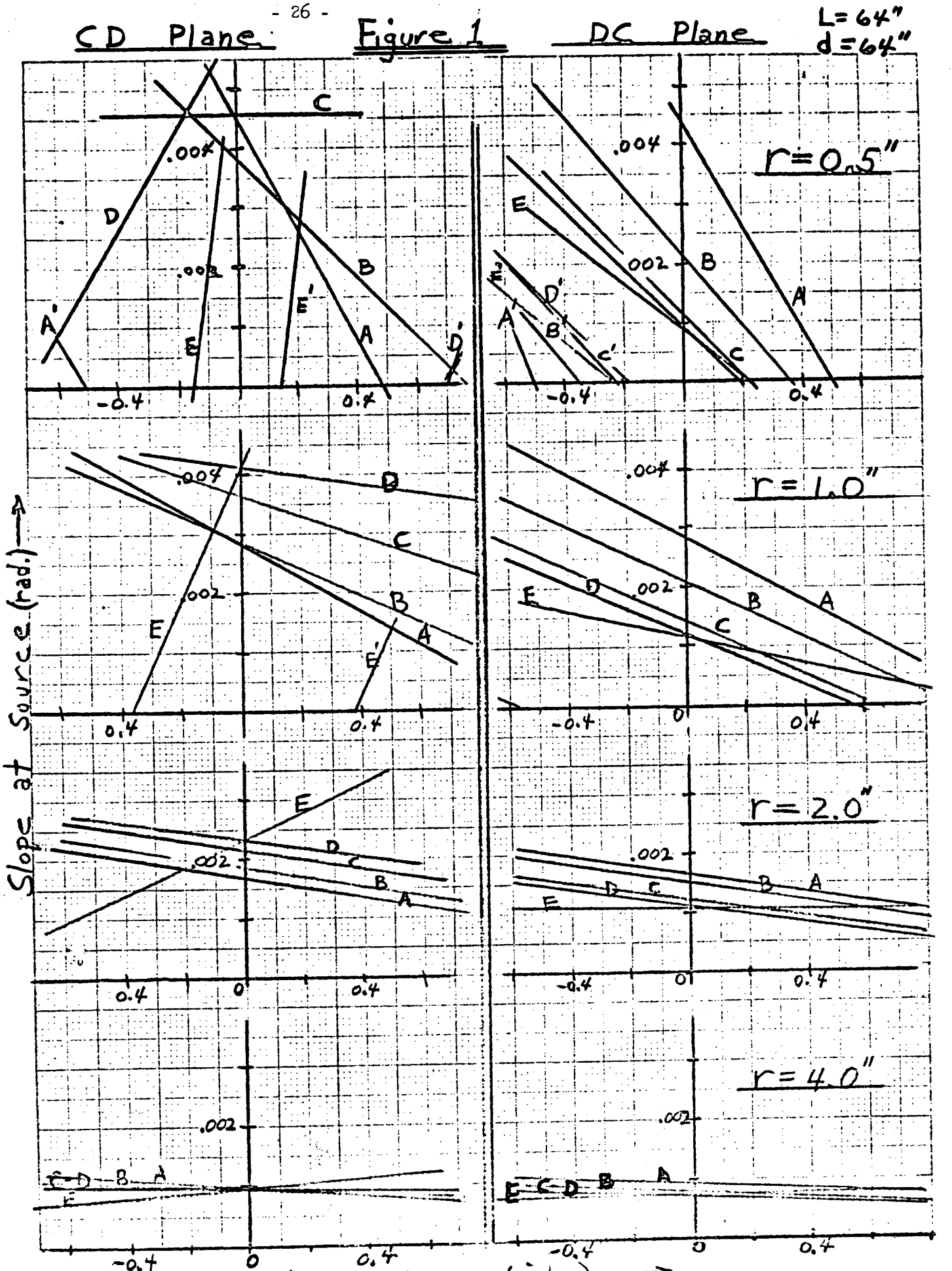
CD Plane
DC Plane
L = 64"
d = 64"
r = 0.5"
r = 1.0"
r = 2.0"
r = 4.0"
Slope at Source (rad.) →
Position at Source (inches) →
.004
.002
0
-0.4
0.4
A
B
C
D
E
A'
B'
C'
D'
E'

This causes a significant increase in solid angle with the 2" radius quadrupole subtending the largest solid angle. Even with 128" sections the object distance of the 4" radius quadrupoles would be 700 inches at 100 GeV/c and over twice as long at 150 GeV/c.

Table IV shows the effect of increasing r while maintaining Z constant at 250" and at the same time increasing L so that the gradients do not exceed $12\ r^{-1}$.

TABLE IV - Variation of Flux accepted with Radius of Quadrupole (Z = 250", $\frac{d}{L} = 1$)

r	L	$G(\frac{KG}{in})$	G_2	$\theta_x(x10^3)$	$\theta_y(x10^3)$	Fraction of total flux accepted (100 GeV/c	"Weight"
1"	74"	12.0	7.8	1.35	3.7	.32	1
2"	123"	5.96	3.25	1.9	6.9	.50	~6
4"	200"	3.05	1.36	2.7	12.6	.65	~40
6"	270"	2.00	0.79	3.17	17.3	.75	~120

In all cases d = L and P = 100 GeV/c. θ_x and θ_y are the half-angles of the acceptance cone in the DC and CD planes respectively. For comparison 70% of the available pion flux is contained within an angle $\theta \approx 4.4 \times 10^{-3}$. In order to maintain the same fraction of the total flux at lower momenta, say 50 GeV/c, we must double r, thereby halving the maximum gradient and increasing θ_x and θ_y by 2. Thus a 4" radius quadrupole will accept 50% of the flux at 50 GeV/c. In table IV, we also give the "weight" of the quadrupoles taking the smallest as the unit. Since the cost tends to increase linearly with weight, this is relevant to the economics of the choice.

The rather small gain in flux with increasing r is due mainly to the fact that most of the increase in solid angle goes into θ_y which is already large compared to the "Cocconi angle" The choice of Z = 250" is arbitrary of course, but if it is increased, r must be even larger to get the same fraction collected (though L can be shorter). If d/L is decreased to make θ_x and θ_y more nearly equal, then L must be made larger to compensate for the weakening of the lens.

The available pion fluxes range from 5×10^7 sec^{-1} at 150 GeV/c to 1.3×10^{10} sec^{-1} at 25 GeV/c with a ± 1% momentum bite.* Even with only 10% of the total collected, these fluxes would be enough to swamp any experiment with counters or spark chambers in the beam. At present, the most practical means of separating beams at these energies seems to be Cerenkov counters so it is quite possible that most of the "nonpermanent" beams may be limited to total fluxes ~ 10^7 particles/sec. For "permanent" beams such as those for neutrino experiments, and perhaps muon experiments; and those with r.f. separators it is reasonable to assume that special quadrupoles will be used. Unless a new technique for mass separation at high energies is developed, it appears there is in general little reason for trying to capture most of the available flux. Thus, for most beams 1" or 2" radius quadrupoles seem to be quite adequate. Quadrupoles with 0.5" -radius bores would be too small for general-purpose use though they may be useful for special applications such as in forming a beam of short-lived particles. If they could be constructed economically and if the assumed gradients of ≈ 24kg/in. could actually be achieved in practice, they could be useful for fairly low-intensity beams. They could not be used economically for transporting beams over large distances because of the short focal lengths involved.

The smaller quadrupoles also have the advantage of smaller overall demensions which makes them easier to bury in a shielding wall and transport. Because of the massive shielding required, it is quite probable that many quadrupoles will remain buried for long periods even though not in use. This is a strong argument for having many inexpensive quadrupoles available.

It would appear that quadrupole "modules" of length approximately 64" and bores of both 1" and 2" radius would be most economical and would satisfy most experimental requirements. For beams of momenta $\gtrsim$ 100 GeV/c two or more of these modules could be put end-to-end to obtain larger solid angles. In certain applications such as muon beams larger bores may be desirable.

---

* This assumes the CKP formula with a proton intensity of 5×10^{12} pps and a target efficiency of 1/3.

Bending Magnets

Once the radii of the quadrupoles is set, it is reasonable to choose bending magnets with the same gap as the quadrupoles (4"). In order to decide on a reasonable length we must set up some criterion for determining the bending angle required. The figure below illustrates schematically the usual situation.

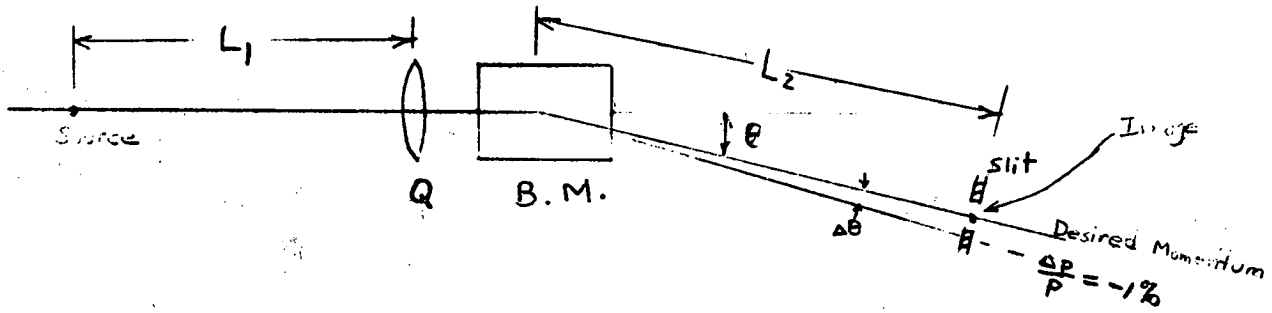

We require that the spatial separation between the image of particles of the desired momentum and that for particles with momentum differing by say 1%, be large compared to the diameter of the images. The most favorable situation is when the quadrupole and the bending magnet are close together. If we neglect their separation, then we require that

$$L_2 \cdot \Delta\theta > \frac{L_2}{L_1} \cdot \text{(diameter of source)}$$

where

$$\Delta\theta \cong \theta \cdot \frac{\Delta p}{p}$$

A reasonable requirement is

$$\Delta\theta = .01 \cdot \theta = 2 \cdot \left(\frac{\text{diameter of source}}{L_1}\right)$$

Referring to Tables I, II, and III, we find $L_1 \sim 400"$ (measured from source to center of quadrupole) for 100 GeV beams. If we assume a source diameter $\approx 0.1"$ as discussed previously, then we need $\theta = .05$ at 100 GeV/c. This requires a magnet approximately 25 feet long with a field of 20 kg. It is probably more practical to build modules 10 or 12 feet long. The width of the pole tip should be at least 10 to 12 inches to allow fairly large bends at lower momenta.

Conclusions

An attempt has been made to determine suitable dimensions for quadrupole and bending magnets to be used for transporting beams of momentum 50 to 200 GeV/c. Quadrupole modules approximately 64" long with 2" and 4" -diameter bores appear to be optimal for most applications. Bending magnets approximately 10 feet long with 4" gaps and 10" wide pole tips would satisfy most experimental requirements. No real attempt has been made to determine the most economic choice of parameters, but those suggested seem very reasonable from an economic point of view. Also a complete study should be made of the magnets required near the production target. In situations where the first quadrupole must be a long distance from the source, it might be desirable to use quadrupoles with an $\approx$ 8" diameter bore; but the length of each section would have to be $\approx$ 12 ft. long for a 150 GeV/c beam.

A 150 GeV/c beam has been designed using magnets of the sizes suggested and is discussed in another report.[3] On the basis of current estimates of available pion fluxes, a beam of 10^7 pions/sec at 150 GeV/c with a momentum spread of $\pm$ 1% is easily obtainable with a proton beam of 5×10^{12}/sec.

The author wishes to thank Dr. Glen Lambertson for many helpful discussions and suggestions.

---

[3] Michael J. Longo, "A 150 GeV/c Beam for Spark Chamber Experiments". July 30, 1964

University of California
Lawrence Radiation Laboratory
Berkeley, California

UCID 10128
AS/Experimental/01
August 13, 1964
Robert W. Williams

THE CHOICE OF PARAMETERS FOR MAGNETS AND BUBBLE CHAMBERS

A. Particle beams and quadrupoles

AGS and CPS experience indicates the validity of the constant-transverse-momentum rule for production of mesons (μ or K) by high energy protons: we assume more than half the mesons are found within an angle

$$\theta_{sec} = \frac{0.44}{p_{sec}} \text{ radians} \qquad (1)$$

(units will be GeV and MKS where possible). This may describe p and $\bar{p}$ also, but the other candidates for beams - $\mu\pm$, $e\pm$ - would have to be considered as special cases. The external beam should have an emittance about 0.05 mm-mr so with a target-spot size matching a 10-cm long target, about 50 μ radius, the secondary angles are dominated by the production angle.

The focal length of a quadrupole doublet is given by the approximate formula,

$$\frac{1}{F} = k^4 \ell^2 \left(\frac{2}{3}\ell + d\right) \quad \left(\text{A singlet focal length is } f_1 = \pm \frac{1}{k^2 \ell} + \frac{\ell}{6}\right) \qquad (2)$$

where ℓ is the length of one quad, d the edge-to-edge separation and $k = \sqrt{0.3\ B'/p}$. This assumes equal gradients in both quads, and is an $\frac{\ell}{F} \ll 1$ approximation; however, it is good to a few percent for $\frac{\ell}{F} \sim \frac{1}{2}$ if one measures correctly from the principle planes. For a first approach we measure everything from the center of the doublet, as though the aperture stop were a diaphragm of radius a in a thin lens at that plane. This overestimates the acceptance by 50% in a numerical example calculated below!

If the quadrupole radius is a, and the maximum usable field at the edge of the aperture is B_o, then $B' = B_o/a$ is the gradient corresponding to the maximum beam momentum p. Equation (2) becomes:

$$\frac{1}{F} = \frac{.09\ B_o^2\ \ell^2}{2\ 2} \left(\frac{2}{3}\ \ell + d\right) \qquad (3)$$

We can investigate several ways of scaling to high momentum, depending on what conditions we impose:

a) Stretch the longitudinal scale, i.e., F, ℓ, d $\rightarrow \alpha$F, $\alpha\ell$, αd. Then (ap) $\rightarrow \alpha^2$ (ap).

b) With the quadrupole dimensions, ℓ and a, fixed, we can still scale the separation, i.e., p $\rightarrow \alpha$p, F $\rightarrow \alpha$F, $(\frac{2}{3}\ell + d)$ = (effective separation) $\rightarrow$ α (effective separation). This is less objectionable when $\frac{F}{\ell}$ is large than in the F $\sim \ell$ range, but of course the solid angle will suffer. At very high energies the angles are naturally small which means that separations of 2ℓ or 3ℓ can be profitable.

c) For maximum intensity we require that the particle production angle θ_{sec} (Eq. (1)) be equal to the acceptance angle. In our approximation, if Z is the source-to-midplane distance, this is $\frac{a}{Z}$ in both planes, and for the formation of a parallel beam, we have Z = F, so the condition is

$$ap = 0.44\ F_{max.\ int.} \tag{4}$$

and the condition for maximum intensity is

$$F_{m.i.} = 0.46\ B_o^{\ 2}\ \ell^2\ (\tfrac{2}{3}\ell + d). \tag{5}$$

This is compatible with the scale of paragraph (b) but is not compatible with the scale of paragraph (a), except for the case a $\alpha \frac{1}{p}$, which leaves the lengths of the quadrupoles invariant.

It is interesting to see what the maximum "capturable" momentum is for the most powerful existing AGS and CPS quadrupoles, taking B_o conservatively as ~ 1.0 T, and putting $d = \frac{1}{3}\ell$.

AGS: 8" x 48", $F_{(p_{max})} \sim 0.8$ m, $P_{max} \sim 3.7$ GeV/c .

. 12" x 60", $F_{(p_{max})} \sim 1.6$ m, $P_{max} \sim 7.1$ GeV/c

CPS: 20 cm x 200 cm, $F_{(p_{max})} \sim 3.7$ m, $P_{max} \sim 16$ GeV/c

We still lack a principle to set the $\frac{a}{\ell}$ ratio for quads designed for higher momenta. Economics might suggest holding ℓ constant and making the aperture (and therefore the bending-magnet apertures) very small. Scaling from CERN, we have a factor 200/25 = 8, so a 2-meter magnet would have a = 1.25 cm, $P_{max} \sim 130$ GeV.

There are several disadvantages to such small apertures for general-use magnets.

1) Beam layouts are awkward because of relatively short focal lengths, since most other beam items - shielding, bending magnets, separators - tend to be in a larger scale. This is especially true for the lower momenta, for which one would have to go to very short distances or else weaken the gradients and lose much of the intensity contained in the cone of Eq.(1). One must study scale drawings of actual layouts (eg, drawings 15A3936 and 15A3946) to see the constraints which force long focal lengths on magnet systems at these energies.

2) To make the very long parallel beams needed for threshold Cerenkov counters or separators, one would not like too large a magnification, since both source size and quadrupole displacements become a problem.

3) The secondary user who must look at a target from some angle other than 0° will need a large-bore quadrupole, as Eq.(1) does him no good at all.

4) The possibility of taking 0° beams without interfering with the primary beam or with each other depends on having enough lateral clearance between beams of different momenta after a certain amount of magnetic analysis. This (unexpectedly, perhaps) argues for a large, since the target-to-quad distance f is proportioned to a, and the lateral separation is proportioned to target distance squared.

Call the ratio of lateral dimension of a quadrupole to its diameter, X. The most compact Bevatron magnets (High Power 8" x 32") have X = 3, and requires about $2\frac{1}{2}$ times the power of the normal (X = 4.8) quads. However, it appears possible[2] to design special quadrupoles for close stacking at the entrance to beam transport systems which would have a ratio of about 1.5, at a power level perhaps 10 times normal. The sketch illustrates one version of the stripped-down quad.

The conditions on a imposed by 0° beam separation in a finite magnetic field arises because the separation is quadratic in the path length while the natural spread of the beam is linear. With a primary momentum p_o, a beam of momentum p, and a lateral displacement y, we have the condition (see sketch on next page)

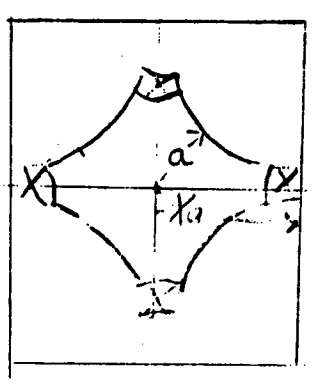

$$y - y_o = X\,a$$

Assuming B = 16,700 gauss,

$$y - y_o = 0.25\,Z^2\left(\frac{1}{p} \mp \frac{1}{p_o}\right)$$

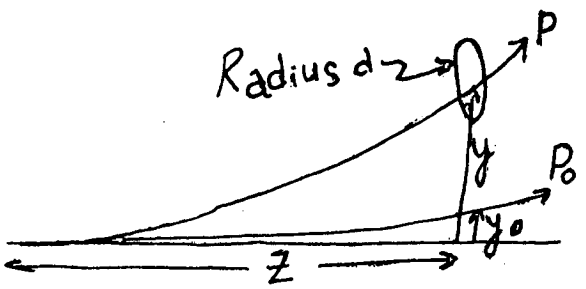

The + sign is for a negative beam. If the primary beam can be "septumed" out after a distance $\ll Z$, then the term $\frac{1}{p_o} \to 0$.

From Eq.(1), $\frac{a}{Z} = \frac{0.44}{P}$

$$\text{whence } Z = \frac{1.76\,X\,p_o}{p_o \mp p}\text{, or for positive beams,}$$

with p_o = 200 GeV/c,

$$Z = \frac{1000}{200 - p} \text{ for no septum and } X = 3, \text{ or } Z = \frac{500}{200 - p} \text{ for } X = 1.5, \qquad (6$$

or Z = 5 meters (or 2.5 meters) for a perfect septum, independent of momentum.

From the latter we see that even with the septum we have a minimum aperture for good intensity, depending on the lowest momentum for which we design a full-intensity beam:

$$a_{min} = 0.78\,\frac{X}{p_{min}} \sim \frac{2.3}{p_{min}} \text{ for } X = 3, \text{ or } \frac{1.2}{p_{min}} \text{ for } X = 1.5$$

Thus a = 10 cm accomodates momenta down to 23 GeV, or 12 GeV, positive or negative.

With no septum, the minimum aperture is given, for various momenta, by the table:

	P	10	20	40	80	160 GeV/c
X = 3	Z	5.3	5.5	6.3	8.3	25 meters
	a	23	12	7	4.5	6.9 centimeters
X = 1.5	Z	2.7	2.8	3.2	4.2	13 meters
	a	12	6	3.5	2.3	3.5 centimeters

It remains to be shown that the crude approximations for quadrupole doublets used here are adequate to support the arguments. The acceptance angles of quadrupole doublets, particularly when focal lengths are not long compared to the magnet lengths, are considerably less in the defocus-focus plane than in the FD plane. I have, therefore, compared the characteristics of a doublet which might be used to render a 100 GeV/c beam parallel, as calculated by rough approximations and by a correct treatment. The example chosen is that of a pair of 20 cm diameter by 600 cm long quadrupole, with 21 meters from the source to the first face of the doublet and 3 meters between the magnets. Also shown are the results of a thin lens approximation of D. Keefe.[3] The results are:

	B_o		Acceptance angle		Fraction of "Cocconi cone"
	Q_1	Q_2	FD	DF	
Approximate	0.98 T	0.98 T	0.0039	0.0039	0.79
Exact	1.24 T	0.97 T	0.0044	0.0023	0.52
Thin lens[3]			0.0044	0.0023	

From this example it appears that the crude approximation used here over-estimates the solid angle by about 50%, while the thin lens is quite adequate.

Conclusion:

General-purpose quads should be fairly large aperture, perhaps a = 10 cm. For the highest energy beams, say 160 GeV c, to get the requisite focal length, one would increase $\underline{d}$ in Eq.(5) to perhaps 2 ℓ, maintaining a suitable focal length with ℓ = 3 meters, which seems a reasonable size.

B. Bubble Chambers

Comments on bubble chambers for very high energies can be found in all the summer study reports. I wish here only to question the conclusion of Pless[4], on the basis of a scaling rule, that "...the momentum measurements in propane are comparable to that of hydrogen." The formulas used by everyone for the fractional momentum error in a bubble chamber track of length ℓ due to (1) multiple scattering, and (2) measurement or setting errors are:

$$\left.\frac{\delta p}{p}\right|_{\text{mult. scatt.}} = \frac{A}{\beta B \sqrt{\ell X_o}}, \qquad \left.\frac{\delta p}{p}\right|_{\text{meas.}} = \frac{C p \epsilon}{B \ell^2},$$

where X_o is the radiation length in meters, and ϵ is the error in measuring the transverse coordinate of the track. The latter does not represent fairly the distortion errors that may be present in a large chamber, but that's another problem.

Pless holds ℓ constant (~ 1.5 meters) and observes that as $\underline{p}$ increases $(\delta p/p)_{meas.}$ increases until it swamps the multiple scattering term, even with $X_o \ll X_{o\ hydrogen}$. There is no reason to hold ℓ constant, however: the fact that 1.5 m is the interaction length in propane cannot be adduced to restrict hydrogen; and the flight path of unstable particles increases linearly with $\underline{p}$. Brookhaven has submitted a serious and detailed proposal for a 4.3 m hydrogen chamber[5]. Wide-angle lenses take the curse off the window, and it appears that only the high cost of magnetic field might hold one back from something truly heroic.

A reasonable scale might be to hold $(\delta p/p)_{meas.}$ constant as $\underline{p}$ increases. Then $p \to \alpha p$ implies $\ell \to \sqrt{\alpha \ell}$, and $\delta p/p)_{m.sc.} \to \alpha^{-1/4}\ \delta p/p)_{m.sc.}$ With this scale one might reduce X_o by 10 (i.e., propane instead of hydrogen) when $\underline{p}$ has increased by 100; but the interaction path in propane is too short.

Perl "proves" from the same formulae[6] that a large magnetic-field spark chamber with built-in hydrogen target is better than a bubble chamber anyway. I will venture a prediction: when such a device is ultimately built, physicists will be unable to resist changing it for each experiment, with the result that its format will never settle down, and the bubble chambers will always publish first.

REFERENCES

1. See also M. Longo, UCID 10124.
2. C. Dols, private communication.
3. D. Keefe, private communication.
4. I. Pless in BNL 7534, Proceedings of the 1964 Summer Study, p. 119.
5. Shutt et al, Recent BNL report.
6. M. Perl, SLAC 5, p. 104.

UCID-10166
AS/Experimental/01
July 6, 1965
Denis Keefe

University of California
Lawrence Radiation Laboratory
Berkeley, California

SCALING OF QUADRUPOLES FOR USE AT THE 200 BEV ACCELERATOR

The Scaling Law: ℓ = const, a = const, u, V, f_1, f_2, and d scaling like p.

(i) What happens when we vary d?

Omit the $\pm \ell/6$ correction to f as an inessential complication.

Nomenclature: For a parallel beam incident

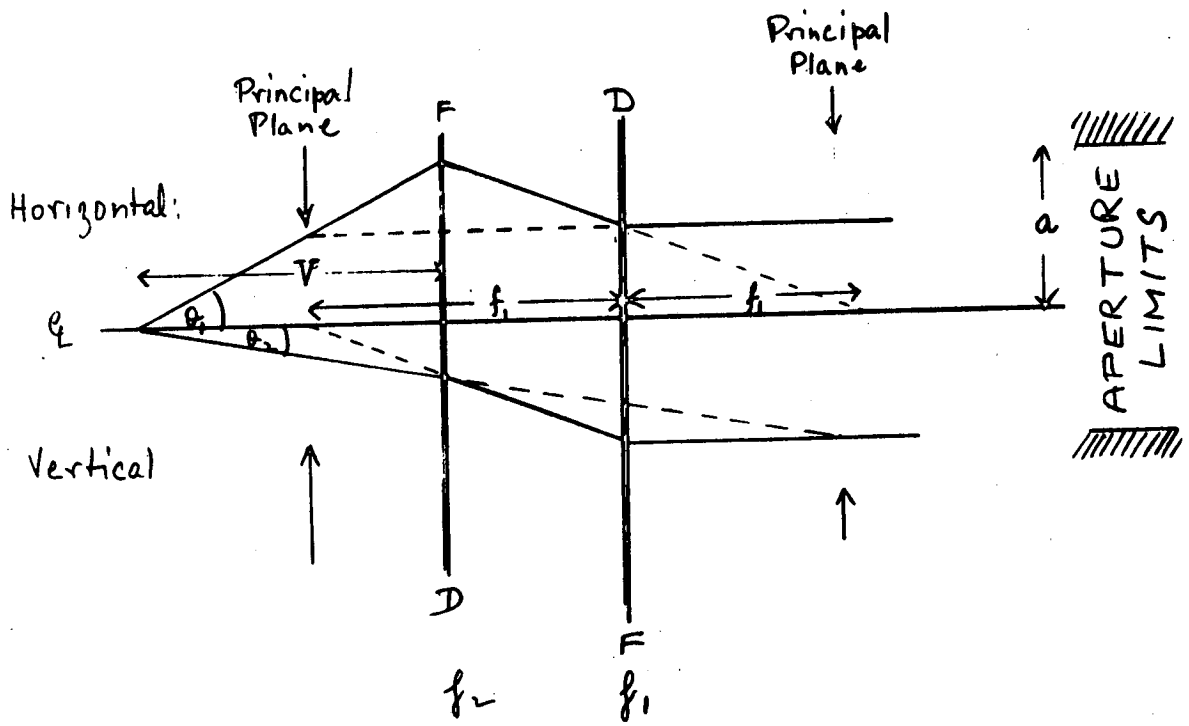

from the right coming to an anastigmatic focus V beyond center of second lens. The extreme excursions occur in the middle of the focussing element, call this limit a the radius of the quadrupole.

Horizontal

Into L_1 Disp = b angle = b/f_1 in L_1

Into L_2 Disp = $b + \frac{db}{f_1}$ angle = $\frac{b}{f_2}(1 + \frac{d}{f_1}) - \frac{b}{f_1}$

$$\therefore V = \frac{b(1 + d/f_1)}{(b/f_2)(1 + \frac{d}{f_1}) - \frac{b}{f_1}} = \frac{1 + d/f_1}{-\frac{1}{f_1} + \frac{1}{f_2} + \frac{d}{f_1 f_2}} = \frac{1 + d/f_1}{1/F_H}$$

Vertical

Change $f_1 \to -f_1$ $f_2 \to -f_2$

$$\therefore V = \frac{d - d/f_1}{\frac{1}{f_1} - \frac{1}{f_2} + \frac{d}{f_1 f_2}} = \frac{1 - d/f_1}{1/F_V}$$

The solid angle available for transmission if the particles issue from a target at the image and are made parallel, is $\pi\, \theta_H\, \theta_V$ where $\theta_H = a/V$

$$\theta_V = a/F_V = a\,(\frac{1}{f_1} - \frac{1}{f_2} + \frac{d}{f_1 f_2})$$

If we scale V proportional to p then $\theta_H \propto 1/p$. If we scale f_1, f_2 and $\underline{d}$ proportional to p then $\theta_V \propto 1/p$ which is the criterion for capture of a constant fraction of flux at all momenta.

Note that while θ_H is independent of the spacing and focal lengths of the elements, θ_V depends on all three. Consider the following: We impose the requirement of anastigmatism;

$$V = (1 + d/f_1)\, F_H\ ; \qquad V = (1 - d/f_1)\, F_V\ .$$

There are four parameters V, d, f_1, and f_2 and we can eliminate one. Most trivial is $\underline{V}$ which then gives a relation between the two focal lengths once we choose d. This is of the form

$$f_2 = \text{function of } f_1^2,\ f_1,\ d$$

Since we wish to retain $\underline{d}$ we will eliminate one of f_1, f_2. Since f_2 occurs only in 1st order, eliminate it.

$$-\frac{1}{f_1}(V + d) - 1 + \frac{V}{f_2}\left(1 + \frac{d}{f_1}\right) = 0 \qquad \times \left(1 - \frac{d}{f_1}\right)$$

$$\frac{1}{f_1}(V + d) - 1 + \frac{V}{f_2}\left(-1 + \frac{d}{f_1}\right) = 0 \qquad \times \left(1 + \frac{d}{f_1}\right)$$

$$\therefore f_1^2 = d\,(V + d)$$

$$\therefore f_1 = \sqrt{d(V + d)}$$

Define:

$$\boxed{\beta = f_1/V = \sqrt{\alpha(1 + \alpha)}} \qquad \text{where} \quad \boxed{\alpha = d/V}$$

Solving for f_2 we have:

$$\frac{1}{f_2}\ V\left(1 + \frac{d}{f_1}\right) = \frac{V + d}{f_1} + 1$$

$$f_2 = V\ \frac{\sqrt{d\,(V + d)} + d}{\sqrt{d\,(V + d)} + V + d}$$

Define:

$$\boxed{\gamma = \frac{f_2}{V} = \frac{\sqrt{\alpha\,(1 + \alpha)} + \alpha}{\sqrt{\alpha\,(1 + \alpha)} + 1 + \alpha} = 1 - \frac{1}{\sqrt{\alpha\,(1 + \alpha)} + 1 + \alpha}}$$

In Fig. 1 β and γ and the ratio of the vertical and horizontal acceptance angles are plotted against α.

Suppose we set the first quadrupole at a fixed distance V from the target and vary the spacing $\underline{d}$, θ_H remains constant but $\theta_V = a/F_V$. But

$$V = (1 - d/f_1)F_V \qquad \therefore \frac{1}{F_V} = \frac{1 - \sqrt{\frac{d}{V+d}}}{V}$$

$$= \frac{1}{V}\left(1 - \sqrt{\frac{\alpha}{1+\alpha}}\right)$$

Consider now the case of maximizing $\Delta\Omega$, i.e., minimum α. Assume now that both elements are the same length $\underline{\ell}$, then L_2 is running hotter than L_1 and it runs first into the limit. It is obviously impossible to have α very small, viz, a very small $\underline{d}$ since we have the condition:

$$d \geq \ell$$

For a given limiting pole-tip field (1 Tesla) and a reasonable aperture, as we try to make f_2 (hence β) as small as possible at the same time keeping the interelement spacing (α) a minimum, we run into a limit on $\underline{\ell}$ and hence on $d \geq \ell$.

To express this limit quantitatively we still have to fix one parameter; most conveniently $\underline{V}$. The pole-tip field limit gives the following

$$f_2 = \frac{B\rho}{B'\ell} = \frac{10}{3} E \frac{a}{\ell} \frac{1}{B_o}$$

$$B_o \leq 1 \qquad \text{Units: Meters, Teslas, GeV}$$

$$\therefore f_2 \geq \frac{10}{3} E \frac{a}{\ell}$$

Pick a value of V, then if we always require a certain fraction of the flux this fixes $\underline{a}$. Take the traditional 70% number — then $a/V = .44/E$

$$\therefore \gamma = f_2/V \geq \frac{10}{3}\,\frac{Ea}{V^2}\,\frac{V}{\ell}$$

$$\geq \frac{10}{3}\,\frac{Ea}{V^2}\,\frac{V}{d} \quad \text{since } d \geq \ell$$

$$= \frac{10}{3}\,\frac{Ea}{V^2}\,\frac{1}{\alpha}$$

$$= \frac{10\ (.44)}{3\ V}\,\frac{1}{\alpha} = \frac{1.5}{V}\,\frac{1}{\alpha}.$$

				V	
If V = 5 m	$\gamma \geq \cdot 3/\alpha$	min α (p.4)	~ 0.5	10	$\cdot 15/\alpha$
15 m	$\gamma \geq \cdot 1/\alpha$	"	~ 0.25	20	$\cdot 075/\alpha$
45 m	$\gamma \geq \cdot 03/\alpha$	"	~ 0.09	30	$\cdot 05/\alpha$

Referring back to the θ_V/θ_H curve we see that over this very wide range of V the α operating point corresponds to a ratio very close to 1/2 for θ_V/θ_H. (Therefore the choice $a/V \simeq 0.44/E$ is not true in both planes and probably the numerator should be taken closer to 0.7 for design purposes.)

The curves now allow us to choose acceptable quadrupole specifications if we have some estimate of V. For example:

Take V = 15 m.

Take a base momentum E = 100 GeV and assume we bolt the two elements close together at this momentum. Then $\alpha \geq 0.25$ (take the equality)

$\therefore \alpha = 0.25$ $\quad\therefore d = 3.75$ m

$\beta = 0.55$ $\quad f_1 = 8$ m

$\gamma = 0.42$ $\quad f_2 = 6$ m

$a/V = 0.44/E$ $\quad = 0.066 \quad = 6.6$ cm

Hence quadrupole singlets are 3.75 m long with a radial aperture of 6.6 cm and should be used 15 m from the target. At higher momenta the distances V, d should be increased in proportion to p and the currents

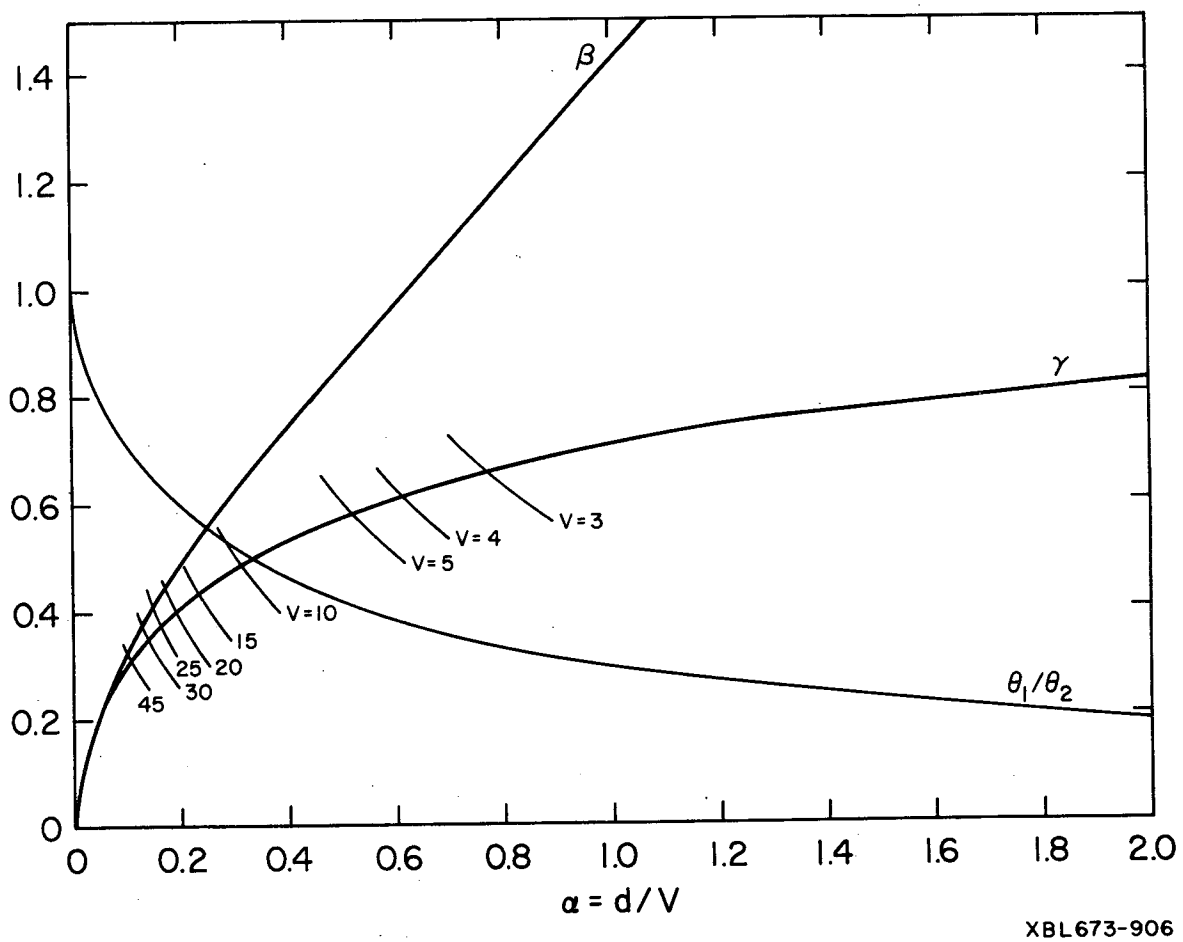

ig. 1. The "reduced" focal lengths, $\beta(= F_1/V)$ and $\gamma(= F_2/V)$, of the two elements of a doublet, plotted as a function of the "reduced" spacing between the elements, $\alpha(= d/V)$. Also shown is the ratio of horizontal and vertical angles θ_1/θ_2.

in the elements held the same.

What happens if we try to use the same elements at lower momentum? Say one half. Then $p \rightarrow \frac{1}{2} p$. Suppose now we try to keep the same flux factor and make $V \rightarrow \frac{1}{2} V$. Then $\alpha \rightarrow 2\alpha$ or from 0.25 to 0.5 decreasing the ratio $\frac{\theta_V}{\theta_H}$ from $0.53 \rightarrow 0.43$ because of the irreducibility of $\underline{d}$. Thus we lose 20% in flux. (Actually not quite this as we should back away again from the target a little bit). If we naively scale $\underline{V}$ downward with momentum then at 25 GeV ($p \rightarrow \frac{1}{4} p$) $\frac{\theta_V}{\theta_H}$ decreases from 0.53 to 0.3 again losing flux. At this stage the solution lies in choosing quadrupoles of shorter length or larger aperture.

UCID 10167
AS/Experimental/01
March 29, 1966
G. H. Trilling

NOTES ON QUADRUPOLE SCALING

A. Quadrupoles

Consider a quadrupole doublet which produces a parallel beam from a point source. Consider the "thin-lens" approximation and let f_1, f_2 be the focal lengths of the two singlet elements 1 and 2, in the plane in which Element 1 is converging (C) and Element 2 diverging (D) (see diagram).

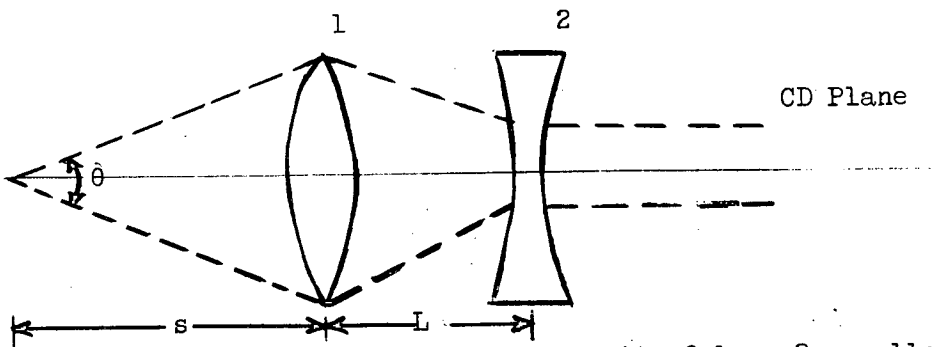

If one requires that the beam emerge from the exit of lens 2 parallel to the axis in both planes, one can easily show that

$$f_1 = s\sqrt{\frac{L}{L+s}}$$

and

$$f_2 = -\sqrt{L}\,\sqrt{L+s}$$

Hence

$$\frac{f_1}{f_2} = -\frac{s}{L+s}$$

If D is the diameter of either quadrupole aperture, the angular acceptance subtended at the point source can be written:

$$\theta = \frac{D}{s} \quad \text{in the plane shown in the figure (CD)}$$

and

$$\theta' = \frac{D}{s} \frac{1}{1 + \sqrt{\frac{L}{s}}\sqrt{\frac{L+s}{s}} + \frac{L}{s}},$$

in the plane at right angles (DC).

An expansion of the above expressions up to first order in $\frac{L}{s}$ will be sufficient for our purposes. Thus,

$$f_1 = \sqrt{Ls} \quad (1 - \frac{L}{2s}) \tag{1}$$

$$f_2 = -\sqrt{Ls} \quad (1 + \frac{L}{2s}) \tag{2}$$

$$\theta = \frac{D}{s} \tag{3}$$

$$\theta' = \frac{D}{s} (1 - \sqrt{\frac{L}{s}}) \tag{4}$$

(Note that if $L \ll s$: $f_1 \approx -f_2 \approx \sqrt{sL}$, $\theta \approx \theta' \approx \frac{D}{s}$)

The characteristics of the production of high-energy secondary particles are such that the production angle containing most of the particles is

$$\theta \approx \frac{1.0}{P}, \text{ (P in BeV/c)} \tag{5}$$

Since $P \alpha H\rho$, we may write this angle as

$$\theta = \frac{\xi}{H\rho}, \text{ where } \xi \text{ is a constant.} \tag{6}$$

For a quadrupole element of length ℓ, the focal length is given by:

$$\frac{1}{f_1} = \frac{H'\ell}{H\rho}, \text{ where H' is the field gradient} \tag{7}$$

$$= \frac{2H_o\ell}{DH\rho}, \text{ where } H_o \text{ is the pole tip field} \tag{8}$$

Combining (1), (7), and (8), we get

$$\ell^{\frac{3}{2}} = \frac{D(H\rho)}{2H_o\sqrt{\lambda s}} \left(1 + \frac{\lambda \ell}{2s}\right) \quad \text{where } \lambda = \frac{L}{\ell} \geq 1 \tag{9}$$

Consider now how the situation may be scaled with momentum. We immediately notice that if we increase P, hence $(H\rho)$, and we change s, λ in the same proportion leaving ℓ, H_o, D the same, i.e., keep the same elements and the same apertures but increase all inter-element spacings in proportion to the momentum, Eq. (9) remains satisfied. From (5), just the same fraction of the flux is captured by keeping to this method of scaling. Thus one could consider using quadrupoles similar in size to those in use at present accelerators for beams at the 200 BeV accelerator and simply expand the beam lengths in proportion to P. This has the serious disadvantage that the real estate taken up by a beam would become unduly large.

Assuming elements with given ℓ, D, we next introduce the requirement that a major proportion of the flux be captured over as large a range of momentum as possible. While the angles of acceptance in the two planes are not the same we can approximately express this condition by using equation (6) only. Thus

$$\theta = \frac{\xi}{(H\rho)} \frac{D}{s} \quad \text{or} \quad D(H\rho) = s\xi \tag{10}$$

which, being combined with equation (9) gives

$$\ell^{3/2} = \frac{\xi}{2H_o} \sqrt{\frac{s}{\lambda}} \left(1 + \frac{\lambda \ell}{2s}\right) \tag{11}$$

Over how large a range of $(H\rho)$ can equations (10) and (11) be satisfied for quadrupoles of chosen dimensions? Define a "design value" of $(H\rho)$, $(H\rho)_d$, a corresponding value of s, s_d, such that for this value λ is unity and H_o has its maximum value $H_{o\,max}$. Then the conditions (equation (10) and (11)) for capturing a major fraction of flux give

$$\ell^{3/2} = \frac{\xi}{2H_{o\ max}} \sqrt{s_d}\ (1 + \frac{\ell}{2s_d}) \qquad (12)$$

$$D(H\rho)_d = s_d \xi . \qquad (13)$$

Now when we consider the case of higher momentum, we cannot increase H_o, and hence can only change λ. As P increases, equation (10) requires that $s \alpha P \alpha (H\rho)$ and further, equation (11) demands, $\lambda \alpha s \alpha P$. Thus we retain our conditions in increasing the momentum by increasing s and L just in proportion to the momentum, as discussed earlier. However, when we consider the situation at lower momentum, we are not allowed to decrease λ since $\lambda = 1$ is the minimum value when the quadrupole singlets are touching each other, but we can decrease H_o. In that case, equation (10) requires

$$s \alpha (H\rho) \alpha P$$

and together with equation (11) we have

$$H_o \alpha \sqrt{s}\ (1 + \frac{\ell}{2s}) \alpha \sqrt{P}\ (1 + \frac{\ell}{2s_d} \sqrt{\frac{P_d}{P}}\ ) \qquad (14)$$

Hence by going down in gradient and s we can keep our conditions satisfied. If we can then go up or down in momentum, what determines the design momentum P_d from which the quadrupole parameters L, D are calculated?

The answer is the following. If we take P_d large, we minimize the real estate used up by the highest energy beams but we do cut down on the flux obtainable from the low energy beams. This is because equation (10) is an approximation which ignores the different angular acceptances in the two planes (θ, θ'). Thus for fixed λ, as s decreases, the acceptance in the initially defocusing plane gets worse. If we take P_d small, then the high energy beams get rather long.

We consider below some numerical examples:

1. Assume $P_d = 100$ BeV/c, $H_{o\ max} = 13$ kG; from (5), (6) $\xi \approx 1300$ if $H\rho$ is in kG-inches, and take $s_d = 12.5\text{m} = 500$ inches

$(H\rho)_d = \frac{100 \text{ BeV/c}}{.762} \times 10^3 = 131{,}000$ kG-inches.

$$D = \frac{s\xi}{H\rho} = \frac{(500)(1300)}{13{,}000} = \underline{5 \text{ inches}}$$

$$\ell^{3/2} = \frac{\xi}{2H_{o\ max}} \sqrt{s_c} \left(1 + \frac{\ell}{2s_d}\right)$$

$$\ell^{3/2} = \frac{1300}{2(13)} \sqrt{500} \left(1 + \frac{\ell}{1000}\right)$$

$$\ell^{3/2} = 1120 \left(1 + \frac{\ell}{1000}\right)$$

or $\underline{\ell = 115 \text{ inches}}$

Thus we get $\underline{\ell = 115", D = 5"}$ for this case.

For 200 BeV/c we would take s = 1000 inches, λ = 2, hence the edge to edge doublet separation would be ~ 115".

The ratio of the angular acceptance in the two planes from (4), is $\sim 1 - \sqrt{\frac{L}{s}} = 1 - \sqrt{\frac{\ell}{s}} = 1 - \sqrt{\frac{115}{500}} \sim 50\%$ which causes a substantial loss in flux. It is then clear that as one proceeds to lower momenta and decreases s, but not λ, the loss in the D.C. plane will be even larger. Thus for lower momentum beams it may be desirable to consider elements which optimize a beam momentum P_d = 50 BeV/c.

2. For P_d = 50 BeV/c, if we take s_d = 250" (smaller than before as one has fewer magnets to go through and thus closer access to the target), then D = 5" and ℓ = 90".

It is of interest to ask what dimensions would be required so that essentially the full flux can be captured. In that case we must set the required production angular width $\theta = \frac{1.0}{P} = \frac{\xi}{(H\rho)}$ equal to the angular acceptance of the doublet when the first element is defocusing (i.e. in the D.C. plane):

Thus

$$\theta' = \frac{\xi}{H\rho} = \frac{D}{s} \frac{1}{1 + \sqrt{\frac{L}{s}} \sqrt{\frac{L+s}{s}} + \frac{L}{s}} \qquad (15)$$

Putting in numerical values, P_d = 100 BeV/c, s_d = 500 inches, L = ℓ, and solving simultaneously with (9) we obtain $\ell \sim 299"$ and $D \sim 10"$. Thus it evidently requires much larger quadrupoles to capture all the flux in one plane, but much easier to do so in the other plane.

B. Bending Magnets

For bending magnets, the vertical apertures should just match the quadrupole aperture. As to the length, we must ask that a magnet give adequate dispersion for good momentum analysis. Let t be the source size, D the horizontal aperture, θ the horizontal angular acceptance, and Φ_m the angle of bend. The dispersion at the target if the aperture D is filled is given by:

$$\Phi_m \left(\frac{D}{\theta}\right) \frac{\Delta p}{p} .$$

If we assume a target size of 1 mm, a momentum bite of 0.1% total and that $\theta = \frac{1.0}{P}$ so that most of the particles can be captured by the quadrupoles, then

$$1 \text{ mm} = .04" = \Phi_m (DP) (.001)$$

$$\Phi_m = \frac{40}{DP}$$

or,
$$\Phi_m = .762 \times 10^{-3} \frac{H\ell}{P}$$

with H in kG
ℓ in inches
P in BeV/c.

Thus,

$$\ell = \frac{5 \times 10^5}{DH}$$

If D = 8" then H = 20 kG and ℓ = 300 inches.

This length is excessive, because it is obtained by combining maximum flux with ±.05% momentum definition. It is quite likely that beams with such a momentum definition can use less than the maximum flux, in which case s can be greater, hence ℓ less in the same proportion.

UCID-10027
AS/Experimental/03
August 11, 1964
C. Dols

SEPTUM QUADRUPOLE MAGNET SUGGESTIONS

This note offers design suggestions for "septum quadrupole" magnets. The first design is derived from a septum bending magnet by the conformal transformation $z = w^2$ (where $z = x + iy$ and $w = u + iv$).

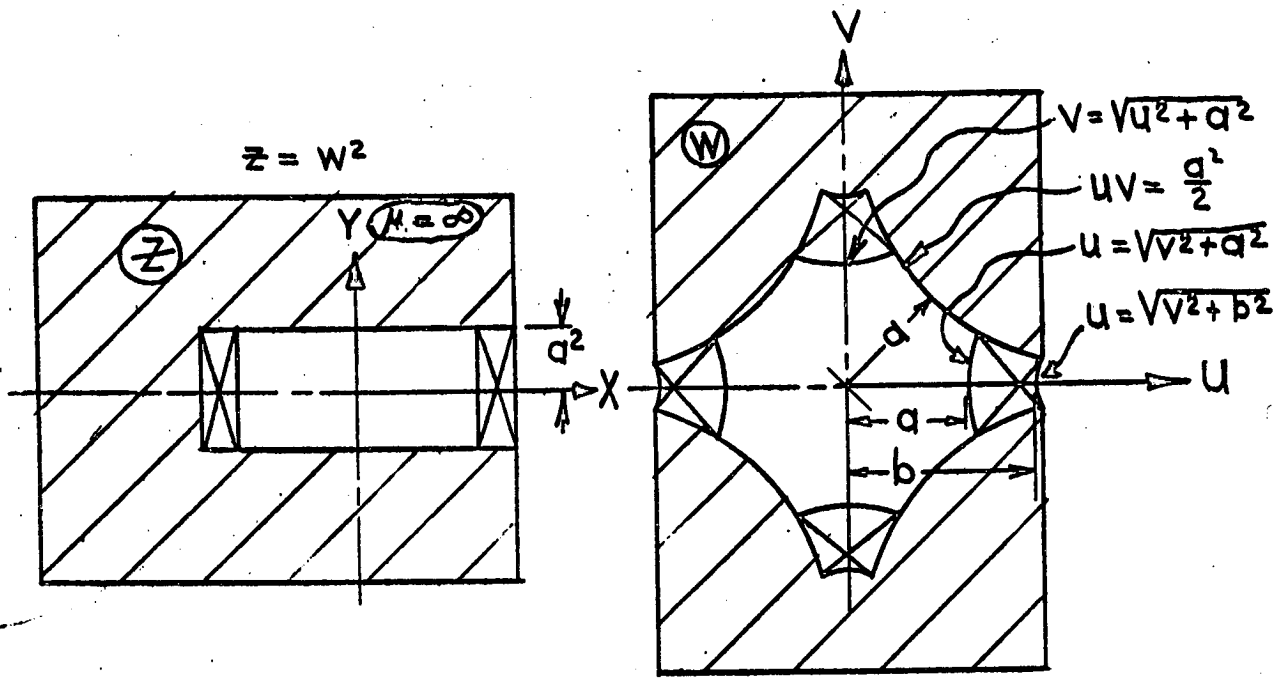

When the distribution of current density in the coil sides satisfies certain restraints, the magnet field is ideally quadrupolar inside the coils and is zero outside of the coils.

When the pole surface is defined by the hyperbola, $v = \frac{a^2}{2u}$, an ideal current distribution is obtained as follows: between any two hyperbolas orthogonal to the pole tip surfaces the relative current density is $\frac{j(u, v)}{j(u_o, v_o)} = \frac{u^2 + v^2}{u_o^2 + v_o^2}$, in general, or, e.g.: $\frac{j(u, v)}{j(u_o, o)} = \frac{u^2 + v^2}{u_o^2}$. (u, v are points in the region and u_o, v_o is any point in the region). Note that each coil side may be divided into any number of such regions.

To obtain a quadrupole field that is relatively free of aberrations, the ideal current density distribution should be approximated fairly well near the aperture. However, uniform current density becomes a fairly good approximation to the ideal for $u > 1.25a$ (say). The pole tip contour corresponding to this approximation would probably have flat portions to permit coil sides of uniform height in those regions.

When the left hand edge of the right hand coil side is at $u = a$ and the right hand edge of the right hand coil side is at $1.5a$, the coil cross-section A_w is $0.40a^2$. When the magnet winding is symmetrical, the total cross-section for conductors is $4 A_w$.

The gradient:

$$G = \frac{j f A_w}{2.02 a^2} \qquad \text{gauss/in with } \underline{a} \text{ in inches}$$

When $A_w = 0.4a^2$ $G = 0.20 f j$

where f is the conductor space factor and

j is the current density in amperes per square inch.

The power per unit length for <u>each</u> of the four conductor bundles:

$$\frac{P}{\ell} = \frac{I^2 R}{\ell} = j^2 f A_w r = \frac{4.08 a^4 G^2 r}{f A_w}$$

with $r = 0.8 \times 10^{-6}$ ohm in (resistivity)

$f = 0.4$ (copper space factor)

$A_w = 0.4 a^2$ (area of coil)

$P/\ell = 0.128 j^2 a^2 \times 10^{-6}$ watts/inch

$= 20 G^2 a^2 \times 10^{-6}$ watts/inch

It is clear that even moderate gradients require much power. Remember, however, to take a realistic duty factor when computing power cost. Many of these magnets will spend a large portion of their useful lives at less than 1/2 rated current (e.g. zero). A duty factor of 0.1 for such a (CW) magnet is probably high.

As a first step in reducing power consumption, the size of the upper and lower coil sides may be increased by using coil sides of conventional size and shape. This approach is particularly appropriate when the required vertical aperture is less than the horizontal. The left and right coil sides may

also be increased in size if a larger ratio of b to a, is allowed. Since the height of the ideal coil sides at the outer edges decreases as b/a is increased the next step would be to depart from the hyperbolic pole contours in the direction implied in the figure below. The aberrations introduced by this non-ideal geometry are acceptable in many applications.

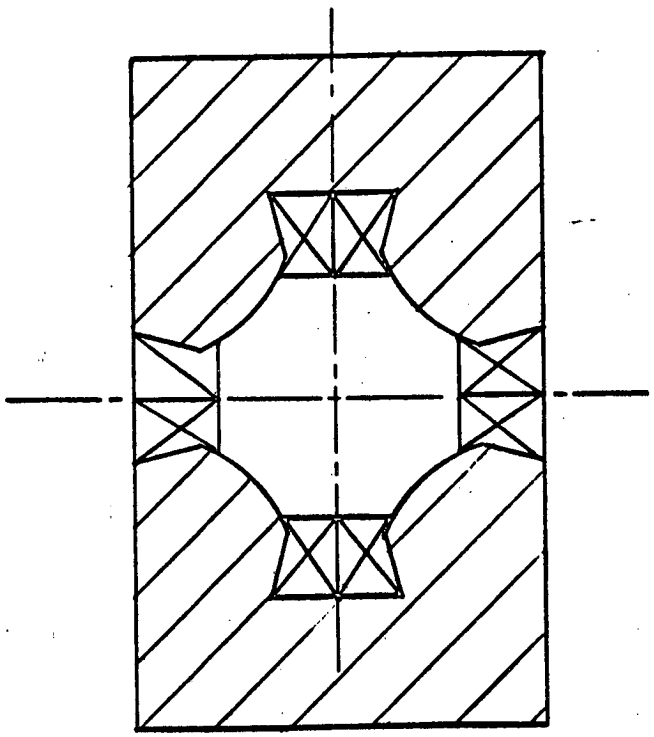

Another form of septum quadrupole magnet has been suggested by Glen Lambertson. This magnet could be called a "bending septum quadrupole" because it has a vertical field at the center of its aperture.

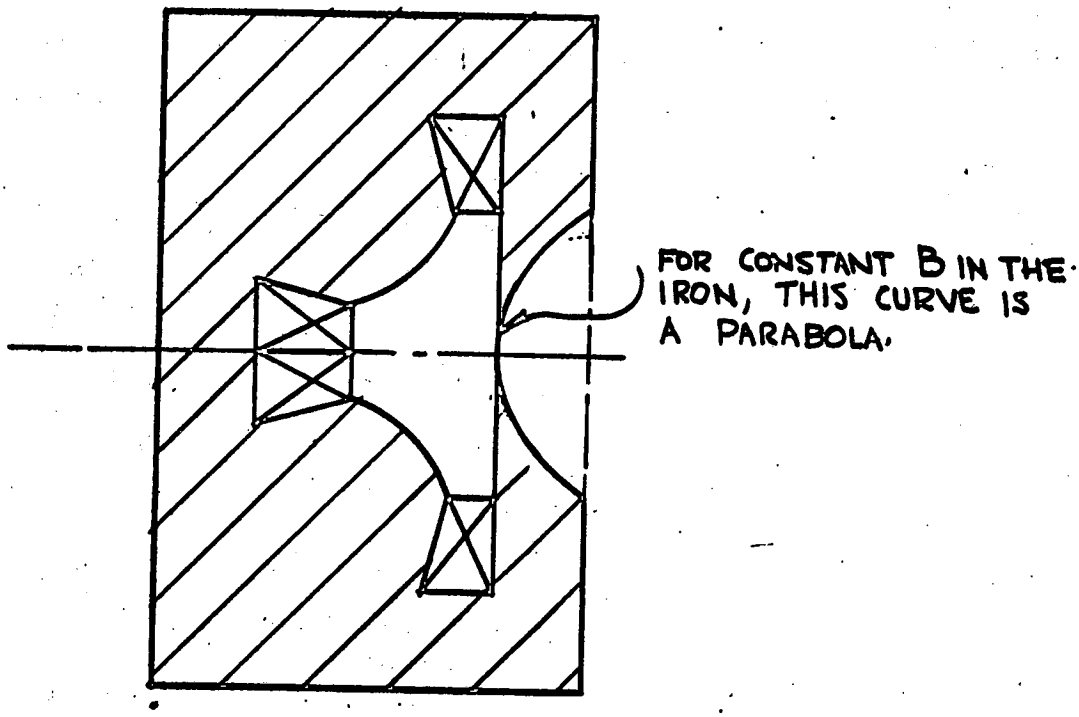

Glen pointed out the interesting possibility of combining two such magnets as shown in the figure below to get a field-free region as close as possible to two bending quadrupole regions. If the restriction on field direction is acceptable the outer iron return paths may be eliminated as shown.

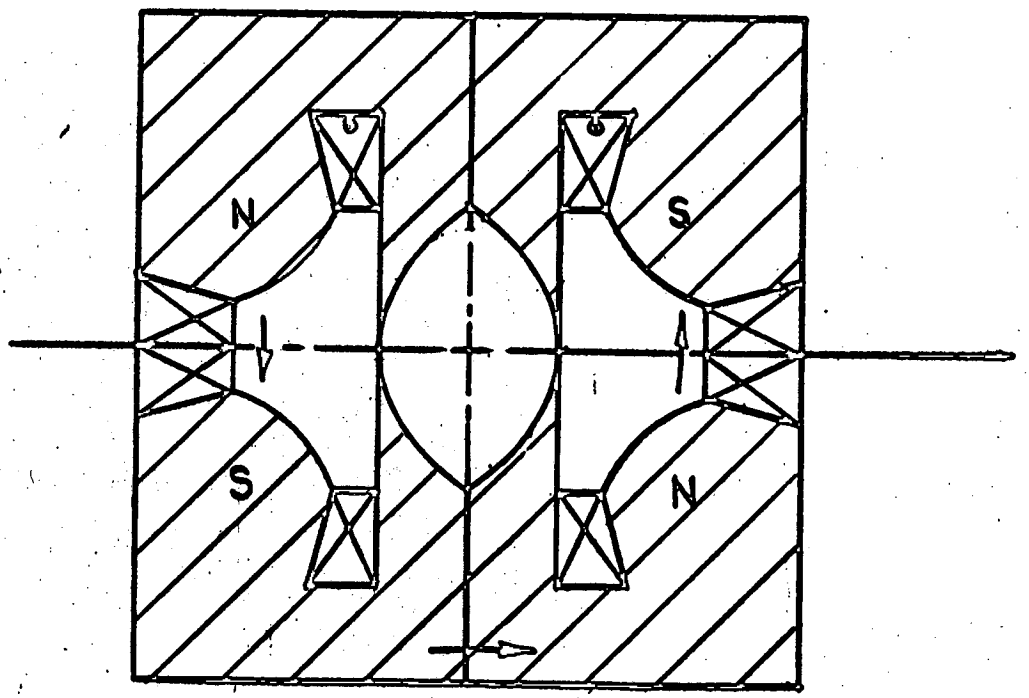

UCID-10163
AS/Experimental/01
August 25, 1965
W. Chinowsky

MONSTER BUBBLE CHAMBER DOCUMENT

I. Physics Utilizing a Hydrogen Bubble Chamber at the 200 BeV Machine

It is necessary to make some judgements about the direction future research in high energy physics will follow. These are necessarily based on present interests and in particular on the problems now raised but unsuccessfully solved. We consider that the present research in strong interaction physics will continue, proceeding to higher energy. Among typical kinds of experiments to be pursued may be listed those studying reactions among known particles with perhaps an elucidation of the "asymptotic" properties of the strong interactions. Further should be cited the continuation of the search for all the strongly interacting particles with the discovery of presently unknown stable particles and resonances. It is to be expected that better and fuller understanding of basic symmetries will follow. The utility of the hydrogen bubble chamber in investigating such problems hardly need be discussed very much. It need only be pointed out that with minor exceptions all particles heavier than ~ 100 MeV have been first detected with visual devices (cloud chamber, emulsion, bubble chamber) and with even fewer exceptions their static properties, spins, parities, etc., have been measured with the use of hydrogen bubble chambers. Decay properties also have been amenable to study particularly with the hydrogen chamber. There seems every reason to expect this kind of physics to continue to be of great interest and to be vigorously continued provided bubble chambers of sufficient size to meet the requirements discussed below are available.

Of great importance and perhaps of even more interest since so little is known at present is the investigation of weak interactions at high momentum transfer. Present knowledge of weak interactions has been obtained from decay properties. The only feasible technique available to extend the study to greater momentum transfer appears to be the investigation of neutrino interactions at high energy. As discussed by D. Keefe[1] and V. Peterson[2] the 200 BeV accelerator will provide neutrino beams of high

intensity with reasonably well-defined momentum. In fact it appears that this will be a unique capability of that machine. It is expected that a major share of the reasearch done with the large bubble chamber will be involved with neutrino interactions with protons and neutrons. In this way knowledge of the structure of the weak interaction will be extended. We discuss neutrino interactions therefore in some detail.

II. Considerations on the Study of Neutrino Interactions in a Liquid Hydrogen-Deuterium Bubble Chamber

A. Introduction

General discussions of high energy neutrino-nucleon interactions have been made many times, among which we particularly mention those of Lee and Yang[3] and a recent review by G. Feinberg[4] where other references may be found. We may summarize some of the general problems for which solutions must be sought. First, the detailing of the structure of the four-Fermion weak interaction and the strangeness - changing weak interaction by determination of the relevant form factors - is necessary. The validity of the low-energy selection rules and conservation laws established in the decays of unstable particles and primitively determined in the low-energy neutrino interaction experiments[5] must be considered at all energies. As will be discussed below somewhat more, it will be possible to study not only nucleon interactions but also electron interactions, so that complications due to strongly interacting particles can be eliminated. This is a direct study then of lepton-lepton interaction, without the introduction of extraneous particles or forces. It will be possible to do such experiments with, however, the total energy in the center of mass system limited to ~ 200 MeV. Even at these relatively low energies there is interest in making detailed, quantitative experiments on processes not available in the naturally occurring decay processes. Also, it may become necessary to depart from the present theoretical framework and introduce an entirely new structure should the high energy weak interaction experiments not be interpretable with present ideas. New phenomena must always be expected to appear.

B. Theoretical Considerations

In order not to work in a complete vacuum, we will find it necessary to use many results obtained in the framework of "conventional" weak interaction theory. We particularly make use of the discussions of Lee and Yang[3] and of Feinberg.[4] In doing this, we may work at various levels of the theory. As discussed by Lee and Yang, these levels may be considered first using only the assumption of point interaction; second adding selection rules; thirdly adding the assumption of the conserved vector current theory. It is well known that this highest level, CVC theory, is very successful at small momentum transfers and it is a valid task to determine whether the theory may be extended to higher energies. We must be prepared, however, to give up any of the conventional assumptions. This point has a direct bearing on the design and analysis of experiments. As an example, consider the reaction $\bar{\nu}_\mu + P \rightarrow \mu^+ + N$, the only allowed two body, $\Delta S = 0$ reaction if the fiat of charged lepton currents is demanded at high energies as it is at low. This being so, it is then required that the positively charged particle be a muon. Then the number of possible particles in the final state is severely restricted and the task of identifying them is made simpler. Were it desired to search for effects of neutral lepton currents then it would be necessary to distinguish between the reactions

$$\bar{\nu} + P \rightarrow \bar{\nu} + P \quad \text{and} \quad \bar{\nu} + P \rightarrow \mu^+ N,$$

for instance. Thus the problem is more formidable if we do not admit of some a-priori selection rules. Thus experiments should be designed so that is is possible to distinguish between events which are examples of these last two reactions. Other examples could be given but are perhaps unnecessary. We may say that eliminating any assumption, permitting then a greater variety of reactions increases the difficulty of making experiments and necessitates providing more sophisticated means of identifying particles. As is usually the situation, the program will then be dichotomic. On the one hand, we will want to make experiments to check predictions of current theoretical models, while, in case of failure of such predictions, keeping alert to observation of effects indicating both the particular reasons for failure (which assumptions are invalid) and important clues to construction of new theories.

III. Event Rate

As shown by V. Z. Peterson, D. Keefe and others, the 200 BeV machine provides beams of neutrinos of sufficient intensity to make experiments in liquid hydrogen at energies much greater than any yet achieved. It has been calculated that at neutrino energies in the range ~ 1 BeV $< E_\nu \lesssim 15$ BeV fluxes of the order of 10^{11} neutrinos per pulse of 10^{13} protons can be made available at a bubble chamber of some 6 meters in diameter, with the neutrino energy defined to $\sim 10\%$. Then, with an interaction cross section $\sigma = 10^{-38}$ cm^2 and assuming a useful path length of 4 meters of liquid hydrogen, we obtain an event rate of $\sim 1/100$ per pulse. If a picture taking rate of 15,000 per day is assumed, we thus obtain about 150 such events per running day. This is then the approximate expected rate of elastic events in the bubble chamber with neutrino energy about 1 BeV. In Table I below we list some relevant kinematical quantities and expected event rates for neutrino-proton and neutrino-electron interactions in the bubble chamber mentioned above, i.e., 6 meters diameter, 4 meters path length. In calculating the event rate we use the qualitative estimate $\sigma \sim G^2 \bar{P}_\nu^2$ where the coupling constant $G^2 \simeq 10^{-5}$ (M_p^{-2}) and $\bar{P}_\nu$ is the neutrino energy in the center of mass system. This gives a cross section for ν-P elastic scattering $\sigma_{EL} \simeq 10^{-38}$ cm^2 at a lab neutrino momentum $P_\nu \approx 4$ BeV/c. Present theoretical prejudices indicate that the cross section should not rise much larger than this. We have, in fact, given the neutrino-proton event rate at 5 BeV/c incident momentum with the assumption of the $\bar{p}_\nu^{\,2}$ dependence. At higher momenta, the event rate is uncertain. Rates for inelastic reactions presumably are greater; those for strangeness-changing reactions perhaps an order of magnitude smaller.[6] It is emphasized that these are qualitative estimates and must be taken in that spirit. The neutrino-electron rates are quite small. For these experiments there may be some advantage to using neon-hydrogen mixtures in the chamber,[7] not merely to increase the rate but to allow the identification of electrons. It has been shown that Ne-H mixtures in almost any combination are usable, producing good tracks at conditions which can be easily achieved in a chamber ordinarily operating with liquid hydrogen. In pure Neon, with density ~ 1.2 gm/cm^3, the electron interaction rate is then ~ 15 times greater than shown in the table, giving the respectable rate of the order of ten events per day.

The available range of momentum transfer* for nucleon interaction is seen to be very large, indeed, ~ 20 times greater than the range of momentum transfer presently covered in electron scattering experiments. Of course, the accuracy achievable here is much smaller, but at any rate it is of great interest to directly compare the ν-nucleon and e-nucleon form factors.

TABLE I.

P_ν (lab)	$\bar{P}_\nu$(c.m.) ν-p	ν-e	$\bar{E}$ (c.m.) ν-p	ν-e	q^2 max ν-p	ν-e $\times 10^3$	Event Rate ν-p	ν-e
1.0	.57	.016	1.67	.032	1.30	1.0	150	0.1
5.0	1.47	.036	3.21	.071	8.65	5.2	1000?	0.6
10.0	2.14	.050	4.43	.10	18.0	10.	?	1.2
15.0	2.56	.061	5.31	.12	26.2	15.	?	
20.0	3.06	.071	6.20	.14	37.4	20.	?	2.3

All units are BeV or BeV/c. Quantities are given, for each incident neutrino momentum, both for neutrino-nucleon interactions (νP) and neutrino-electron interactions. Maximum momentum transfer squared (q^2_{max}) is given for elastic scattering, as is the event rate, calculated according to $\sigma = G^2\bar{P}_\nu^2$, in a volume of liquid hydrogen 6 m x 6 m x 4 m, the latter in the beam direction.

---

* For a two body interaction

$$\nu + N_1 \rightarrow \ell + N_2$$

of a neutrino with target particle N_1 producing lepton ℓ and recoil particle N_2, the momentum transfer squared is defined as

$$q^2 \equiv (\vec{P}_{n_1} - \vec{P}_{n_2})^2 = (E_{n_2} - M_{n_1})^2 - P^2_{n_2}$$

where $\vec{P}_{n_1}$, $\vec{P}_{n_2}$ are the four-momenta of N_1, N_2; E_{n_2}, P_{n_2} the energy and momenta of N_2; M the target mass.

The event rate is essentially proportional to the volume of detector.

It is seen that the expected energies and intensities are such as to enable a full program of study of neutrino interactions, permitting quantitative results with reasonable statistical accuracy in times short compared to physicist mean productive lives. To achieve this, bubble chamber dimensions of several meters are required. As we discussed below, approximately similar dimensions are required to the necessary measurement precision and to permit identification of the reaction products by decay and/or secondary interaction in the liquid hydrogen.

III. "Conventional" Weak Interaction Theory

Consider first the class of two-body reactions.

$$\bar{\nu}_\ell + P \rightarrow \ell^+ + Y^o$$

$$\bar{\nu}_\ell + N \rightarrow \ell^+ + Y^-$$

$$\nu_\ell + N \rightarrow \ell^- + Y^+$$

where ℓ^+, ℓ^- are leptons corresponding to the "lepton-ness" of the neutrino; Y^+, Y^-, Y^o are particles with baryon number one. Among the latter may be nucleons, hyperons and baryon-meson resonances. In writing these reactions it has been implicitly assumed that the usual conservation laws are valid and that only neutral lepton currents occur. Reactions forbidden by these selection rules are great in number and are not listed here. Indeed, as mentioned above, the determination of the validity of the low-energy conservation laws in this higher energy region is of great importance, but it does not seem worthwhile to consider them in a very general way and so for now, we restrict the discussion to the reactions above. We will state here, at the risk of being repetitious and boring, some known results which are relevant.

In a theory which assumes a point interaction, in a current-current form, with lepton current

$$J_\rho = \bar{U}_{\ell'} \gamma_\rho (1 + \gamma_5) U_\ell$$

and nucleon current

$$J_\rho = \bar{U}_2 \left[\gamma_\rho \left(g_v + G_A\gamma_5 \right) + \ell(P_{1\rho} + P_{2\rho})(f_v + f_A\gamma_5) + \right.$$

$$\left. + i(P_1 - P_{2\rho})(h_v + h_A\gamma_5)\right] U_1$$

describing the process

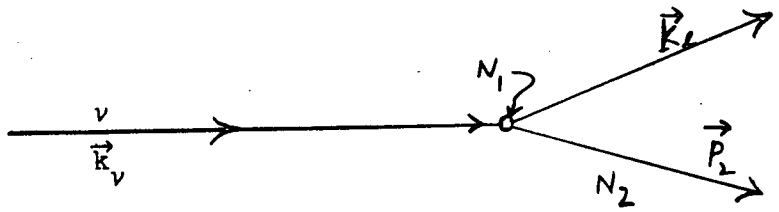

where $\vec{P}_1$ is the four-momentum of the initial baryon, the expressions for the differential cross section have been calculated by Lee and Yang. With the approximation $v_\ell \cong c$, these are, for neutrinos and anti-neutrinos respectively,

$$d\sigma_{\substack{\nu \\ \overline{\nu}}} = \frac{1}{8\pi k_\nu^2} \left[(k_\nu + k_\ell)^2 - P_2^2\right] \times \left[\frac{k_\nu + k_\ell \pm P_2}{k_\nu + k_\ell \pm P_2} a_+ (q^2) + \right.$$

$$\left. + \frac{k_\nu + k_\ell \pm P_2}{k_\nu + k_\ell \pm P_2} a_- (q^2) + b\,(q^2)\right] dq^2$$

In this expression k_ν, k_ℓ, P_2 are the magnitudes of the neutrino, lepton and outgoing baryon momenta, respectively; q^2 is the four-momentum transfer, $\vec{q}^2 = (\vec{P}_2 - \vec{P}_1)^2$. All momenta and energies are laboratory quantities. Here a_+, a_- and b are functions of q^2 only. These functions depend on the form-factors g_v, g_A, etc., in complicated ways restricted to some extent by the conservation laws, e.g., in this case both h_A and h_v do not contribute to the matrix element. It is important to realize that this form of $\frac{d\sigma}{dq^2}$ follows only from the assumption of a "point structure" for the lepton current. In particular, the energy dependence of the differential cross section is independent of the details of the strong current form factors. These details are in the structure functions a_+, a_- and b. We may consider as useful experimental problems the determination of the energy dependence of $\frac{d\sigma}{dq^2}$ for as great a range of momentum

transfer as is available. To see how the experimental uncertainties affect the results, we consider this expression somewhat more. First, rewrite this in a more convenient form. Noticing that

$$q^2 = (\vec{P}_2 - \vec{P}_1)^2 = -(E_2 - M_1)^2 + P_2^2 = 2M_1E_2 - M_1^2 - M_2^2$$

so that

$$E_2 = \frac{q^2}{2M_1} + \frac{M_1^2 + M_2^2}{2M_1} = \sqrt{M_2^2 + P_2^2}$$

it follows that q^2 is determined by P_2, the momentum of the final state baryon. Thus q^2 is directly determined from measurement of the momentum of the scattered nucleon except, of course, for events producing neutrons, $\bar{\nu} + P \rightarrow \mu^+ + N$ or the neutral strange particles which do not decay in the chamber. Clearly it is of great advantage to have a chamber of a size sufficient to permit secondary neutron interactions and strange particle decays to occur within the chamber volume in a large number of cases. The only other kinematic variable occuring in $\frac{d\sigma}{dq}_2$ is the incident neutrino energy, k_ν. With the use of energy-momentum conservation, we get $k_\nu + k_\ell = 2k_\nu - \frac{q^2}{2M_1} - \frac{(M_2 - M_1)}{2}$. Then, with straight-forward arithmetic manipulation, the formula above may be rewritten, in lab,

$$\frac{d\sigma}{dq^2} = \frac{1}{8\pi k_\nu^2} \left[f_o(q^2) + k_\nu f_1(q^2) + k_\nu^2 f_2(q^2)\right]^8$$

so we may equivalently call the f's the necessary structure constants to determine the form factors. Clearly the scattering experiments must be done in such a way that the neutrino energy and the momentum transfer are well known for each event. This expression has also been given by Lee and Yang in terms of the form factors of the nucleon current

$$\frac{d\sigma}{dq^2} = \frac{1}{4\pi}\left(\frac{1}{k_\nu^2}\right) q^2 (g_A^2 - g_v^2) + (g_A - g_v)^2 + \left[1 - \frac{q^2}{2Mk_\nu}\right]^2 (g_A + g_v)^2 + \left[2 - \frac{q^2(M + 2k_\nu)}{2Mk_\nu^2}\right]\left[(4M^2 + q^2) f_v^2 - 4Mf_v g_v\right]$$

Again to give some idea of the kind of angular distribution to be expected, we have calculated $\frac{d\sigma}{dq^2}$ for the process $\bar{\nu}_\mu + P \rightarrow \mu^+ + N$ with the assumption of conserved vector current theory. That is, put

$$g_v(q^2) = G_v [F_Q(q^2) + (\mu_p - \mu_N) F_M(q^2)]$$

$$f_v(q^2) = G_v(\mu_p - \mu_N) F_M(q^2)/2M$$

where $F_Q(q^2)$ and $F_M(q^2)$ are the vector electromagnetic charge and magnetic moment form factors. For these we use[9]

$$F_Q = F_M = -0.2 + \frac{1.20}{1 + 0.1\, q^2}$$

with q^2 in $(\text{Fermi})^{-2}$.
Further it is assumed

$$g_A(q^2) = 1.2[g_v(q^2) - 2M\, f_v(q^2)],$$

which is known to be correct at zero momentum transfer but has only specificity to recommend it here. This then gives

$$g_A(q^2) = 1.2\, G_v\, F_Q(q^2).$$

Figure 1 is a plot of this angular distribution for an incident momentum of 10 BeV/c. The relation between q^2 and the lepton angle is

$$q^2 = 2P_\nu\, P_\ell\, (1 - \cos\theta_\ell) \quad (\text{lab})$$

where P_ℓ is the lepton momentum at the angle θ_ℓ. For small momentum transfer, $P_\ell \approx P_\nu$ and we may put

$$q^2 \approx P_\nu\, P_\ell\, \theta_\ell^2 \approx P_\nu^2\, \theta_\ell^2$$

For 10 BeV/c incident this gives

$$\theta \approx \frac{q^2}{25.7} \times 10^{-1}.$$

From Fig. 1 it is seen that statistical inaccuracy will probably limit the range of momentum transfer to $\lesssim 20\ F^{-2}$. Within this range the form factors can be determined with reasonable precision. Note further that the emission angle should be known to $\sim 0.4^{\circ}$, an accuracy easily obtained with bubble chamber measurements. The direction of the incident beam also should be determined to $\sim 0.1^{\circ}$. As a last point, we mention that precise determination of the q^2 dependence of the form factors (or the "structure functions" introduced by Lee and Yang) will also provide information on the existence of the intermediate boson. Should an intermediate boson exist, the vector form factor should be multiplied by $[1 + \frac{q^2}{MW^2}]$ so that detailed knowledge of the form factors should allow a measure of the consistency of the data with this form and also a measurement of the mass.

We have indicated that for this particular proposed investigation, determinations of the form factors in the nucleon current, it is required to know the energy and angle dependence of the "elastic" process. The required precision is obtainable if the bubble chamber is large enough and provision is made for identification of the reaction products.

IV. Identification of Neutrino Reactions.

A. General Remarks

To permit identification of products of neutrino interactions it is necessary to make use of all possible aids. These include particle decays, secondary strong interactions, conversion of π^{o}-decay photons, electron bremsstrahlung and others less general, as well as the usual application of energy-momentum conservation to constrain measured quantities. All these require, at the energies considered here, rather large path length. As discussed in the Brookhaven proposal[9], this long length can be in many cases obtained for charged particles if the magnetic field is sufficiently large. If pions, muons, etc., can be made to make many turns within the chamber volume, then clearly the interaction and decay probabilities increase. This point has been discussed in some detail and we

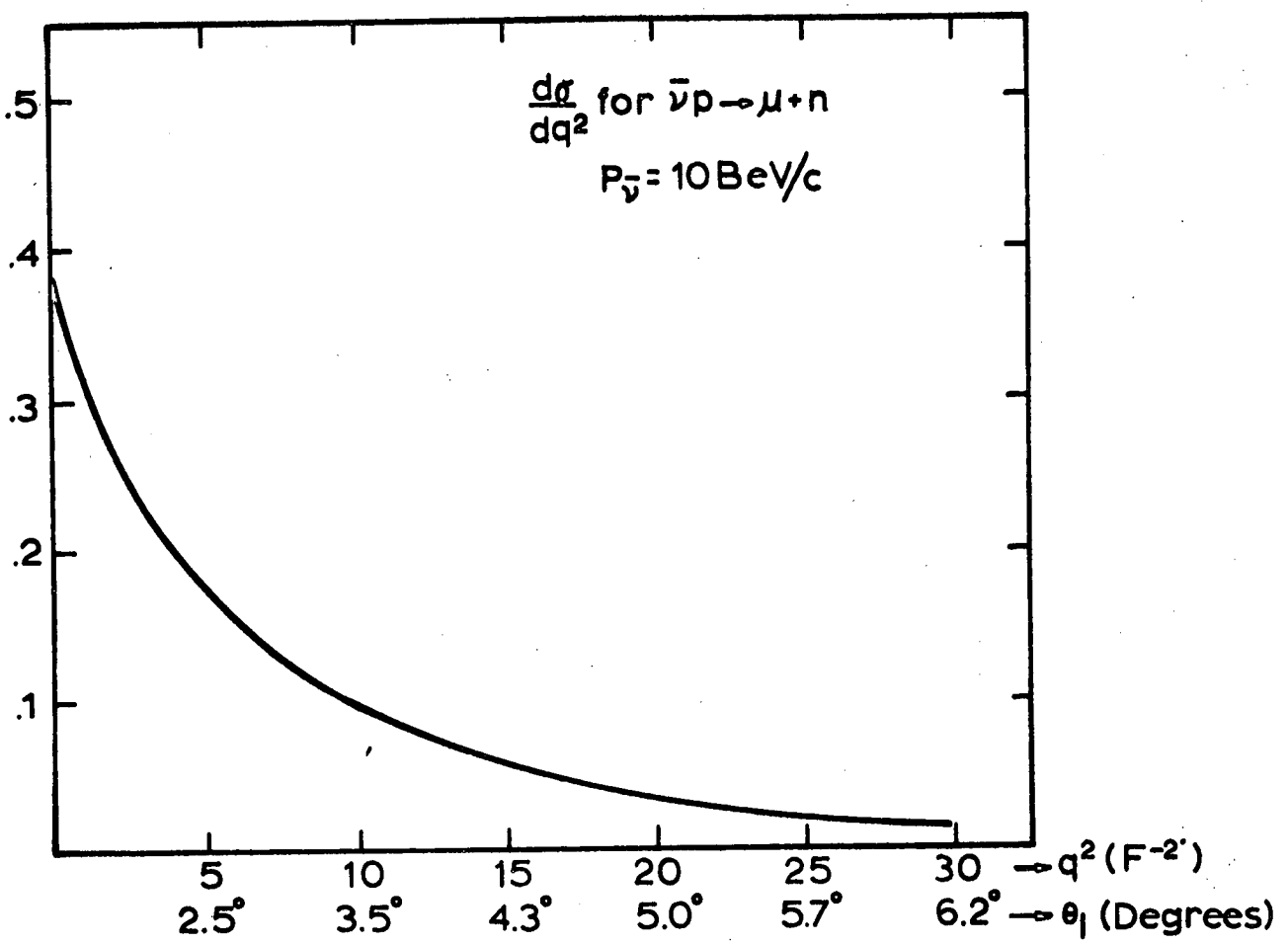
$\frac{d\sigma}{dq^2}$ for $\bar{\nu}p \rightarrow \mu + n$
$P_{\bar{\nu}} = 10$ BeV/c
.5
.4
.3
.2
.1
5
10
15
20
25
30
$\rightarrow q^2$ (F^{-2})
2.5°
3.5°
4.3°
5.0°
5.7°
6.2°
$\rightarrow \theta_l$ (Degrees)

fig. 1

leave it with the remark that this is one of the advantages to be gained with huge magnetic fields. The decay paths of neutral strange particles as a determinant of the size of the bubble chamber has been stressed by Trilling[10] in a SLAC report where it is indicated that mean decay lengths are of order 0.5-2 meters for strange particles of mementa 5-30 BeV/c appropriate to the 200 BeV/c machine. Thus already chamber dimensions as great as 4 meters are indicated. Secondary interactions of neutrals has been considered by Stevenson.[11] Again dimensions of many meters are required to provide electromagnetic interaction length (mean free path ~ 10 meters) and strong interaction length (mean free path ~ 5 meters) so that a reasonable sample of events with identified missing neutrals may be selected from the total. In general these considerations indicate the desirability of a chamber of dimension 5-6 meters and preferably even larger.

B. Measurement Precision

To aid in understanding the problem of fitting to particular hypotheses, we give here the appropriate formulae for errors in momentum and direction. The sources of these uncertainties are the errors in coordinate measurement of points on tracks due to setting errors in the measuring machine, and the multiple scattering in the bubble chamber liquid. These expressions are written down in many places and are more-or-less well-known, but are copied down here for convenience of reference. My favorite discussion is by Gluckstern[12], giving complete and straightforward derivations. The uncertainties, due to rms setting error ϵ, in momentum, projected angle and dip angle are

$$\left(\frac{\Delta P}{P}\right)_M \simeq \frac{\epsilon}{L^2} \times \frac{8 \times 10^2}{3} \times \frac{P}{B}$$

$$\Rightarrow \quad (\Delta\theta)_M \approx 4\,\frac{\epsilon}{L}$$

$$(\Delta\alpha)_M \approx \frac{\epsilon}{L} \times \sqrt{\frac{12}{N}} \times \sqrt{2}\,R \approx 1.5\,\frac{\epsilon R}{L}.$$

In the last expression R is the stereo ratio when the reference "horizontal" plane is perpendicular to the magnetic field direction (assumed to be constant). The units of B are kilogauss, L and ϵ are in meters, P is in

BeV/c. The exact expressions, given by Gluckstern, depend, of course, on the number, N, of points, measured on the track as well as the assumed form of the curve, here parabolic. For present purposes we have given the values appropriate for seven points measured. One sees immediately the virtue of long tracks and large magnetic field and small setting error. Further, ϵ should include also any random effects of distortions. It is assumed that non-random distortions, e.g., those due to imperfect lenses used in photographing, may be removed in the computer reconstruction of the tracks in space. The corresponding errors resulting from multiple scattering are

$$\left(\frac{\Delta P}{P}\right)_s \simeq \frac{.2}{\beta B\sqrt{L}}$$

$$(\Delta\theta)_s \approx .0016\ \sqrt{L}/\beta P$$

$$(\Delta\alpha)_s = .0023\ \sqrt{L}/\beta P$$

These neglect the contribution of nuclear scattering. The multiple scattering errrors are proportional to (rms projected scattering angle per unit length) to which there are in fact three contributions, the coulomb scattering by the proton and the atomic electrons and the nuclear scattering.

The nuclear scattering contribution is

$$\langle \theta_N^2 \rangle \simeq 7 \times 10^{-14} \times \sigma_{ToT}^2 \times P_{BeV/c}^2$$

while the coulomb scattering contribution is

$$\langle \theta_c^2 \rangle \simeq \frac{0.4}{P^2\beta^2} \times 10^{-6}$$

At momenta of order 10 BeV/c, the total cross section $\sigma_T \approx 30$ mb, $\sigma_T^2 \sim 10^3$; so

$$\langle \theta_N^2 \rangle \tilde{=} 7 \times 10^{-14} \times 10^3 \times 10^2 = 7 \times 10^{-9}$$

$$\langle \theta_c^2 \rangle \sim 4 \times 10^{-9}$$

So the nuclear scattering contribution is large and error estimates given above are small by a factor ~ 1.5 at the highest momenta we consider here. If we put the condition that the multiple scatter error dominate the momentum uncertainty, i.e.,

$$\frac{.2}{\beta L} \gg \frac{270\epsilon P}{L^2}$$

with P = 10 BeV/c and $\epsilon = 50\mu$, then the condition is

$$L^{3/2} \gg 2.70 \times .50 \times 10^{-6} \times 1.0 \times .5 = .68$$

or $L \gg \sim 1$ meter.

So for track lengths greater than one meter, only a slow improvement, a $(L)^{1/2}$ dependence, results with increasing length. Such a track is measured with a momentum accuracy $\frac{\Delta P}{P} \approx .015$. A factor two increase is gained by increasing magnetic field to 40 kilogauss, or increasing length to 4 meters. The former is the preferable direction to follow, should it prove technically feasible to make superconducting magnets of the size considered here. This will be discusses at bit further below. We list now all the contributions to the measurement uncertainties for a 5 BeV/c track length L = 1 meter in a field B = 20 kilogauss, with position measurement accuracy 50μ. We assume a stereo ratio R = 5.

$$\left(\frac{\Delta P}{P}\right)_M = .003 \qquad \left(\frac{\Delta P}{P}\right)_S = .01$$

$$(\Delta\theta)_M = 0.011^\circ \qquad (\Delta\theta)_S = .02^\circ$$

$$(\Delta\alpha)_M = 0.022^\circ \qquad (\Delta\alpha)_S = .03^\circ$$

The multiple scattering errors dominate. Longer tracks would mean larger errors in angle measurements. Larger magnetic field would then bring the greatest increase in precision. These considerations indicate a chamber size of about three meters is desirable, with magentic field as can be achieved.

C. An Example of Fitting The reaction $\bar{\nu} + P \rightarrow \mu^+ + \Lambda^o$

The question which we attempt to answer is--are the measurements sufficiently precise to enable one to do physics, and particularly to study neutrino interactions? If it proves possible to uniquely identify all reaction products, on the basis of consistency with the kinematic conservation laws, bubble density of tracks and possible secondary interactions, then the answer is yes. If not, then qualifications must be made. To illustrate with a specific example, consider the reaction

$$\bar{\nu}_\mu + P \rightarrow \mu^+ + \Lambda^o$$

from which we may learn the form factor for strangeness changing weak interaction as a function of momentum transfer. Only events with visible Λ^o decay are considered. The topology is as shown

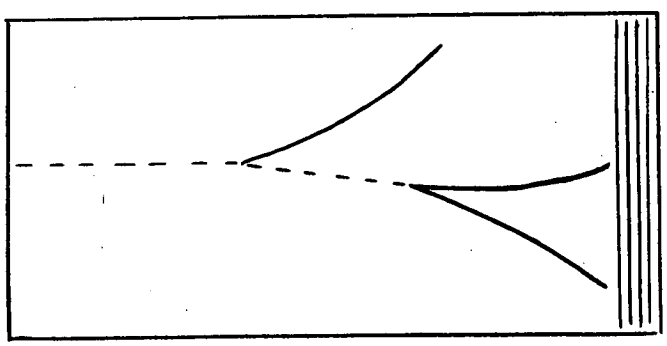

The possible reactions with the topology are

$$\bar{\nu}_\mu + P \rightarrow \mu^+ + \Lambda^o$$
$$\mu^+ + \Lambda^o + \pi^o$$
$$\mu^+ + \Lambda^o + K^o$$
$$\mu^+ + K^o + N$$
$$\mu^+ + K^o + \Lambda^o$$
$$\mu^+ + K^o + \Xi^o$$

In addition, any number of neutral pions may be produced, limited by the kinematics and the Λ^o may result from the decay $\Sigma^o \rightarrow \Lambda^o + \gamma$. We have generated, using the program FAKE,[13] events of this type and made fits to the other five hypotheses listed above. Those reactions not satisfying the small momentum transfer conservation laws, e.g.,

$$\bar{\nu} + P \rightarrow \pi^+ + \Lambda^o$$
$$e^+ + \Lambda^o$$
$$\pi^+ + \Lambda^o + \bar{\nu}$$
$$P + K^o$$

and many others, were not fitted. Events were generated with incident momentum 10.0 ± 2.5, 10.0 ± 5.0 and 5.0 ± 1.25 BeV/c within a fiducial volume 5 meters in the beam direction, 4 meters x 4 meters transverse to the beam. It is important to keep in mind that no production dynamics are included in the generating program, all distributions are produced according to phase space. A setting error of 50μ was assumed.

Of the five "spurious" hypotheses the first two involve only an additional neutral particle, with no change in the identity of the two observed particles. With an incident momentum uncertainty of 25% it was not possible to exclude this hypothesis in more than a few cases, as seen from the χ^2 distribution of Fig. 2. Even with the incident momentum defined to 5%, only one-third of the fits with a spurious π^o could be excluded, as indicated in the χ^2 distribution of Fig. 3. The characteristic feature

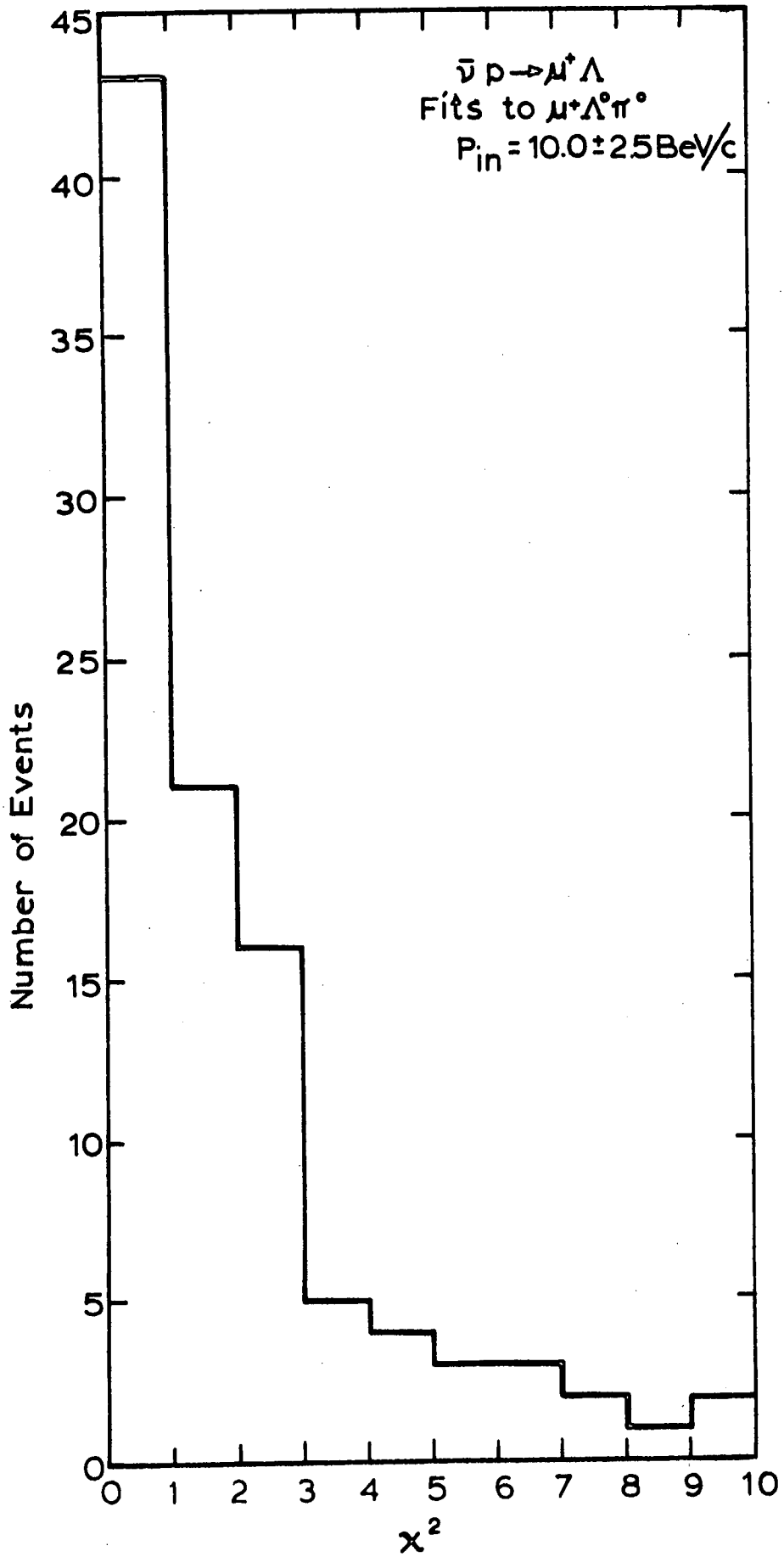
$\bar{\nu}\, p \rightarrow \mu^+ \Lambda$
Fits to $\mu^+ \Lambda^0 \pi^0$
$P_{in} = 10.0 \pm 2.5$ BeV/c
Number of Events
χ^2
0
5
10
15
20
25
30
35
40
45
0 1 2 3 4 5 6 7 8 9 10

fig. 2

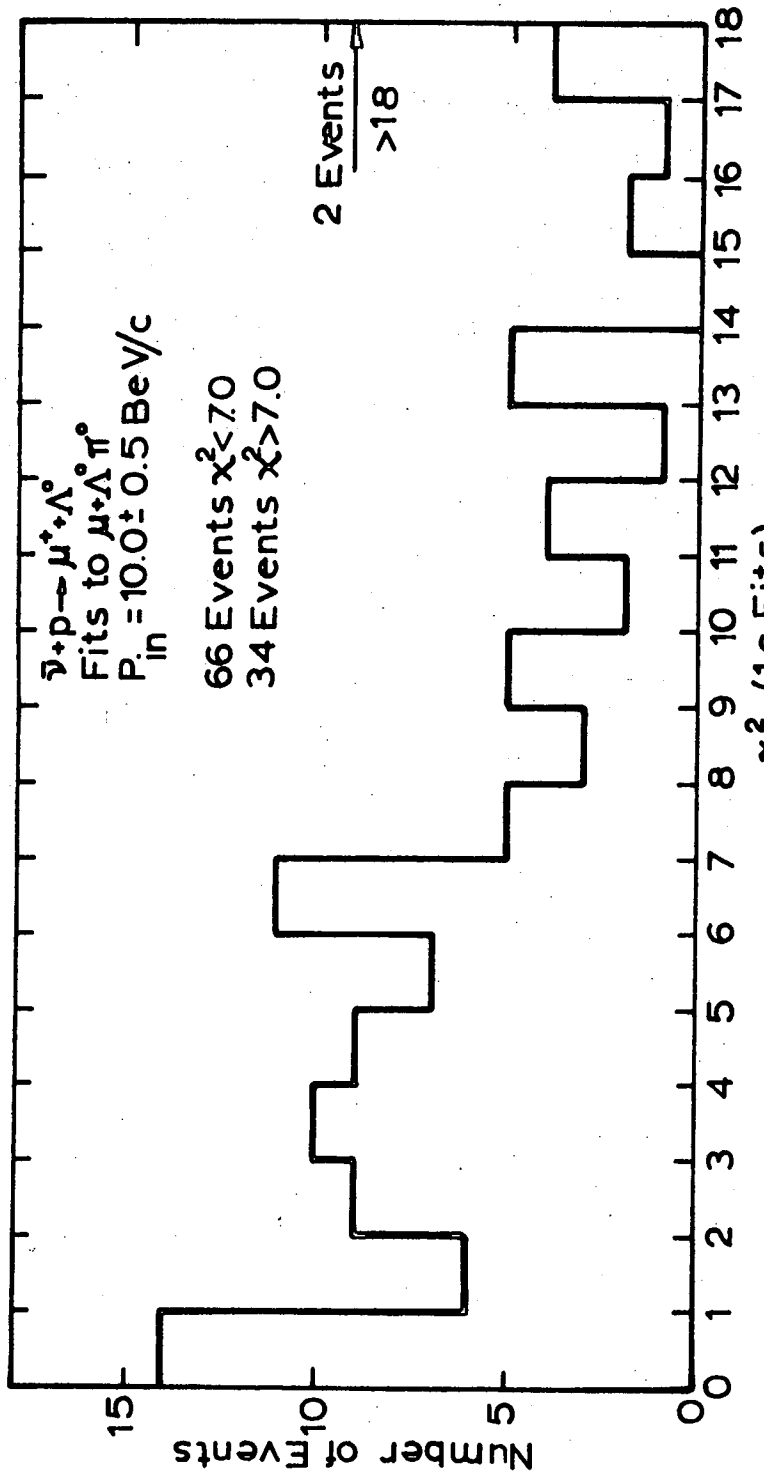
$\bar{\nu}+p \rightarrow \mu^+ + \Lambda^\circ$
Fits to $\mu^+ \Lambda^\circ \pi^\circ$
$P_{in} = 10.0 \pm 0.5$ BeV/c
66 Events $\chi^2 < 7.0$
34 Events $\chi^2 > 7.0$
2 Events >18
Number of Events
χ^2 (1c Fits)

fig 3

of these spurious fits are first, a greater beam momentum definition is needed to fit and second the π^o is emitted essentially along the beam direction. The first feature is illustrated in Figs. 4, 5, and 6 in which are plotted the "true" and "spurious" fitted neutrino momenta and the fractional difference between the spurious fitted momentum and that obtained from the fit to the true, elastic hypothesis. It is seen that momentum definition of a few percent is necessary to eliminate the fits with an additional pion. This is confirmed by the results obtained with the 5% momentum definition. Thus it appears unlikely that a beam can be made with neutrino momentum sufficiently well defined to eliminate the spurious fits. Similar conclusions result from examinations of the data with 5 BeV/c incident momentum. Figures 7 and 8 show the angle of emission of the neutral pion with respect to the incident direction. The π^o's are limited to very small angles. It is clear that these characteristics result from the associated good precision of measurement. The error in transverse momentum is quite small. We have, for each outgoing particle, transverse momentum

$$P_x = P \sin(\theta - \theta_\nu) \approx P(\theta - \theta_\nu)$$

so the error is given by

$$(\Delta P_x)^2 = [(\theta - \theta_\nu)\,\Delta P]^2 + [P\,\Delta\theta]^2 + [P\,\Delta\theta_\nu]^2$$

$$= P^2\left[(\theta_\nu \frac{\Delta P}{P})^2 + (\Delta\theta)^2 + (\Delta\theta_\nu)^2\right]$$

We have shown that $\frac{\Delta P}{P} \approx .01$, $\Delta\theta \approx .05^o$ and we assume also $\Delta\theta_\nu \approx .05^o$. Typical outgoing momenta are $\lesssim$ 5 BeV/c and angles are $\lesssim 20^o$ ($\sim\frac{1}{3}$ radian). So

$$(\Delta P_x)^2 \approx (5)^2\left[(.003)^2 + (.001)^2 + (.001)^2\right]$$

So

$$\Delta P_x \lesssim 20 \text{ MeV/c}.$$

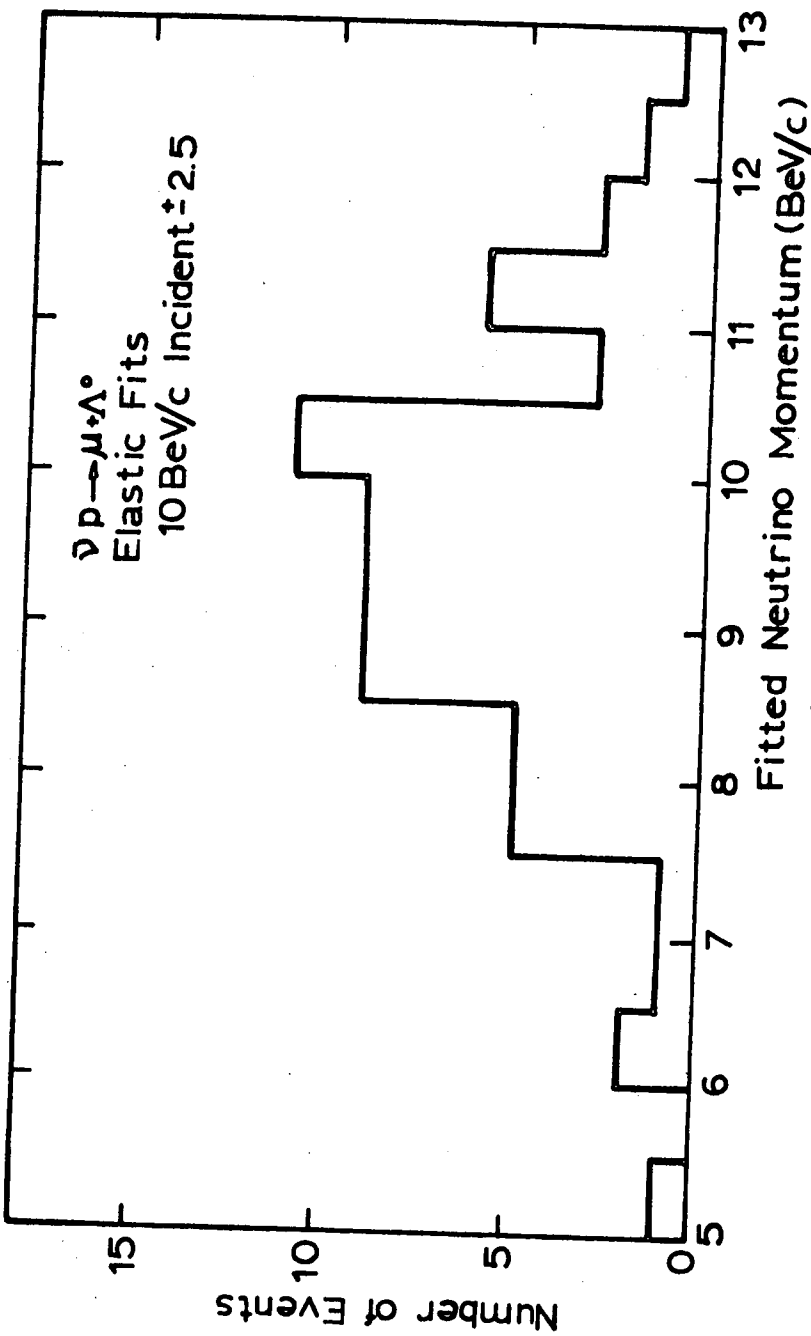
$\bar{\nu}p \rightarrow \mu^+\Lambda^\circ$
Elastic Fits
10 BeV/c Incident ± 2.5
Number of Events
0
5
10
15
5
6
7
8
9
10
11
12
13
Fitted Neutrino Momentum (BeV/c)

fig. 4

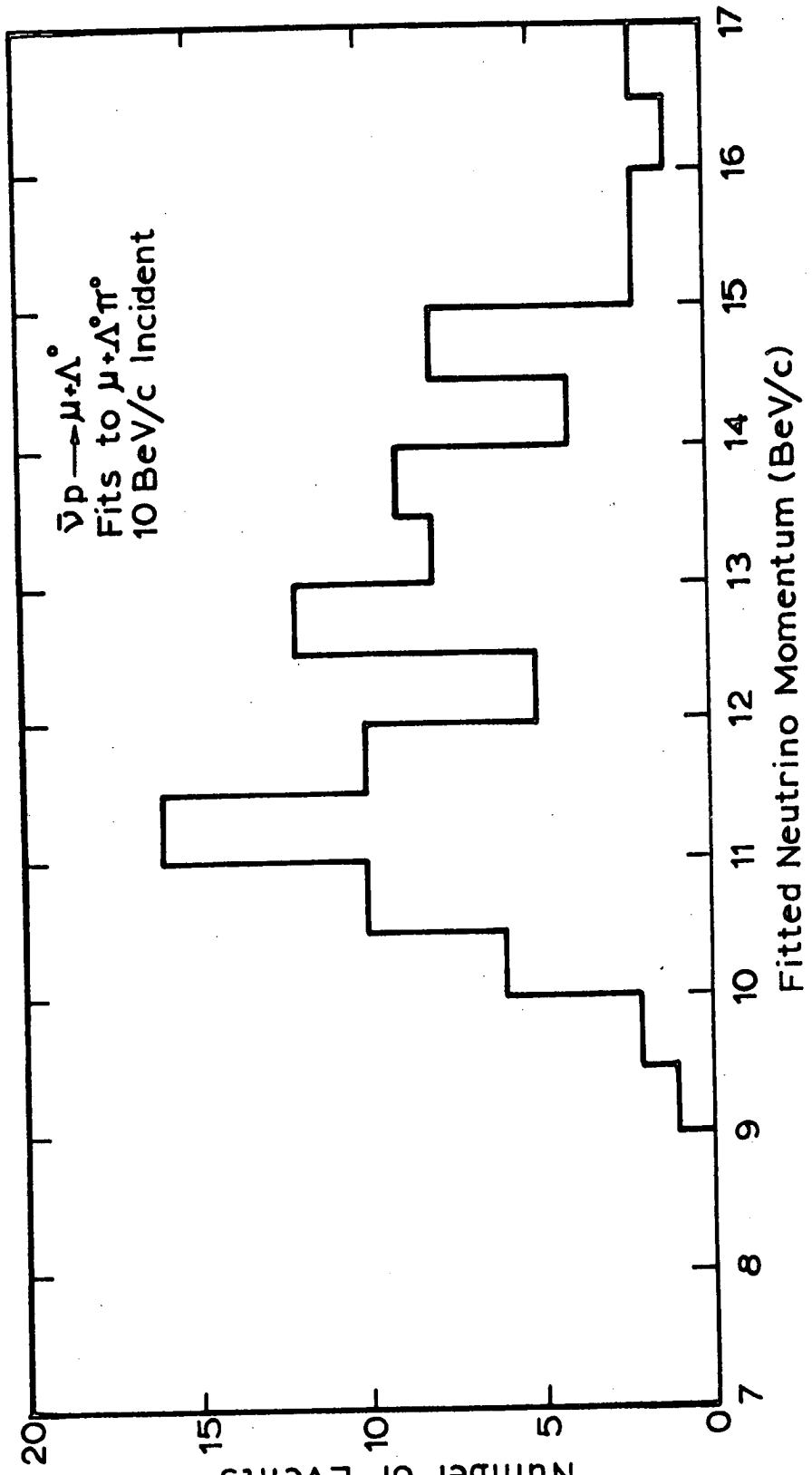
$\bar{\nu}p \longrightarrow \mu^+\Lambda^\circ$
Fits to $\mu^+\Lambda^\circ\pi^\circ$
10 BeV/c Incident
Number of Events
Fitted Neutrino Momentum (BeV/c)
0
5
10
15
20
7
8
9
10
11
12
13
14
15
16
17

fig. 5

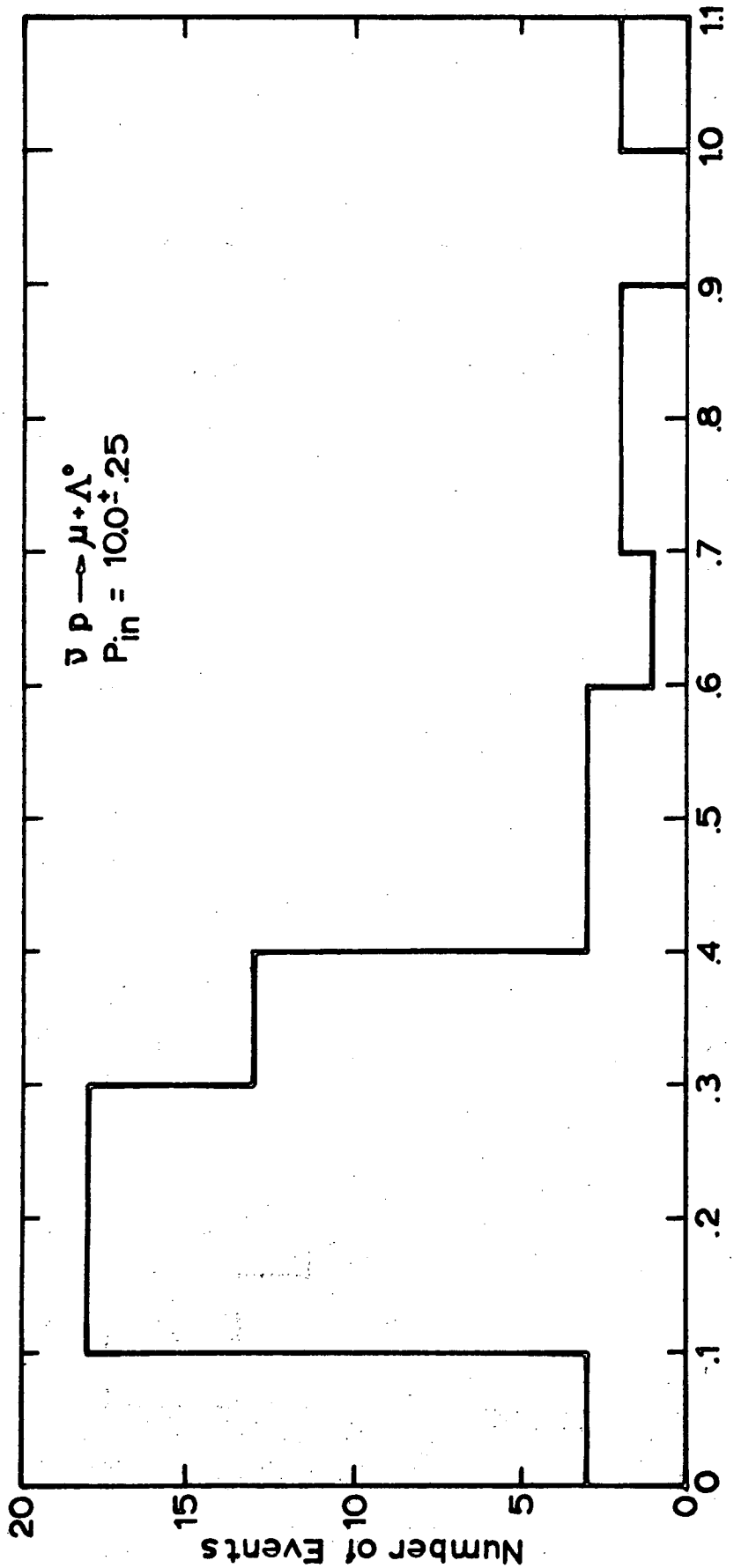
$\nu p \rightarrow \mu^- \Lambda^\circ$
$P_{in} = 10.0 \pm .25$
Number of Events
0
5
10
15
20
0
.1
.2
.3
.4
.5
.6
.7
.8
.9
1.0
1.1
$\frac{P(\pi^\circ fit) - P(Elastic\ fit)}{P(Elastic\ fit)}$

fig. 6

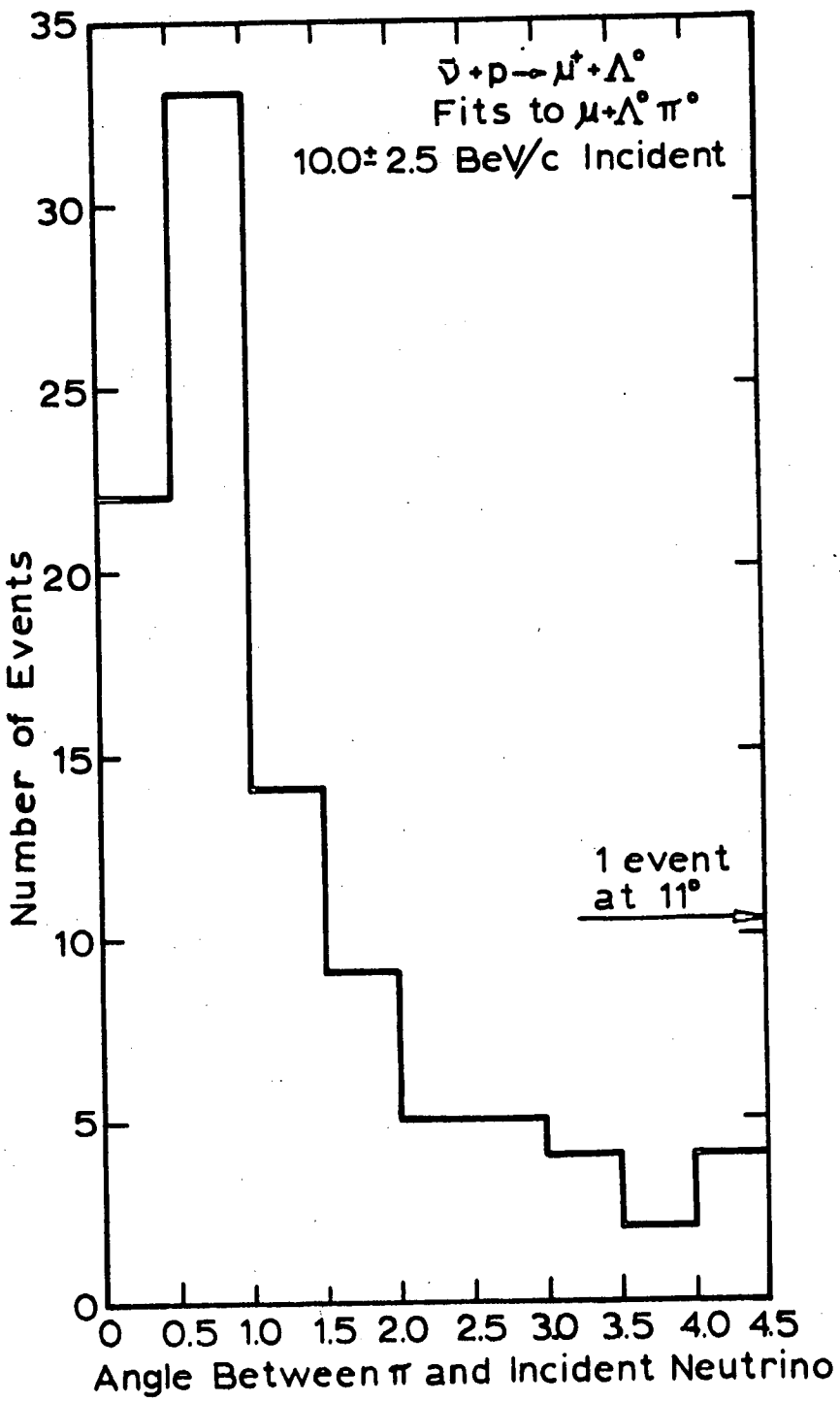
$\bar{\nu} + p \rightarrow \mu^+ + \Lambda^\circ$
Fits to $\mu + \Lambda^\circ \pi^\circ$
10.0 ± 2.5 BeV/c Incident
1 event at 11°
Number of Events
Angle Between π and Incident Neutrino
0
5
10
15
20
25
30
35
0 0.5 1.0 1.5 2.0 2.5 3.0 3.5 4.0 4.5

fig. 7

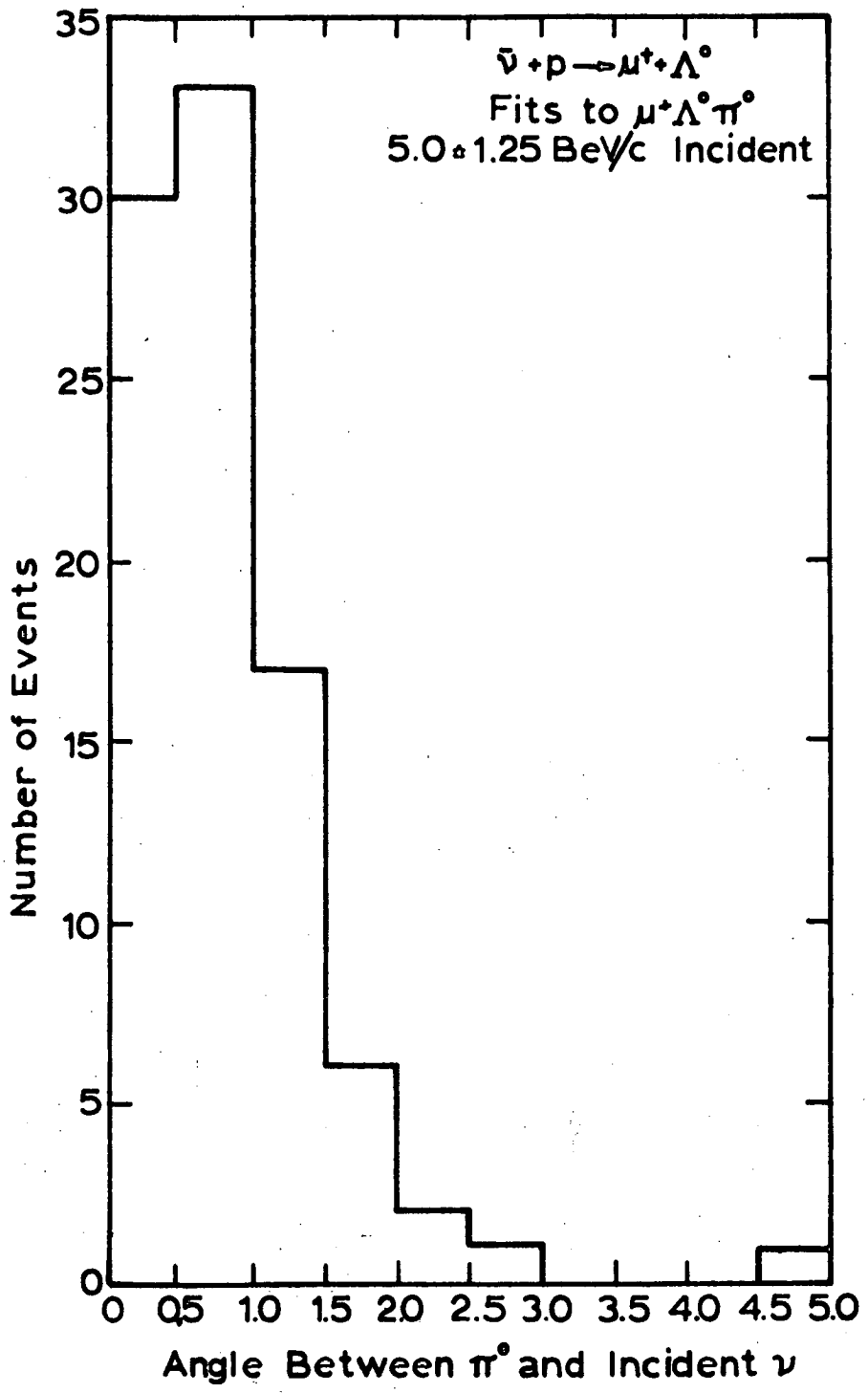
$\bar{\nu} + p \rightarrow \mu^+ + \Lambda^\circ$
Fits to $\mu^+ \Lambda^\circ \pi^\circ$
5.0 ± 1.25 BeV/c Incident
Number of Events
0
5
10
15
20
25
30
35
0 0.5 1.0 1.5 2.0 2.5 3.0 3.5 4.0 4.5 5.0
Angle Between π° and Incident ν

fig. 8

To conserve energy, the momentum of the missing π^o is made large compared to its mass and this momentum added to the incident neutrino, so that energy and momentum are conserved. Thus it is expected that the π^o will be generated at angles $\theta_{\pi^o} \approx \frac{20 \text{ Mev/c}}{1000}$, so, of the order of one degree. This is indeed the case. This being so, such fits could be easily eliminated with a series of lead plates at the far end of the chamber, as sketched.

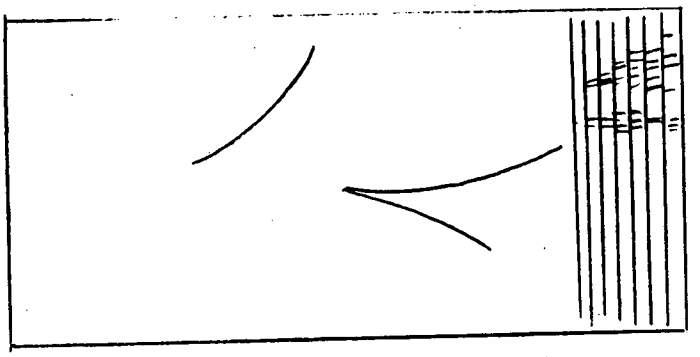

Perhaps ten plates, each of 1/2 cm thickness, providing then 10 radiation lengths for conversion would be sufficient to ensure essentially 100% efficient γ-ray conversion. Spacing the plates 5 cm apart would allow measurement also of the direction of the γ-rays and aid in analysis of events with real π^o's produced. This increases the necessary length of the chamber by about 50 cm. In this way, events with zero missing neutral pions could be identified with good efficiency and Σ^o production events eliminated.

Spurious fits to the reaction $\bar{\nu} + P \rightarrow K^o + \mu^+ + N$ are not as serious a difficulty. Again the good measurement accuracy insures that in a large number of cases the V^o decay does not fit the kinematics of $K^o \rightarrow 2\pi$ decay. Of the 100 generated events, only 33 successfully fitted K^o decay, with the χ^2 distribution shown in Fig. 9. These then fit the production vertex with the χ^2 distribution of Fig. 10 and the fitted neutrino momentum distribution of Fig. 11. The angular distribution is more sharply peaked than that of the π^o given above. Thus the conclusions about identifying the spurious fits are valid here also. Beam momentum definition of sufficient precision is probably not possible. High-efficiency downstream neutron conversion is necessary here to eliminate the false fits. We have not attacked the very complex inverse question, the likelihood that

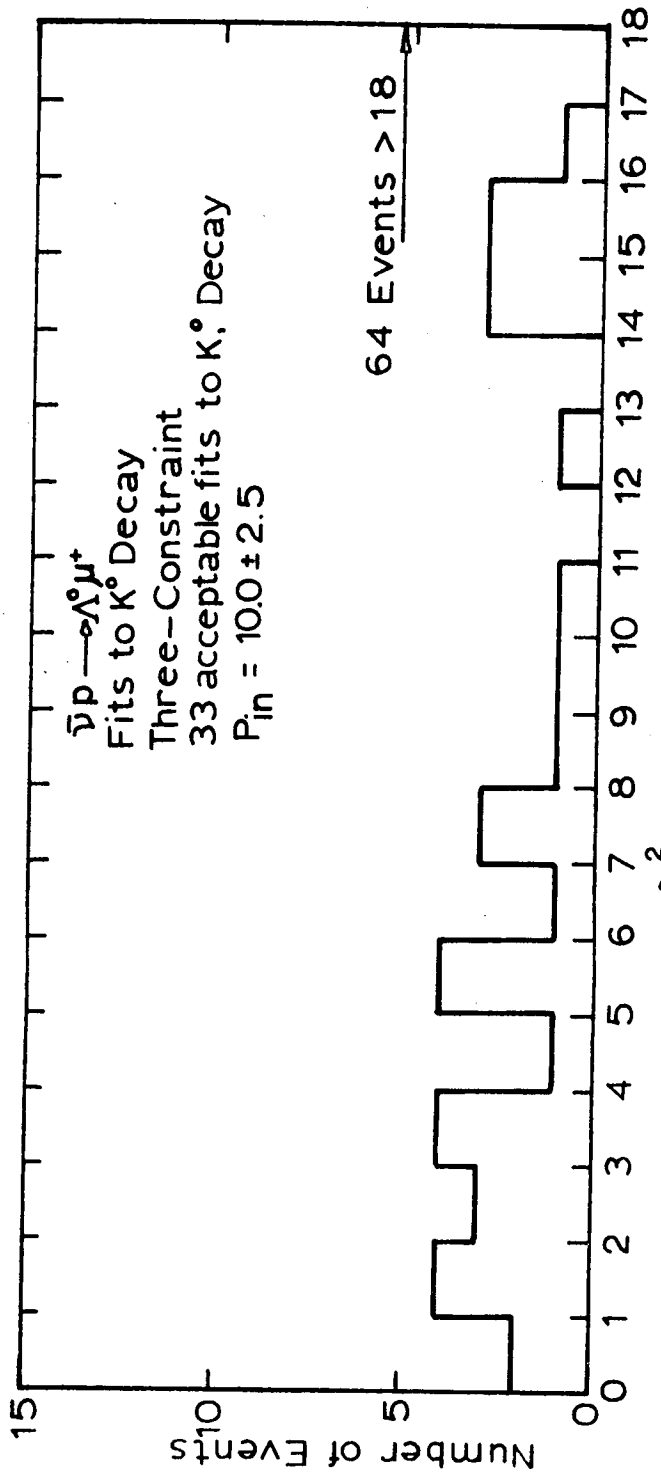
$\bar{\nu}p \rightarrow \Lambda^0\mu^+$
Fits to K^0 Decay
Three-Constraint
33 acceptable fits to K^0 Decay
$P_{in} = 10.0 \pm 2.5$
64 Events > 18
Number of Events
15
10
5
0
0 1 2 3 4 5 6 7 8 9 10 11 12 13 14 15 16 17 18
χ^2

fig. 9

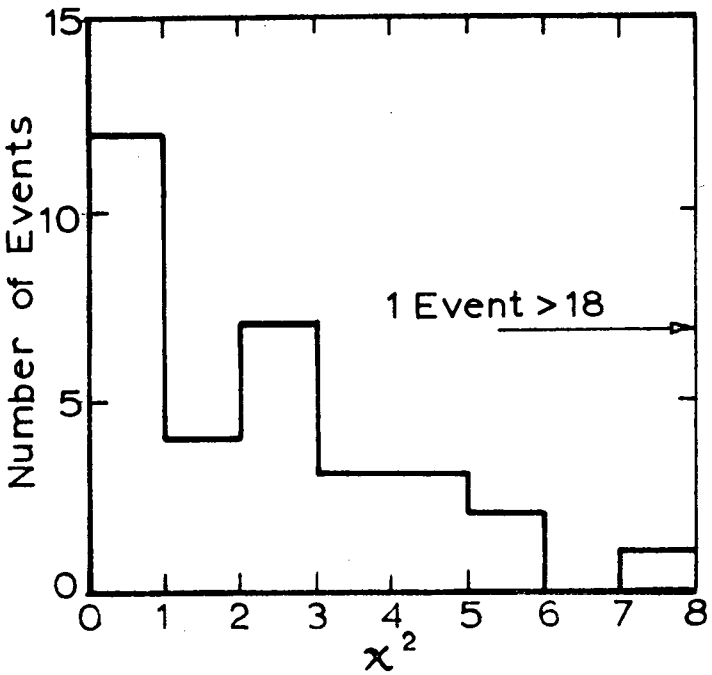
Number of Events
15
10
5
0
1 Event > 18
0 1 2 3 4 5 6 7 8
χ^2

fig. 10

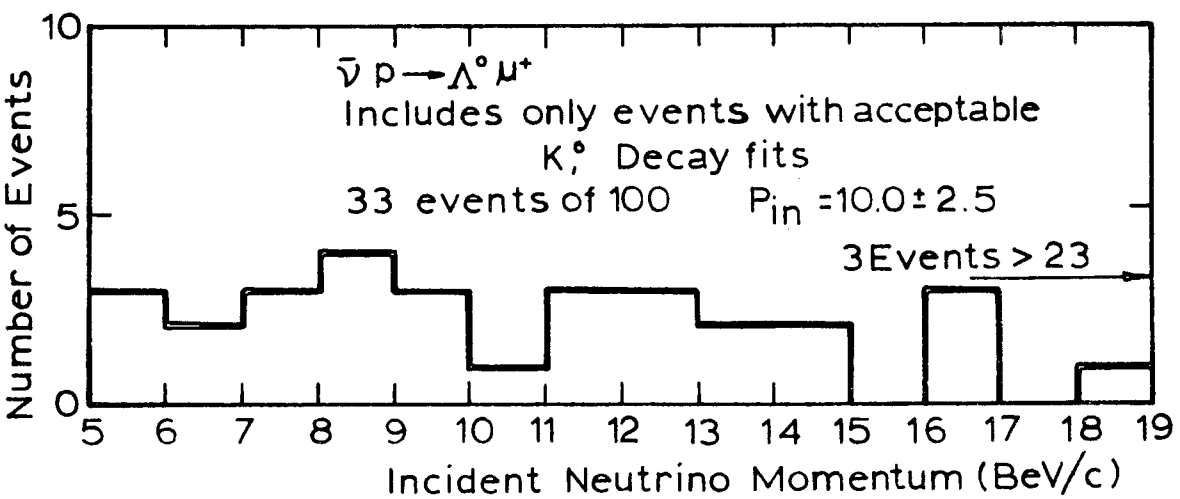
Number of Events
10
5
0
$\bar{\nu}\, p \rightarrow \Lambda^\circ \mu^+$
Includes only events with acceptable
K° Decay fits
33 events of 100
P_{in} =10.0 ± 2.5
3 Events > 23
5 6 7 8 9 10 11 12 13 14 15 16 17 18 19
Incident Neutrino Momentum (BeV/c)

fig 11

an inelastic event, e.g., an example of $\bar{\nu} + P \rightarrow \mu^+ + \Lambda^o + \pi^o$, would be so measured that a good fit would be obtained for the elastic reaction $\bar{\nu} + P \rightarrow \mu^+ + \Lambda^o$. Again we might expect the forward going missing neutrals to be the biggest source of spurious elastic fits, so that high γ-ray conversion efficiency would permit these to be identified. Missing neutrals at large angles would also be detected, albeit with less efficiency and so would permit a means of correcting the elastic-fit events. It would seem that only an overwhelmingly larger "background" of inelastic events would seriously affect the elastic sample, but the point needs more study.

The general conclusion is then that it is reasonable to expect to identify reactions provided the assumed conditions can be met. For good setting accuracy, distortions must be small, certainly not larger than those in present chambers; path lengths of several meters length are necessary to give sagittas large compared to setting errors; detection of secondary neutrals is essential.

We know of only one technique at present which can be applied to in fact improve the situation -- higher magnetic field using superconducting coils. To demonstrate the feasibility we append here some conclusions from cost analysis studies made by R. Yourd.[14] Figure 12 shows calculated costs for construction and operation of a magnet with copper coils compared to one with superconducting coils. Sketches of the shapes of the coils are shown in Fig. 13. For details of the calculation, refer to the report of Yourd. One incidental interesting feature is that addition of an iron yoke does not yield a lower cost magnet. Based on these results and consideration of the likelihood that techniques for producing long pieces of stabilized superconducting alloys will continue to improve as it has in the past, it is clear that the design of a superconducting coil to provide a magnetic field of some 50 kilogauss should proceed.

Other technical points of the design will not be discussed here. Speaking in general, such features as expansion system, refrigeration and other mechanical features are being actively pursued at other laboratories. Optical problems associated with probable impossibility of using a large glass area will probably lead to use of wide angle lenses. Again other groups are pursuing solutions to problems of illuminations and viewing.

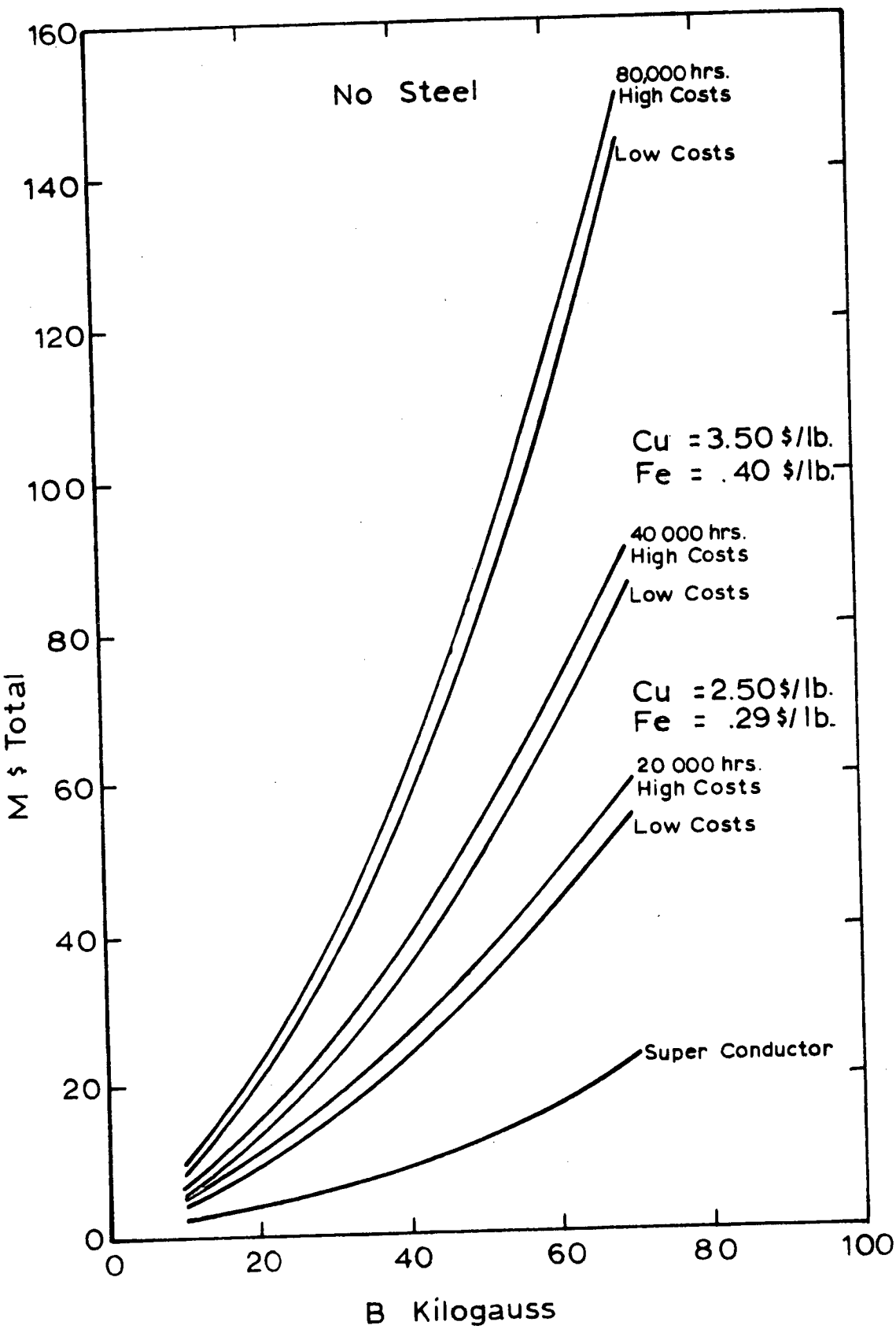
No Steel
80,000 hrs.
High Costs
Low Costs
Cu = 3.50 $/lb.
Fe = .40 $/lb.
40 000 hrs.
High Costs
Low Costs
Cu = 2.50 $/lb.
Fe = .29 $/lb.
20 000 hrs.
High Costs
Low Costs
Super Conductor
M $ Total
B Kilogauss
0
20
40
60
80
100
120
140
160

fig. 12

Coil shapes for minimum cost to provide 20 kG with copper or 40 KG superconducting.

Supercoil width W_S =13"

Copper Coil width W_C =48"

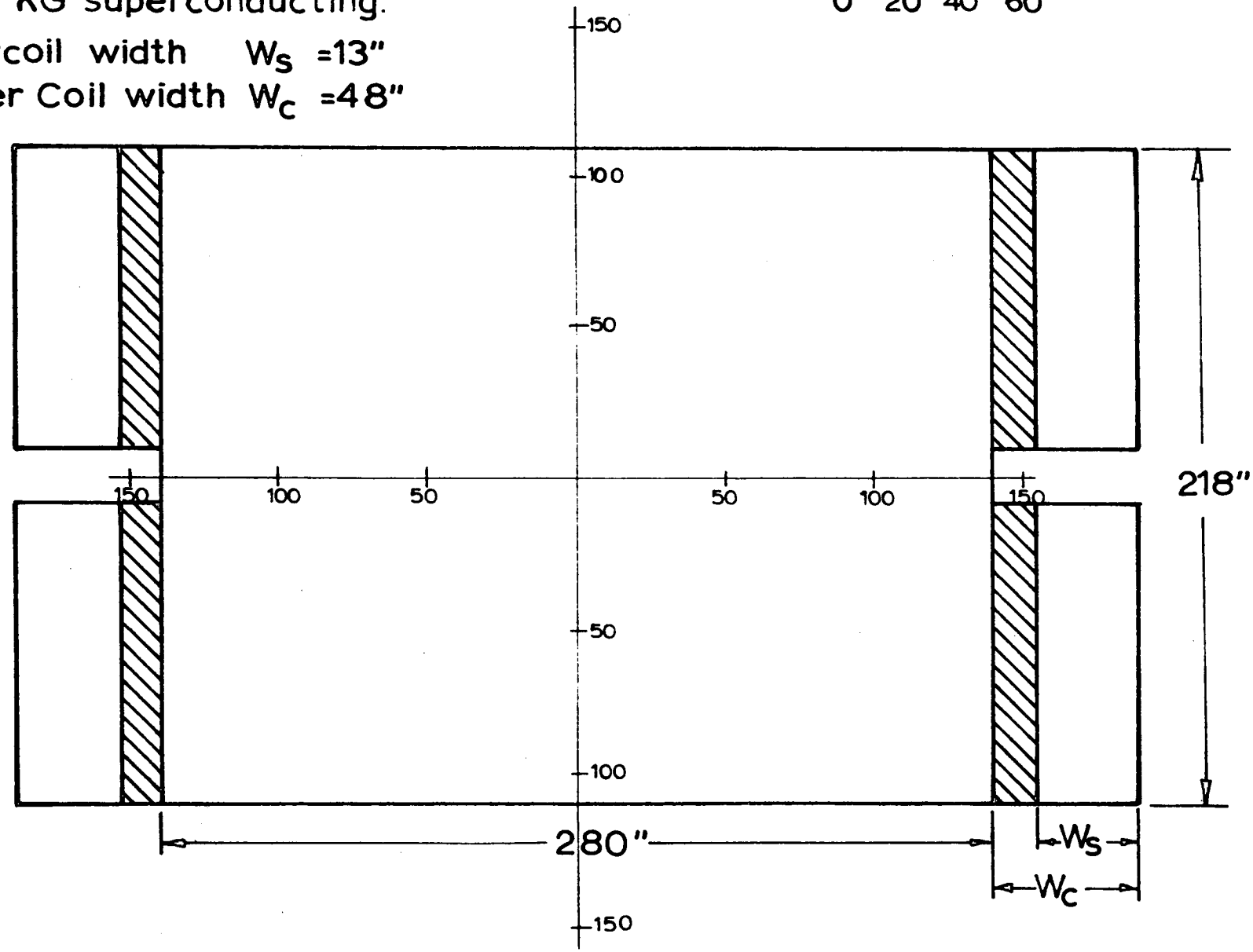

fig.13

These technical problems do not appear formidable. In many cases, present design can be scaled. The cost is large,[15] but perhaps not staggering considering that such a device would be a principal experimental tool of a large number of physicists, for a large number of years.

REFERENCES

1. D. Keefe, "Neutrino Beams at High Energy", UCID-10131, Sep. 1964.

2. V. Z. Peterson, "A Monochromatic Neutrino Beam", UCID-10028, Nov. 1964.

3. T. D. Lee and C. N. Yang, Phys. Rev. 126 , 2239, 1962.

4. G. Feinberg, "Brandeis Summer Institute in Theoretical Physics", p. 277, 1963.

5. G. Danby, et. al., Phys. Rev. Letters 9, 36, 1962.

6. H. A. Bingham, et. al., Proc. Int. Conf. on Elementary Particles, Vol. I, p. 555, Siena, 1963.
   M. Block, et. al., Physics Letters 12, 281, 1964.

7. A. Prodell, Bull. Am. Phys. Soc. 10, 445, 1965.

8. R. Hofstadter and R. Herman, Phys. Rev. Letters 6, 293, 1961.

9. "Proposal for 14 Foot Bubble Chamber", BNL 8266 and BNL 8266 (R).

10. G. Trilling, SLAC 5-D, SLAC Report No. 5, p. 40, Summer 1962.

11. M. L. Stevenson, "Bubble Chamber Physics at the 200 BeV Accelerator", UCID-10152, May 1965.

12. R. L. Gluckstern, Nuclear Inst. and Methods, 24, 381, 1963.

13. G. Lynch, "Program FAKE", UCRL-10335.

14. R. Yourd, "Cost Comparison for Copper and Superconducting Coils - Six Meter Bubble Chamber Magnet", Lawrence Radiation Laboratory Eng. Note., Aug. 10, 1965.

15. D. Keefe, ed., "Major Items of Scientific Equipment Expected to be in Use at the 200 BeV Accelerator Laboratory", UCID-10168, Jan. 1965.

UCID-10152
AS/Experimental/01
May 24, 1965
M. L. Stevenson

BUBBLE CHAMBER PHYSICS AT THE 200 BEV ACCELERATOR

M. L. Stevenson

University of California
Lawrence Radiation Laboratory
Berkeley, California

LAWRENCE RADIATION LABORATORY - UNIVERSITY OF CALIFORNIA
PHYSICS NOTES
- 87 -
MEMO NO. 553
PAGE 1

SUBJECT
Bubble Chamber Physics at the 200 GeV Accelerator

NAME M. L. Stevenson

DATE 5/24/65

TABLE OF CONTENTS

SUBJECT

NAME M. L. Stevenson

DATE 5/24/65

A. Introduction

The purpose of this note is to speculate on what kinds of physics will be done in large liquid hydrogen (deuterium) chambers at a 200 GeV accelerator. As a result of these speculations we hope to find some general physical characteristics of the chamber that will give the maximum possible utility and flexibility.

B. Possible Bubble Chamber physics of the 1970's

1. Strong Interactions

Currently the discovery of resonant states of mesons and baryons and the study of the production characteristics of the "two-body" final states are the major activities of strong interaction bubble chamber physics.

Already we see attempts to deal with reactions in which more than one neutral particle emerges in the final state (e.g. lead plates, and lead glass inserted into the 72" hydrogen bubble chamber). In most instances the missing particles are gamma rays and in some instances they are neutrons.

a) Classification of resonant states

By the 1970's much of the classification as to spin, parity, and other quantum numbers of the known resonances will have been completed but not all of it. This is likely to continue as one of the most exciting aspects of the strong interactions;

b) Branching ratios of resonant states

The major decay modes of many resonances will be known but many of the rarer modes of decay will still be unknown. In particular, those rare modes that involve a production process in which more than one neutral emerge either as a production particle or as a decay fragment will likely still be unmeasured.

c) Production characteristics of "two body" final states

Even though most of the excitement today is in finding and classifying new resonant states there is a hope that out of the production process of the two body final states will come reliable determinations of coupling constants and form factors. Since many of the reactions involve particles of high spin it is desirable to determine the spin correlation matrix (density matrix). Many physicists feel that the density matrix will be an effective way of understanding the production mechanisms.

Presently not enough data exist to accurately determine the elements of the density matrix for most of the interesting reactions. Furthermore, the cross sections for "two-body" processes are decreasing as the energy increases because of increased competition as more final state channels open up. The total number of observed interactions must be substantially increased if the production mechanisms are to be understood.

A large sized bubble chamber can help in this regard.

d) Production characterisitcs of the "many body" final states.

These reactions form a background for the more interesting resonant states. At present this subject is dispensed with by comparing the observations with the predictions of Lorentz invariant phase space. Perhaps in the future we can expect these "many body" final states to be studied for their own value.

In many of the reactions there may be more than one neutral particle in the final state. The ratio of the phase space for the "many body" reactions to that for the "two body" reactions will increase with bombarding energy and consequently the many body processes will become more important not for their simplicity but because their cross section is larger.

A bubble chamber that can better resolve ambiguities between reactions that have no missing π^0's and those that do will be helpful at higher bombarding

energies.

2. Weak Interactions

a) Decay processes of strongly produced particles

Already a great deal is known about the weak, non-leptonic decay processes for many of the strange particles. Perhaps by the 1970's we can expect that the properties of Ω^- decay will be known.

The leptonic decay of the strange particles being $\sim 10^{-3}$ of that for non leptonic decay will not be so well known. Events of this type will be a by-product of the strong interaction experiments.

b) Neutrino-Nucleon Interactions

Here we have a new and important field of study that will certainly not be completely understood. For the purposes of this disucssion we shall assume lepton conservation.

1. $\Delta S = 0$ interactions

Thus far most of the reported work from BNL and CERN have dealt with reactions of the "elastic"type,

$$\bar{\nu}_e + p \rightarrow e^+ + n. \qquad (1)$$

$$\bar{\nu}_\mu + p \not\rightarrow e^+ + n \qquad (2)$$

$$\nu_e + n \rightarrow e^- + p \qquad (3)$$

$$\nu_\mu + n \not\rightarrow e^- + p \qquad (4)$$

and of the "inelastic" type*,

---

*The superscript "o"on(pions)^o merely denotes that the net charge of the pions is zero.

$$\bar{\nu}_\ell + p \longrightarrow \ell^+ + n + (\text{pions})^\circ \qquad (5)$$

$$\longrightarrow \ell^+ + p + \pi^- + (\text{pions})^\circ \qquad (6)$$

$$\nu_\ell + p \longrightarrow \ell^- + p + \pi^+ + (\text{pions})^\circ \qquad (7)$$

$$\longrightarrow \ell^- + n + \pi^+ + \pi^+ + (\text{pions})^\circ \qquad (8)$$

$$\nu_\ell + n \longrightarrow \ell^- + p + (\text{pions})^\circ \qquad (9)$$

$$\longrightarrow \ell^- + n + \pi^+ + (\text{pions})^\circ \qquad (10)$$

$$\bar{\nu}_\ell + n \longrightarrow \ell^+ + n + \pi^- + (\text{pions})^\circ \qquad (11)$$

$$\longrightarrow \ell^+ + p + \pi^- + \pi^- + (\text{pions})^\circ \qquad (12)$$

Many events of the "inelastic" type are probably of a "two-body" variety where the primary production is of the form

$$\bar{\nu}_\ell + p \longrightarrow \ell^+ + (\Delta^\circ \longrightarrow p + \pi^- \text{ or } n + \pi^\circ) \qquad (13)$$

$$\nu_\ell + n \longrightarrow \ell^- + (\Delta^+ \longrightarrow p + \pi^\circ \text{ or } n + \pi^+) \qquad (14)$$

2. $\Delta S = 1$ interactions

a) $\Delta S = \Delta Q$

$$\bar{\nu}_\ell + p \longrightarrow \ell^+ + \Lambda \qquad (15)$$

$$\longrightarrow \ell^+ + \Sigma^\circ \qquad (16)$$

$$\bar{\nu}_\ell + n \longrightarrow \ell^+ + \Sigma^- \qquad (17)$$

$$\bar{\nu}_\ell + p \longrightarrow \ell^+ + \Lambda + (\text{pions})^\circ \qquad (18)$$

$$\longrightarrow \ell^+ + \Sigma^\circ + (\text{pions})^\circ \qquad (19)$$

$$\bar{\nu}_\ell + n \longrightarrow \ell^+ + \Sigma^- + (\text{pions})^\circ \qquad (20)$$

b) $\Delta S \neq \Delta Q$

Reactions of the following type will test, as a function of momentum transfer, the $\Delta S = \Delta Q$ rule

$$\nu_e + n \longrightarrow e^- + \Sigma^+ \quad (21)$$

$$\longrightarrow e^- + \Sigma^0 + \pi^+ \quad (22)$$

$$\longrightarrow e^- + \Lambda + \pi^+ \quad (23)$$

$$\nu_e + p \longrightarrow e^- + \Sigma^+ + \pi^+ + (\text{pions})^0 \quad (24)$$

$$\longrightarrow e^- + \Sigma^0 + \pi^+ + \pi^+ \quad (25)$$

$$\longrightarrow e^- + \Lambda + \pi^+ + \pi^+ \quad (26)$$

and so on.

3. $\Delta S = 2$ interactions

$$\nu_e + p \longrightarrow e^+ + \Xi^0 \quad (27)$$

$$\nu_e + n \longrightarrow e^+ + \Xi^- \quad (28)$$

$$\bar{\nu}_e + n \longrightarrow e^- + \Xi^0 + \pi^+ \quad (29)$$

$$\bar{\nu}_e + p \longrightarrow e^- + \Xi^0 + \pi^+ + \pi^+ \quad (30)$$

$$\bar{\nu}_e + n \longrightarrow e^- + \Xi^- + \pi^+ + \pi^+ \quad (31)$$

4. $\Delta S = 3$ interactions

$$\nu_e + n \longrightarrow e^+ + \Omega^- \quad (32)$$

$$\nu_e + p \longrightarrow e^+ + \Omega^- + \pi^+ \quad (33)$$

$$\bar{\nu}_e + n \longrightarrow e^- + \Omega^- + \pi^+ + \pi^+ \quad (34)$$

5. Production of Intermediate vector mesons

$$\begin{matrix}\bar{\nu} \\ \nu\end{matrix} + p \longrightarrow e^{\pm} + p + W^{\mp} \quad (35)$$

The final topology depends upon how the W decays. If it decays into pions

it will be found in topologies (6) and (7). If it decays leptonically it will be found as follows

$$\nu_e + p \rightarrow \ell^- + p + (W^+ \rightarrow \ell'^+ + \nu_\ell) \quad (36)$$

$$\bar{\nu}_e + p \rightarrow \ell^+ + p + (W^- \rightarrow \ell'^- + \bar{\nu}_\ell) \quad (37)$$

c) Neutrino-electron interactions

Here we consider the interactions that will occur between the incident neutrino and the atomic electron of hydrogen. We assume that only the $\bar{\nu}_e$ interacts with the electron. These neutrinos come from a minor decay mode of the K mesons and hence the flux will be quite low.

If 30 GeV/c is the maximum practical momentum for $\bar{\nu}_e$, the maximum practical energy in the $\bar{\nu}_e - e$ c.m.s. is 173 MeV. The following reactions are energetically possible,

$$\bar{\nu}_e + e \rightarrow e + \bar{\nu}_e \quad (38)$$

$$\rightarrow \mu^- + \bar{\nu}_\mu \quad (39)$$

The outgoing $\bar{\nu}_\ell$ cannot be detected and, therefore, the events will be under constrained.

$$\bar{\nu}_e + e \rightarrow \pi^- + \gamma \quad (40)$$

The following very interesting reactions require $\bar{\nu}_e$ momenta beyond the capabilities of the 200 GeV accelerator.

	Lab. Threshold (GeV/c	
$\bar{\nu}_e + e \rightarrow \pi^- + \pi^0$	78.5 GeV/c	(41)
$\rightarrow K^- + \pi^0$	404 GeV/c	(42)
$\rightarrow K^- + K^0$	983 GeV/c	(43)
$\rightarrow \bar{p} + n$	3,520 GeV/c	(44)

3. Electromagnetic Interactions

a) The electromagnetic decay of strongly produced particles is already an interesting field of bubble chamber physics. Most frequently the electromagnetic

decay involves the emmission of a photon. If a π^0 is produced along with the resonant particle, the reaction becomes under constrained.

b) It is conceivable that a beam of high energy photons might be passed through the bubble chamber. The identification of photon interactions and neutrino interaction will have common problems. For this reason we will not consider photo-production in detail.

C. Experimental Problems

1. Loss of vital information about neutral particles in the reactions.

a) All neutrino interestions lack information about the incident momentum. We shall assume that the chamber is located sufficiently far from the small neutrino source that the direction of the neutrino will be well know. One of the 4 constraint equations can be used to solve for this unknown momentum leaving 3 contraints in the problem. For those ν interactions that have no neutral particles in the final state the kinematic constraint class in 3C. In more than half of the listed reactions a neutral particle can emerge in the final state. The reaction then becomes a "zero-constraint class" (0C) reaction or an unfittable reaction. Present experience at low energies shows us how difficult it is to do reliable physics with (0C) reactions.

It is absolutely essential that we obtain some information about the outgoing neutral particle (or particles). The conversion of photons in the hydrogen could give <u>both</u> momentum and direction information and could restore the constraint class to 3C.

Photon conversion in a lead plate will lack sufficiently accurate information about the momentum. (Roughly speaking, the error in the momentum of the photon will be the same as the conversion efficiency of the plate.) The over-all constraint class will be <u>less</u> than 3C. Conversion in hydrogen is ideal. The radiation length, however, is 10 meters.

When the missing neutral is a neutron we must observe a subsequent np interaction. Generally at high momentum the most we can expect to determine is the direction of the neutron. The constraint class will be 2C. The neutron mean free path is roughly 10 meters in hydrogen.

High energy neutral strange particles can be detected provided sufficient path length exists for decay. If, in addition, sufficient track length exists for the decay fragments the momentum and direction can be determined. For example, a 15 GeV/c K_1^o meson has a mean decay length of 1 meter.

Clearly a chamber that would provide 3 meters from the interaction point to the nearest wall would go far in solving the problem of missing neutrals.

2. Identification of charged particles in the reactions.

The identification of reactions requires more than detection of outgoing neutrals. Even though the reactions are over constrained the problem of ambiguity must be solved. Several hypothetical reactions may have equally good chi-squared values.

Here we note a useful feature of the neutrino interactions. Generally, whenever a ν_ℓ ($\bar{\nu}_\ell$) is incident the outgoing negative (positive) particle is a ℓ^- (ℓ^+). Therefore, the neutrino beam must be produced from a momentum analyzed positive (negative) meson beam as described by Keefe,[a] and Peterson [b,c]

Lead (or Tantalum) plates would serve to identify electrons and muons (provided they were thick enough).

Delta rays produced by the large momentum transfer collisions between the particle and the atomic electron can yield information on the mass of the particle.

---

[a] D. Keefe "Neutrino Beams at High Energy" UCID 10131

[b] V. Peterson "A" Monochromatic Neutrino Beam from a High Intensity 200 GeV Proton Synchrotron." AS/Experimental/01 November 30, 1964

[c] D. Keefe and V. Peterson "Neutrino Beams from a High Intensity 200 GeV Proton

tgoing strange particles can interact and yield secondary strange particles that y serve to identify the original particle. Again the mean free path for such teractions will be roughly 10 meters of hydrogen.

3. Momentum measurement accuracy of charged particles of high momentum.

The value of having long unobstructed tracks in liquid hydrogen for e purpose of determining both direction and magnitude of momentum hardly needs ntioning.

4. The small production cross section of neutrino interactions.

If the chamber is made sufficiently large the problem of the small utrino cross section is solved. For example, a 100 m^3 chamber containing 6 tons hydrogen exposed to one of the beams (neutrino energies between 10 and 25 GeV) scribed by Peterson [b] would produce approximately 300 events per 12 hour period 10^{-38} cm^2. (Included in this estimate is a long term running efficiency factor $\frac{1}{2}$). The production cross section for W mesons could be from 10^{-39} to 10^{-37} . (The c.m.s. energy for a 10 GeV neutrino is 4.5 GeV would be the threshold rgy for a W meson of mass 3.5 GeV.) Even if only 10°/o of these events were ful this is a reasonable yield.

We place the "small cross section difficulty" last in importance for deciding the configuration and size of the chamber. The requirements set by sections 1, nd 3 are more important.

Chamber Size and Configuration

From what we have discussed in the previous sections a chamber that would vide 3 meters from the center of the chamber to the nearest wall would convert o 30 percent of the photons, and neutrons. A sphere of 3 meters radius with top and bottom meters sliced off to allow the pole tips of the magnet to come er together has a volume of 96 m^3. (6 tons of hydrogen) Should the chamber be made longer -- in

the form of a 6 meter diameter cylinder? We think not. Firstly the volume and cost becomes excessive. Secondly, we feel that for some reactions, e.g. $\nu_\mu + p \rightarrow \mu^- + \Sigma^o$ a spherical shape is adequate. In this example the reaction is produced predominatly with low momentum transfer, the Σ^o moves slowly in the laboratory and the γ from its decay can go equally likely in all directions. Further details on the production dynamics of some of the reactions are contained in the appendices. They are the work of two summer research students Mr. Robert Goren and Mr. John Moriarty both of the University of California. Lastly, the fabrication cost can be minimized for a spherically shaped chamber.

We shall leave a detailed discussion of chamber configuration to a later date after a more thorough engineering study has been made.

E. Technical Difficulties

1. Can tracks be photographed accurately through 6 meters of liquid hydrogen?

This, we consider, is the most important unanswered technical question concerning chambers of this size. The distortions that arise because of the thermal variation of the index of refraction (heat waves) must be studied on large samples of hydrogen. We shall follow with great interest the test results of the Argonne and Saclay groups on these systems.

2. Conventional, Cryogenic, or Super conducting magnet?

There are indications that the technology of cryogenic and super conducting magnets will develop fast enough to allow us to use one or the other of them. In the summary, cost estimates are based upon a conventional magnet.

F. Summary

The following is a reproduction of an Alvarez Group Physics Note by the author. It is essentially a summary of the present paper. It includes rough cost estimates by Paul Hernandez and also reflects discussions held with William Chinowsky.

SUBJECT: PRELIMINARY PROPOSAL FOR A 100 CUBIC METER LIQUID HYDROGEN AND DEUTERIUM BUBBLE CHAMBER (6 TONS OF HYDROGEN)

NAME: M. L. Stevenson

DATE: 12-20-64

F. Summary (cont'd.)

A. The Interesting Physics

The need for a large liquid hydrogen (deuterium) chamber for use with the 200-Gev proton sychrotron is based on the necessity to further our understanding of weak, strong, and electromagnetic interactions. Notable among the experiments for which the bubble chamber is ideally suited are the following:

1. Neutrino interactions
2. Decay of strange particles
3. Electromagnetic decay of strongly produced resonant states
4. Strong-interaction reactions with outgoing neutral and charged particles

B. The Experimental Difficulties of Bubble Chamber Physics at High Energy

The experimental difficulties can be summarized as follows:

1. The loss of vital information about a reaction because outgoing neutral particles escape detection in the chamber.
2. The difficulty of identifying outgoing charged particles as pions, kaons, protons, muons or electrons.
3. Momentum measurement accuracy of charged particles of high momentum.
4. The small production cross section of neutrino interactions.

C. How the 100 cubic meter chamber can solve these difficulties.

Considered in the above order, the solutions are:

1. Neutrons, neutral pions $\rightarrow$ γ rays, and neutral strange particles can be detected provided sufficient path length exists between the primary interaction and the walls of the chamber. Keeping in mind that, a) the neutron -proton mean free path is 10 meters, b) the γ -ray radiation length is 10 meters, c) the mean decay length of a 15 Gev/c K_1^0 meson is one meter, and d) roughly one meter of high momentum track length is

necessary for accurate momentum measurement of the secondary tracks, one realizes that 3 meters from the primary interaction to the nearest wall would be very helpful. Twenty to thirty per cent of all neutrons and γ rays will convert in this distance. For those experiments that would require a larger γ conversion efficiency there would be sufficient space to put lead plates.

2. The existence of lead plates surrounding the primary interaction volume would also aid in the identification of electrons. Additional plates, provided they were thick enough, would aid in the identification of muons. In practice the best way of identifying the leptons emerging from neutrino interactions is to use a beam known to consist of either neutrinos or antineutrinos. If lepton conservation is strictly obeyed, then in most reactions the negative (positive) particle emerging from a neutrino (antineutrino) interaction is a lepton. For this reason it is essential to produce the neutrino beams from momentum analyzed meson beams as described in section X of the main report.

3. The value of having long, unobstructed, tracks in liquid hydrogen for the purpose of determining both direction and magnitude of momentum hardly needs mentioning.

4. The need for large volume is usually considered to be required primarily by the low neutrino cross section. We place it last in importance because the reason we propose a 100 m^3 chamber rather than 50 m^3 is because of topics 1, 2, and 3 above. The 200 Gev accelerator will produce adquate neutrino fluxes to give reasonable counting rates for both 50 m^3 and 100 m^3 chambers.

D. Estimated Construction Cost

Detailed proposals for 40 m^3 and 26.5 m^3 chambers have been made by the BNL and Argonne laboratories, with estimated costs of $15 and $14 million respectively. The chamber configuration that we propose differs little from these proposals. The size is greater. A possible shape is that of a 6 meter diameter sphere with 1 meter sliced off both top and bottom to allow the pole tips of the magnet to be placed closer together.

Preliminary estimates, aided by the more detailed cost estimates of BNL, suggest a total cost of $38.5 million distributed as follows:

		1st estimate	2nd estimate
1.	Chamber and Expansion	$ 6.0 m.	9.0
2.	Magnet* (20 kilogauss) and Power Supply	11.2	10.0
3.	Cryogenics	4.7	6.7
4.	Optics	2.4	2.4
5.	Electronic controls	2.6	2.6
6.	Building	11.6	6.0
	Total	$38.5	34.7

* Conventional magnet. Development of cryogenic magnets for this purpose may alter this cost estimate.

E. Operational costs

These costs are estimates assuming a full time crew of operators working three shifts. It is further assumed that the chamber will be taking pictures approximately fifty percent of the operating time of the accelerator ($\approx$ 4 million pictures/year).

1.	Magnet power + crew	$3.0 million
2.	Film (20 cm, 3 views/pulse)	3.0
	Total	$6.0

F. Appendices

1. Chamber configuration

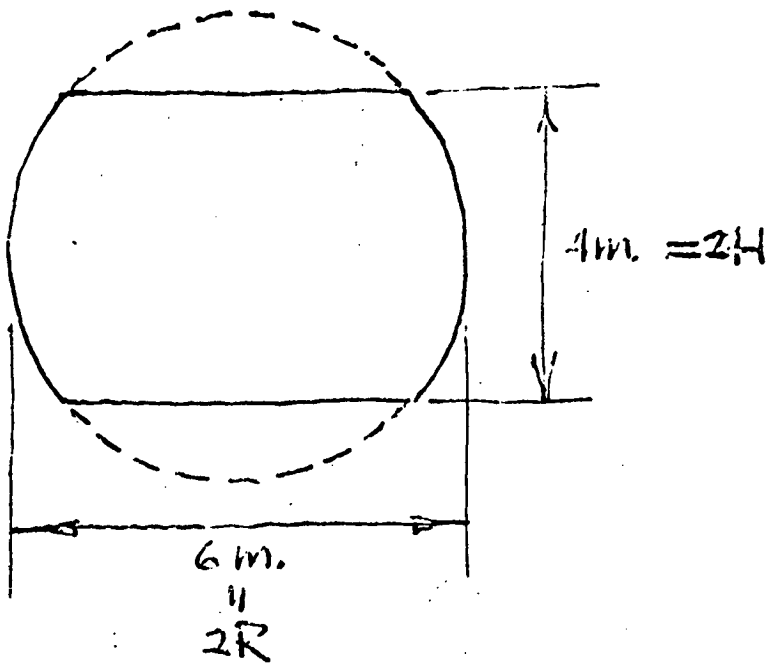

$V = 2\pi (R^2 H - 1/3\ H^3)$

$R = 3m$

$H = 2m$

$V = 96\ m^3$

SUBJECT

NAME M.L. Stevenson

DATE 12-20-64

January 5, 1965

MEMORANDUM

To: M.L. Stevenson

From: H. Paul Hernandez

Subject: 100 Cubic Meter Liquid Hydrogen Bubble Chamber

The BNL report gives a chamber volume of 40 cubic meters and a cost of 15 million dollars. The ZGS report gives the chamber volume of 26.5 cubic meters and a cost of 14 million dollars.

The cost of the 100 cubic meter chamber might be as follows:

		Million Dollars
1.	Chamber and Expansion	6.00
2.	Magnet and Power Supply (20 kG)	11.2
3.	Cryogenics	4.7
4.	Optics	2.4
5.	Electronic Controls	11.6
6.	Building	2.6
7.	Beam Transport Equipment and Neutrino Shielding	1.5
	Total	40.0

Beam transport equipment and neutrino shielding might be low if this is a very complicated beam line and the shielding is massive. On the AGS studies, the shielding estimates have been running low.

The operating cost paragraph might read as follows:

> The chamber is assumed to have a full-time crew of operators working three shifts and will be taking pictures fifty per cent of the operating time of the accelerator. The operating cost will be about 3.3 million dollars per year, including film. The film* cost is estimated at around $300,000.

Paul Hernandez

* I gave Paul the wrong film size. It was a factor 3 too small.

MLS

ALVAREZ GROUP
PHYSICS NOTE 55

Appendix 1. of UCID 10152

A Brief Summary of a Paper to be Published in the Physical Review

HYPERON PRODUCTION BY NEUTRINOS IN AN SU_3 MODEL

N. Cabibbo

CERN

and

Frank Chilton

Stanford University

by Robert Goren
November 19, 1964

B

The SU_3 model of weak interactions and the Conserved Vector Current theory are used to discuss cross sections for hyperon production by neutrinos. In particular the reactions

$$\bar{\nu} + p \rightarrow \Lambda + \mu^+$$
$$\bar{\nu} + n \rightarrow \Sigma^- + \mu^+$$
$$\bar{\nu} + p \rightarrow \Sigma^0 + \mu^+$$

are considered.

In $\Delta S = 0$ reactions the vector form factors are related through the CVC hypothesis to the electromagnetic form factors of the nucleon. Cabibbo assumes a certain universality in the weak interactions so as to write the weak current of strongly interacting particles as

$$J_\lambda = \cos\theta\, J_\lambda^{(0)} + \sin\theta\, J_\lambda^{(1)}, \quad \theta = 0.26$$

where $J_\lambda^{(0)}$ and $J_\lambda^{(1)}$ are the $\Delta S = 0, 1$ members of an octet of currents and are each part vector and part axial vector. From CVC the vector part is in the same octet as the electromagnetic current.

The six form factors usually used to describe the matrix elements of mixed vector and axial vector currents are treated as follows:

1.) G_V and F_V are expressed in terms of the proton and neutron electromagnetic form factors as justified above from the CVC and SU_3 hypotheses.

2.) G_A is also expressed in terms of the analagous form

factor for $\Delta S = 0$ processes + one other parameter which can be experimentally measured in the zero momentum transfer leptonic decay of hyperons.

3.) F_A and H_V which result from S.Weinberg's so called "second class" currents are set =0.

4.) H_A is ignored since it is multiplied by the square of the mass of the lepton and contributes on the order of 1% at most.

Expressions are given in laboratory variables for

$$\frac{d\sigma}{dt}\ ,\quad \frac{d\sigma}{d\cos\theta_2}\ ,\quad \frac{d\sigma}{d\cos\theta_2}\ ,\quad \sigma$$

where t= (momentum transfer)^2 and θ_2, θ_ℓ are the laboratory scattering angles of the hyperon and lepton respectively. Numerical examples are computed for the Λ and Σ^- reactions with those for Σ^0 given by $d\sigma(\Sigma^0) = \frac{1}{2} d\sigma(\Sigma^-)$

The plot of the differential cross section in the lab lepton angle (E_ν = 2 BEV) reveals substantial forward peaking due primarily to the monotonic decrease of the form factors as a function of t. For increasing E_ν the forward peaking becomes sharper.

The graph of $\frac{d\sigma}{d\cos\theta_2}$ has been plotted in a double valued fashion to distinguish the two different baryon lab momenta occuring for each lab angle. With increasing E_ν the maximum angle slowly becomes larger.

" The distributions in the heavy particle angle have one feature that may be of some technical value. At any particular energy the maximum baryon angle is fairly sensitive to the mass

of the baryon. Further the cross sections increase rapidly in the vicinity of the maximum angle. This may permit one to discriminate between the masses of the recoil baryons and to construct an uncontaminated sample of neutrino events. For example, if $E_\nu = 2$ BEV then roughly 30% of the Λ events fall at larger angles than would be possible for Σ^0. The same idea could be applied to nucleon - N^0 discrimination to obtain an uncontaminated sample of elastic events. In this case the mass difference is larger so that the difference of maximum angles would also be larger."

The asymptotic forms of the total cross sections are evaluated to estimate the hyperon to nucleon ratios:

$$\frac{\sigma_\Lambda}{\sigma_N} \sim \frac{1}{19}$$

$$\frac{\sigma_\Sigma}{\sigma_N} \sim \frac{1}{18}$$

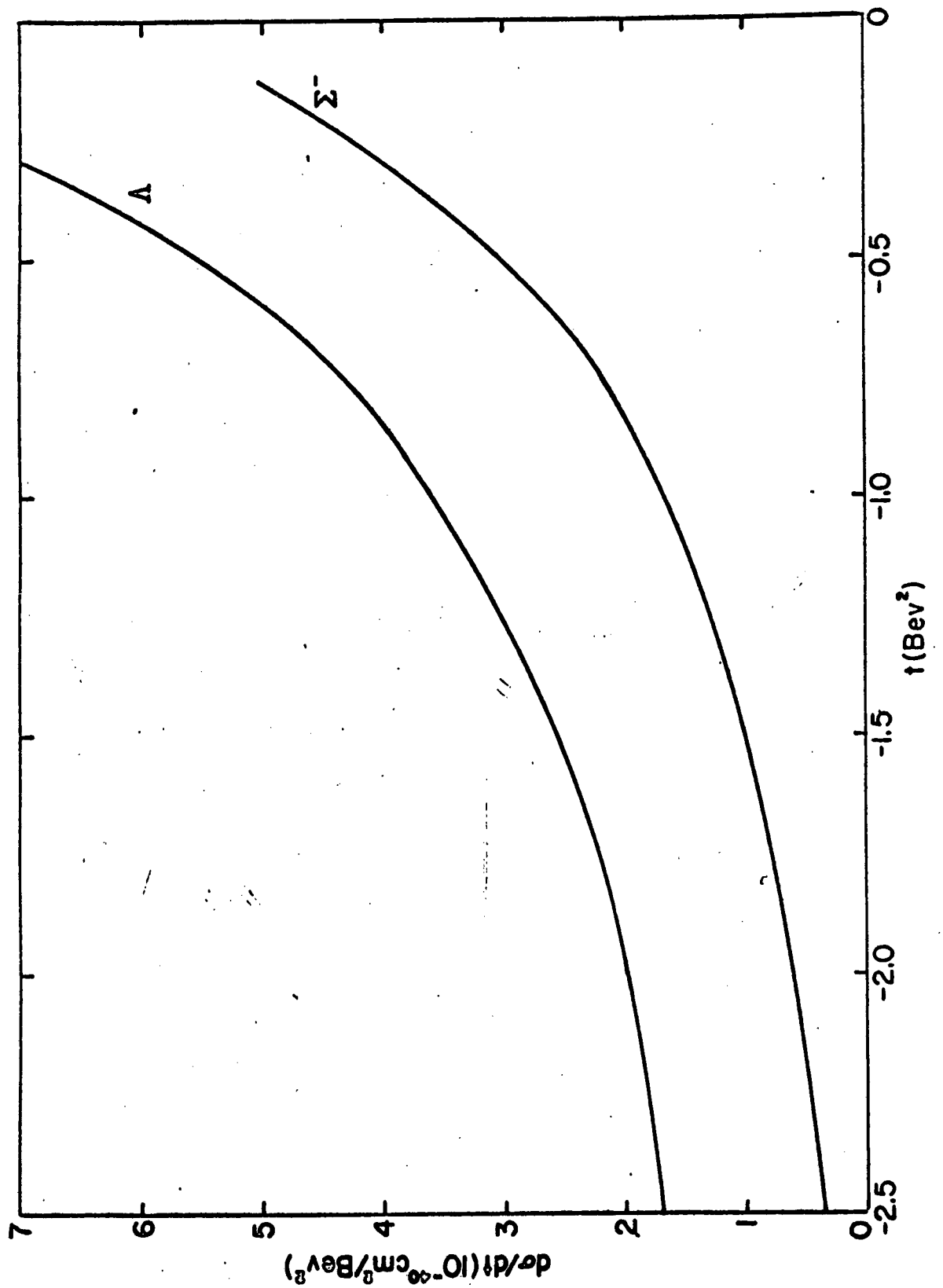
Λ
Σ⁻
dσ/dt (10⁻³⁰ cm²/Bev²)
t (Bev²)
0
1
2
3
4
5
6
7
-0.5
-1.0
-1.5
-2.0
-2.5

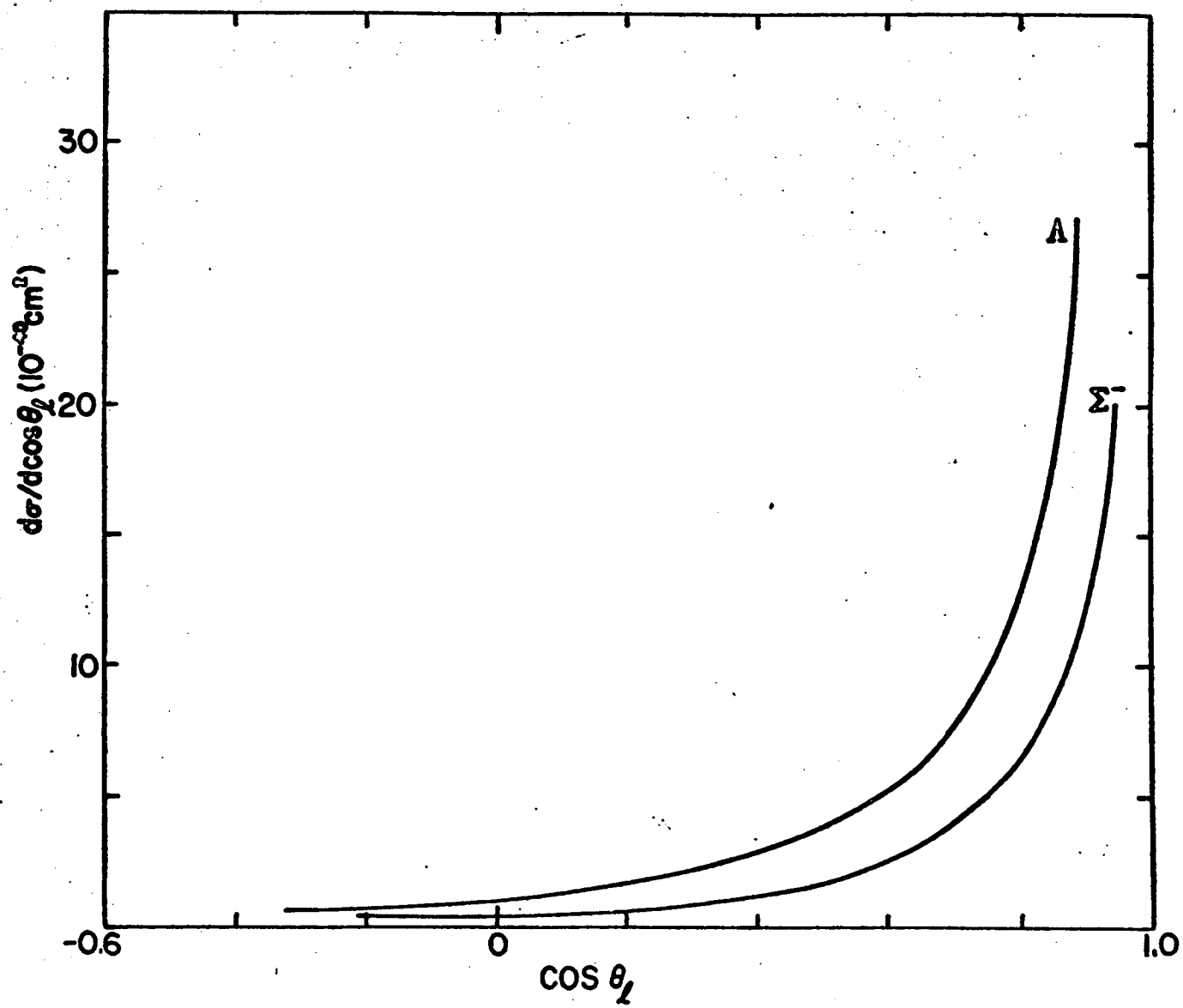
30
20
10
-0.6
0
1.0
$d\sigma/d\cos\theta_l$ ($10^{-39}cm^2$)
$\cos\theta_l$
Λ
Σ^-

$E_\nu = 2$ BEV.

TJ

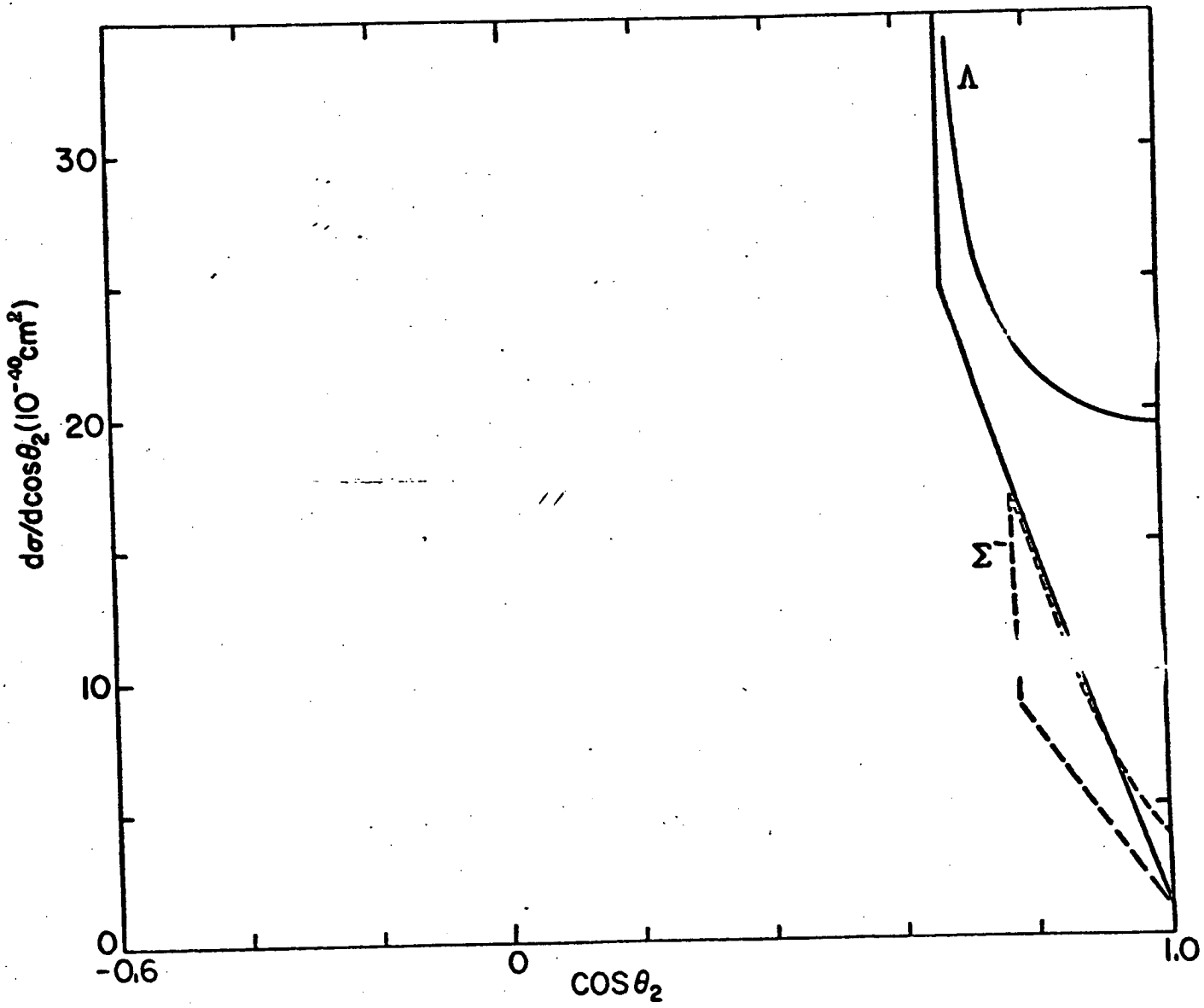

E_ν = 2 BEV.

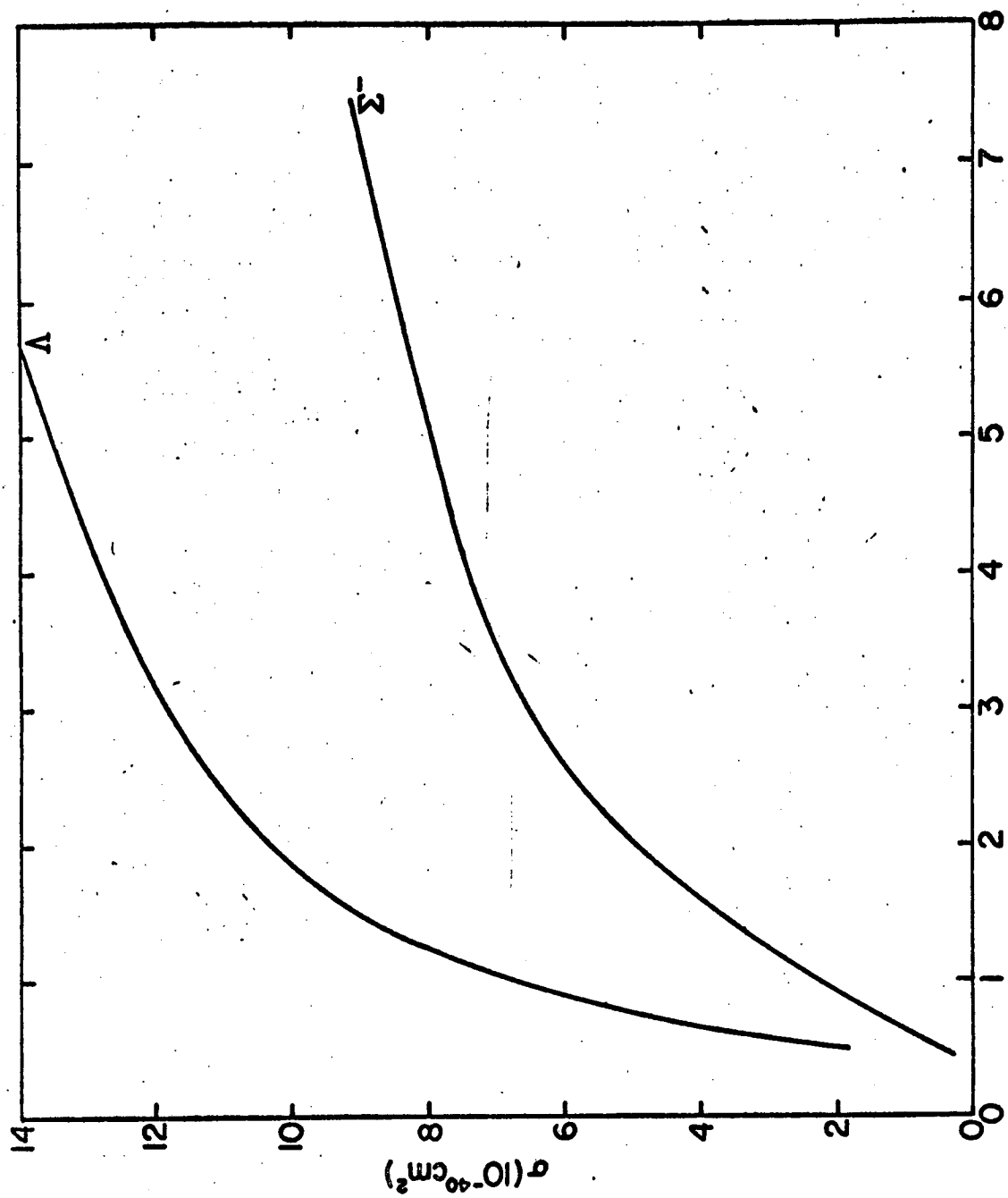
Λ
Σ⁻
σ(10⁻⁴⁰cm²)
E_ν(Bev)
0
2
4
6
8
10
12
14
1
3
5
7

I

POLARIZATION EFFECTS IN HIGH ENERGY WEAK INTERACTIONS

~~Cabibbo and Gatto~~ S.L. Adler

Nuovo Cimento 30, 1020(1963)

Gives expressions for the final lepton and baryon polarization and for correlation effects involving both polarizations expressed in terms of weak interaction form factors. A test of time reversal in high energy weak interactions is suggested. One can look for a term in the cross section

$$\sim \hat{u}_\pi \cdot \hat{n}'$$

where $\hat{u}_\pi$ is the direction of the π from hyperon decay and , in the barycentric system

$$\hat{n}' = \hat{k}_2 \times \hat{n}$$

where $\hat{k}_2$ is along the baryon momenta and $\hat{n}$ & $\hat{k}_2$ are in the plane of the reaction.

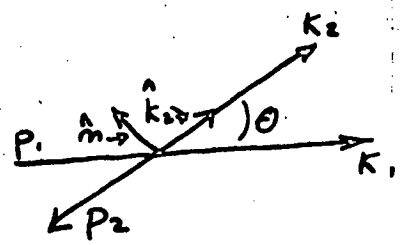

Summarized by Robert Goren
~ Nov. 19, 1964

SUBJECT
Momentum Vector Diagrams for Neutrino Interactions

NAME John Moriarty

DATE 5/25/65

I. Introduction

Each ellipse is a graphic illustration of how the momentum of the particles produced from two particle interactions or from decays varies with the production angle. This so called "ellipse method" is outlined in "Reaction Dynamics for Scanners" by M. L. Stevenson.

II. Explanation of symbols used

(a) $\vec{P}$ - momentum of a particle in the lab frame of reference (lab frame). The length of the vector is proportional to $|\vec{P}|$ at the given angle.

(b) $\vec{P}^*$ - momentum of a particle in the center of mass frame of reference (c.m. frame)

(c) θ_1 and θ_2 - production angles of particles in the lab frame

(d) θ' - production angle of the particles in the c.m. frame

(e) o and o" (in pencil) - each ellipse drawn such that o and o" are the collision vertices in the lab frame for the particles whose momentum vectors radiate from o and o" respectively

(f) o' - collision vertex in c.m. frame

(g) E' = total energy in the c.m. frame

(h) $\bar{\beta} = \bar{V}/C$ = (speed of c.m./speed of light)

(i) $\bar{\gamma} = 1/\sqrt{1 - \bar{\beta}^2}$

(j) $\bar{\eta} = \bar{\beta}\,\bar{\gamma}$

(k) $\bar{\ell}$ = Mean decay length in the lab frame of a particle at the corresponding momentum ($\eta = \frac{PC}{m_0 C^2}$ and t_0 = mean lifetime)

SUBJECT
NAME John Morarity
DATE 5/25/65

Index for Momentum Diagrams (1 BeV/c)

→ 1 Rank ←

$\nu + p \to \mu^+ + n$

0 938 106 939

$$\bar{\beta} = \frac{cP_1}{E_1+E_2} = \frac{1}{\sqrt{1^2+0.938}} = \frac{1}{1.94} = 0.515 = \bar{\beta}$$

$\bar{\gamma} = 1.17$ $\quad \bar{\eta} = \bar{\beta}\bar{\gamma} = 0.602$

$$p^* = \frac{1}{2m^*}\left\{(m^*+\mu+n)(m^*+\mu-n)(m^*-\mu+n)(m^*-\mu-n)\right\}^{1/2}$$

$$m^* = \frac{E_1+E_2}{\bar{\gamma}} = \frac{1+0.94}{1.17} = \frac{1.94}{1.17} = 1.66 \text{ B/c}$$

$$\Rightarrow p^* = \frac{1}{3.32}\left\{(1.66+0.106+0.94)(1.66+0.106-0.94)(1.66-0.106+0.94)(1.66-0.106-0.94)\right\}^{1/2}$$

$$= \frac{1}{3.32}\left\{(2.71)(0.826)(2.49)(0.614)\right\}^{1/2} = \frac{1.86}{3.32} \Rightarrow p^* = 0.56 \text{ B/c}$$

$$E'_\mu = \sqrt{p^{*2}+\mu^2} = \sqrt{.311+.011} = \sqrt{0.322} = .567 \Rightarrow E'_\mu = 567 \text{ MeV}$$

$$E'_n = \sqrt{p^{*2}+n^2} = \sqrt{0.311+0.88} = \sqrt{1.19} = 1.09 \Rightarrow E'_n = 1090 \text{ MeV}$$

$\bar{\beta}\, p^* = 653$ M/c

$\bar{\gamma}\, E'_\mu = 342$ MeV

$\bar{\gamma}\, E'_n = 657$ MeV

$\gamma + p \rightarrow \nu^+ + \pi$ at 1 Bev,

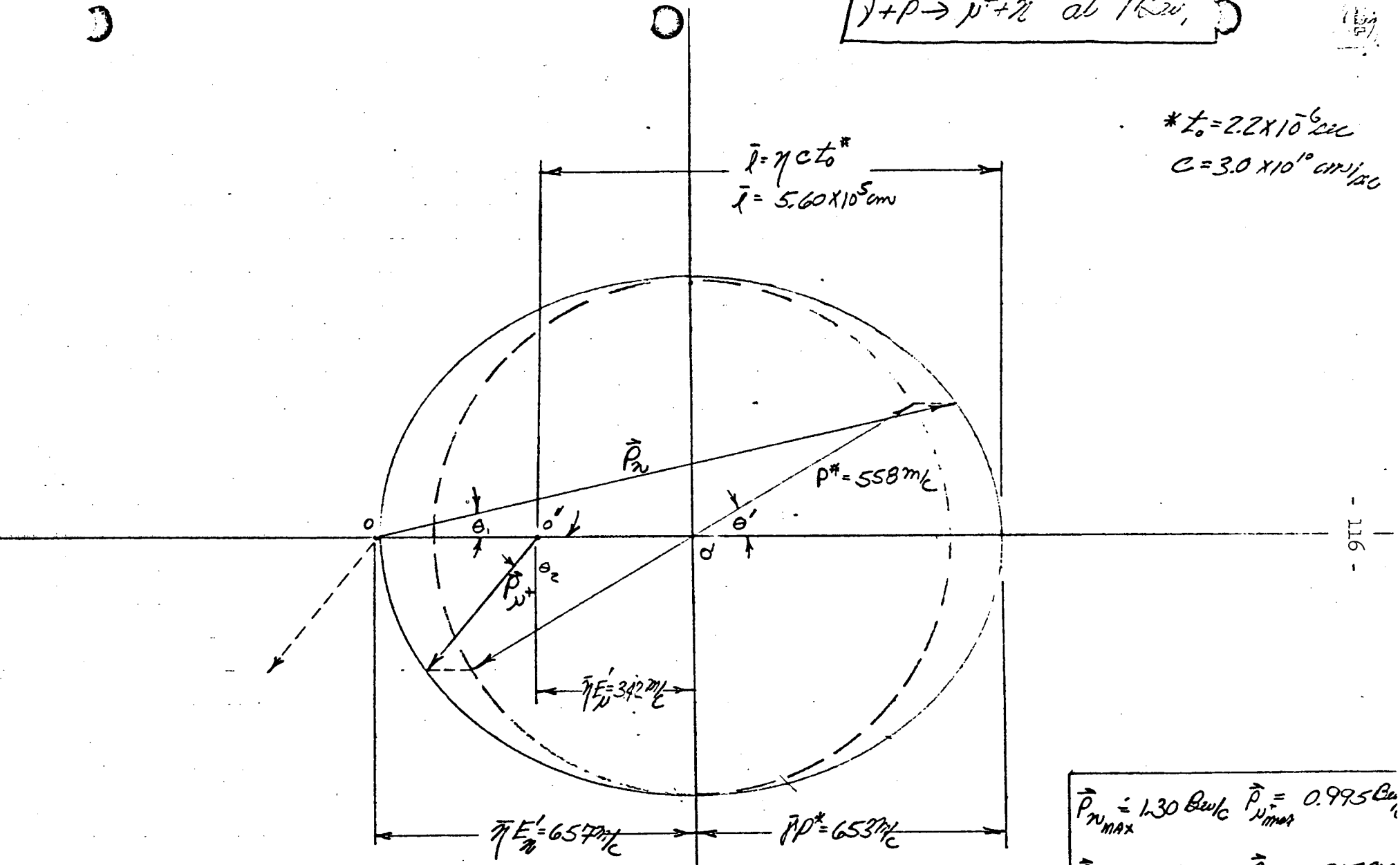

$*t_0 = 2.2 \times 10^{-6}$ sec

$c = 3.0 \times 10^{10}$ cm/sec

$\vec{P}_{\nu_{MAX}} \doteq 1.30$ Bev/c $\quad \vec{P}_{\nu^-_{max}} = 0.995$ Bev/c

$\vec{P}_{\nu_{min}} \doteq 4$ mev/c $\quad \vec{P}_{\nu^+_{min}} = 315$ mc

$\theta_{\nu_{max}} \doteq 90°$

$\nu + p \rightarrow \Sigma^0 + \mu^+$ at 1 Bev/c

0 938 1195 106

$\bar{\beta} = \frac{cp_1}{E_1+E_2} = \frac{1}{1.94} = 0.515 = \bar{\beta}$

$\bar{\gamma} = 1.17$ $\bar{\eta} = 0.602$

$m^* = E^* = \frac{E_1+E_2}{\bar{\gamma}} = \frac{1+0.94}{1.17} = 1.66$ Bev

$\Rightarrow p^* = \frac{1}{3.32}\{(1.66+1.195+0.106)(1.66-1.195+0.106)(1.66+1.195-0.106)(1.66-1.195-0.106)\}^{1/2}$

$= \frac{1}{3.32}\{(2.96)(.571)(2.75)(.359)\}^{1/2} = \frac{1.29}{3.32} = 0.389$ Bev/c

$p^* = 389$ Mev/c

$\bar{\gamma} p^* = 456$ Mev/c

$E'_\nu = \sqrt{p^{*2}+\nu^2} = \sqrt{.152+0.011} = \sqrt{0.163} = 0.403$ Bev

$E'_\nu = 403$ Mev

$\bar{\eta} E'_\nu = 243$ Mev

$E'_\Sigma = \sqrt{.152+(1.195)^2} = \sqrt{0.152+1.43} = \sqrt{1.58} = 1.26$ Bev

$E'_\Sigma = 1260$ Mev

$\bar{\eta} E'_\Sigma = 757$ Mev

$\nu + p \to \Sigma^0 + \mu^+$ at 1 Bev/c

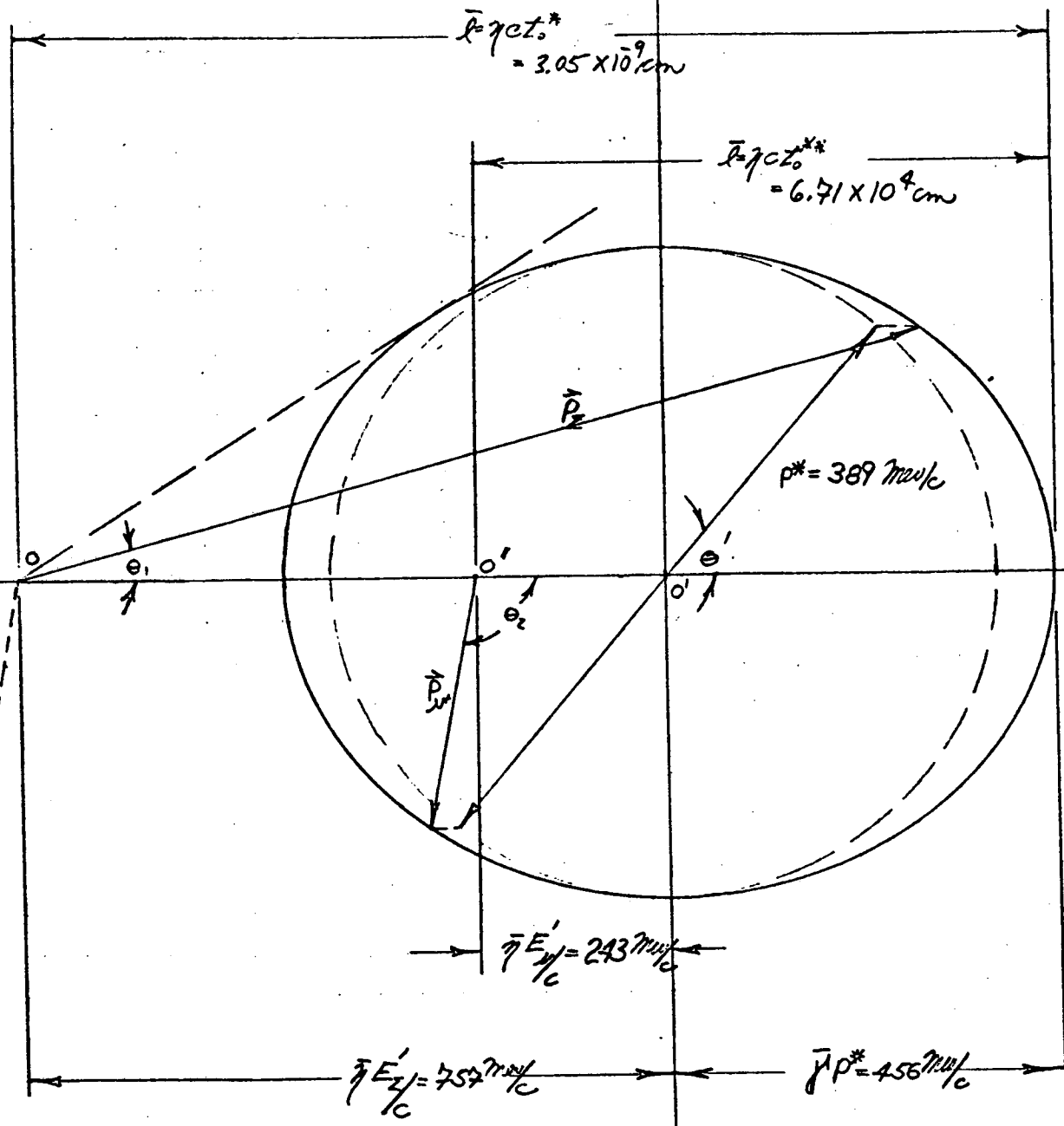

$\tau_0^* = 10^{-19}$ sec
$\tau_0^{**} = 2.2 \times 10^{-6}$ sec

$\vec{P}_{\Sigma max} = 1.213$ Bev/c	$\vec{P}_{\Sigma min} = 301$ Mev
$\vec{P}_{\nu max} = 699$ Mev	$P_{\nu min} = -213$ Mev
$\theta_{1 max} = 32.5°$	

Memo 5555

Index for Momentum Diagrams (5 BeV/c)

$\nu + p \rightarrow \mu^+ + n$ → at 5 Bev/c ←

0 938 106 939

$\bar{\beta} = \frac{cp_1}{E_1 + E_2} = \frac{5}{5 + 0.938} \doteq \frac{5}{5.94} = 0.842 = \bar{\beta}$

$\bar{\gamma} = 1.85$ $\bar{\eta} = 1.56$

$M^* = E^* = \frac{E_1 + E_2}{\bar{\gamma}} = \frac{5.94}{1.85} = 3.21$ Bev

$\Rightarrow p^* = \frac{1}{6.42}\{(3.21 + 0.106 + .939)(3.21 + 0.106 - 0.939)(3.21 - 0.106$

$(3.21 - 0.106 -$

$= \frac{1}{6.42}\{(4.36)(2.38)(4.04)(2.16)\}^{1/2} \doteq \frac{9.55}{6.42} = 1.48$ Bev/c

$\Rightarrow p^* = 1480$ Mev/c

$\bar{\gamma} p^* = 2740$ Mev/c

$E'_\mu = \sqrt{p^{*2} + \mu^2} = \sqrt{2.19 + 0.01} = \sqrt{2.20} \doteq 1.48$

$\Rightarrow E'_\mu = 1480$ Mev

$\bar{\eta} E'_\mu = 2310$ Mev

$E'_n = \sqrt{p^{*2} + n^2} = \sqrt{2.19 + 0.88} = \sqrt{3.07} = 1.75$ Bev

$\Rightarrow E'_n = 1750$ Mev

$\bar{\eta} E'_n = 2730$ Mev

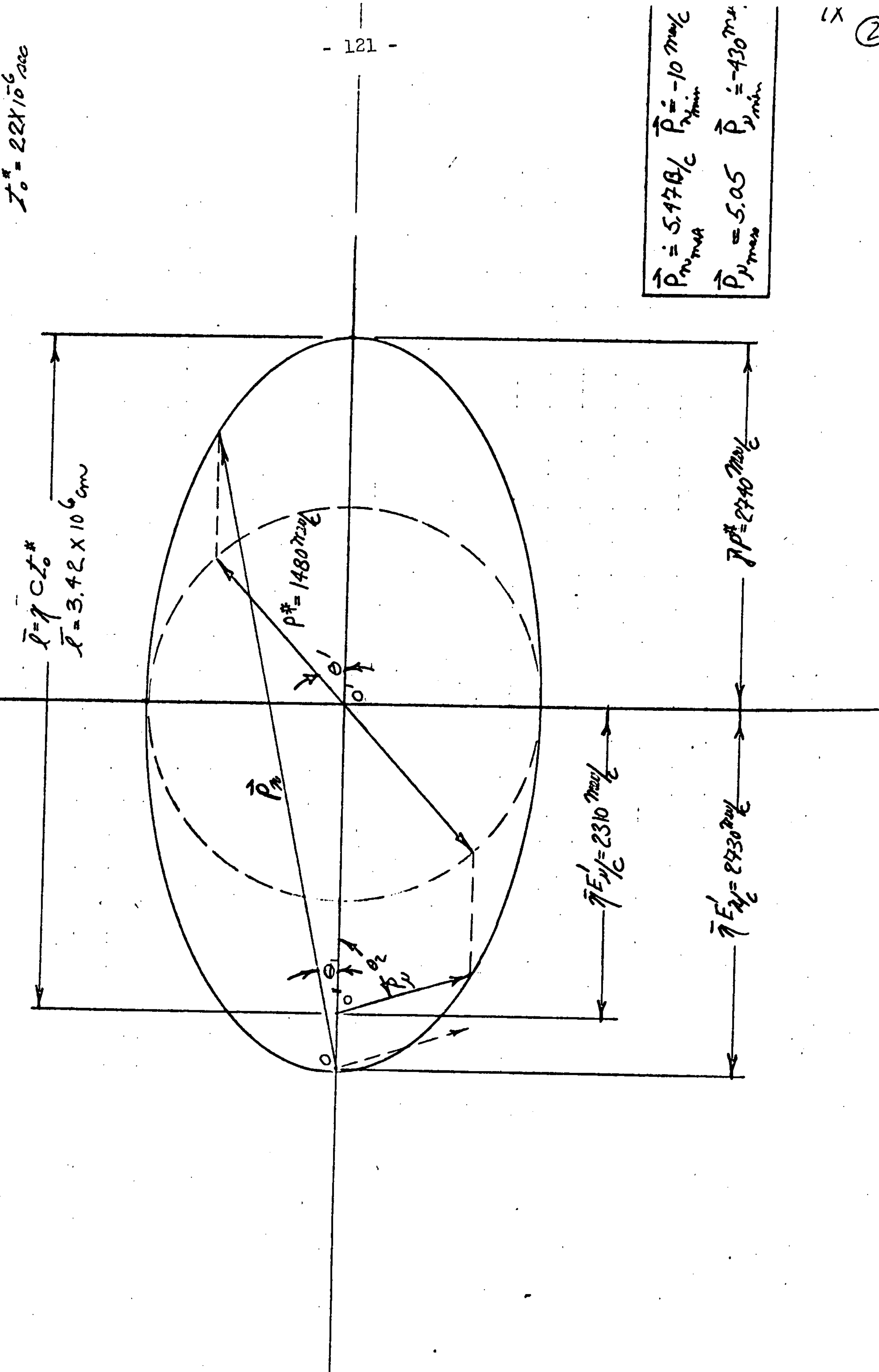
IX ②
$t_0^* = 22 \times 10^{-6}$ sec
$\hat{p}_{\pi\,max} \doteq 5.47$ B/c
$\hat{p}_{\pi\,min} \doteq -10$ mev/c
$\hat{p}_{\nu\,max} = 5.05$
$\hat{p}_{\nu\,min} \doteq -430$ mev.
$\bar{\ell} = \bar{\eta} c t_0^*$
$\bar{\ell} = 3.42 \times 10^6$ cm
$p^* = 1480$ mev/c
θ'
$\hat{p}_\pi$
θ_1
θ_2
$\hat{p}_\nu$
$\bar{\eta} p^* = 2740$ mev/c
$\bar{\eta} E'_\nu/c = 2310$ mev/c
$\bar{\eta} E'_\nu/c = 2730$ mev/c

$\nu + p \rightarrow \Sigma^0 + \mu^+$ at 5 Bev/c

$\bar{\beta} = 0.842$ $\bar{\gamma} = 1.85$ $\bar{\eta} = 1.56$

$$p^* = \frac{1}{6.42}\{(3.21 + 0.106 + 1.195)(3.21 + 0.106 - 1.195)(3.21 - 0.106 + 1.195)(3.21 - 0.106 - 1.195)\}$$

$$= \frac{1}{6.42}\{(4.51)(2.12)(4.30)(1.91)\}^{1/2} = \frac{8.86}{6.42} = 1.38 \text{ Bev/c}$$

$\Rightarrow$ $p^* = 1380$ Mev/c

$\bar{\gamma} p^* = 2550$ Mev/c

$$E'_\mu = \sqrt{p^{*2} + \mu^2} = \sqrt{(1.38)^2 + (.106)} \doteq 1.38 \text{ Bev}$$

$\Rightarrow$ $E'_\mu = 1380$ Mev

$$E'_\Sigma = \sqrt{(1.38)^2 + (1.195)^2} = \sqrt{3.33} = 1.82 \text{ Bev}$$

$\Rightarrow$ $E'_\Sigma = 1820$ Mev

$\bar{\eta} E'_\Sigma = 2840$ Mev

$\bar{\eta} E'_\mu = 2150$ Mev

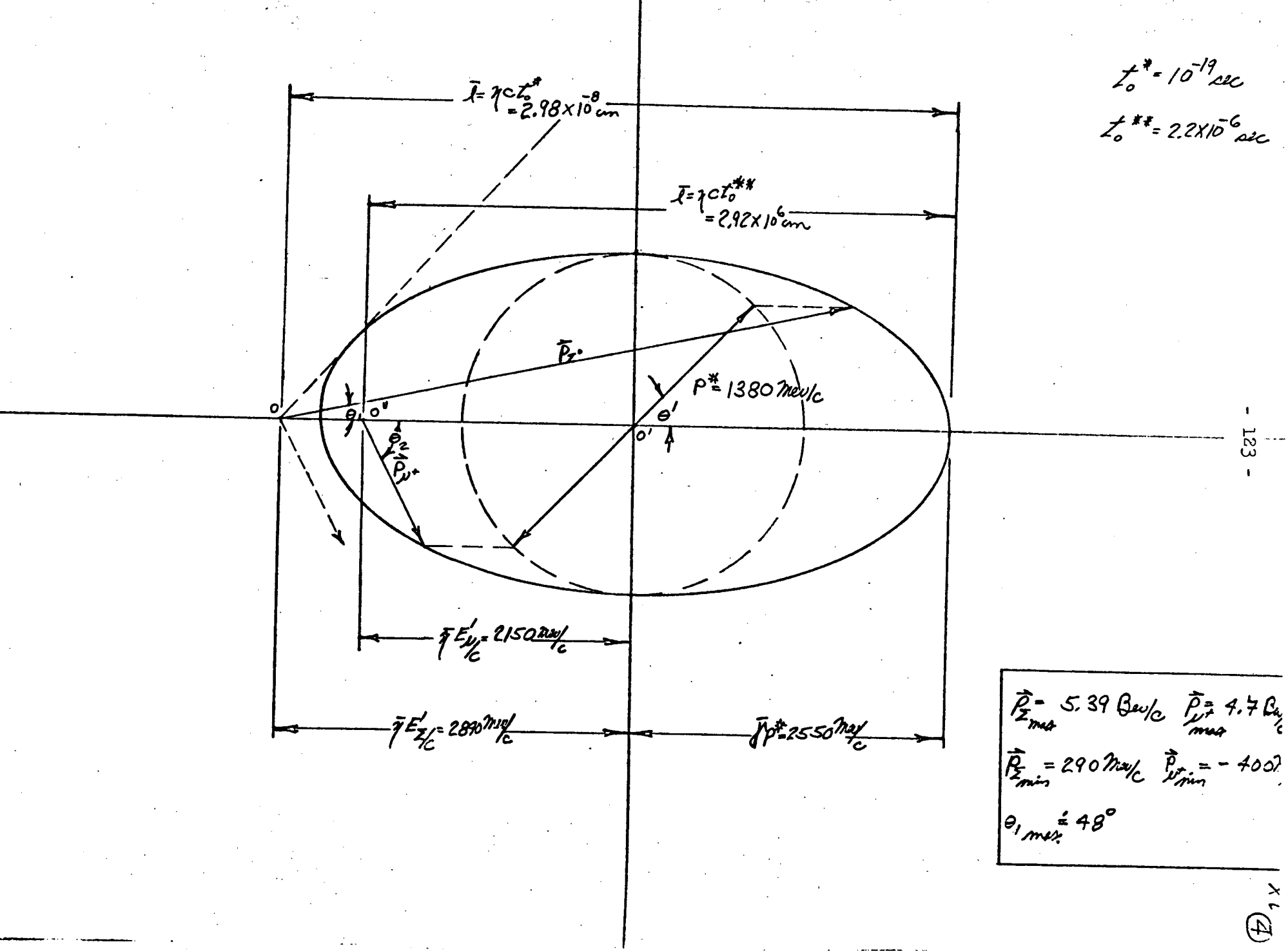

$t_0^* = 10^{-19}$ sec

$t_0^{**} = 2.2 \times 10^{-6}$ sec

$\bar{P}_{z_{max}} = 5.39$ Bev/c $\quad \bar{P}_{y^+_{max}} = 4.7$ Bev/c

$\bar{P}_{z_{min}} = 290$ mev/c $\quad \bar{P}_{y^+_{min}} = -400$ mev/c

$\theta_{1\,max} \doteq 48°$

(4)

$\mu + p \to \pi^+ + n$ → at 5 Bev/c ←

0 938 140 939

$\bar{\beta} = 0.842$ $\quad \bar{\gamma} = 1.85$ $\quad \bar{\eta} = 1.56$

$$M^* = E^* = \frac{E_1 + E_2}{\bar{\gamma}} = \frac{5.91}{1.85} = 3.21 \text{ Bev}$$

$$p^* = \frac{1}{6.42}\{(3.21 + 0.14 + 0.94)(3.21 + 0.14 - 0.94)(3.21 - 0.14 + 0.94)(3.21 - 0.14 - 0.94)\}$$

$$p^* = \frac{1}{6.42}\{(4.29)(2.41)(4.01)(2.13)\}^{1/2} = \frac{9.40}{6.42} = 1.46 \text{ Bev/c}$$

$p^* = 1460$ Mev/c

$\bar{\gamma} p^* = 2700$ Mev/c

$$E'_\eta = \sqrt{p^{*2} + \eta^2} = \sqrt{(1.46)^2 + (0.94)^2} = \sqrt{2.14 + 0.88} = \sqrt{3.02} = 1.74$$

$\Rightarrow E'_n = 1740$ Mev

$\bar{\eta} E'_n = 2710$ Mev

$$E'_\pi = \sqrt{p^{*2} + \pi^2} = \sqrt{2.14 + .02} = \sqrt{2.16} = 1.47$$

$E'_\pi = 1470$ Mev

$\bar{\eta} E'_\pi = 2290$ Mev

$\gamma + p \to \pi^+ + n$ at 5 Bev/c

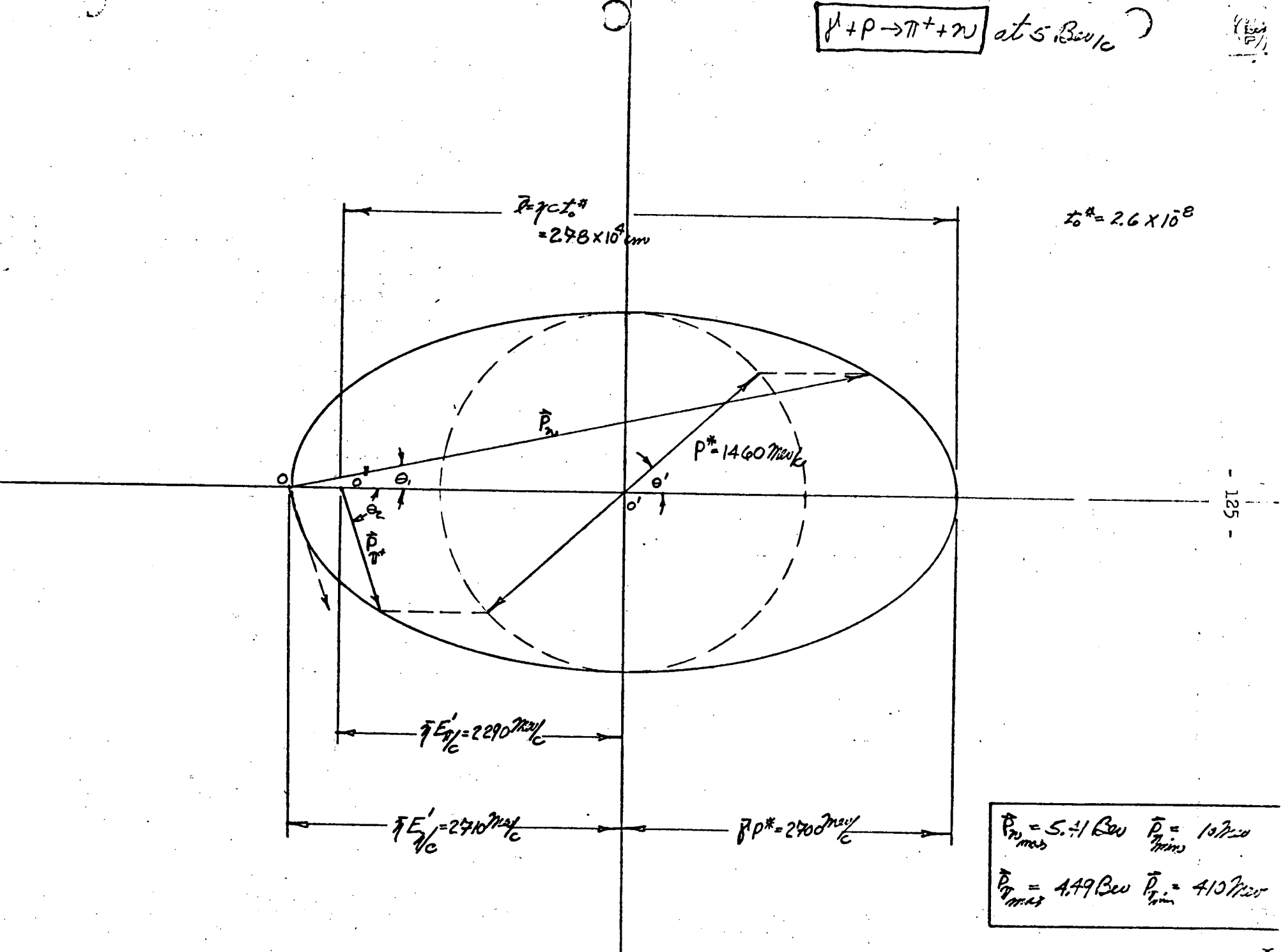

$P_{n\,max} = 5.1$ Bev $P_{\pi\,min} = 10$ Mev

$P_{\pi\,max} = 4.49$ Bev $P_{\pi\,min} = 410$ Mev

XLV (47)

$\gamma + p \rightarrow \Sigma^+ + K^\circ$ ← at 5 Bev/c ←

0 938 1190 500

$\bar{\beta} = \frac{cp_1}{E_1 + E_2} = \frac{5}{5 + 0.94} = \frac{5}{5.94} = 0.842 = \bar{\beta}$

$\bar{\gamma} = 1.85$ $\bar{\eta} = 1.56$

$M^* = E^* = \frac{E_1 + E_2}{\bar{\gamma}} = \frac{5.94}{1.85} = 3.21$ Bev

$$p^* = \frac{1}{6.42}\left\{(3.21+1.19+0.50)(3.21+1.19-0.50)(3.21-1.19+0.50)(3.21-1.19-0.50)\right\}^{1/2}$$

$$= \frac{1}{6.42}\left\{(4.90)(3.90)(2.52)(1.52)\right\}^{1/2} = \frac{8.56}{6.42} = 1.33 \text{ Bev/c}$$

$\Rightarrow p^* = 1330$ Mev/c

$\bar{\gamma} p^* = 2470$ Mev/c

$E'_\Sigma = \sqrt{p^{*2} + \Sigma^2} = \sqrt{1.78 + 1.42} = \sqrt{3.20} = 1.79$ Bev

$E'_\Sigma = 1790$ Mev

$\bar{\eta} E'_\Sigma = 2790$ Mev

$E'_{K^\circ} = \sqrt{p^{*2} + K^{\circ 2}} = \sqrt{1.78 + 0.25} = 1.43$ Bev

$E'_{K^\circ} = 1430$ Mev

$\bar{\eta} E'_K = 2220$ Mev

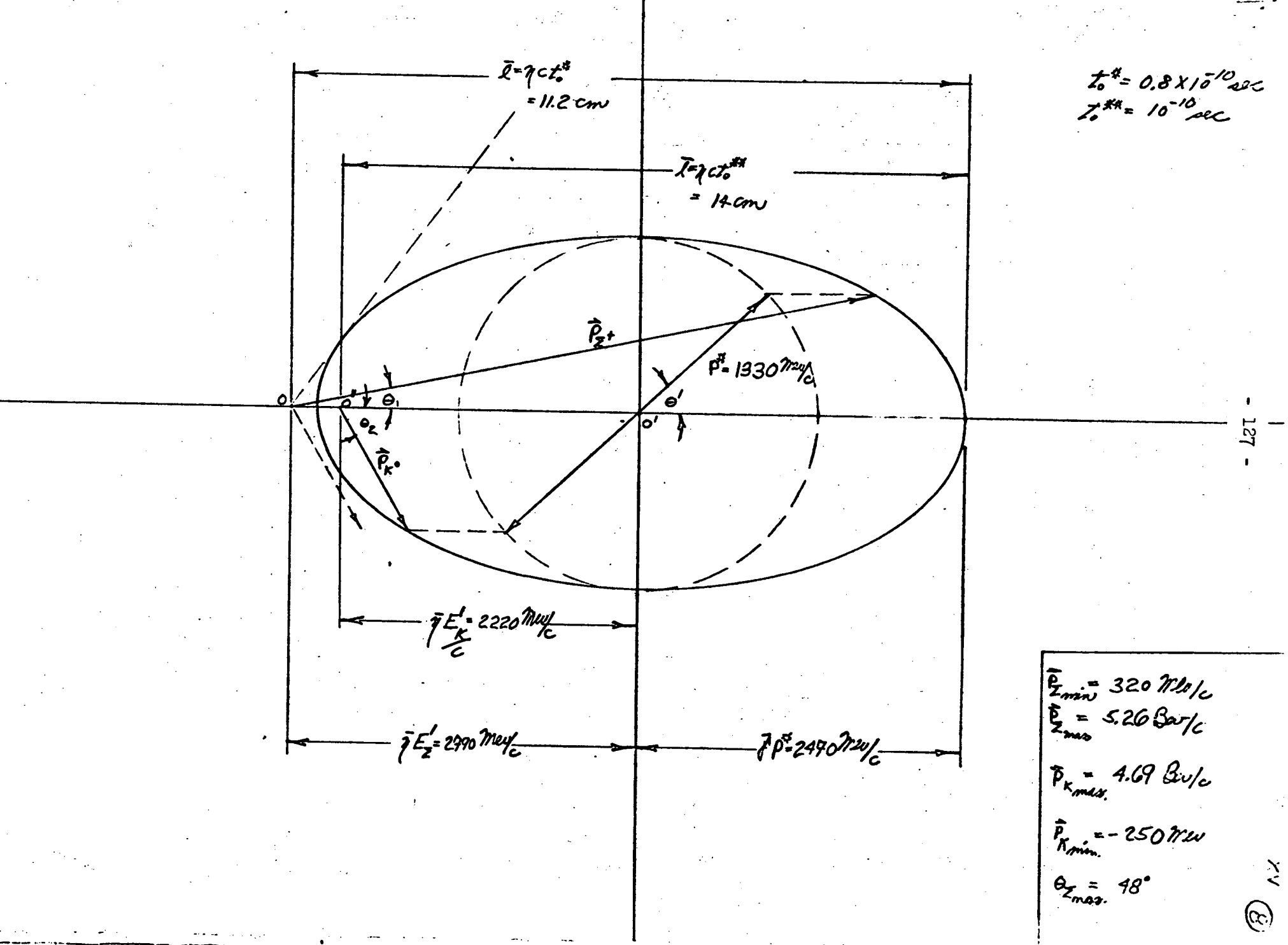

$t_0^{*} = 0.8 \times 10^{-10}$ sec

$t_0^{**} = 10^{-10}$ sec

$\bar{p}_{z\,min} = 320$ Mev/c

$\bar{p}_{z\,max} = 5.26$ Bev/c

$\bar{p}_{K\,max.} = 4.69$ Bev/c

$\vec{p}_{K\,min.} = -250$ mev

$\theta_{z\,max.} = 48°$

XV ⑧

SUBJECT

NAME John Moriarty

DATE 5/25/65

Index for Momentum Diagrams (10 BeV/c)

(*Note: $\pi^- p \rightarrow K^+ \Sigma^-$; $K^- p \rightarrow K^+ \Xi^-$; $K^- p \rightarrow \pi^\pm \Sigma^\pm$ similar also at 10 BeV/c)

→ 10 B/c ←

ν	+ p	→ μ^+	+ π
0	938	106	939

(DATA FOR $\pi^+ + p \to \pi^+ + \pi$ ALMOST THE SAME AT 10 BEV/c.)

$$\bar{\beta} = \frac{cp_1}{E_1 + E_2} = \frac{10}{\sqrt{10^2} + 0.94} = \frac{10}{10.94} = 0.914 = \bar{\beta}$$

$$\bar{\gamma} = 2.46 \qquad \bar{\eta} = \bar{\beta}\bar{\gamma} = 2.25$$

$$p^* = \frac{1}{2m^*}\left\{(m^* + \mu + \pi)(m^* + \mu - \pi)(m^* - \mu + \pi)(m^* - \mu - \pi)\right\}^{1/2}$$

$$m^* = E^* = \frac{E_1 + E_2}{\bar{\gamma}} = \frac{10.94}{2.46} = 4.45 \text{ B/c}$$

$$\Rightarrow p^* = \frac{1}{8.90}\left\{(4.45 + 0.106 + 0.94)(4.45 + 0.106 - 0.94)(4.45 - 0.106 + 0.94)(4.45 - 0.106 - 0.94)\right\}^{1/2}$$

$$= \frac{1}{8.90}\left\{(5.50)(3.62)(5.28)(3.40)\right\}^{1/2} = \frac{18.9}{8.90} = 2.12 \text{ B/c}$$

$$\Rightarrow \boxed{p^* = 2120 \text{ m/c}}$$

$$E'_\nu = \sqrt{p^{*2} + \mu^2} = \sqrt{(2.12)^2 + (0.116)^2} \cong 2.12 \text{ B/c}$$

$$\Rightarrow \boxed{E'_\nu \doteq 2120 \text{ Mev}}$$

$$E'_n = \sqrt{p^{*2} + (0.94)^2} = \sqrt{4.51 + 0.88} = \sqrt{5.39} \doteq 2.32 \text{ B/c}$$

$$\Rightarrow \boxed{E'_n \doteq 2320 \text{ Mev}}$$

$\bar{\gamma} p^* \doteq 5220$ Mev/c

$\bar{\gamma} E'_\nu \doteq 4780$ Mev

$\bar{\gamma} E'_n \doteq 5220$ Mev

$\nu + p \rightarrow \nu^+ + n$ at 10 Bev/c

(PLOT FOR $\Lambda + p \rightarrow \Sigma^+ + \pi$ ALMOST THE SAME)

* $\tau_0 \equiv 2.2 \times 10^{-6}$ sec
$c = 3.0 \times 10^{10}$ cm/sec

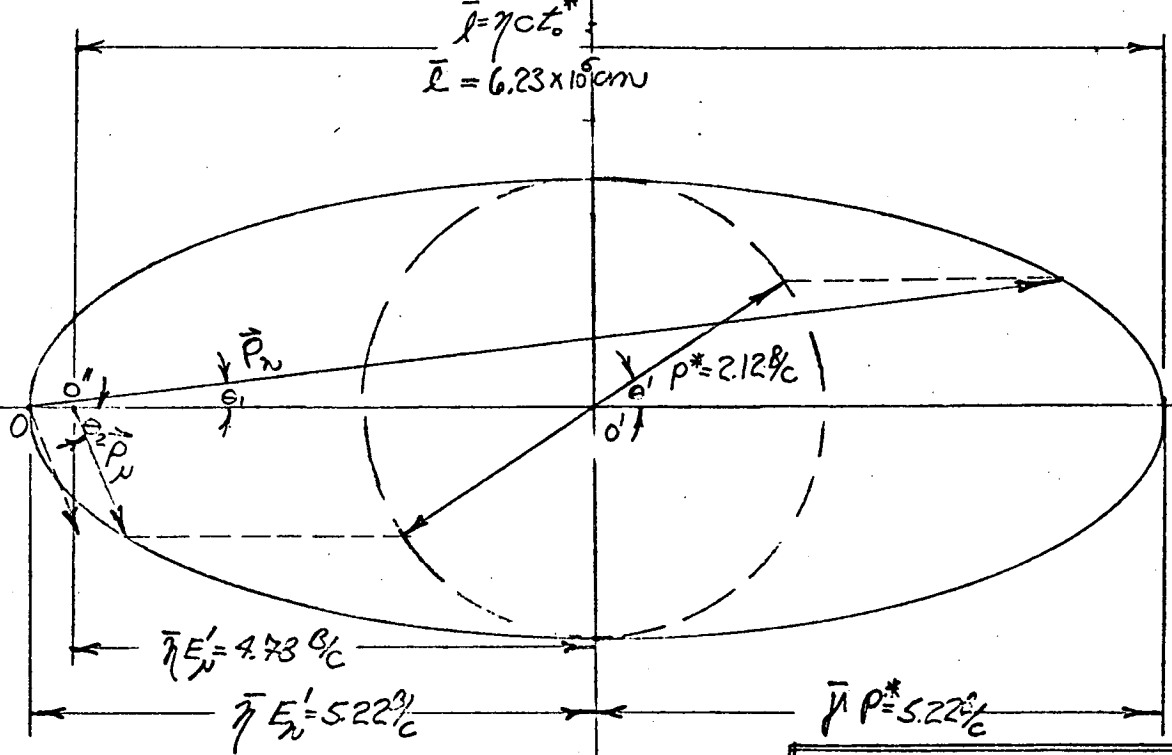

$\vec{P}_{\nu_{max}} \doteq 10.4$ B/c	$\vec{P}_{\nu_{max}} \doteq 10.0$ B/c
$\vec{P}_{\nu_{min}} \doteq -0.4$ B/c	$\vec{P}_{\nu_{min}} \doteq 0.0$ B/c
for n: $\theta_{max} \doteq 90°$	for ν^+: $\theta_{max} \doteq 180°$

xix (3)

$\nu + p \rightarrow \Sigma^0 + \mu^+$ at 10 Bev/c

0 938 1195 106

$\bar{\beta} = \frac{cp_1}{E_1 + E_2} = \frac{10}{10.94} = 0.914 = \bar{\beta}$

$\bar{\gamma} = 2.46$ $\bar{\eta} = 2.25$

$M^* = 4.45$ Bev/c

$p^* = \frac{1}{8.90}\{(4.45+0.106+1.195)(4.45+.106-1.195)(4.45-.106+1.195)(4.45-.106-1.195)\}^{1/2}$

$= \frac{1}{8.90}\{(5.75)(3.36)(5.54)(3.15)\}^{1/2} = \frac{18.3}{8.90} = 2.06$ Bev/c

$\Rightarrow p^* = 2060$ mev/c

$E'_{\mu^+} = \sqrt{p^{*2} + \mu^2} = \sqrt{4.25 + .01} = 2.06$

$E'_{\mu^+} = 2060$ mev

$E'_{\Sigma_0} = \sqrt{p^{*2} + \Sigma^2} = \sqrt{4.25 + 1.43} = 2.38$

$E'_{\Sigma_0} = 2380$ mev

$\bar{\gamma} p^* = 5070$ mev/c

$\bar{\eta} E'_{\mu^+} = 4640$ mev

$\bar{\eta} E_{\Sigma_0} = 5360$ mev

Followed by $\Sigma^0 \rightarrow \Lambda\gamma$

① This Σ_0 on plot is 9.4 Bev/c

$\bar{\eta} = \frac{cp_1}{M_0c^2} = \frac{9.4}{1.195} = 7.86 = \bar{\eta}$

$\bar{\gamma} = \sqrt{(7.86)^2 + 1} = 7.91 = \bar{\gamma}$

$$p^* = \frac{1}{2.39}\left\{(1.195+1.120)^2(1.195-1.120)^2\right\}^{1/2}$$

$$= \frac{1}{2.39}(2.32)(0.075) = 0.073 \text{ Bev/c}$$

$$\boxed{p^* = 73 \text{ Mev/c}}$$

$$\boxed{\bar{\gamma} p^* = 576 \text{ Mev/c}}$$

$$E'_\Lambda = \sqrt{p^{*2} + \Lambda^2} = \sqrt{(.073) + (1.12)^2} = \sqrt{.0053 + 1.25} \doteq \sqrt{1.26} \doteq 1.12$$

$$\Rightarrow \boxed{E'_\Lambda = 1120 \text{ Mev}}$$

$$\boxed{\bar{\eta} E'_\Lambda = 8840 \text{ Mev}}$$

$$\boxed{E'_\mu = 73 \text{ Mev}}$$

$$\boxed{\bar{\eta} E'_\mu = 573 \text{ Mev}}$$

② This Σ_o on plot is about 1.1 Bev/c

$$\bar{\eta} = \frac{cp_1}{m_o c^2} = \frac{1.1}{1.195} = \boxed{0.921 = \bar{\eta}}$$

$$\bar{\gamma} = \sqrt{(0.921)^2 + 1} = \sqrt{1.849} = \boxed{1.36 = \bar{\gamma}}$$

$$\boxed{p^* = 73 \text{ Mev/c}} \qquad \boxed{\bar{\gamma} p^* = 100 \text{ Mev/c}}$$

$$\boxed{E'_\Lambda = 1120 \text{ Mev}} \qquad \boxed{\bar{\eta} E'_\Lambda = 1030 \text{ Mev}}$$

$$\boxed{E'_\mu = 73 \text{ Mev}} \qquad \boxed{\bar{\eta} E'_\mu = 67.2 \text{ Mev}}$$

③ This Σ_0 on plot is 290 Mev/c

$$\bar{\eta} = \frac{cP_1}{M_0 c^2} = \frac{0.290}{1.195} = \boxed{0.242 = \bar{\eta}}$$

$$\bar{\gamma} = \sqrt{(0.242)^2 + 1} \doteq \sqrt{0.059+1} \doteq \sqrt{1.06} = \boxed{1.03 = \bar{\gamma}}$$

$\boxed{p^* = 73 \text{ Mev/c}}$ $\Rightarrow$ $\boxed{\bar{\gamma} p^* = 75.2 \text{ Mev/c}}$

$\boxed{E'_\Lambda = 1120 \text{ Mev}}$ $\boxed{\bar{\eta} E'_\Lambda = 271 \text{ Mev}}$

$\boxed{E'_\mu = 73 \text{ Mev}}$ $\boxed{\bar{\eta} E'_\mu = 17.7 \text{ Mev}}$

(DECAY $\Sigma^0 \to \Lambda + \gamma$)

(SCALE 5X)

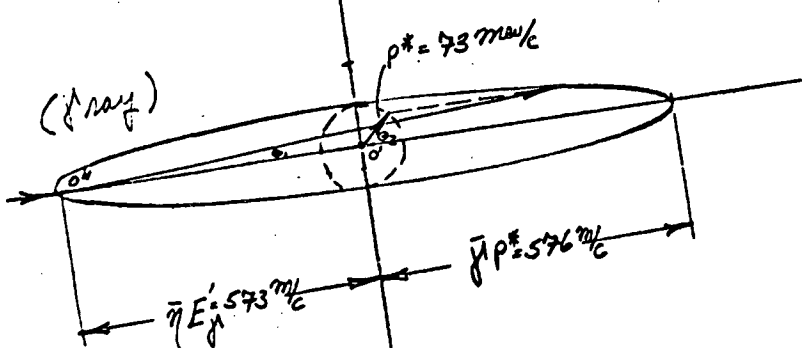

Σ^0 at ~ 9.4 Bev/c
(at $\theta_1 = 8°$)

$\bar{p}_{\mu\,max} = 1150$ mev/c

$\bar{p}_{\mu\,min} = 3$ mev/c

(DECAY $\Sigma^0 \to \Lambda + \gamma$)

(SCALE 10X)

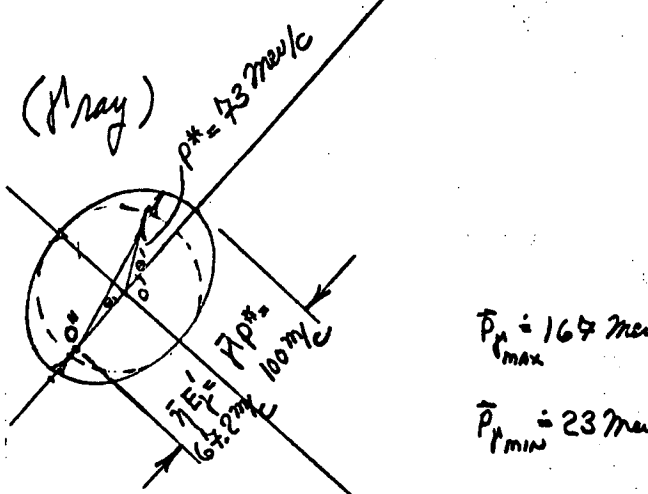

Σ^0 at ~ 1.1 Bev/c
(at $\theta_1 = 49°$)

$\bar{p}_{\mu\,max} = 164$ mev

$\bar{p}_{\mu\,min} = 23$ mev

(DECAY $\Sigma^0 \to \Lambda + \gamma$)

(SCALE 25X)

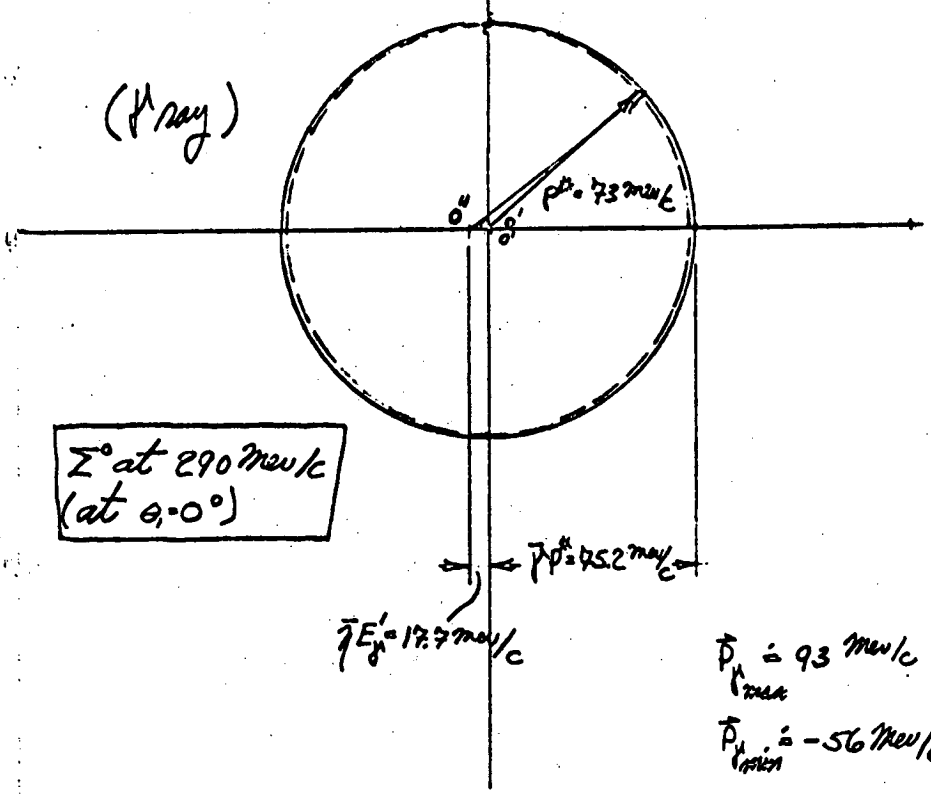

$p_{\gamma_{max}} \doteq 93$ mev/c

$p_{\gamma_{min}} \doteq -56$ mev/c

$\nu + p \rightarrow \Sigma^0 + \nu^+$ at 10 Bev/c.

$\hookrightarrow \Lambda + \gamma$

(SCALE IX)

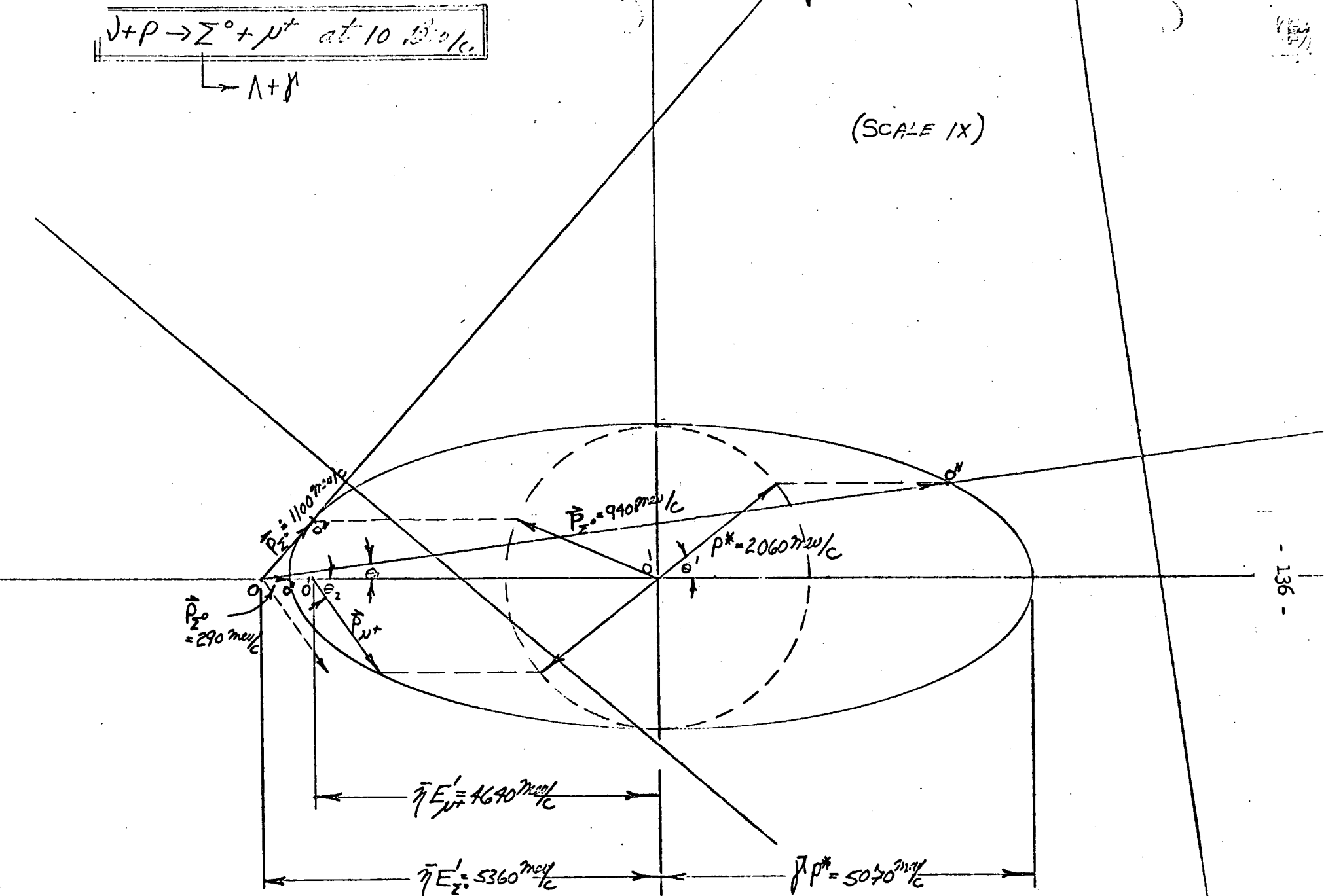

$\vec{P}_{\Sigma^0}{}_{max} = 10.43$ Bev/c	$\vec{P}_{\nu^+}{}_{max} = 9.71$ Bev/c
$P_{\gamma} = 290$ mev/c	$\vec{P}_{\Lambda} = 430$ mev/c

$\nu + p \rightarrow \mu^+ + \Delta^\circ$ $\quad \Delta^\circ \rightarrow \begin{cases} n\pi^\circ \\ \text{or} \\ p\pi^- \end{cases}$ $\rightarrow$ at 10 Bev/c $\leftarrow$

0 938 106 1238

$$\bar{\beta} = \frac{cp}{E_1 + E_2} = \frac{10}{10 + 0.938} = \frac{10}{10.94} = \boxed{0.914 = \bar{\beta}}$$

$$\boxed{\bar{\gamma} = 2.46} \qquad \boxed{\bar{\eta} = \bar{\beta}\bar{\gamma} = 2.25}$$

$$M^* = E^* = \frac{E_1 + E_2}{\bar{\gamma}} = \frac{10.94}{2.46} = 4.45 \text{ Bev/c}$$

$$\Rightarrow p^* = \frac{1}{8.90}\left\{(4.45 + 0.106 + 1.238)(4.45 + 0.106 - 1.238)(4.45 - 0.106 + 1.238)(4.45 - 0.106 - 1.238)\right\}^{1/2}$$

$$= \frac{1}{8.90}\left\{(5.79)(3.32)(5.58)(3.11)\right\}^{1/2} = \frac{18.3}{8.90} = 2.05$$

$$\Rightarrow \boxed{p^* = 2050 \text{ Mev/c}}$$

$$\boxed{\bar{\gamma} p^* = 5050 \text{ Mev/c}}$$

$$E'_\mu = \sqrt{p^{*2} + \mu^2} = \sqrt{(2.05)^2 + (0.106)} = 2.05$$

$$\Rightarrow \boxed{E'_\mu = 2050 \text{ Mev}}$$

$$\Rightarrow \boxed{\bar{\eta} E'_\mu = 4620 \text{ Mev}}$$

$$E_{\Delta^\circ} = \sqrt{p^{*2} + \Delta^{\circ 2}} = \sqrt{(2.05)^2 + (1.238)^2} = \sqrt{(4.22) + (1.53)} = 2.40$$

$$\Rightarrow \boxed{E_{\Delta^\circ} = 2400 \text{ Mev}}$$

$$\boxed{\bar{\eta} E_{\Delta^\circ} = 5400 \text{ Mev}}$$

① This Δ° on plot is 9450 Mev/c

$$\Delta^\circ \rightarrow \begin{cases} n\pi^\circ \\ p\pi^- \end{cases}$$

1238 940 140

$$\bar{\gamma} = \frac{cp_1}{m_0c^2} = \frac{9.45}{1.238} = \boxed{7.64 = \bar{\gamma}}$$

$$\bar{\mu} = \sqrt{\bar{\gamma}^2 + 1} = \sqrt{(7.64)^2 + 1} = \sqrt{59.3} = \boxed{7.70 = \bar{\mu}}$$

$$p^* = \frac{1}{2(1.238)} \{ (1.238 + .940 + 0.140)(1.238 + 0.940 - 0.140)(1.238 - 0.940 + 0.1 \\ (1.238 - 0.940 - 0.$$

$$= \frac{1}{2.47} \{ (2.32)(2.04)(0.438)(0.158) \}^{1/2} = \frac{0.572}{2.47} = .263 \text{ Bev/c}$$

$$\Rightarrow \boxed{p^* = 232 \text{ Mev/c}}$$

$$\boxed{\bar{\mu} p^* = 1780 \text{ Mev/c}}$$

$$E_\pi' = \sqrt{(p^*)^2 + \pi^2} = \sqrt{(0.232)^2 + (0.14)^2} = \sqrt{.0536 + .0196} = 0.271 \text{ Bev}$$

$$\boxed{E_\pi' = 271 \text{ Mev}}$$

$$\boxed{\bar{\gamma} E_\pi' = 2070 \text{ Mev}}$$

$$E_{p\pi n}' = \sqrt{p^{*2} + (p_{\pi n})^2} = \sqrt{0.0536 + 0.894} = \sqrt{0.948} = 0.972$$

$$\Rightarrow \boxed{E_{p\pi n}' = 972 \text{ Mev}}$$

$$\boxed{\bar{\gamma} E_{p\pi n}' = 7430 \text{ Mev}}$$

② This Δ° amplitude is 1100 MeV/c

$$\Delta^\circ \to \left\{ \begin{matrix} n\pi^\circ \\ \text{or} \\ p\pi^- \end{matrix} \right\}$$

$$\bar{\eta} = \frac{1.1}{1.24} = \boxed{0.888 = \bar{\eta}} \qquad \bar{\gamma} = \sqrt{(.888)^2 + 1} = \sqrt{1.79}$$

$$\boxed{\bar{\gamma} = 1.34}$$

$$\boxed{p^* = 232 \text{ MeV}/c}$$

$$\boxed{\bar{\gamma} p^* = 311 \text{ MeV}/c}$$

$$\boxed{E'_\pi = 271 \text{ MeV}}$$

$$\boxed{\bar{\eta} E'_\pi = 241 \text{ MeV}}$$

$$\boxed{E'_{p\,or\,n} = 972 \text{ MeV}}$$

$$\boxed{\bar{\eta} E'_{p\,or\,n} = 863 \text{ MeV}}$$

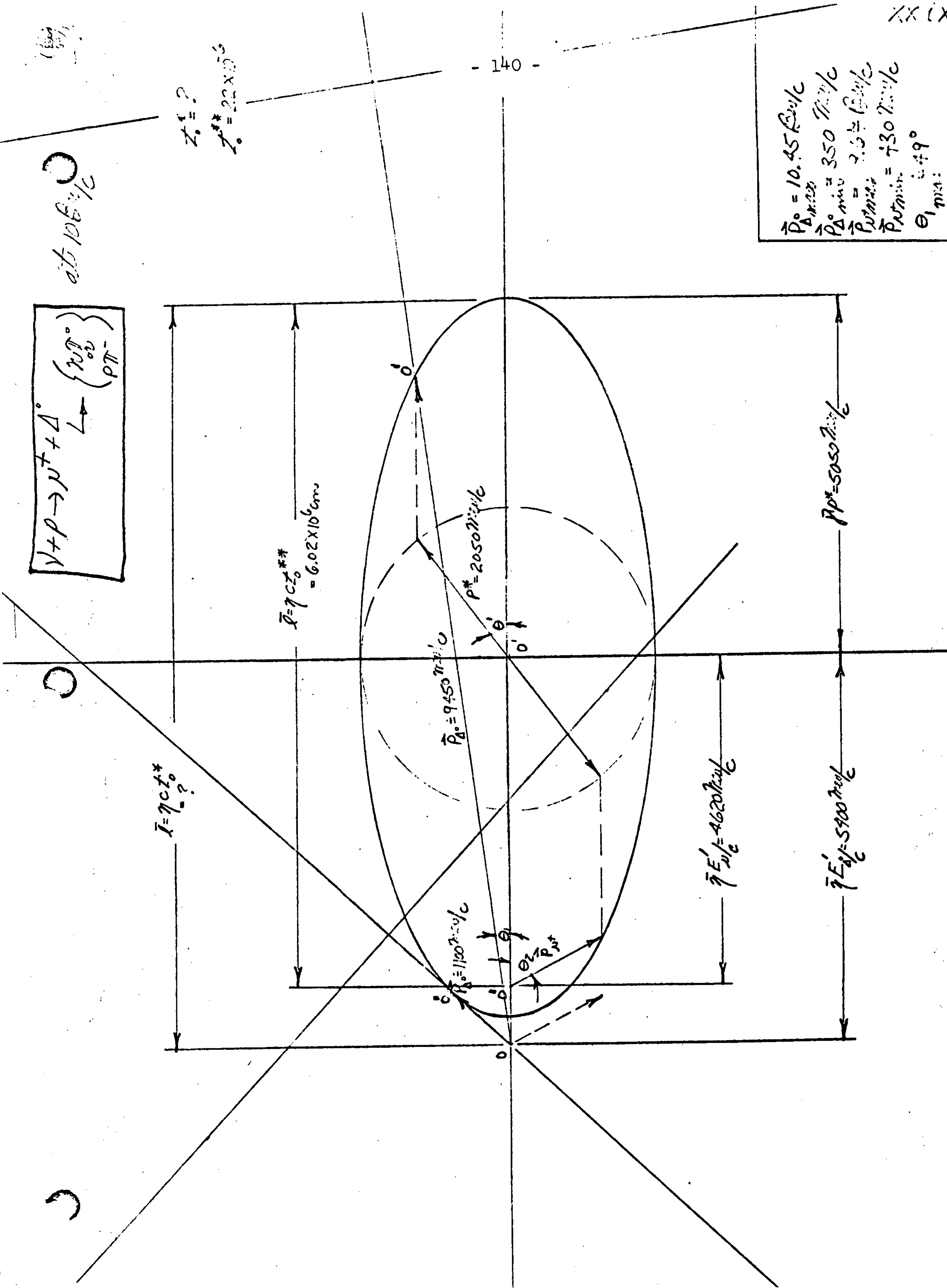
ν + p → μ+ + Δ°
p π−
l = ηcτ0* = ?
l̄ = ηcτ0** = 6.02 X 10^6 cm
p̄Δ° = 9450 MeV/c
p* = 2050 MeV/c
p̄Δ° = 1100 MeV/c
ηE'μ/c = 4620 MeV/c
ηE'Δ/c = 5400 MeV/c
ηp* = 5050 MeV/c
p̄Δ°max = 10.45 GeV/c
p̄Δ°min = 350 MeV/c
p̄μmin = 730 MeV/c
O
O'
θ1
θ2
pμ+

(DECAY $\Delta^0 \to \begin{Bmatrix} p\pi^- \\ n\pi^0 \end{Bmatrix}$)

(10.8)

(SCALE 2X)

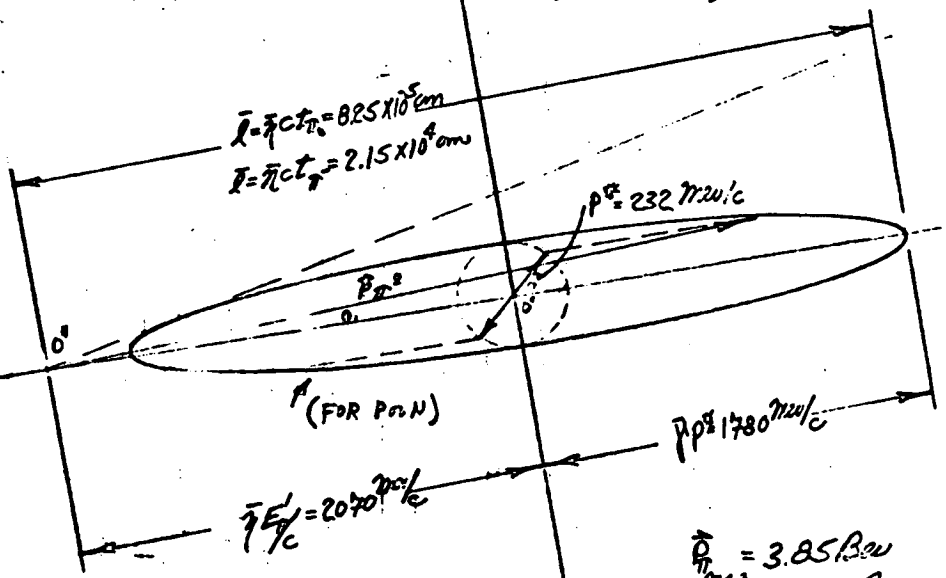

$\vec{p}_{\pi\,max} = 3.85$ Bev

$p_{\pi\,min} = 290$ mev

$\theta_{\pi\,MAX} \doteq 12.5°$

$t_{\pi^-} = 2.6 \times 10^{-8}$ sec

$t_{\pi^0} = 10^{-16}$ sec

π^0 at ~ 9.45 Bev
(at $\theta = 8.5°$)

(10.9)

(DECAY $\Delta^0 \to \begin{Bmatrix} p\pi^- \\ n\pi^0 \end{Bmatrix}$)

(SCALE 5X)

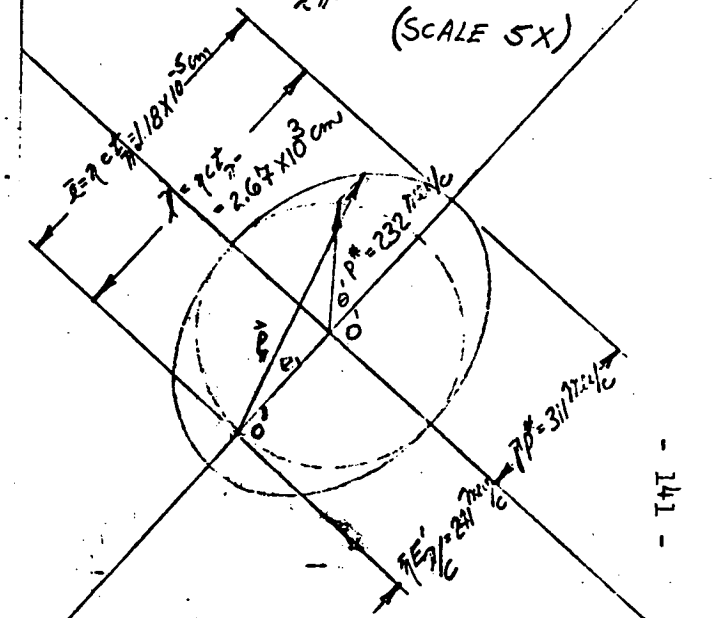

$t_{\pi^0} = 10^{-16}$ sec

$t_{\pi^-} = 10^{-16}$ sec

$\vec{p}_{\pi\,max} \doteq 552$ mev

$p_{\pi\,min} \doteq 70$ mev

π^0 at ~ 1100 mev
(at $\theta = 9°$)

$\gamma + p \to \Sigma^+ + K^0$ at 10 Bev/c ← (DATA BELOW ALSO GOOD APPROXIMATION OF $\gamma + p \to \Sigma$ ... $\gamma + p \to \Lambda$ ... at 10 B...

0 938 1190 500

$$\bar{\beta} = \frac{cP_1}{E_1+E_2} = \frac{10}{10+.94} = \frac{10}{10.94} = \boxed{0.914 = \bar{\beta}}$$

$$\boxed{\bar{\gamma} = 2.46} \qquad \boxed{\bar{\eta} = \bar{\beta}\bar{\gamma} = 2.25}$$

$$M^* = E^* = \frac{E_1+E_2}{\bar{\gamma}} = \frac{10.94}{2.46} = 4.45 \text{ Bev/c}$$

$$\Rightarrow p^* = \frac{1}{8.90}\left\{(4.45+1.19+0.5)(4.45+1.19-0.5)(4.45-1.19+0.5)(4.45-1.19-0.5)\right\}^{1/2}$$

$$p^* = \frac{1}{8.90}\left\{(6.14)(5.14)(3.76)(2.76)\right\}^{1/2} = \frac{18.1}{8.90} = 2.03 \text{ Bev/c}$$

$$\Rightarrow \boxed{p^* = 2030 \text{ Mev/c}}$$

$$E'_{\Sigma^+} = \sqrt{p^{*2} + \Sigma^{+2}} = \sqrt{(2.03)^2 + (1.19)^2}$$

$$= \sqrt{4.13 + 1.42} = \sqrt{5.55} \doteq 2.36 \text{ Bev}$$

$$\Rightarrow \boxed{E'_{\Sigma^+} \doteq 2360 \text{ Mev}}$$

$$E'_{K^0} = \sqrt{4.13 + 0.25} = \sqrt{4.38}$$

$$\doteq 2.09 \text{ Bev}$$

$$\Rightarrow \boxed{E'_{K^0} \doteq 2090 \text{ Mev}}$$

$\bar{\gamma} p^* = 5000$ Mev/c
$\bar{\eta} E'_K = 4700$ Mev
$\bar{\eta} E_\Sigma = 5310$ Mev

→ $\pi^- p \to K^+ \Sigma^-$ at 10 Bev/c ← - 143 -

140 938 495 1200

$$\bar{\beta} = \frac{c p_1}{E_1 + E_2} = \frac{10}{\sqrt{(10)^2 + (.14)^2} + 0.938} \doteq \frac{10}{10.94} = \boxed{0.914 = \bar{\beta}}$$

$$\boxed{\bar{\gamma} = 2.46} \qquad \boxed{\bar{\gamma}\bar{\beta} = 2.25}$$

$$m^* \equiv E^* = \frac{E_1 + E_2}{\bar{\gamma}} = \frac{10.94}{2.46} = 4.45 \text{ B/c}$$

$$\Rightarrow p^* = \frac{1}{8.90}\left\{(4.45 + 0.495 + 1.2)(4.45 - 0.495 + 1.2)(4.45 + 0.495 - 1.2)(4.45 - 0.495 - 1.2)\right\}^{1/2}$$

$$= \frac{1}{8.9}\left\{(6.14)(5.16)(3.74)(2.76)\right\}^{1/2} = \frac{18.1}{8.9} = 2.03 \text{ B/c}$$

$$\Rightarrow \boxed{p^* = 2030 \text{ mev/c}}$$

$$E'_{K^+} = \sqrt{p^{*2} + K^2} = \sqrt{(2.03)^2 + (.494)^2} = 2.09 \text{ B/c}$$

$$\boxed{E'_{K^+} = 2090 \text{ mev}}$$

$$E'_{\Sigma} = \sqrt{p^{*2} + \Sigma^2} = \sqrt{4.12 + 1.44} = \sqrt{5.56} = 2.36 \text{ Bev}$$

$$\Rightarrow \boxed{E'_{\Sigma^-} = 2360 \text{ mev}}$$

$$\boxed{\bar{\gamma} p^* = 5000 \text{ mev/c}}$$

$$\boxed{\bar{\gamma} E'_K = 4900 \text{ mev}}$$

$$\boxed{\bar{\gamma} E'_\Sigma = 5310 \text{ mev}}$$

(NOTE: THIS DATA IS SAME AS THAT ON LAST PAGE FOR $\Lambda + p \to K^0 + \Sigma^+$)

$K^- + P \rightarrow K^+ + \Xi^-$ at 10 Bev/c

495 938 495 1320

$$\bar{\beta} = \frac{CP_1}{E_1 + E_2} = \frac{10}{\sqrt{(10)^2 + (.495)^2} + (.938)} \doteq \frac{10}{10.94} \doteq \boxed{0.914 = \bar{\beta}}$$

$\boxed{\bar{\gamma} = 2.46}$ $\boxed{\bar{\eta} = \bar{\beta}\bar{\gamma} = 2.25}$

$M^* = 4.45$ Bev/c

$$p^* = \frac{1}{8.90}\left\{(4.45 + 0.495 + 1.32)(4.45 - 0.495 + 1.32)(4.45 + 0.495 - 1.32)(4.45 - 0.495 - 1.32)\right\}^{1/2}$$

$$p^* = \frac{1}{8.90}\left\{(6.26)(5.28)(3.62)(2.64)\right\}^{1/2} = \frac{17.8}{8.90} = 2.00 \text{ Bev/c}$$

$\boxed{p^* = 2000 \text{ Mev/c}}$

$$E'_K = \sqrt{p^{*2} + K^2} = \sqrt{4 + 0.245} = 2.05 \text{ Bev/c}$$

$\Rightarrow \boxed{E'_K = 2050 \text{ Mev}}$

$$E'_\Xi = \sqrt{p^{*2} + \Xi^2} = \sqrt{4 + 1.74} = 2.40 \text{ Bev/c}$$

$\Rightarrow \boxed{E'_\Xi = 2400 \text{ Mev}}$

$\boxed{\bar{\gamma}p^* = 4920 \text{ Mev/c}}$

$\boxed{\bar{\gamma}E'_K = 4620 \text{ Mev}}$

$\boxed{\bar{\gamma}E'_\Xi = 5410 \text{ Mev}}$

(DATA FOR $K^-P \rightarrow \pi^{\pm}\Sigma^{\mp}$ SIMILAR AT 10 Bev/c

XXXV (14)

(B) $K^- P \to \pi^- \Sigma^+$ (partly cut off)

(C) $K^- P \to \Lambda K^+$ ARE SIMILAR

2 PLOTS FOR: (A) $\pi^- P \to \Sigma^+ K^0$

(B) $\pi^- P \to \Sigma^0 K^+$ ARE ALMOST THE SAME

at 10 Bev/c

(all at 10 Bev/c)

$^* \tau_0 = 1.6 \times 10^{-10}$ sec

$^{**} \tau_0 = 10^{-10}$ sec

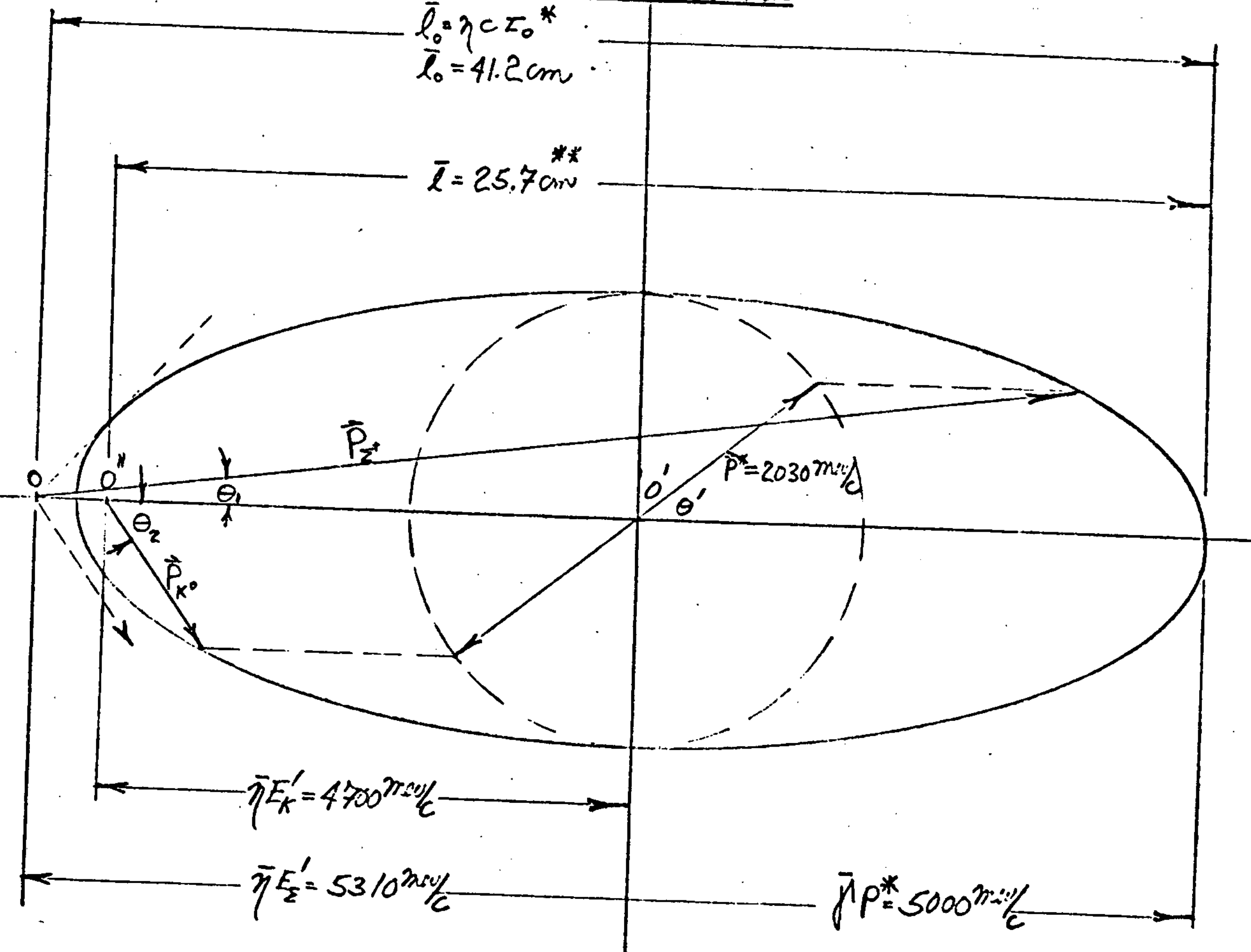

$\vec{P}_{\Sigma_{max}} \doteq 10.3$ Bev/c	$\vec{P}_{K_{max}} \doteq 9.7$ Bev/c
$\vec{P}_{\Sigma_{min}} \doteq 310$ mev/c	$\vec{P}_{K_{min}} \doteq -300$ mev/c
$\theta_{1_{max}} \doteq 45°$	

Mean Path of γ Ray in Hydrogen from $\nu + p \rightarrow \Sigma^{\circ} + \mu^{-}$, $\Sigma^{\circ} \rightarrow \Lambda + \gamma$

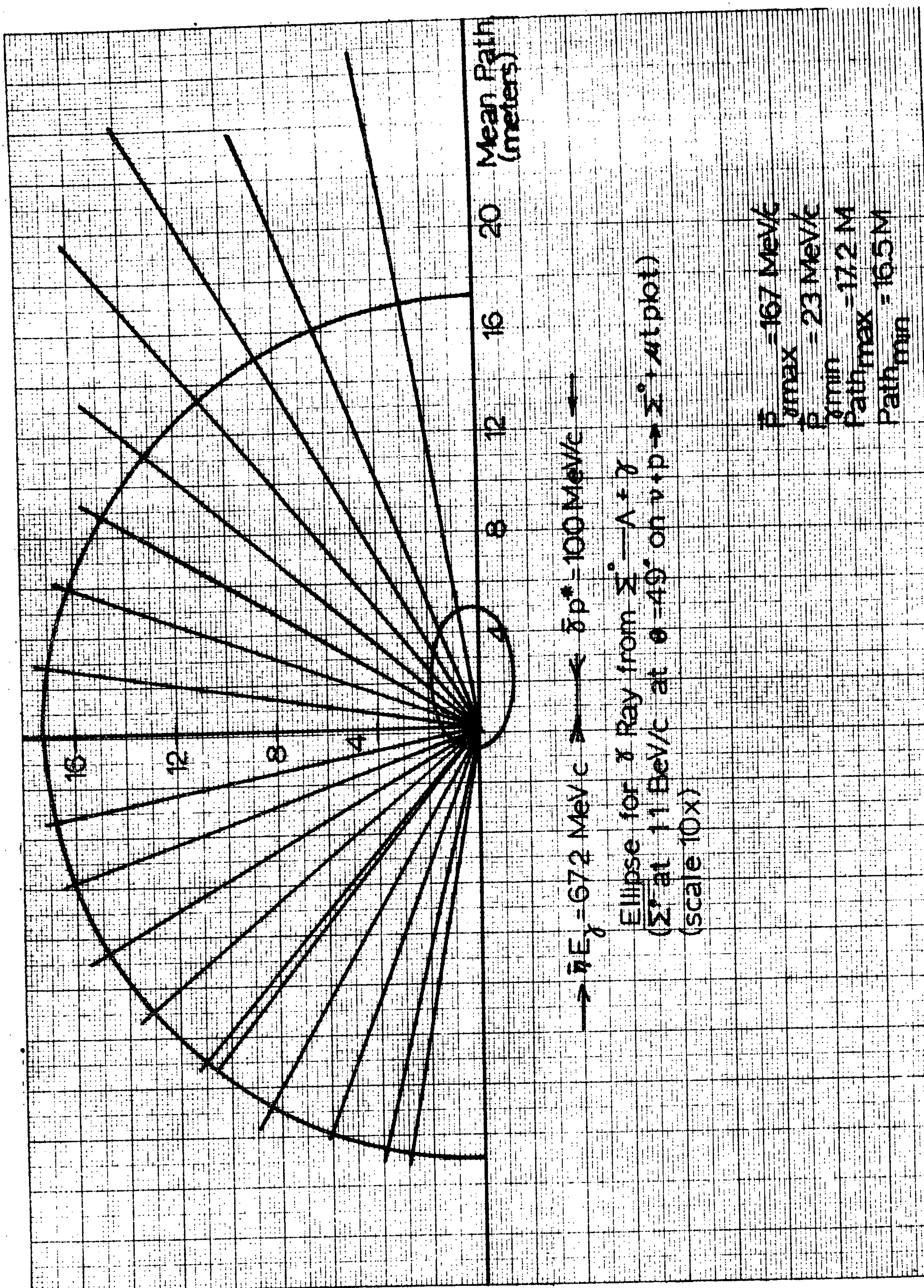

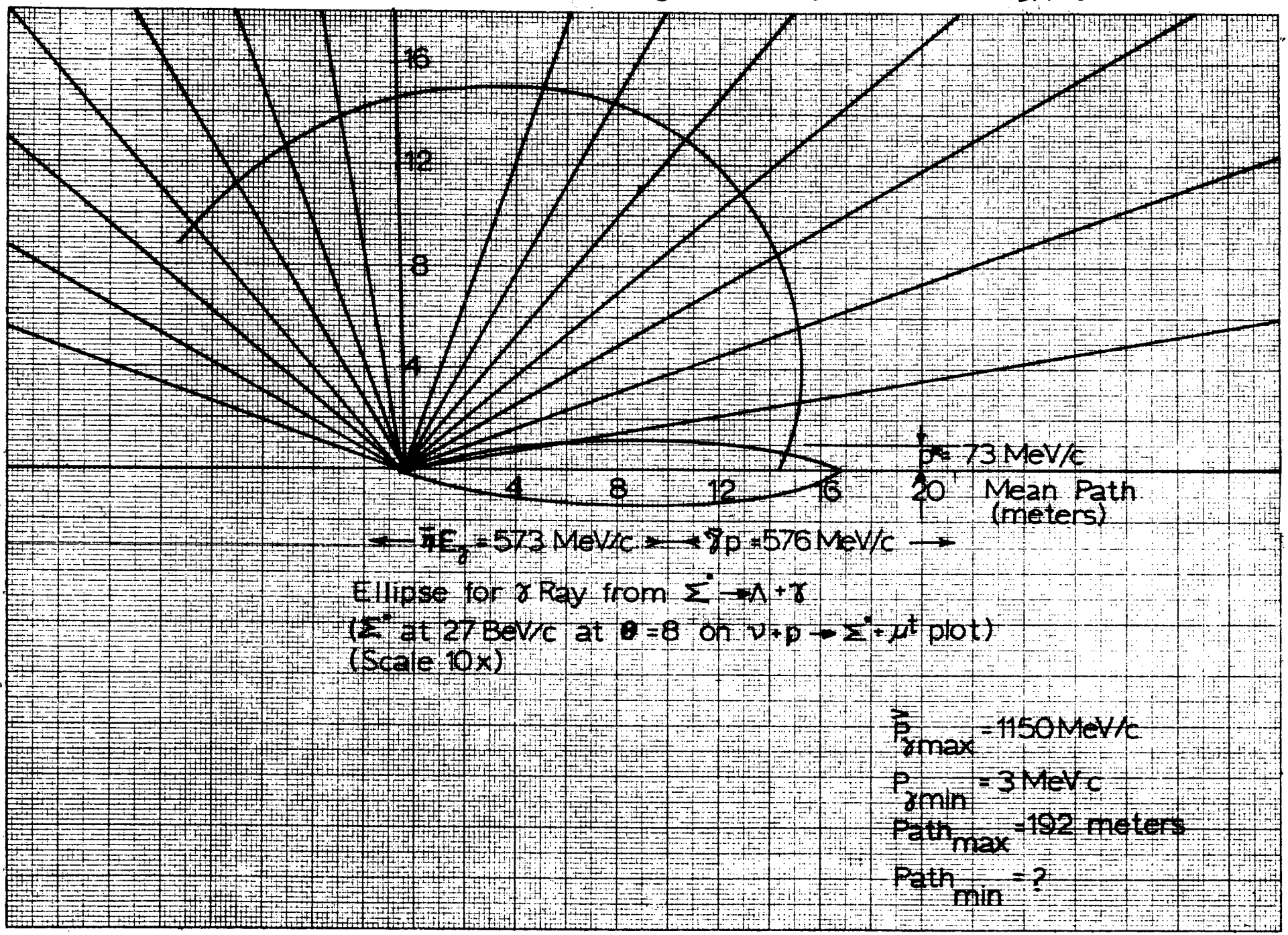
Mean Path in Hydrogen of γ Ray from ν+p → Σ⁺+μ⁺, Σ⁺ → Λ+γ
16
12
8
4
4
8
12
16
20
Mean Path (meters)
p = 73 MeV/c
← π E_γ = 573 MeV/c → ← γp = 576 MeV/c →
Ellipse for γ Ray from Σ⁺ → Λ + γ
(Σ⁺ at 27 BeV/c at θ = 8° on ν + p → Σ⁺ + μ⁺ plot)
(Scale 10x)
P_γmax = 1150 MeV/c
P_γmin = 3 MeV c
Path_max = 192 meters
Path_min = ?

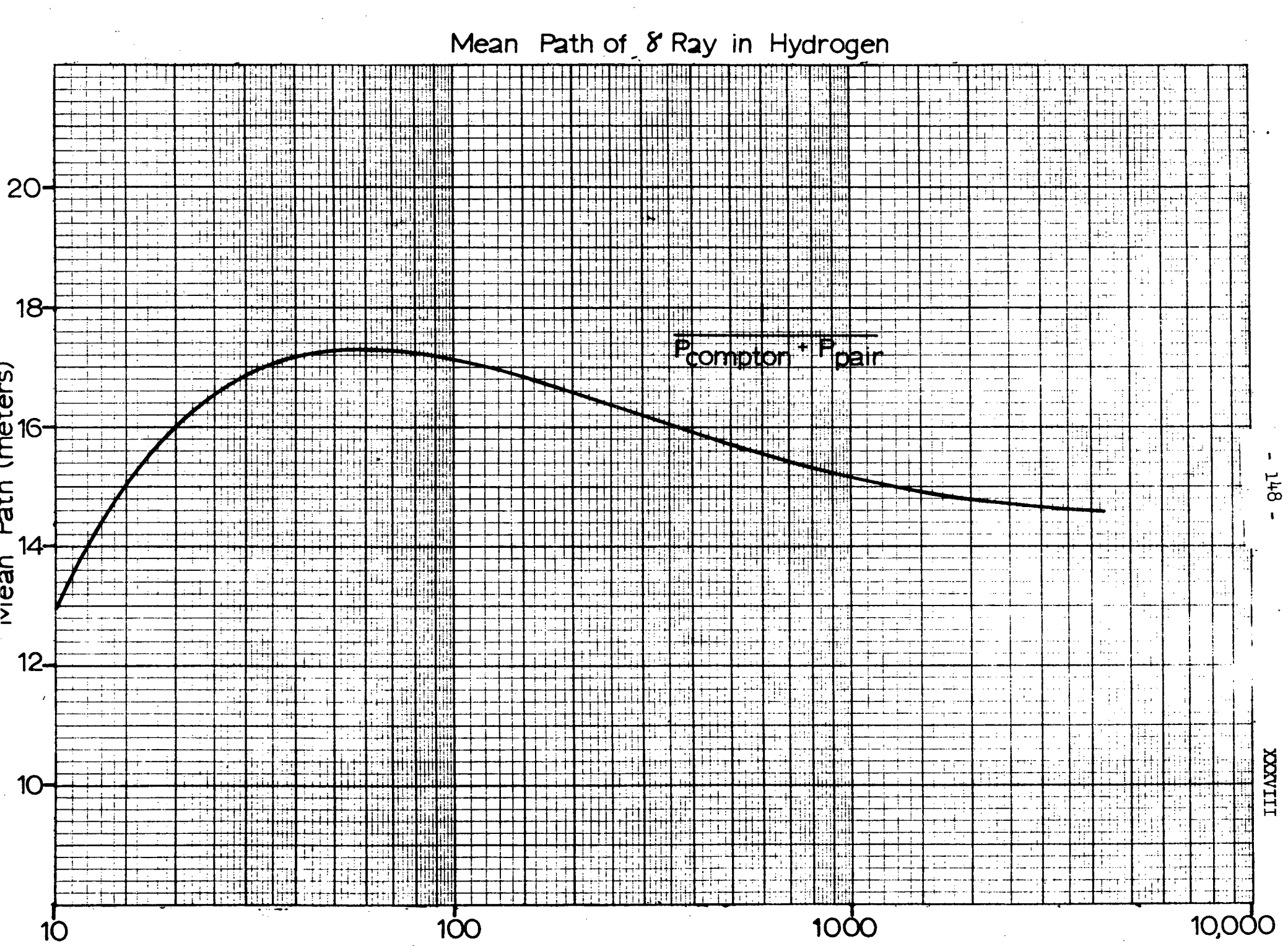
Mean Path of δ Ray in Hydrogen
Mean Path (meters)
20
18
16
14
12
10
10
100
1000
10,000
$\overline{P_{comptor} + P_{pair}}$

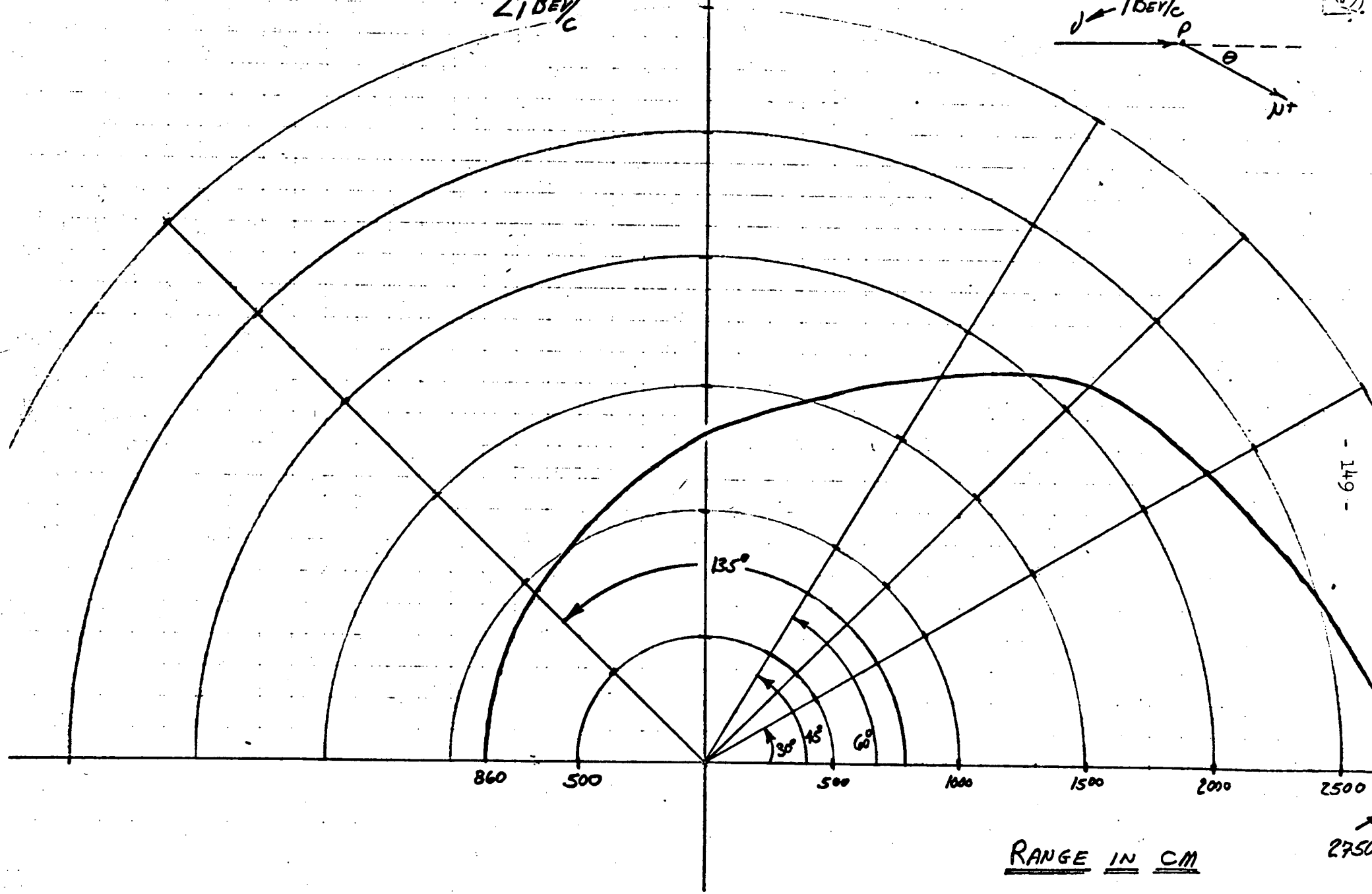
2.1 BEV/c
1 BEV/c
p
θ
π+
135°
30°
45°
60°
860
500
500
1000
1500
2000
2500
2750
RANGE IN CM

$p + p \rightarrow \Delta(1238) + p$ (① ② ③ ④) at 10^3 BeV/c ($= p_1$)

$\Delta \rightarrow p + \pi^0 \rightarrow \mu\mu$ (③ ⑤ ⑥ ⑦⑧)

$\bar{\beta} = \dfrac{p_1}{E_1 + E_2}$, $E_1 = \sqrt{p_1^2 + M_1^2}$, $E_2 = M_2$

$\bar{\gamma} = \dfrac{1}{\sqrt{1-\bar{\beta}^2}}$; $\bar{\eta} = \bar{\gamma}\bar{\beta}$

$M_1 = 0.9382 = M_2 = M_4 = M_5$

$M_3 = 1.238$

$M_6 = 0.13500$

$M_7 = M_8 = 0.000$

$$M^* = E^* = \frac{E_1 + E_2}{\bar{\gamma}}$$

$$p^* = \frac{1}{2M^*}\left\{(M^* + M_3 + M_4)(M^* - M_3 + M_4)(M^* + M_3 - M_4)(M^* - M_3 - M_4)\right\}^{1/2}$$

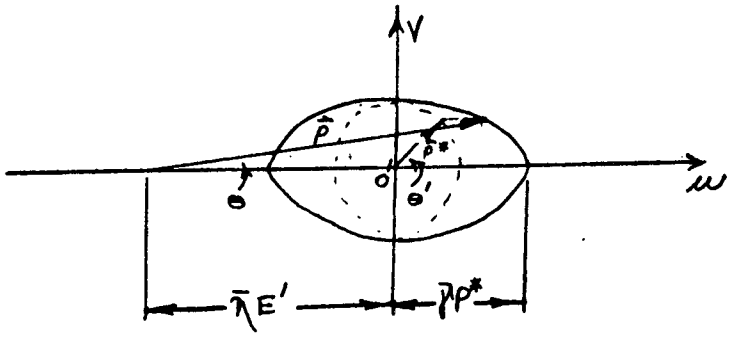

$$\boxed{\begin{aligned} w &= \bar{\gamma} p_w^* = \bar{\gamma} p^* \cos\theta' = p\cos\theta - \bar{\eta}E' \\ V &= p_V^* = p^* \sin\theta' = p\sin\theta \end{aligned}} \qquad (1)$$

Equation of an ellipse:

$$\frac{w^2}{(\bar{\gamma}p^*)^2} + \frac{V^2}{(p^*)^2} = 1$$

$$\Rightarrow \frac{(p\cos\theta - \bar{\eta}E')^2}{(\bar{\gamma}p^*)^2} + \frac{(p\sin\theta)^2}{(p^*)^2} = 1$$

$$\Rightarrow p^2\cos^2\theta - 2\bar{\eta}E'p\cos\theta + (\bar{\eta}E')^2 + (\bar{\gamma}p\sin\theta)^2 = (\bar{\gamma}p^*)^2$$

$$\Rightarrow p^2(\cos^2\theta + \bar{\gamma}^2\sin^2\theta) - p(2\bar{\eta}E'\cos\theta) + (\bar{\eta}E')^2 - (\bar{\gamma}p^*)^2 = 0$$

$$\Rightarrow p = \frac{2\bar{\eta}E'\cos\theta \pm \sqrt{4\bar{\eta}^2E'^2\cos^2\theta - 4(\cos^2\theta + \bar{\gamma}^2\sin^2\theta)(\bar{\eta}^2E'^2 - \bar{\gamma}^2p^{*2})}}{2(\cos^2\theta + \bar{\gamma}^2\sin^2\theta)}$$

$$\Rightarrow \boxed{p = \frac{\bar{\eta} E \cos\theta \pm \bar{\mu}\sqrt{p^{*2}(\cos^2\theta + \bar{\mu}^2\sin^2\theta) - \sin^2\theta\,\bar{\eta}^2 E'^2}}{(\cos^2\theta + \bar{\mu}^2\sin^2\theta)}} \quad (2)$$

$$p^2(\cos^2\theta + \sin^2\theta) = \bar{\eta}^2 E'^2 + 2\bar{\eta}E'\bar{\mu}p^*\cos\theta' + p^{*2}\sin^2\theta' + \bar{\mu}^2 p^{*2}\cos^2\theta'$$

$$\Rightarrow \boxed{p = \pm\sqrt{p^{*2}(\sin^2\theta' + \bar{\mu}^2\cos^2\theta') + 2\bar{\eta}E\bar{\mu}p^*\cos\theta' + \bar{\eta}^2 E'^2}} \quad (3)$$

$$\frac{p^*\sin\theta'}{\bar{\mu}p^*\cos\theta'} = \frac{p\sin\theta}{p\cos\theta - \bar{\eta}E'}$$

$$\Rightarrow \tan\theta' = \frac{\bar{\mu}p\sin\theta}{p\cos\theta - \bar{\eta}E'}$$

$$\Rightarrow \boxed{\theta' = \arctan\frac{\bar{\mu}p\sin\theta}{p\cos\theta - \bar{\eta}E'}} \quad (4)$$

$$\frac{p\sin\theta}{p\cos\theta} = \frac{p^*\sin\theta'}{\bar{\eta}E' + \bar{\mu}p^*\cos\theta'} \cdot \tan\theta$$

$$\Rightarrow \boxed{\theta = \arctan\frac{p^*\sin\theta'}{\bar{\eta}E' + \bar{\mu}p^*\cos\theta'}} \quad (5)$$

XLii (3)

To find θ_{max} -

$$p^{*2}(\cos^2\theta + \bar{\gamma}^2 \sin^2\theta) = \sin^2\theta\, \bar{\eta}^2 E'^2$$

$$\Rightarrow p^{*2}(\cot^2\theta + \bar{\gamma}^2) = \bar{\eta}^2 E'^2$$

$$\Rightarrow \cot^2\theta = \frac{\bar{\eta}^2 E'^2}{p^{*2}} - \bar{\gamma}^2$$

$$\Rightarrow \tan\theta = \frac{1}{\sqrt{\frac{\bar{\eta}^2 E'^2}{p^{*2}} - \bar{\gamma}^2}}$$

$$\Rightarrow \boxed{\tan\theta_{MAX} = \frac{p^*}{\sqrt{(\bar{\eta}E')^2 - (\bar{\gamma}p^*)^2}}} \quad (6)$$

$$\tan\theta_{MAX} = \frac{p^* \sin\theta_0'}{\bar{\eta}E' + \bar{\gamma}p^*\cos\theta_0'} = \frac{p^*}{\sqrt{(\bar{\eta}E')^2 - (\bar{\gamma}p^*)^2}}$$

$$(\sin\theta_0')\sqrt{(\bar{\eta}E')^2 - (\bar{\gamma}p^*)^2} = \bar{\eta}E' + \bar{\gamma}p^*\cos\theta_0'$$

$$\Rightarrow (\sin^2\theta_0')[(\bar{\eta}E')^2 - (\bar{\gamma}p^*)^2] = (\bar{\eta}E')^2 + 2\bar{\eta}E'\bar{\gamma}p^*\cos\theta_0' + (\bar{\gamma}p^*)^2\cos^2\theta_0'$$

$$\Rightarrow (\sin^2\theta_0' - 1)(\bar{\eta}E')^2 - \sin^2\theta_0'(\bar{\gamma}p^*)^2 - 2\bar{\eta}E'\bar{\gamma}p^*\cos\theta_0' + (\bar{\gamma}p^*)^2\cos^2\theta_0'$$

$$\Rightarrow 2\bar{\eta}E'\bar{\gamma}p^*\cos\theta_0' + (\bar{\gamma}p^*)^2\cos^2\theta_0' + \cos^2\theta_0'(\bar{\eta}E')^2 + \sin^2\theta_0'(\bar{\gamma}p^*)^2 = 0$$

$$\Rightarrow \cos^2\theta_0'(\bar{\eta}E')^2 + 2\bar{\eta}E'\bar{\gamma}p^*\cos\theta_0' + (\bar{\gamma}p^*)^2 = 0$$

$$\Rightarrow \cos\theta_0' = \frac{-\bar{\gamma}\bar{\gamma}E'\bar{\beta}p^* \pm \sqrt{4\bar{\gamma}^2E'^2\bar{\beta}^2p^{*2} - 4(\bar{\gamma}E')^2(\bar{\beta}p^*)^2}}{2(\bar{\gamma}E')^2}$$

$$\Rightarrow \boxed{\cos\theta_0' = -\frac{\bar{\beta}p^*}{\bar{\gamma}E'}} \quad (7)$$

θ_0' corresponding to θ_{max}

$$\sin\theta_0' = \sqrt{1-\cos^2\theta_0'}$$

$$= \sqrt{1-\left(\frac{\bar{\beta}p^*}{\bar{\gamma}E'}\right)^2}$$

$$\Rightarrow \tan\theta_0' = \frac{-(\bar{\gamma}E')\sqrt{(\bar{\gamma}E')^2-(\bar{\beta}p^*)^2}}{(\bar{\beta}p^*)(\bar{\gamma}E')}$$

$$\Rightarrow \boxed{\tan\theta_0' = -\frac{\sqrt{(\bar{\gamma}E')^2-(\bar{\beta}p^*)^2}}{\bar{\beta}p^*}} \quad (8)$$

$p + p \rightarrow \Delta(1238) + p$ at 1000 Bev/c

E_1	$\bar{\beta}$	$\bar{\gamma}$	$\bar{\gamma}$	M^*c^2	p^*	E'_Δ	E'_p	$\bar{\gamma}p^*$	$\bar{\gamma}E'_\Delta$	$\bar{\gamma}E'_p$
1000.	0.9991	23.10	23.07	43.34	21.64	21.68	21.66	499.8	500.2	499.8

(IN UNITS OF Bev)

$\Delta(1.238) \rightarrow p + \pi^\circ$

$M^{**}c^2$	p^{**}	E'_p	E'_π
1.238	0.2348	0.9672	0.2708

$\pi^\circ \rightarrow \gamma + \gamma$

$M^{***}c^2$	p^{***}	E'_γ
0.1350	0.0675	0.0675

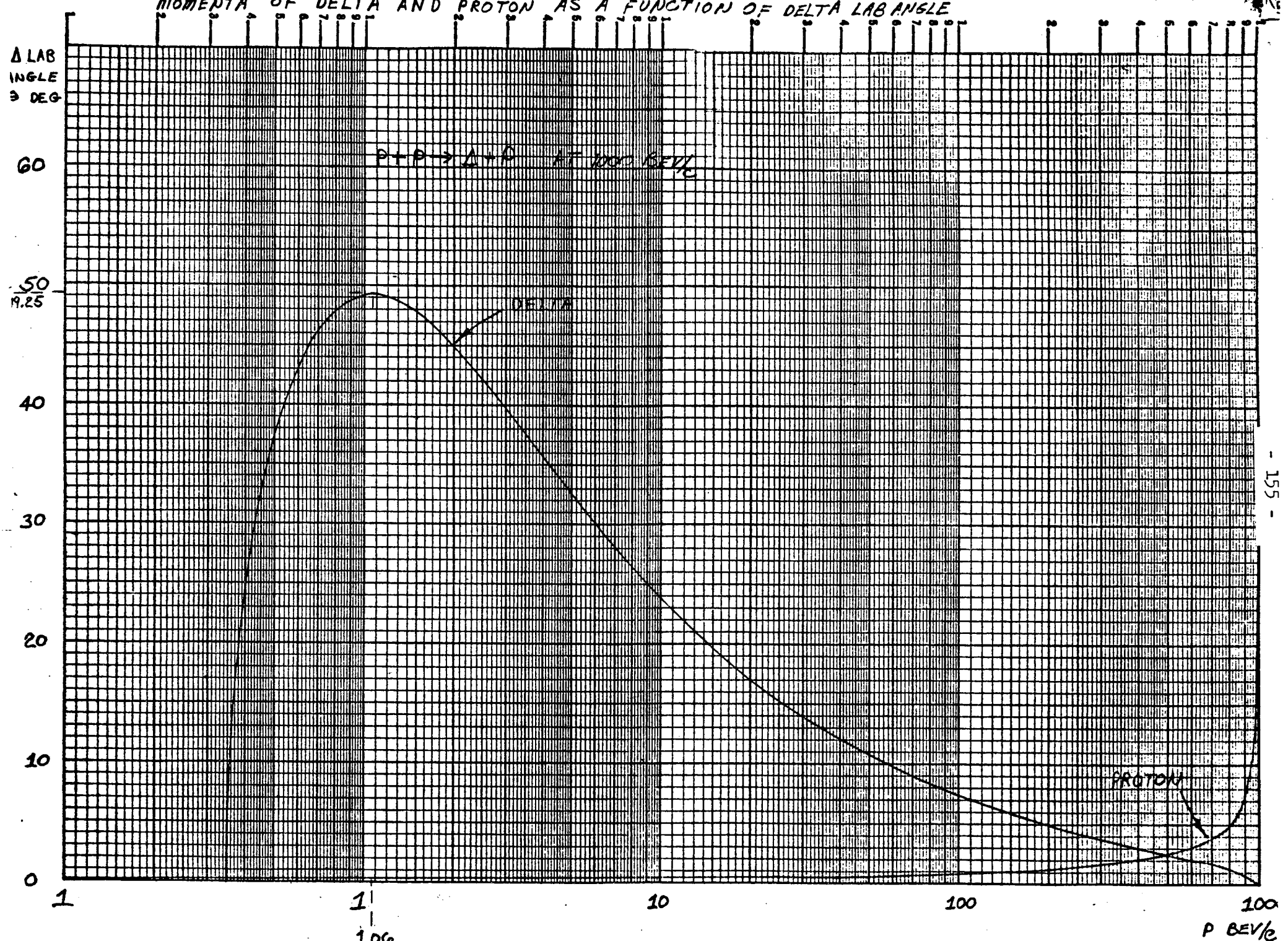
MOMENTA OF DELTA AND PROTON AS A FUNCTION OF DELTA LAB ANGLE
Δ LAB INGLE 3 DEG
60
50
19.25
40
30
20
10
0
p+p→Δ+0 AT 200 BEV/c
DELTA
PROTON
1
1
10
100
100
1 DG
P BEV/c

Explanation of Fortran Symbols Used in Program Delta

Fortran	Explanation	Fortran	Explanation
W1	M_1 (mass of incident proton)		DELTA, "+" solution to
W2	M_2 (mass of rest proton)		equation #2 pg 2)
W3	M_3 (mass of delta)	P3B	P_3 ("-" solution to eq
W4	M_4 (mass of exit proton)	TP3A, TP3B	corresponding θ_Δ' for
P1	P_1 (incident momentum of M_1)		delta of momentum P
			P3B (Eq. #4 pg 2)
P2	P_2 (momentum of M_2)	TP3A1D, TP3A2D	TP3A in degrees
E1	E_1 (total energy of M_1)	TP3BD	TP3B in degrees
		TP4A1D, TP4A2D; TP4BD	corresponding θ_p' fo
E2	E_2 (total energy of M_2)		proton in degrees f
			delta momentum P3A
BB	$\bar{\beta}$ (cm beta)		P3B
GG	$\bar{\gamma}$ (cm gamma)	TP4A1, TP4A2, TP4B	TP4A1D, TP4A2D, TP4B
YY	$\bar{\eta}$ (cm nu)		in radians
EZ	$E^* = (E_1 + E_2)/\bar{\gamma}$	T4A1, T4A2, T4B	corresponding θ_p fo
WZ	$M^* = E^*$		proton in radians
PZ	p^* (momentum in cm)	T4A1D; T4A2D1, T4A2D2;	T4A1; T4A2; T4B in
EZ3	E_Δ' (enegy of M_3 in cm)	T4BDEG	degrees
EZ4	E_p' (enegy of M_4 in cm)	P4A1, P4A2, P4B	corresponding momen
X1	$\bar{\gamma} p^*$		of proton for $\theta_p' =$
X2	$\bar{\eta} E_\Delta'$		T4A1, T4A2, T4B
X3	$\bar{\eta} E_p'$	T3MAX	θ maxiumum for delt
T3	Angle θ for delta (in radians)		(in radians)
		TP3MAX	corresponding θ' fo
T3DEG	θ in degrees		delta, for θ=T3MAX
DEL	.5 degrees in Radians		(in radians)
DEL DEG	.5 degrees	P3MAX	corresponding delta
P3A	P_3 (momentum of		momentum

FORTRAN	EXPLANATION
T3MAXD, TP3MXD	T3MAX, TP3MAX IN DEGREES
TP4MXD	CORRESPONDING θ' FOR PROTON (IN DEGREES)
TP4MAX	TP4MXD IN RADIANS
T4MAX	CORRESPONDING θ FOR PROTON (IN RADIANS)
T4MAXD	T4MAX IN DEGREES
P4MAX	CORRESPONDING MOMENTUM OF PROTON
TP	θ' (AS MEASURED FOR Δ)
U, V	COORDINATES OF PRODUCTION ELLIPSE
W5	M_5 (MASS OF 2ND EXIT PROTON)
W6	M_6 (MASS OF π^0)
EZZ	E^{**}
WZZ	$M^{**}=E^{**}$
PZZ	p^{**}
EZ5	E'_p (ENERGY OF M_5 IN CM)
EZ6	E'_{π^0} (ENERGY OF M_6 IN CM)
TP3	θ' FOR DELTA (IN RADIANS)
JTP3DEG	θ' IN DEGREES
DELT	15° IN RADIANS
JDELT	15 DEGREES
TH3	θ FOR DELTA CORRESPONDING TO θ' ABOVE (IN RADIANS)
TH3DEG	TH3 IN DEGREES
P3	CORRESPONDING MOMENTUM OF DELTA
XNU1, GAMMA1, BETA1	γ, γ', β FOR DELTA
X4(I)	γp^{**}
X5(I)	$\gamma E'_p$
X6(I)	$\gamma E'_{\pi^0}$
T5MAX, T6MAX	θ MAXIMUM FOR p, π^0 FOR GIVEN θ (OF DELTA)
W7	M_7 (MASS OF δ^1)
W8	M_8 (MASS OF δ^1)
EZZZ	E^{***}
WZZZ	$M^{***}=E^{***}$
PZZZ	p^{***}
EZ7	E'_μ (ENEGY OF M_7 IN CM)
EZ8	E'_μ (ENEGY OF M_8 IN CM)
P6MAX(K)	MAXIMUM MOMENTUM OF π^0 FOR GIVEN θ (OF DELTA)
P5MIN(K)	CORRESPONDING MOMENTUM OF PROTON
XNU2A, GAM2A, BETA2A	γ, γ', β FOR π^0 OF MOMENTUM P6MAX(K)
X7A, X8A, X9A	$\gamma p^{***}, \gamma E'_\mu, \gamma E'_\mu$
P7AMAX, P7AMIN	MAXIMUM AND MINIMUM MOMENTUM OF δ RAY FROM π^0 OF MOMENTUM P6MAX

D. TARGETING, EXPERIMENTAL AREAS, AND FACILITIES

V International Conference on High Energy Accelerators - Frascati (Italy)

UCRL-16223

UNIVERSITY OF CALIFORNIA

Lawrence Radiation Laboratory
Berkeley, California

AEC Contract No. W-7405-eng-48

THE DESIGN OF EXPERIMENTAL FACILITIES AT THE PROPOSED 200-GeV ACCELERATOR

Denis Keefe

August 25, 1965

UCRL-16223

THE DESIGN OF EXPERIMENTAL FACILITIES AT THE PROPOSED 200-GeV ACCELERATOR

Denis Keefe

Lawrence Radiation Laboratory
University of California
Berkeley, California

August 25, 1965

I. Introduction

The basic starting point in trying to define and specify the nature of the experimental areas and facilities is to consider, first, the output of the accelerator--viz., types and fluxes of various elementary particles--and second, the ways in which these particles might conceivably be used. The abundance and distribution of particles produced in high-energy interactions have a vital influence on the shielding configuration (especially, close to targets), on how efficient targeting arrangements can be achieved for high-energy particle beams, and on the nature of experimental activity, since this is largely controlled by the qualities of the available beams. Although it is impossible to be prescient about the experiments of most interest in physics a decade from now, one can nevertheless proceed quite far in exploring the general properties of beams and certain boundary conditions associated with them, at least in terms of the known elementary particles. A second aspect of the experimental use, which was a necessary ingredient of the 200-GeV Accelerator Design Study, is the consideration of the level of use, viz., the number of experimental arrangements which could be set up and how many could operate simultaneously within broad limits. This helps define whether the number of experimental areas in the design is too meager or too lavish.

II. Particle Production at High Energies

The measurements of fluxes of secondary particles as a function of angle and momentum produced by high-energy protons still leaves a lot to be desired. The data obtained by Dekkers et al.[1] are the most useful set because they included measurements at 0 deg production angle. Their results indicate that at CPS energies there are two components, one of low energy and one of high energy in the c. m. system, in the production of pions and kaons. Using this model and making certain assumptions about how to extrapolate it to 200 GeV, Trilling[2] has arrived at estimates of particle production for pions and kaons. Data from the same experiment were also used to estimate proton (neutron) and antiproton fluxes. These forecasts are shown in Figs. 1, 2, and 3. In the meson flux extrapolations, the effect of the separation of the two energy components (in the laboratory system) at high energies can be seen. For comparison, the form predicted by the Cocconi-Koester-Perkins formula[3] is also shown. An interesting feature of the more recent extrapolation is that the expressions for the double differential cross sections all contain terms of the type $\exp(-\text{const.}\ \theta^2)$ and only the terms describing the high-energy component of the pions contains the familiar term $\exp(-\text{const.}\ \theta)$ predicted in Ref. 3. The value of the mean transverse momentum associated with this high-energy term alone is about 0.5 GeV/c, rather higher than hitherto assumed.

III. Targeting

It is fair to assume that a 200-GeV accelerator should be optimized to provide beams in the energy regions beyond the efficient reach of the CPS or AGS, say above 15 to 20 GeV/c. (Beams of lower energy are, of course, obtainable as easily as at present accelerators.) Targeting problems arise, then, because high-energy secondary particles are

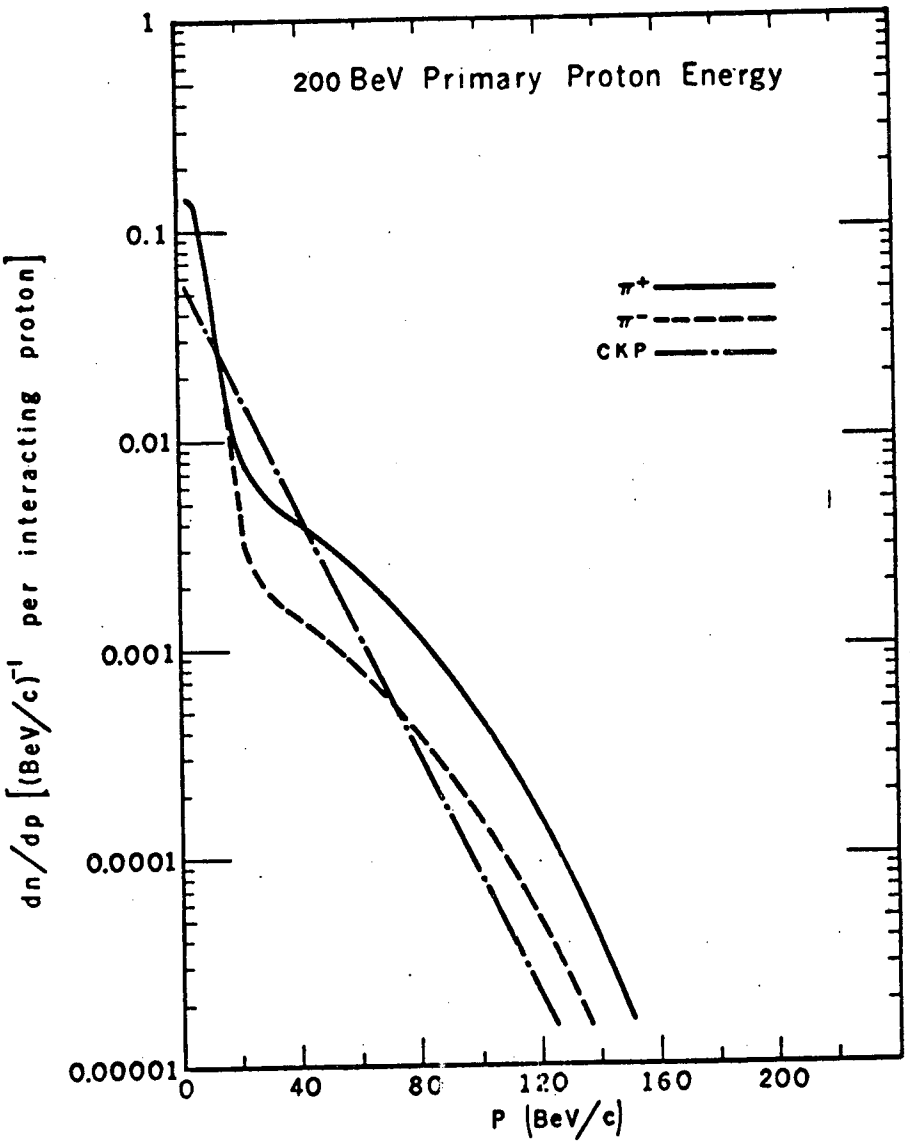

Secondary Pion Momentum Spectrum
Integrated Over All Angles

Fig. 1 MUB-6402

Figure Captions

Fig. 1. Secondary pion momentum spectrum dn/dp. The kaon spectrum is assumed to be one-tenth of this.

Fig. 2. Secondary proton momentum spectrum.

Fig. 3. Secondary antiproton momentum spectrum.

Fig. 4. Internal multiple-traversal target efficiency for different energies of the circulating beam. Note the drastic reduction in efficiency at reduced primary energy.

Fig. 5. External target efficiency (RYE) for different materials of different lengths (measured in terms of the nuclear absorption length, λ). The standard of reference is a perfectly efficient internal multiple-traversal target--RYE = 1.

Fig. 6. Proposed configuration of the experimental areas at three adjacent straight sections (H, I, and J).

Fig. 7. The internal target area with some hypothetical-beam layouts.

Fig. 8. A backstop area in the EPB.

Fig. 9. The long EPB area, showing the switchyard.

Fig. 10. Some typical beams originating from one of the backstops in the long EPB area (after A. L. Read).

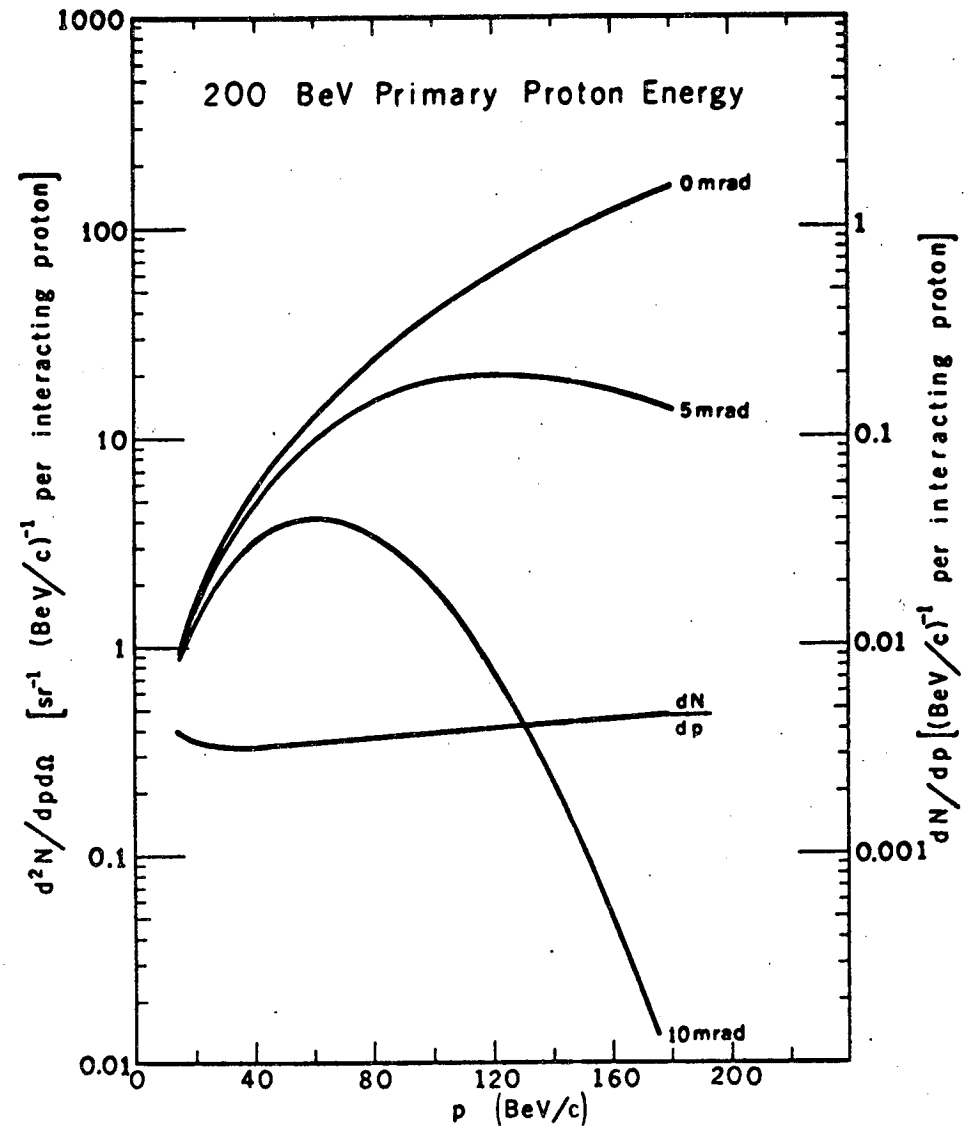

Secondary Proton Momentum Spectrum

Fig. 2 MUB-6403

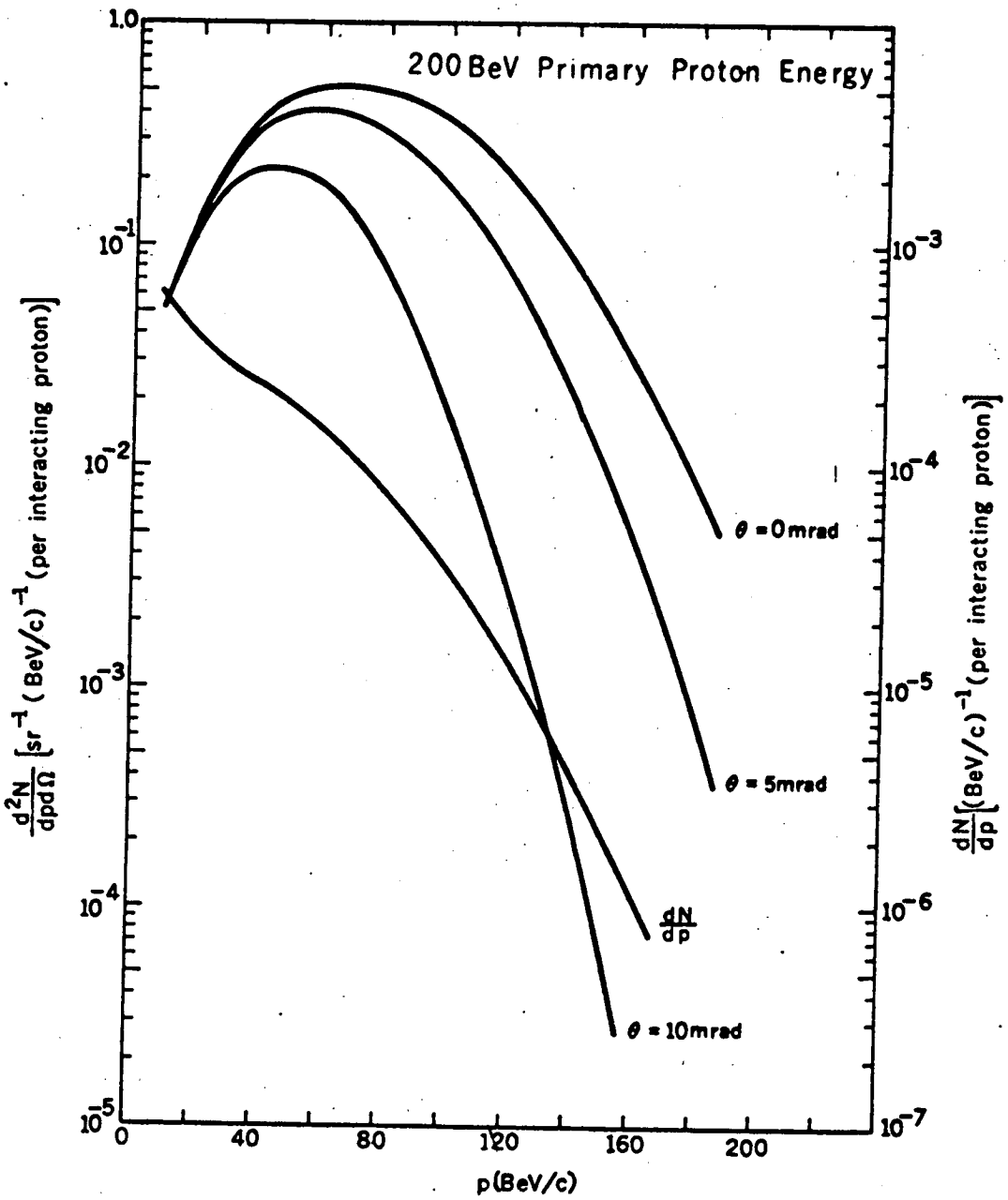

Secondary Antiproton Momentum Spectrum

Fig. 3

MUB-6404

produced in abundance only at very small angles to the forward direction. If we define a "typical" angle of production $a = 0.25/p$ (where p is in GeV/c), then about one-third of the flux is contained within a cone of half-angle a and more than half within a cone 2a. A secondary beam which can capture one-third the available flux when looking at 0-deg production angle will capture only 1% of the flux if forced to look at the target at an angle about 3a to 4a.

For a secondary momentum of 100 GeV/c, a is 2.5 mrad. In using a target in a field-free straight section, either in the internal or external beam, it is difficult to set up equipment at production angles less than 10 mrad, and if several experimenters are using the same target, most must accept much larger angles. Thus yields from targets in a straight section are certain to be inefficient.[4] This inefficiency is a consequence of the fact that the angle of production is small and is therefore a poor effect to exploit to achieve spatial displacement between the primary proton beam and the desired secondary beam. Magnetic fields supply a much more powerful means of creating physical displacement. In a field of B (tesla) of length L (meters), the angle of bend is

$$\phi = \frac{BL}{B\rho} = \frac{3BL}{10p} = a, \text{ if } BL = 0.8.$$

Thus a field of 1.6 T just 0.5 meter long is sufficient to give angular deflections comparable to the production angle. A field a few meters long is therefore sufficient to cause angular deflection of secondary particles much greater than attainable by using production-angle effects. In particular, for a secondary beam, the entire forward cone can be diverted away from the proton beam, and capture into the secondary channel can be achieved

at a production angle of 0 deg. Thus targeting in a magnetic field can be highly efficient. There are three obvious ways in which to achieve this: first, to use a target in the gradient-magnet part of the accelerator; second, to use a group of bending magnets in a Collins straight section;[3] and, third, to use target magnets in the external beam.[4] The last allows the most flexible arrangement and minimizes the coupling of the secondary beams with the accelerator.

For this reason, considerable effort has been expended on a critical examination of the relative advantages of internal and external beam operation and how far the desirable features associated with internal beam operation at AG synchrotrons can be achieved externally. In brief, the conclusion is that the major part of the physics program can be operated with assurance, and often with advantages, externally, but that at the moment one cannot eliminate from the design some sort of internal area, however rudimentary. When this study was begun the external proton beam (EPB) at the Cosmotron was being used and preliminary work with the Bevatron external beam being begun. The later experiments and discoveries about the efficiency of resonant extraction from AG machines greatly bolstered the arguments described below.

First, a major emphasis on the use of external beams provides critical advantages in the preservation of the accelerator (namely, ease of maintenance, lifetime of components, and minimum interferences with operation) and in the overall running efficiency of the accelerator and physics program. These advantages are:

(i) Because internal-target areas are directly coupled to the main ring, the accelerator must be turned off to allow setup or repair of the front end of an experiment. The unstacking of the enormous mass of shielding and

the handling and surveying of equipment in a radioactive environment involve shutdown times of several weeks. Conversely, if troubles develop in the early transport sections of an experiment, repairs will have to be delayed until a shutdown of substantial length can be negotiated. The more internal-target areas there are, the more interferences with continuous beam operation will follow. Since similar disadvantages are associated with a single EPB area, it is desirable to have a minimum of two extracted beams. Each of the two external beams--and, independently, certain of the target areas in each beam--can be easily turned off without halting operation of the internal beam and with only partial interruption to the experimental program.

(ii) Work in an internal-target area must be started immediately after turnoff because accelerator time is at a premium; this is the time of highest radioactivity. In an external area, a cool-down period of several days is not difficult to arrange.

(iii) If the extraction efficiency is approximately 90% for slow beams and approximately 100% for fast beams, the induced activity and the radiation damage in the accelerator are smaller by a factor of approximately 20 than for internal targets, for both local and distributed losses. Development of the extraction system to permit simultaneous extraction in two separate straight sections is possible with a doubling of the total beam loss.

(iv) Movement and restacking of large amounts of shielding close to a target can result in misalignments of neighboring magnets. This may be annoying but tolerable in an external beam, which the protons traverse only once, but intolerable in the main ring. An allied effect, also resulting in closed-orbit deviations, arises from the proximity of pieces of

experimenters' equipment to the target, such as separators or magnets with stray fields. Again the EPB is much less sensitive to this effect.

(v) In the external-beam target areas, crane handling is freed of the restrictions of the magnet structure and enclosure, and also from the maximum pressure for reassembly of the shielding in the shortest possible time.

Second, there are also distinct gains in the ease of targeting.

(i) The cooling problem is reduced in proportion to the single-to-multiple traversal ratio. Further the freedom of access to the EPB vacuum chamber allows the use of more complicated target arrangements, e.g., a ribbon target cooled from the edges and through radiation to surfaces placed nearby, above and below it.

(ii) For plunge or flip targets the travel distance need be only a few millimeters, because allowances for a large beam at injection are not needed.

(iii) A system using small deflecting magnets and the long lever arms available in the EPB can be used to achieve rapid and controlled switching from target to target, thereby minimizing the need for mechanically moved targets. Such a system is in one-to-one correspondence with the methods applied to control of spills from many internal targets by using closed-orbit perturbations.

Third, from the experimenters' point of view, the main advantages of using external beams can be summarized as follows:

(i) Access to 0-deg production angle for both positive and negative beams, a necessity for high energies, is easily achieved by means of a targeting magnet in the external beam.

(ii) Very good target optics (transverse target size of the order of 0.005 in.) are possible, because the external beam has small emittance and can be focused. If the emittance of the external beam is πA, then it can be matched into a target of height $h = 2\sqrt{AL}$. With A = 0.03 mm-mrad and L = 15 cm, then h = 0.13 mm = 0.005 in.

(iii) A single-target efficiency very close to that obtainable with a multiple-traversal internal target can be obtained. In general, the accelerator productivity integrated over all experiments can be as good as the best achievable internally. The internal and external target efficiencies for a single target in the 200-GeV design are shown in Figs. 4 and 5 respectively. Note, however, that with multiple targets, at most 74% of the protons can be usefully employed internally but the extracted protons can essentially all be used.[6]

(iv) For low-energy (0 to 30 GeV) parasitic experiments with decoupled secondary momenta, operation off a "straight section" target in the external beam allows access to smaller angles of production than internally, because the smaller size of vacuum chamber constitutes a smaller transverse interference.

(v) The possibility of rebuilding the configuration of the target magnets to cater to special experimental setups is an important illustration of the flexibility of external-beam targeting. The EPB channel has constraints, but these still allow considerable latitude in the positioning of the individual magnets making up the target-magnet complex. These magnets can be interchanged or moved apart, or, for special reasons, a very-high-field short magnet can be substituted in their place.

(vi) Another form of rebuilding of the target station is possible when maximum flux is of utmost importance. The target can be moved upstream

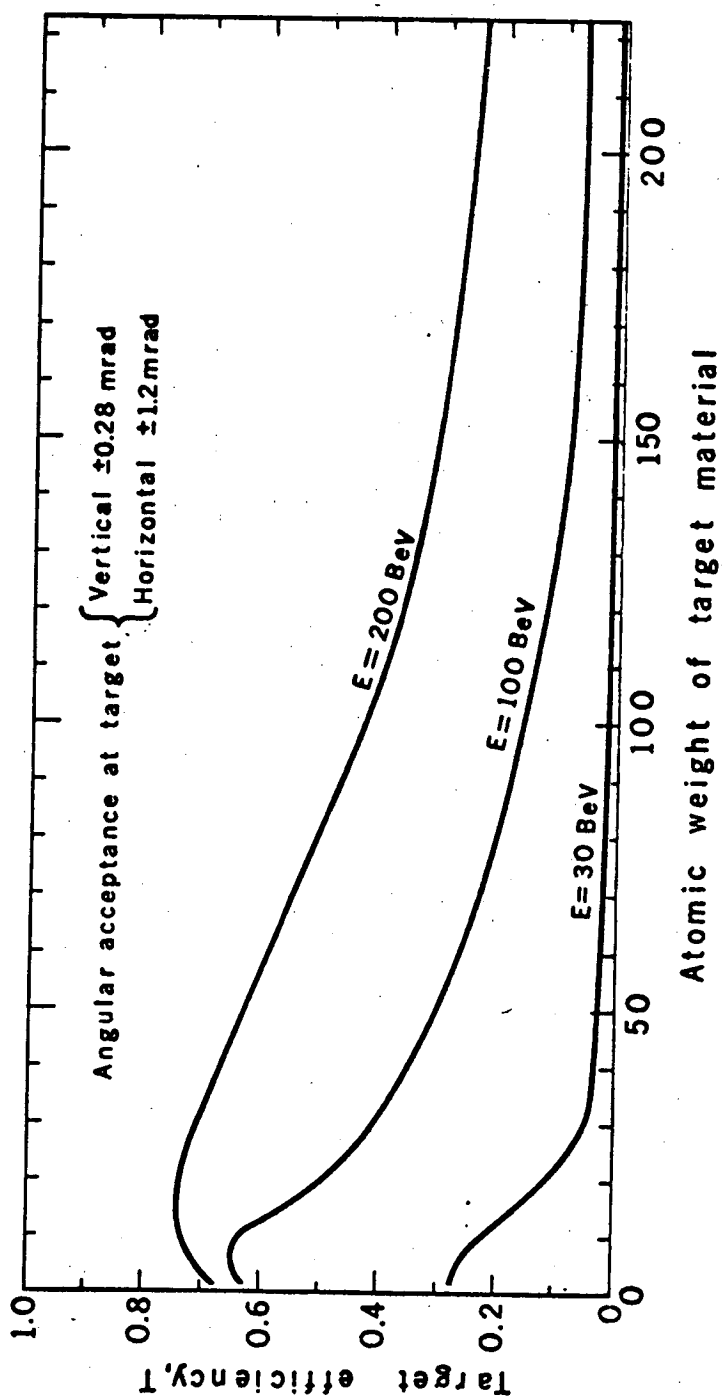

Internal-Target Efficiency, T,
as a Function of Atomic Weight

Fig. 4

MUB-6409

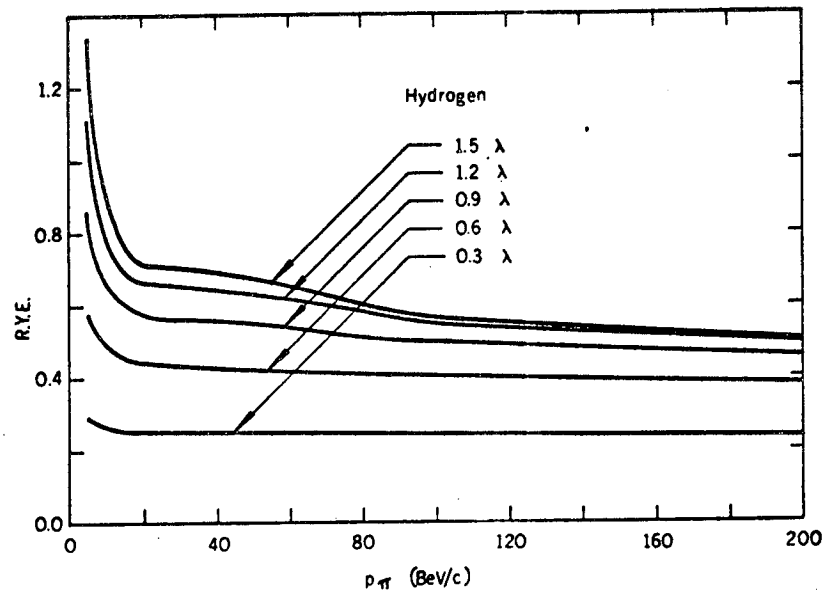

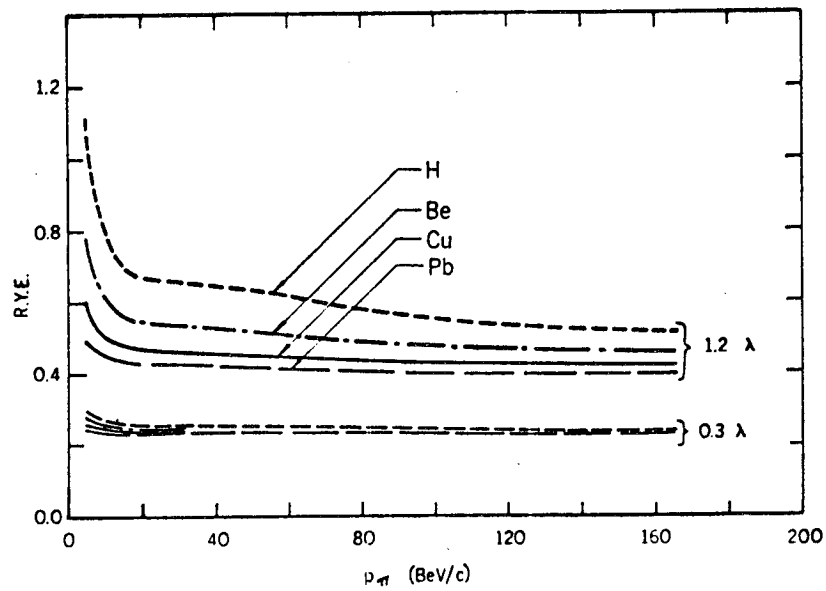

R.Y.E. for Pions

Fig. 5

MUB-6466

from the target magnet and a quadrupole placed between target and magnet. Thus focusing of the secondary beam can begin before dispersion. In some cases it may be necessary to have it only 2 to 3 m from the target, whereas downstream from the target magnet, the quadrupole is required to be $\gtrsim$ 10 m away.

(vii) Multiple secondary-beam setups are easily achieved because the target magnet fans out beams of different momenta and charge. There is a distinction between the number of secondary beams operating from a given target (for example, between three and five) and the number of experiments that can actually use the same beam spill on the same target at that station (for example, two or three). In general, several targets will be available at any target station, but perhaps only one operating at a given time for certain prime users--the other installed channels accepting particles of any momentum in order to time counters, test spark chambers, etc.

IV. The Role of the Internal-Target Area

Although the case for placing heavy reliance on external-target areas for serving the physics program is very strong, it is too soon to argue for complete abandonment of all internal-target facilities. Given, however, the existance of external beams serving several target areas, it is unreasonable to consider the inclusion of more than one internal area in the initial design. Not enough experience has yet been gained with external beams at AG machines to be certain that there are not some practical difficulties associated with running a large experimental program entirely externally. Features in favor of the retention of some internal-target facilities are:

(i) Physics experiments utilizing an experimental target in the circulating

beam, rather than using an internal metal target to produce secondary particles for experimental use. One good example is the use of a thin polyethylene foil target or a gaseous hydrogen target, to study low-momentum-transfer p-p interactions. In this case, the thickness of the target is determined only by the need to allow low-energy protons to escape from the target without too much scattering or energy loss. As a second example, large energy loss may dictate the use of a thin production target in searching for the magnetic monopole. Such experiments may require a straight section free of accelerator equipment to allow the secondary analyzing and detection channel to be set up. These provisions constitute a rudimentary internal area, although the shielding need be far less extensive than in a conventional internal area.

(ii) Production of fewer electrons from thin rather than thick targets because of the decreased absorption of γ rays.

(iii) The tune-up period after turn-on. For several months, secondary-beam survey work and certain experiments could usefully be operating from an internal target, when the beam is naturally low and when the damage and activation due to internal targeting are least.

(iv) Decoupled "point" optics. When studied in detail, the advantages for high-energy beams have been found to be rather marginal compared with external beams.

(v) Indefinitely small target emittance. In principle, an extremely small target can be inserted in the internal beam and, provided a long enough flat-top is available, all particles in the circulating beam (apart from those lost to the walls) will eventually interact in the target. This is a fundamental point of superiority of internal over external targets, but it is not clear that the gain is not illusory in that it implies conditions

that cannot be exploited. The design of internal targets of very small dimensions is hampered by the problems of finite target-holder size and of cooling.

(vi) Convenience for future modifications. The crane cover and modular shielding blocks at the internal-target area would provide convenient access to a straight-section area if, for example, some major and massive piece of equipment needed to be added to the accelerator facility at some future date.

In conclusion, it appears that some form of modest internal area with crane cover and shielding is necessary. It should be possible to define better the most appropriate extent of the internal area in the next few years, after experience has been gained from external-beam operation at the CPS and the AGS.

V. Interpretation of These Considerations in the Proposed Design

The configuration of the experimental areas chosen for initial installation at the 200-GeV accelerator is shown in Fig. 6. They are located at adjacent Collins straight sections and comprise an internal area (H), a "short" EPB area (I), and a "long" EPB area (J). The internal area is of conventional design, where the earth shielding around the ring is interrupted for 400 ft and replaced by modular heavy concrete blocks handled by overhead cranes. The internal target is assumed to be located in the Collins straight section and an upper limit of 10 to 15% of the beam spilled on it. The target could be moved upstream into the curved section of the ring, but then extra precautions must be taken against muons because their angular spread would be increased by dispersion in the magnetic field. This area is shown in more detail in Fig. 7.

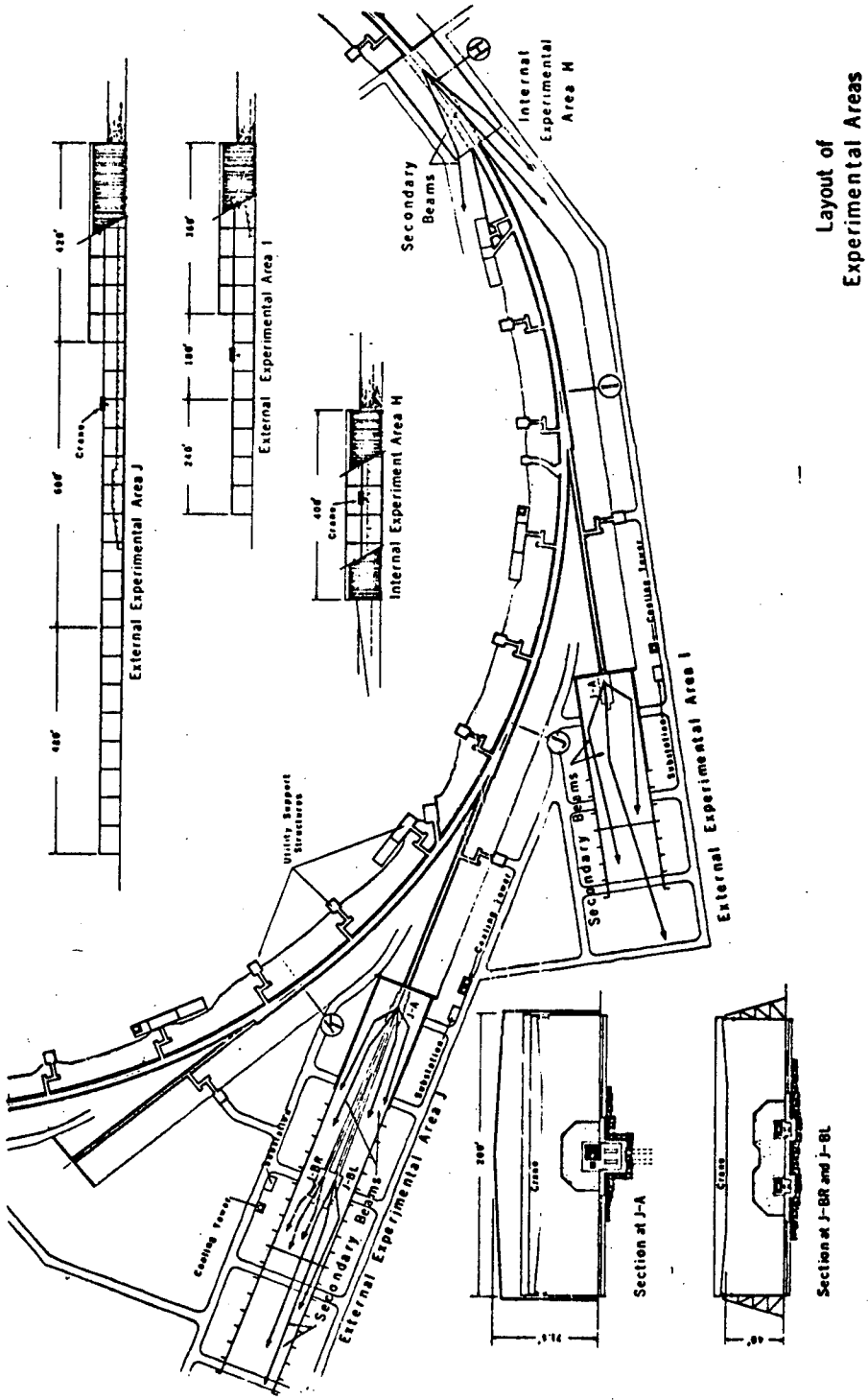

Layout of Experimental Areas

Fig. 6

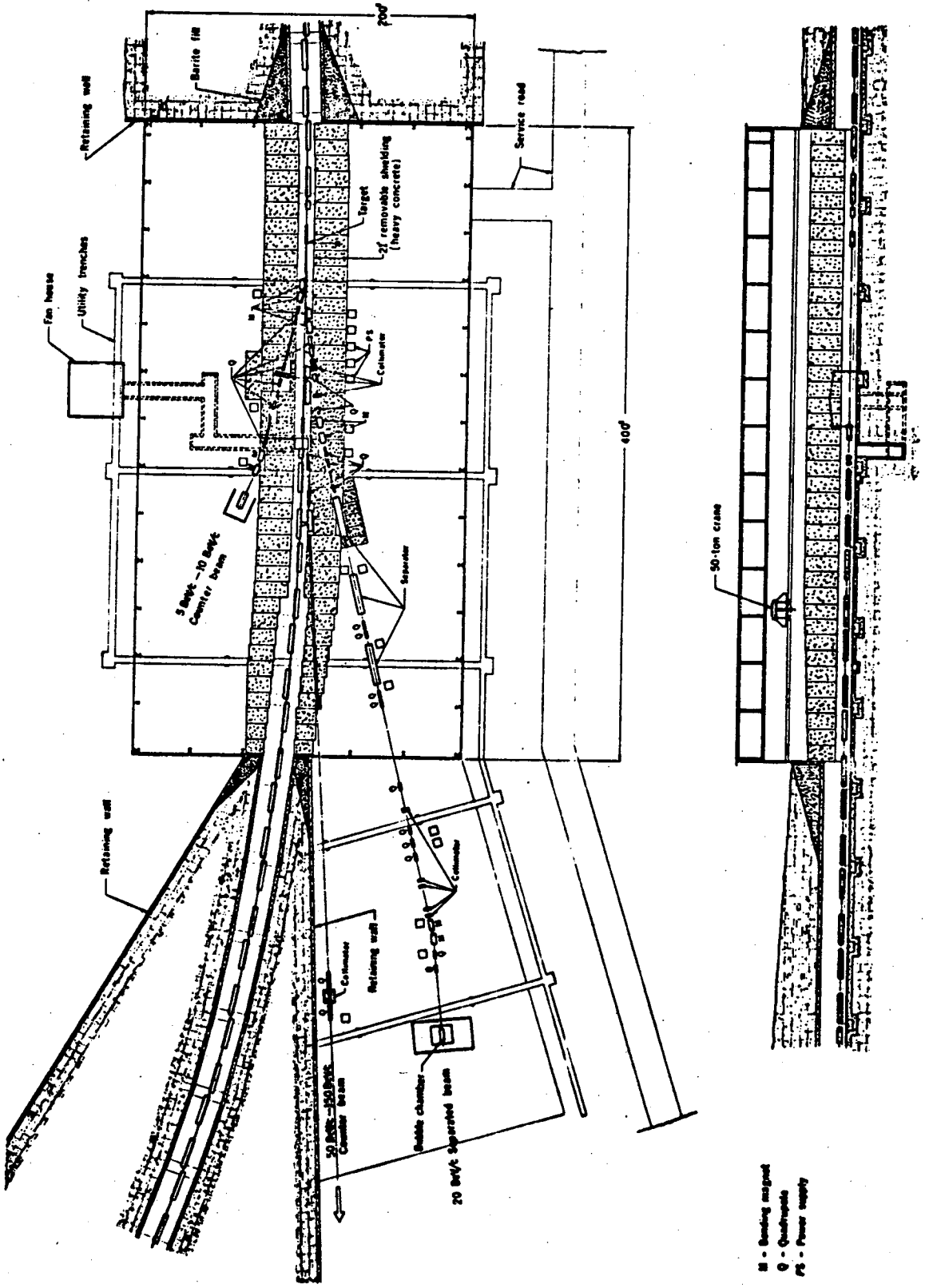

Internal-Target Area H

Fig. 7

In the "short" EPB area, the full beam can be spilled. Either a slow or fast external beam is brought outside the shield wall to a target placed at a target magnet. The target magnet is designed in four separate units for ease of handling (see Fig. 8). Targets can be placed at different longitudinal locations to provide a degree of freedom in selecting different momenta down a secondary channel. Transversely the shield is composed of an inner layer of steel and an outer layer of heavy concrete. Longitudinally the shielding requirement is dominated by the need to eliminate muons. A high-Z material is desirable because it results in enhanced collision losses, while a high-density material is desirable because the shield can be made compact and so allow experimental beams to emerge quickly into the outside world. Uranium has been proposed in the initial design; it is possible that it could be superseded by lead as a result of further studies, with some saving in cost and some loss in compactness.

The "long" EPB area includes an upstream target magnet which also forms a switchyard to divert the external beam into one of two downstream backstop target stations (Fig. 9). Targeting in a "straight section" can be accomplished in the straight EPB runs between target stations. A feature of the switchyard target-magnet complex is that it is composed of magnets with different fields to allow secondary momenta to be varied without altering the EPB angle or position at emergence.[4]

VI. Remarks on Physics Program

The possible nature of secondary beams and physics experiments has been studied in some detail to make sure the areas are adequate at least for those beams one might construct with present-day equipment. In electronically separated beams, Cerenkov counters remain supreme in providing

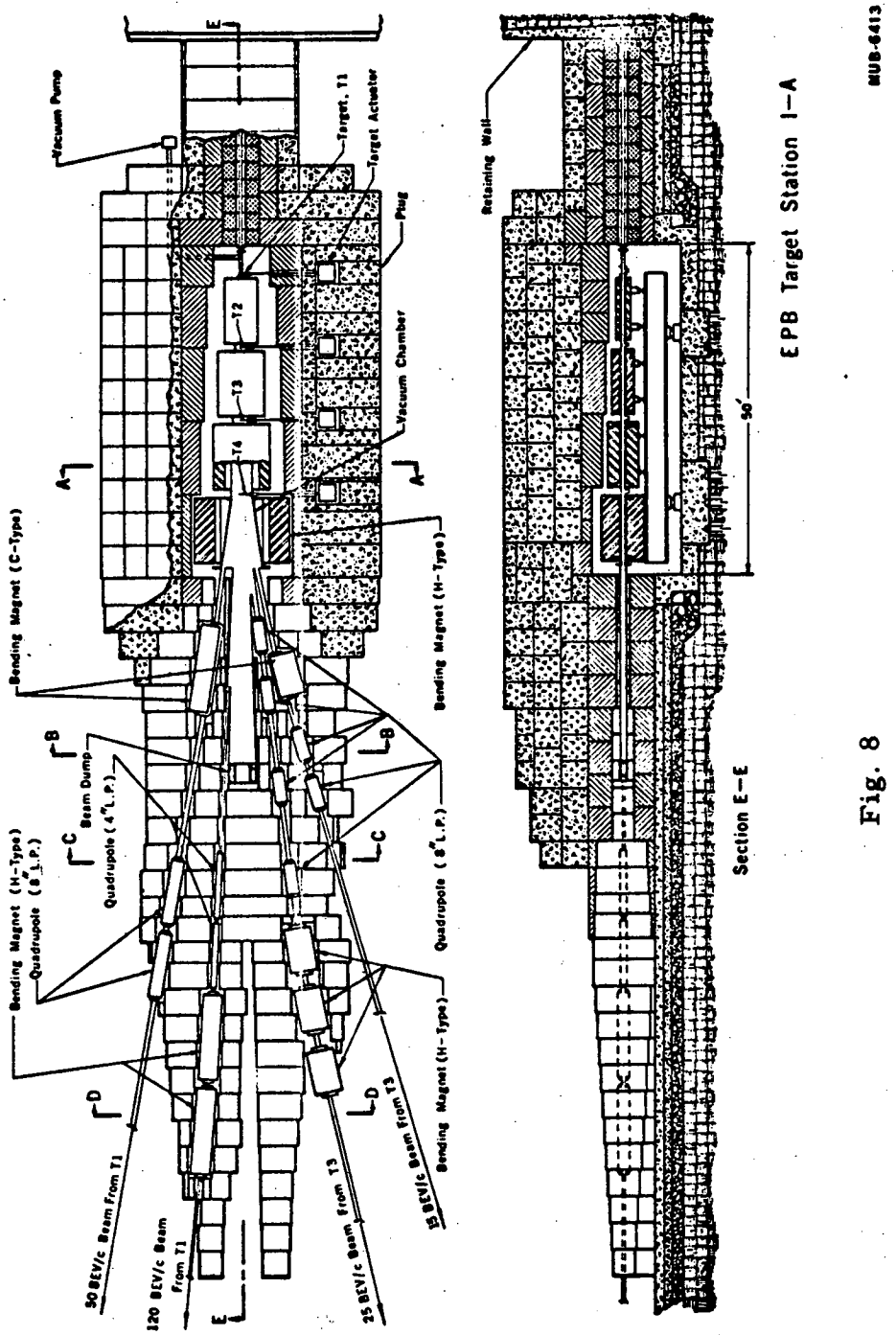
Vacuum Pump
Target, T1
Target Actuator
Plug
Vacuum Chamber
Bending Magnet (C-Type)
Bending Magnet (H-Type)
Quadrupole (8"L.P.)
Beam Dump
Quadrupole (4"L.P.)
Bending Magnet (H-Type)
Quadrupole (8"L.P.)
Bending Magnet (H-Type)
30 BEV/c Beam from T1
120 BEV/c Beam from T1
25 BEV/c Beam from T3
15 BEV/c Beam from T3
Retaining Wall
50'
Section E-E
EPB Target Station 1-A
MUB-6413

Fig. 8

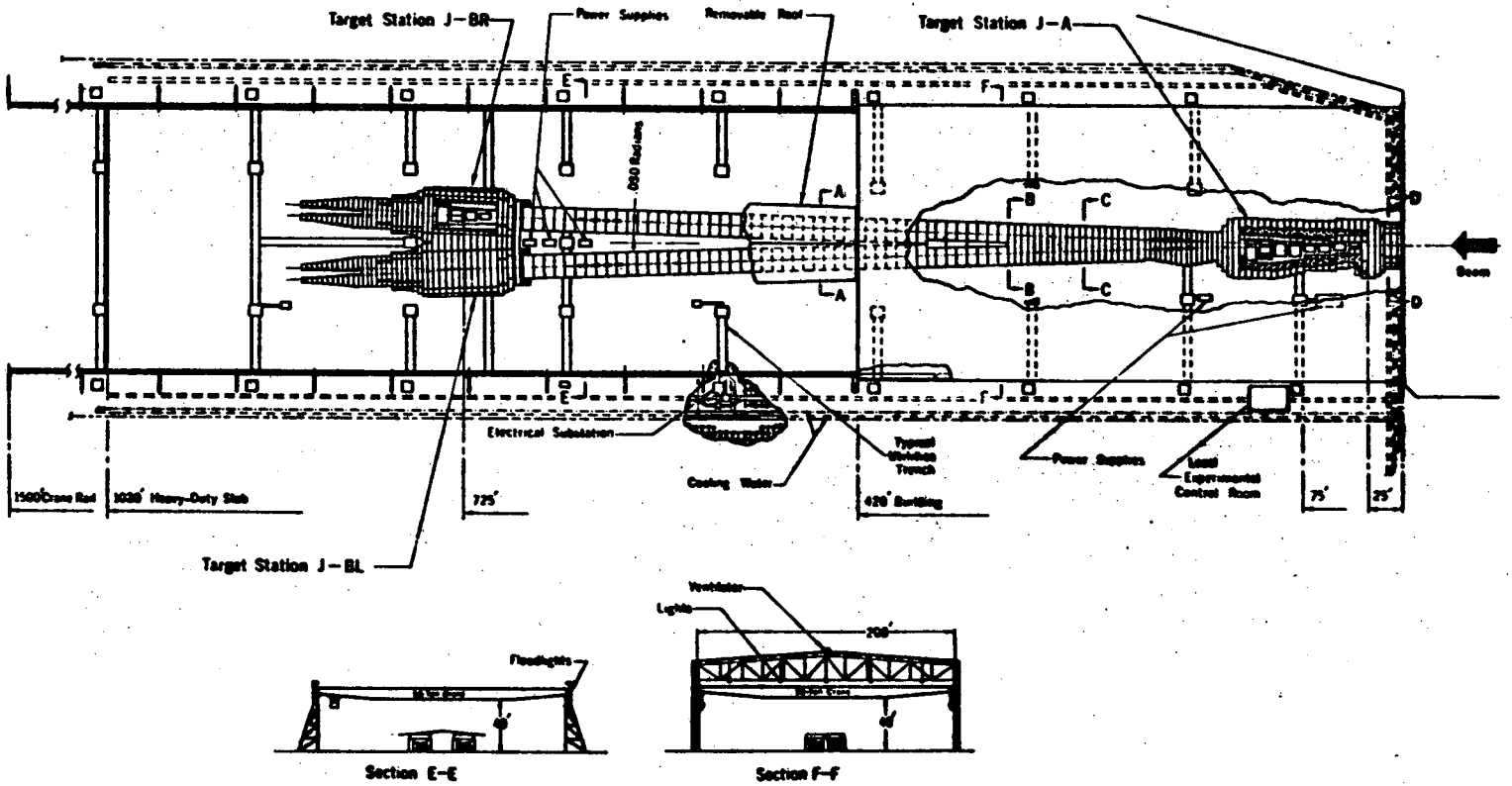
Target Station J-BR
Power Supplies
Removable Roof
Target Station J-A
Target Station J-BL
Electrical Substation
Cooling Water
Typical Ventilation Trench
Power Supplies
Local Experimental Control Room
Beam
1500' Crane Rail
1038' Heavy-Duty Slab
725'
420' Building
75'
25'
Floodlights
Ventilator
Lights
200'
Section E-E
Section F-F
EPB Area J

Fig. 9

clean separation at these energies, although other types of counter, e.g., those relying on the relativistic rise effect, could be useful in special circumstance. The technique of rf separation using frequencies of 10 or even 20 kMc/sec looks extremely attractive in the new energy range. Long spill times (≈ 100 millisec) seem achievable even without resorting to superconducting cavities.

About 4 years after turn-on it is believed that the experimental target facilities could support about 25 experimental beams set up, with more than half capable of simultaneous running. Figure 10 shows some typical layouts in the long-EPB area. Current estimates indicate individual beam lengths may be between 300 and 4000 feet. The total integrated length of beam at that time may be about 5 miles. This can be compared with an integrated length of approximately one-half mile at the AGS or CPS today.

References

1. D. Dekkers et al, Phys. Rev. 137, B962 (1965).
2. G. H. Trilling, Pion and Proton Fluxes from High-Energy Proton Collisions, Lawrence Radiation Laboratory Report UCID-10148, July 1965.
3. G. Cocconi, L. J. Koester, and D. H. Perkins, UCRL-10022, January 1962, p. 167.
4. D. Keefe, Design of Target Facilities at the 200 BeV Accelerator, Lawrence Radiation Laboratory Report UCID-10138, Dec. 1964.
5. L. T. Kerth, in the Berkeley High-Energy Physics Study, UCRL-10022, Jan. 1962, p. 47.
6. 200 BeV Accelerator Design Study, UCRL-16000, June 1965.

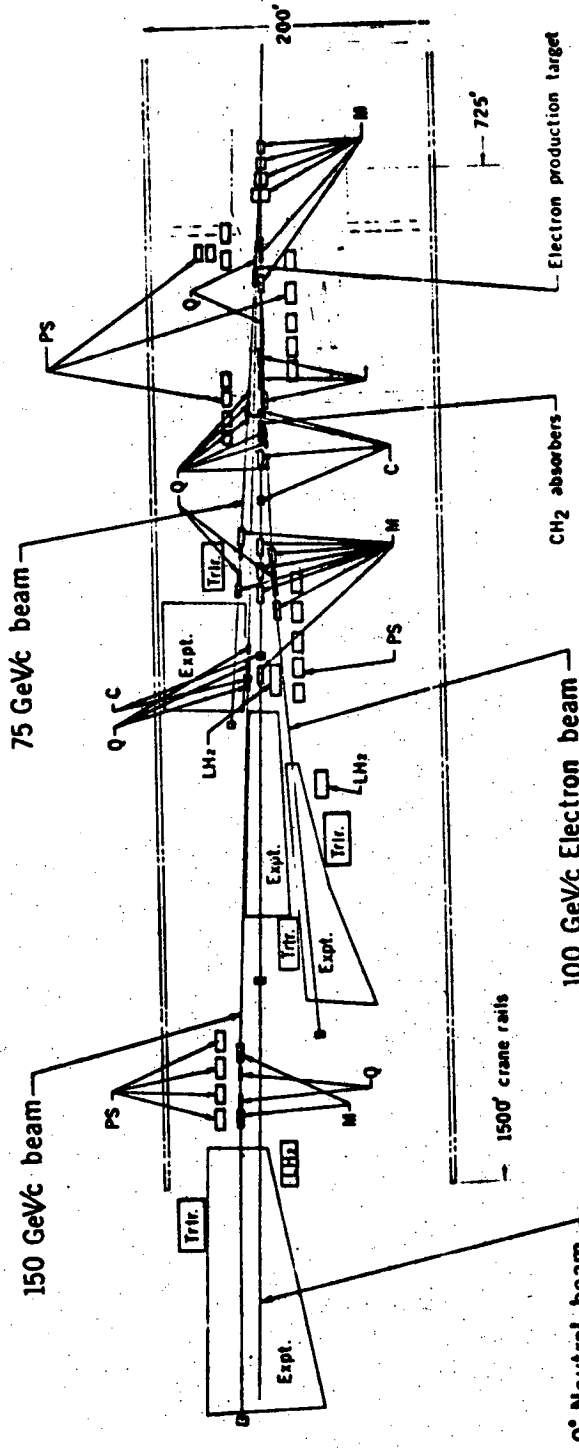
200'
725'
Electron production target
PS
Q
C
M
Trtr.
Expt.
LH₂
75 GeV/c beam
CH₂ absorbers
100 GeV/c Electron beam
150 GeV/c beam
150d' crane rails
0° Neutral beam

Fig. 10

UCID-10138
AS/Experimental/01
December 9, 1964
Denis Keefe

University of California
Lawrence Radiation Laboratory
Berkeley, California

DESIGN OF TARGET FACILITIES AT THE 200 GEV ACCELERATOR

Denis Keefe

DESIGN OF TARGET FACILITIES AT THE 200 GEV ACCELERATOR

I. INTRODUCTION

Design criteria and specifications for experimental areas and target facilities at the 200 GeV accelerator are considerably less definite than the criteria and specifications of the components of the machine. There are large unknowns in the nature of experimental activity in the field of elementary particle physics a decade hence. We do not know what the division of use will be between high and low flux beams, between short and long beam spills, between internal and external target use, etc. If a new invention, for example a new method of mass separation, a new detector, or a new kind of beam, arrives, it may well change greatly the demands on target facilities.

Nevertheless, there are conclusions which can be drawn concerning target facilities from the nature of the accelerator, the beams it produces and the unquestioned heavy demand for use of the facility. It is the purpose of this report to collect together the arguments for and against various targetting procedures and to show that they lead to quite strong conclusions about the need for highly developed external beam areas and about the marginal nature of the advantages of internal beam facilities.

II. CHARACTERISTICS OF THE 200 GEV MACHINE

In making comparisons with the two existing high energy proton AG machines, certain fundamental differences need to be noted:

(i) Beam Power: With a design energy of 200 GeV and intensity of 1.5×10^{13} pps, the beam power will be 500 kW. This is to be compared with about 1.5 kW of beam power at the PS and the AGS. The improved AGS is expected to operate at 100 kW.

(ii) μ-Meson Shielding: The higher intensity and energy make the problem of shielding muons in a target area much different from anything experienced up to the present.[1] A few extra nuclear mean free paths (1 n mfp = 130 gm cm^{-2}) is enough to take care of the higher flux and energy as far as the strongly interacting

particles are concerned. But for muons the effective removal length is in the region of 6000 gm cm^{-2} (it is about one-fourth of this at the 30 GeV accelerators). The exact dimensions of the shield needed depend[1] on how efficiently the π-mesons can be eliminated, but, in general, at a target area, the muon shield will be about 100 m Fe equivalent long and about 15 m wide, with an outside layer of concrete blocks. This presents a formidable stacking and unstacking problem when making changes in a target area, irrespective of whether it is an internal or external area.

(iii) Radiation Problems: The problem of induced activity and radiation damage associated with distributed loss around the ring do not scale with beam power, but with intensity only, since the circumference has been increased proportionally to the energy. However, close to a target area the radiation damage and activity will scale almost as the beam power--not quite, since most of the activity will be deposited within about one-half betatron-wavelength downstream, and this will be more than twice as far in linear distance at the 200 GeV machine compared to the PS and the AGS. Radioactivity levels will thus be ~ 200 times more than at the target areas of these machines. Thus, in the target areas certain types of remote handling techniques are required for a distance of about $\pi\bar{\beta} \sim 120$ m. Around the main ring boronization of the concrete and local shields on the open side of the C-magnets are expected to take care of the induced activity problem.[2]

(iv) Aperture and Phase Space: Several seemingly small differences in parameters occur in the scaling to higher energies which will be seen later generally to diminish the importance of internal targetting and enhance the advantages of targetting in the external beam. The vertical aperture will be about 5 cm, smaller than that in the PS (7 cm) and the AGS (7 cm), $\frac{R}{\nu} = \bar{\beta}$ (= betatron wavelength/2π) will be 40 meters, or more than twice that in the PS and the AGS, and the emittance of the beam

at full energy will be $\pi(0.05)$ mm-mrad vertically, and the same horizontally for 1×10^{13} ppp. The revolution time will be 15 μs compared with approximately 2 μs at the PS and the AGS.

(v) Long Straight Sections and Beam Extraction: Since the construction of the PS and the AGS, there have been two inventions which can be exploited--long straight sections and beam extraction systems. We assume that 12 long straight sections of the $\pi/2$ type[3] or π-type[4], or a mixture of both, will be included. Either the first or second choice leads to an increase in momentum compaction factor $\hat{\alpha}$(*) of a factor of about two--and the mixture to a greater increase--demanding therefore a large radial aperture. However, Garren et al,[4] have shown that the large momentum compaction factor $\hat{\alpha}$, can be greatly reduced by including bending magnets at the beginning and ends of a π-type straight section. Figure 1 shows the parameters for a $\pi/2$ type and a compensated π-type straight section. A disadvantage of the $\pi/2$ type is that there is a practical limit of ~ 30 m on the free-space length, whereas the π-type can be made with a drift length just as short, or substantially longer, as one chooses. An attractive possibility is a machine with straight sections exclusively of the π-type, possibly some of them having different lengths, e.g., 9 at 30 m, 3 at 50 m, etc.

Fast extraction using a pulsed kicker has been demonstrated experimentally at both the PS and the AGS. The efficiency is 100% (however, a small amount of the circulating beam in bad regions of phase space may be scraped off on the effective aperture of the magnet.) The emittance of the extracted beam is the same as that of the internal beam. Slow extraction using a non-linear magnetic perturbation to drive firstly the large-amplitude, and later the small amplitude particles into resonance[5] has been achieved at CERN. The first experiments had an efficiency of 50% with a spill time of ~ 100 ms; the

---

*The parameter $\hat{\alpha}$ is defined by $\frac{\Delta R}{R} = \hat{\alpha} \frac{\Delta p}{p}$.

π/2 STRAIGHT SECTION

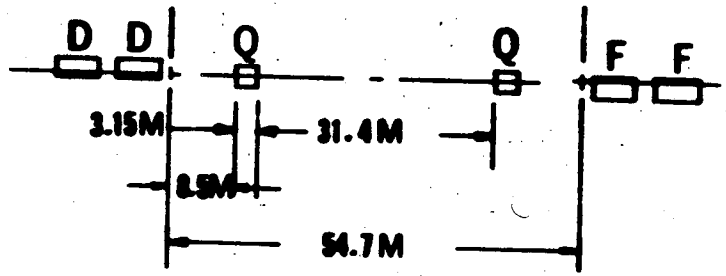

Q - 3.15 M
AG - 5.82M

B^{l} - 1.35 kg/cm
k - 3.17 M^{-1}

fig.1a

π STRAIGHT SECTION

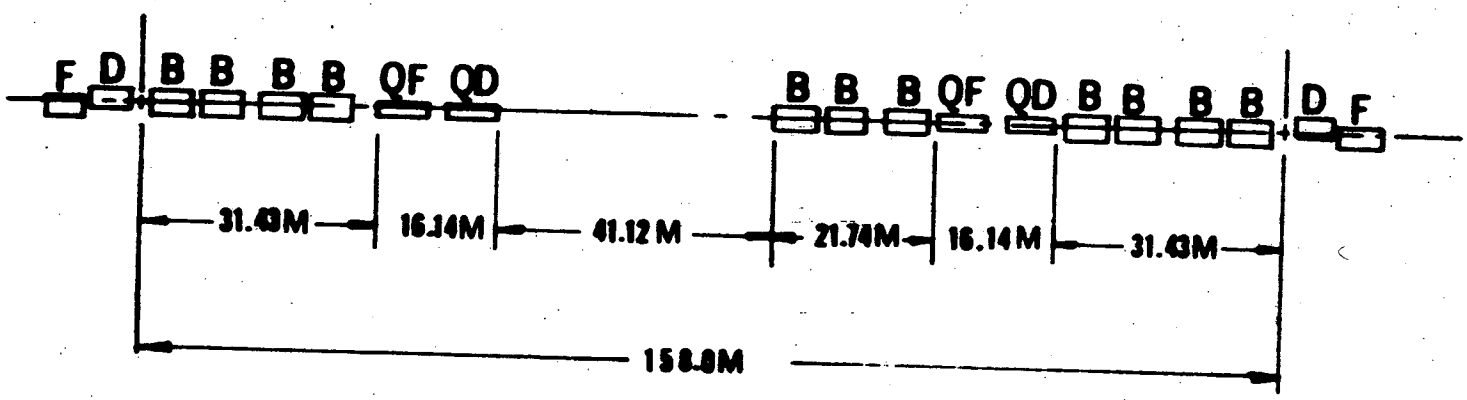

Scale: 1cm. = 10M.

Q - 6.821M
B - 6.08 M
AG - 5.07 M

B^{l} - 0.6382 kg/cm
B^{l} - 0
k - 4.693 M^{-1}

fig.1b

horizontal emittance, as predicted, was much smaller than that of the internal beam and the vertical emittance was about the same.[6] The most impressive feature is the agreement between the calculated and the observed properties, so that it is not being too optimistic to believe our calculations of the properties of an extracted beam from the 200 GeV machine. With a scheme similar to that described by de Raad[7], using two septum magnets, the first with a 1 mm wide septum, the second with a septum almost 1 cm wide located (in the shadow of the first) about one magnet period downstream, a beam displacement of about 4 cm can be achieved at the beginning of the drift space in a long straight section. Here a third magnet (which now can have plenty of copper in the median plane) about 15 m long can steer the beam away from the machine at an angle of $\sim 2^{o}$, sufficient to clear any expected downstream obstructions. The extraction efficiency is 90% and is determined by the choice of 1mm for the width of the first septum. The horizontal emittance is again expected to be less than that of the circulating beam. Exact details depend on the choice of the straight section parameters; a diagram of one scheme due to G. Lambertson is shown in Fig. 2. We will assume that the emittance of the extracted beam in either plane is $\pi(0.05)$ mm-mrad.

III. SOME OBSERVATIONS ON THE NATURE OF EXPERIMENTAL ACTIVITY IN THE FUTURE

The design of general-purpose target areas is dependent on the nature of experimental activity in the future. This is the aspect of the accelerator design most vulnerable to error because of the difficulty of visualizing the state of the experimenters' art at that time.

It seems appropriate, however, to make some reference to the shape of experimental activity we might expect a decade hence. If we pause long enough to examine how far from the present-day picture such crystal-gazing would have been if attempted in 1953, the prospect of being even remotely successful seems slight! At that time, strong-focussing lenses, electrostatic and r-f separators as beam transport elements for high energy beams did not exist, plastic scintillators and cerenkov counters had yet to become standard beam-counting elements, while bubble chambers

EXTRACTION TRAJECTORIES (MACHINE B12/108 ν=19 1/4 − 0.15 = 19.1 β_F = 47m)

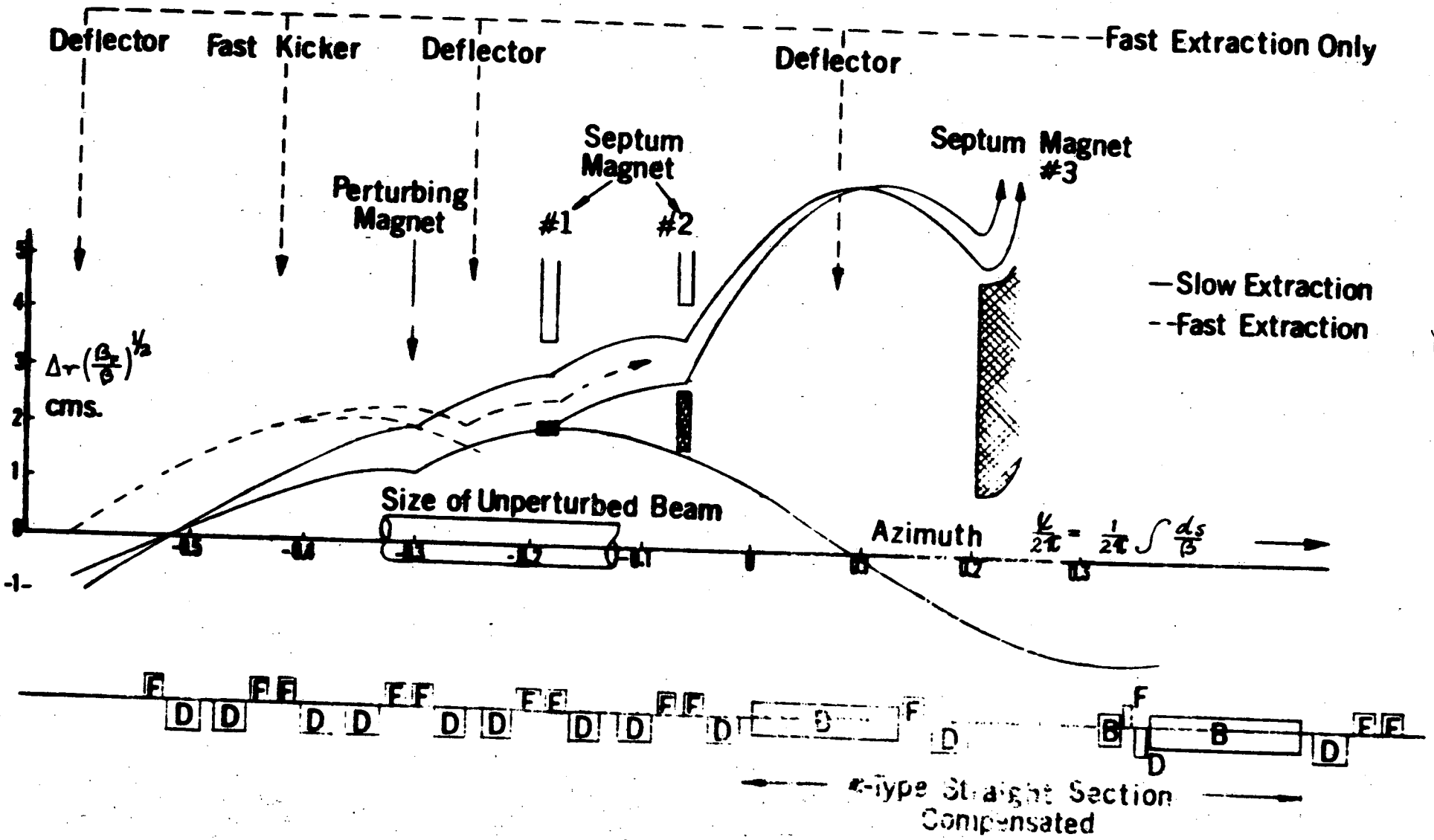

fig 2

and spark chambers had not yet been exploited as detection devices. If we look around the floor of an experimental area at any major elementary particle facility today, we find that vacuum pipes and bending magnets are about the only components consistent with the 1953 extrapolation. To predict new inventions is impossible, but at least we can guess at the technical improvements possible in known techniques.

(1) Dimensions of Secondary Beams: A number of hypothetical experimental beam set-ups have been examined and the preliminary conclusions --based on a small sample--are summarized here. Certain beams will scale in length as p^2, e.g., the 100 GeV r-f separated beam is 1.3 km long, although Murray has pointed out[8] that a scaling law closer to the first power of momentum could be achieved. One may choose to scale other beams as p, an example is the case of a neutrino (or μ-meson) beam arising from the decay of approximately monochromatic π-mesons of K-mesons.[9] The mean decay length for π-mesons is 55 E m and for K-mesons 7.4 E m (where E is in GeV.) Thus for some optimum choice of the ratio of beam length to decay length, the overall beam length will scale directly as the momentum (e.g., at 20 GeV λ_π = 1100 m). In the case of electronically separated beams, the choice of quadrupole elements stronger than those in use at present results in beams which, compared with those at existing facilities, scale more nearly as $p^{1/2}$. One example of a beam using cerenkov counters to identify π-mesons or K-mesons or protons with a momentum range between 50 and 150 GeV/c has been designed to be 240 m in length.[10] An interesting conclusion, which has important implications in the choice of the size of buildings, is that the transverse displacement of the experimental equipment at the end of the secondary beam from the initial proton beam direction can be kept in the region of 10 - 30 m irrespective of momentum. The dispersion near the target is large for low-momentum beams, which can be kept short, and small for the high momentum beams, which are long, thus leading to a situation where the area of active experimental equipment is confined, at least in the EPB area, to a swath of space ~ 50 m wide, straddling the mean direction of the EPB.

It is assumed that counter telescopes and spectrometers, spark chamber arrays and bubble chambers will be the major forms of detector. The former categories can be tailored to suit any experiment, and in the latter case we assume that several moderately-sized chambers (~ 1 m to 2 m) will be available in addition to a giant bubble chamber in the 10^5 liter class. Elsewhere[9] we assume the existence of a hydrogen/deuterium chamber of 10^5 liters for the purpose of computing the rate of neutrino events; there are extant several proposals for chambers about half this size while the construction of one twice this size seems very far in the future; thus for the purpose of calculating reliable rates for very rare events to within a factor of two, this seems a reasonable choice in size.

(ii) Momentum Requirements for Secondary Beams: One of the major difficulties which will be adverted to later (Section VII) concerns the setting up of several experiments accepting beam from the same target, viewed through a magnetic field, during the same beam spill. A quadrupole system accepting one beam momentum will inevitably cast a momentum shadow so that another channel cannot accept a momentum close to that of the first. Also, it is difficult to create two secondary systems with arbitrary and independent control over their individual momenta. This leads us to examine whether we may expect differences from present-day practices in the high energy region in the momenta requirements of secondary beams.

There will certainly be a need for beams covering a very large momentum range, for example an experiment studying the asymptotic behavior of cross-sections and the comparison of particle and anti-particle cross-sections, would have such a need. The first point to observe is that there will be relatively a more rapid change in flux over wide momentum ranges the higher the energy, E_o, of the accelerated protons. For example, the parameter T, in the formula of Cocconi, Koester and Perkins[11], which is proportional to $E_o^{3/4}$ and measures the mean energy of the (high energy) mesons, has a value 4 GeV at

30 GeV and 16 GeV at 200 GeV. Thus, if we compare a beam which spans $(1/2)E_o$, or 15 GeV in one case, and 100 GeV in the other, we see from the CKP formula[11] that the total flux ratios between the lowest and highest energies are $e^{15/4}$ (= 43) and $e^{100/16}$ (= 530) respectively. (The relative solid angle acceptance will scale similarly in the two examples and can be ignored in the comparison.) Since one of the criteria of a widely variable channel is a tolerable flux over the whole range, the difficulties will be greater at the higher energy and channels will probably be less ambitious in total range.

Furthermore, it seems likely that the exact choice of energy in many cases may not be too important. Again to quote an example: if one wishes to study the mechanism of high energy production of π-mesons, strange particles, and anti-nucleons in a series of bubble chamber runs at 50 GeV, 100 GeV and 150 GeV, it is probably not important if he has to settle for primary energies of 40 GeV, 90 GeV and 160 GeV. In other words, for many elementary particle mechanisms which are expected to vary smoothly, it is likely that <u>any</u> set of widely spaced points is the main requirement rather than particular magic values for each point. This trend is apparent already in some experiments at present machines--numerous studies of di-boson production have been and are scheduled to be made and in most cases, except for matters of detail, it is not too important if the primary particle has an initial energy of 4 GeV or 5 GeV or 6 GeV--any high energy within broad limits would do. This point of view is partly bolstered by the predicitions that as the energy of interactions becomes great compared with a few GeV, resonance phenomena will become much more smeared, and diminish in amplitude. The discovery of resonances of the order of a few hundred microbarns above the continuum in πp collisions in the region of 2 GeV was a recent <u>tour de force</u> at the AGS.[12] There seems little likelihood of successfully pursuing this sort of search at energies an order of magnitude higher and the accent may well shift to exploring other types of phenomena of specifying particular secondary processes. It is not clear whether the pursuit of resonant effects far into the high energy region will

be necessary--one is reminded of the situation in atomic physics half a century ago when the line-series formulae were established and explained on the basis of the observations of a relatively small number of energy levels, and the later observation of very closely spaced lines lying close to the continuum was a feat of spectroscopic virtuosity of purely confirmatory character.

Our present ideas about the desirability of an exact choice of a specific momentum for a secondary beam are largely dictated by the experience of working in an energy region teeming with interesting thresholds. An experiment on hyperon polarization at one enrgy may be unfeasible at an energy only 10% different because the polarization has changed for the worse. Cusp phenomena and, generally, effects depending on the hope of drastic simplifications in the analysis in terms of angular momentum states all require precise choice of momentum close to threshold. As one proceeds further away from the threshold for a particular reaction there seems, in general, to be less pressure to choose a very specific energy for an experiment.

The purpose of these remarks is to indicate that scheduling compatible runs may well be easier than we would anticipate if indeed an experimenter can accomplish the same physics in a beam of 80 GeV or 100 GeV or 120 GeV. It is a degree of flexibility uncommon at lower energies. A circumstance which could destroy the general applicability of these remarks would be the discovery of particles with much higher mass than the nucleon, thus creating a field of study of threshold effects at energies much higher than we are accustomed to today. Furthermore, these remarks are not intended to refer to weak-interaction physics--μ mesons and neutrino interactions--where the problems in both cases are quite different and especially in the latter, only poorly understood.

(iii) Beam Transport Equipment: The use of hard superconductors seems a very likely development for both bending magnets and quadrupoles. The scaling of the latter[13] does not result in a gross increase in size and cost, largely because the compaction in solid angle

of high momentum secondary beams allows one to save in aperture. Bending magnets, however, become very long and expensive and it is here that the greatest saving in cost would lie. If used in conventional transport elements it is not clear whether superconductors would utilize the ferro-magnetic properties of iron; certainly some structurely strong material is needed for coil support and, even if used at fields in the 2 Tesla region, it would be a valuable innovation to save power. In the case of special detection equipment, there is little doubt that very high-field superconducting magnets will be used, e.g., with bubble chambers. It would be wrong at this time to consider serious design of the conventional transport equipment, with attendant cost estimates, on the basis of hard superconductors--there is too much room for considerable improvement in fabrication techniques, reliability and the development of new materials which would change the cost drastically. The situation is somewhat analogous to the situation in the transistor field in the early 1950's when severe problems of fabrication control and reproducibility had to be faced and the development of very high-current transistors looked unlikely. If, for example, a new material costing tens, and not hundreds of dollars per pound were to emerge on the market, the impetus in this field could within a few years produce a revolution.

Restricting consideration to conventional copper-and-iron transport equipment, one observes that where several beams have to be served at one target station, the need for the leading elements in the secondary beams to be packed close together laterally is aggravated beyond that at existing machines because of the higher energy. This can be alleviated somewhat by the use of targetting magnets to fan out the secondary beams, but the need for transport elements compact transversely is as critical as ever. If the physical width is $\underline{b}$ and the available full aperture is $\underline{a}$, then in the case of bending magnets $b/a \gtrsim 2$, and it is impossible (at high fields) to do any better. A high-power (about ten times optimum) quadrupole has been described by Dols which has $b/a = 1.5$.[14] It has the disadvantage of an

upper limit on the gradient ~ 4 Tm^{-1}; in the same report, a septum quadrupole-cum-bending-magnet with b/a = 2 is described, which has the available aperture asymmetrically located so that the transverse interference on one side can be made almost zero. (See Fig. 3.)

(iv) Spatially Separated Beams: While beams using electrostatic separators will probably be used at the 200 GeV machine, we assume that they will not deal with momenta beyond 10, or at most 15 GeV/c. There seems to be a fundamental limit, set by the requirements of stability and homogeneity of the electric field, at about 10 GeV/c. Even allowing for technological improvements, the extension beyond this limit can be only minor because of the $(\text{momentum})^3$ scaling law. With r-f separated beams, on the other hand, it seems feasible to extend the energy range to 100 GeV.[15] The two main problems to be solved in this case are how to improve the acceptance and the duty factor. Tubes in the kilomegacycle range typically can have pulse lengths of a few microseconds only, which permits r-f separated beams to be quite adequate for bubble chamber operation. For counter experiments, new possibilities would be opened up if the pulse length could be made tens or hundreds of milliseconds. Improvement in power tube design gives some small hope; the major breakthrough seems more likely to come from the development of superconducting cavities.

(v) Electronically Separated Beams: The remarks expressed in a previous report[16] still seem generally valid. It is hard to imagine electronic resolution times much less than 1 ns in common use; in this region the temperature stability of the long cables needed, the rise time of photo-tubes, the transit-time spread of photons in a scintillator and dispersion of gases in gas cerenkov counters, all become serious problems. (Certain experiments will probably, however, make use of the 50 Mc/s bunch structure or 3 kMc/s if a pre-buncher is built.[17] Low energy beams will continue to use conventional time-of-flight

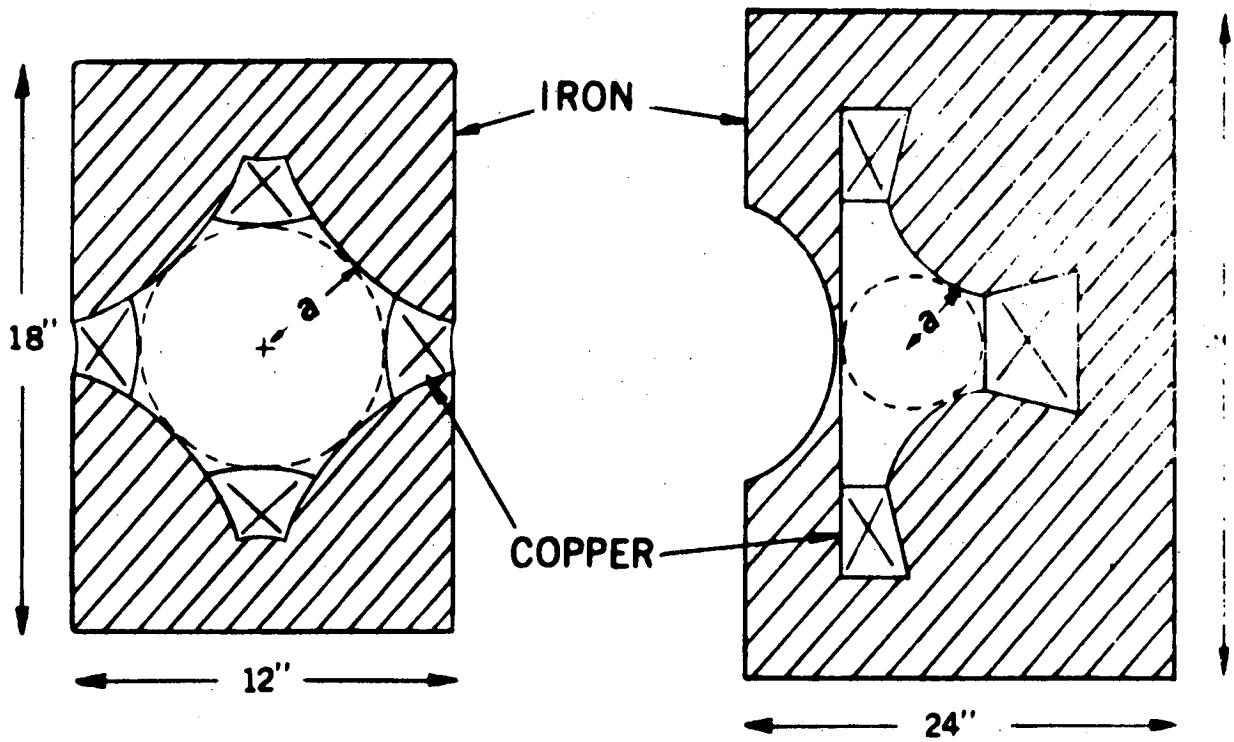

a = Radius of Useful Aperture
= 4"
B' = 1 Kilogauss/inch

fig. 3

techniques as an aid in separation. If indeed very massive particles weighing several GeV exist--for example the α and β triplets[18]--then clearly time-of-flight techniques would again become important.) Thus it seems probable that many experimenters will continue to demand beams with an intensity of the order of 10^6 particles per pulse and a long flat-top spill in order that accidental rates can be kept to a small fraction of one percent. An upper limit on beam intensity per unit time in the case of spark chamber experiments is imposed by the requirement that the logic of the triggering system be completed before the pulsing of the chambers can be initiated. At very high energies, a precision in momentum measurement by means of spark chambers can be obtained which is far in excess of bubble chamber measurements provided long lever arms can be used. The kinematics of high energy interactions, while it has the desirable consequence of relieving the need for much larger aperture magnets, has the unfortunate effect of stretching out the arrangement of equipment linearly. There is a greater time-delay in pulsing the initial chambers because the transit time of the triggering particles to the last counters is correspondingly increased. Thus, while we can visualize improvements in the logic speed and in the pulsing equipment with time, they will probably be offset by the extended disposition of the chambers. The resolving time is assumed to remain in the 1 μ sec region and ten or twenty percent accidental tracks in the photography to be tolerable. Thus, this again leads us to believe that beams of $\sim 10^6$ particles per second will continue to be a commonplace requirement.

IV. THE USES OF EXTERNAL AND INTERNAL TARGETS AND A COMPARISON OF THEIR ADVANTAGES

(1) Advantages of Internal Targets in Present AG Machines: Among the many advantages of internal targets in AG machines currently operating, are the following--and they are in striking contrast with targetting in CG machines:

(a) High Target Efficiency: The targetting efficiency can be high because the high momentum compaction in AG machines permits a proton to traverse the target many times despite energy loss. In going one nuclear mean free path, a proton loses ~ 200 MeV and at the 200 GeV machine, where $\Delta p/p$ at full energy $\sim 10^{-4}$, this would result in high multiple traversal efficiency. Multiple coulomb scattering and nuclear diffraction determine the upper limit of target efficiency which usually is in the region of 60% to 80% The efficiency for different target elements placed close to the upstream (horizontally defocussing) quadrupole in a $\pi/2$ straight section is shown in Fig. 4 for different primary energies.[19]

(b) Multiple Targets: The fact that there is a large number of betatron wavelengths around the machine allows one to distort the closed orbit independently at different azimuths so that several targets can be struck at once. This feature of series targetting is relatively unimportant for short spills, but a great advantage where several groups wish to utilize the high duty factor provided by the full flat-top time.

(c) Target Optics: A target, very small in both transverse and longitudinal dimensions, can be used so that experimenters who view the target away from 0-deg production angle can still secure essentially point optics and also are free to vary independently their secondary momentum. Alternatively an experimental beam at angle θ to the internal beam can operate from a thin rod-target inserted into the beam at angle θ, and the apparent target size still appears only as the transverse size of the rod although interactions are taking place throughout its volume.

These are the main attractive and advantageous features of internal targets as used at present. Next, we compare them with what can be obtained using thick targets in an external beam--a situation proposed below (Sections VI and VII).

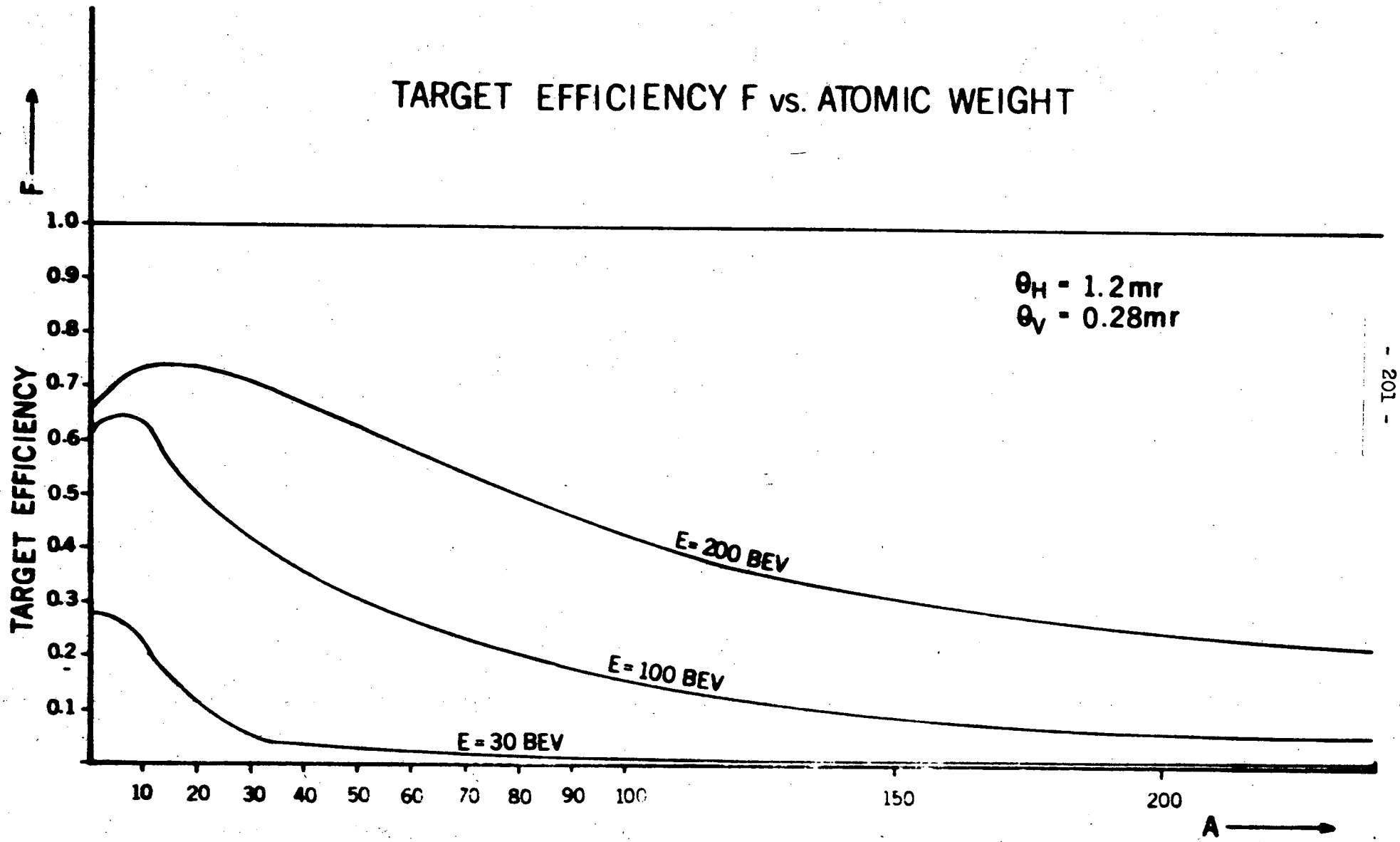
TARGET EFFICIENCY F vs. ATOMIC WEIGHT
F
1.0
0.9
0.8
0.7
0.6
0.5
0.4
0.3
0.2
0.1
TARGET EFFICIENCY
θ_H = 1.2mr
θ_V = 0.28mr
E = 200 BEV
E = 100 BEV
E = 30 BEV
10
20
30
40
50
60
70
80
90
100
150
200
A

Fig. 4

(ii) Scaling of These Advantages for the 200 GeV Machine: Almost all of the advantages can be achieved to a close degree by operating with external targets and many others availed of in addition.

(a') High Target Efficiency: Several features of the 200 GeV machine tend to offset the gains of multiple traversal targets. The long betatron wavelength and rather small vertical aperture result in particles being lost to the walls because of small nuclear or coulomb angular deviations in the target. The efficiency of targets has a maximum of ~ 80% at full energy for light elements (Fig. 4), but falls drastically if the primary energy is lowered (the maximum is ~ 60% at 100 GeV and ~ 40% at 30 GeV.)[19] It is reasonable to assume that for a large fraction of time the accelerator will run at less than full energy (v. experience at CPS and AGS). Secondly, if a short spill is required, multiple traversals are of no advantage. For example, if a bubble chamber needs a spill of 100 μ sec, the long revolution time of 15 μ sec allows only 6 passages of the circulating protons. However, the fact that the machine has a quarter-integral tune means that a small angular deviation in one passage of the target--assumed to be small transversely--will virtually guarantee that the proton will miss the target on the next and every alternate passage thereafter, so that the average number of traversals is close to three. To maximize the efficiency in this case requires a target close to one nuclear mean free path long. A similar efficiency, and optics at least as good, can be obtained in the external beam.

Thirdly, it is often stated that the maximum efficiency of an external target is 0.37 when it is 1 n.m.f.p. ($= \lambda_a$) in length. This is based on the assumption that the incident protons and the secondary particles produced are absorbed with a m.f.p. of λ_a and that only the interactions of the primary protons need be considered in the production of

secondary particles. This leads to an expression of the form

$$\frac{x}{\lambda} \quad e^{-x/\lambda}$$

for the efficiency of a target of length x, which has a maximum value of 1/e when $x = \lambda$. When the effects of the high energy cascade in producing secondaries is included the efficiency is enhanced. The results of a calculation by Riddell[20], (which actually underestimates the magnitude of the effect) are shown in Fig. 5. From this we see that for low energies (~ 20 GeV) the efficiency in copper can be as high as 80%--the maximum attainable with internal targets.

Fourthly, part of the relative inefficiency of external targets arises from the fact that the optimum thickness of the target results in a substantial fraction of the primary protons emerging from the target without interaction. The angle of coulomb scattering (~ 0.03 mr) is negligible since, if targetting is carried out at a focus, there is only a minute increase in emittance of the external beam. If series targets are used, the surviving protons can be used to feed another target. Consider a simple (and pessimistic) illustration in which the efficiency of targets is 0.37 and the fraction of transmitted protons at each target is 0.37. Then, defining the productivity as the total efficiency of all targets (in number, n_t) we have

$$\text{Productivity} = \sum \text{(Efficiency) (Incident Protons)}$$

$$= \sum_{n=1}^{n=n_t} \left(\frac{1}{e}\right)^n$$

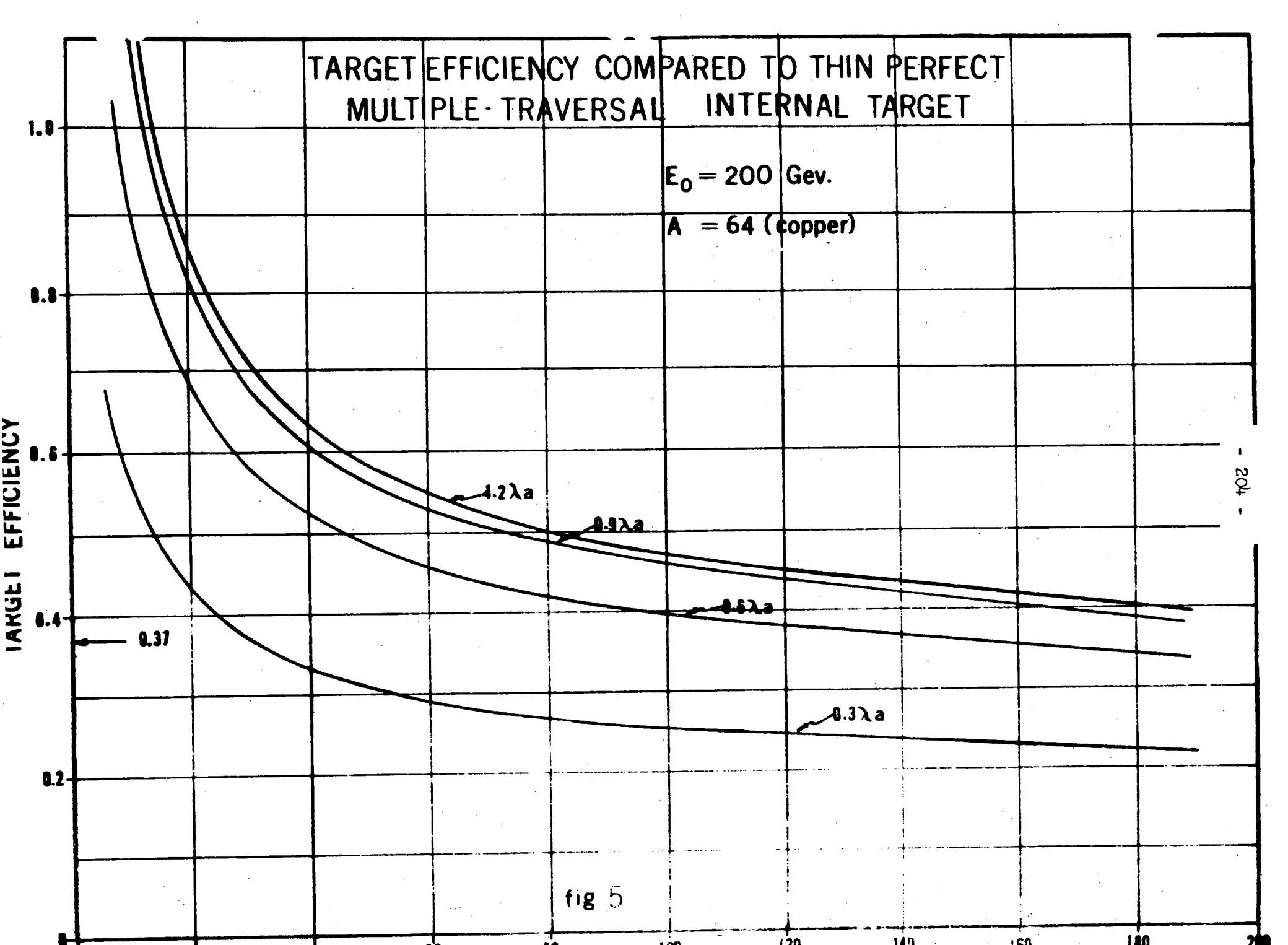
TARGET EFFICIENCY COMPARED TO THIN PERFECT
MULTIPLE-TRAVERSAL INTERNAL TARGET
$E_0 = 200$ Gev.
A = 64 (copper)
TARGET EFFICIENCY
1.0
0.8
0.6
0.4
0.2
0
1.2λa
0.9λa
0.6λa
0.3λa
0.37
140
160
180

fig 5

$$= .37 \text{ for } n_t = 1$$
$$= .51 \text{ for } n_t = 2$$
$$= .56 \text{ for } n_t = 3$$

Consider that we have a maximum efficiency of 0.8 obtainable internally. Thus in this case if we imagine three series targets all λ in length, while the experiment at the first target is suffering by having to run at an efficiency of about one-half that attainable internally, the two remaining targets are being used to serve other parts of the experimental program and the total relative productivity is $0.56/0.80 = 0.70$. To be more realistic and less pessimistic consider a case where high flux is needed at three copper targets (each of length = λ) at energies 100 GeV, 50 GeV and 10 GeV. Then the productivity is (using Fig. 5):

$$(.46) + 0.37\ (.57) + 0.37^2\ (1.15) = 0.83$$

which in fact represents an improvement over the internal target case. If the targets were placed in reverse order, the productivity would be

$$(1.15) + 0.37\ (0.57) + 0.37^2\ (0.46) = 1.42$$

an even greater improvement. If productivity were the only goal, this number could be improved upon by choosing somewhat different lengths for the individual targets. The object here however is only to illustrate that comparison of individual target efficiency is only part of the story.

Finally, it would seem that far too much weight is attached to the efficiency of a target in relation to the number of particles <u>produced</u> rather than in relation to the number of particles <u>captured</u>. For example, at the AGS and CPS only about 1% or less of the available flux is typically captured into a secondary channel, largely because of interferences between the secondary transport equipment and the

main ring magnet and vacuum tank. To argue about production efficiencies differing at most by a factor of two between internal and external targets is then to miss the most important point. In fact, apart from the neutrino experiments performed at the AGS and CPS where every effort was made to capture the maximum flux, in the opinion of the author far too much empahsis has been placed upon the need to increase the number of circulating protons by factors like 2 or 4 or 8 and not enough upon the development of efficient targetting techniques where factors between 2 and 3 orders of magnitude are lurking.

In an external beam it is possible, by means of bending magnets, to arrange for targetting at 0-deg. In fact, for high energy beams, there is no other choice but to use the forward cone. Production angles of even a few degrees correspond to losses in flux of many orders of magnitude since the cross-section per unit solid angle decreases exponentially[11,21] with angle with an e-folding angle of $\frac{0.22}{E}$ (for example 2.2 mr at 100 GeV). Beams of reasonably low energy (say, 10 GeV) could still be obtained away from 0-deg from a target without the use of a magnet. Even in this case of a "straight section target", the efficiency of capture is higher in the EPB since, firstly, the length of the straight section can be very long, and secondly, the transverse equipment is with a vacuum pipe about 2 cm across and not with the full machine vacuum vessel 12 cm across (not to mention the machine magnets).

(b') Multiple Targets: The use of several internal targets all being traversed simultaneously by the circulating beam in order to provide a large duty factor at independent target stations, can only be matched in a purely external beam facility if several series target stations are developed in at least one channel. We have seen in the last paragraph that a set of thick targets in series in the EPB can approach or exceed the total productivity of a similar number of

multiple traversal internal targets. Let us ignore the small difference in productivity and postpone discussion of the number of series targets for optimum conditions--it is clear that 95% of the protons can be exhausted in as few as three thick targets, each 1 n.m.f.p. thick. Then there is a striking analogy between the case of series targets inside and outside the machine. The gross control of the intensity distribution among the external targets is best done by choice of the target thicknesses, but the fine details of beam partition can be accomplished by exactly the same trick as used internally of "shaving" beam off the various targets.* Traditionally with internal targetting this is done by control of the perturbed orbit in the horizontal plane; in translating the system to external beam operation we have chosen the vertical plane as the more convenient in which to operate. This is largely because the position of targets, slits, transport elements, etc., can be more easily monitored and held stable in their vertical location and because one is less sensitive to jitter in the inevitable magnetic dispersion which is predominantly (and usually exclusively) in the horizontal plane. As an example, most mass-separators are for similar reasons preferentially oriented to operate in the vertical plane. In general, more precise target optics involve exact definition in one plane with more relaxed requirements in the other. Thus we tend to think, for ultimate requirements, in terms of ribbon targets in which the vertical dimension is defined by the optics of the incident proton beam. In principle the focal spot of the external beam could be used to define the source horizontally and vertically and all transverse dimensions of the target made large--which helps enormously the cooling problem; this technique will

*A further dimension of control suggested by Lambertson is the use of a wedge target so that by varying the transverse position different thicknesses can be presented to the beam.

certainly be adequate for a large number of experiments. However, when precise optics in one plane are needed it is preferable to avoid any jitter or misalignment in the EPB transport system and to rely on the target height for source definition. Furthermore, the emittance of the EPB at full intensity may be less vertically than horizontally because the use of multiturn injection results in a much larger radial emittance, which may not be recovered completely by the properties of the slow ejection system.

The scheme then proposed for series targetting which is illustrated in Fig. 6, is to bring the EPB to an initial focus, F_o, at a "clean-up" collimator at the exit from the shielding wall and thereafter to re-image the beam at each successive target. Four quadrupole singlets are used between successive images--two are needed to achieve the anastigmatic image condition and the remaining two to control the magnification independently in both planes (about a factor of 5 variation in horizontal or vertical magnification can be obtained with the placement of lenses shown in Fig. 6.) Two pairs of displaced bending magnets, (each 1.2 Tm) allow for correction of angle and position of the EPB before it enters the main channel. These must be laminated and could be servoed to correct for jitter in the extraction system. The targetting bending magnets needed to deflect the forward cones of secondary particles away from the EPB direction are placed just downstream of each focus; in the approximation of being small in extent and exactly at a focus the tracking requirements on these targetting magnets are quite modest. In addition, close to each intermediate lens is a kicker magnet of 0.6 Tm, which can be used to deflect the beam above the downstream target. No extreme requirement on timing is envisaged, viz., a laminated iron magnet with a response time in the millisecond range is quite adequate. The choice of magnetic deflection above a target serves another important purpose, namely to minimize the need for flip-target mechanisms. In some cases flip-targets would be feasible, but undesirable,

SCHEMATIC LAYOUT OF E.P.B. OPTICS WITH SERIES TARGETS

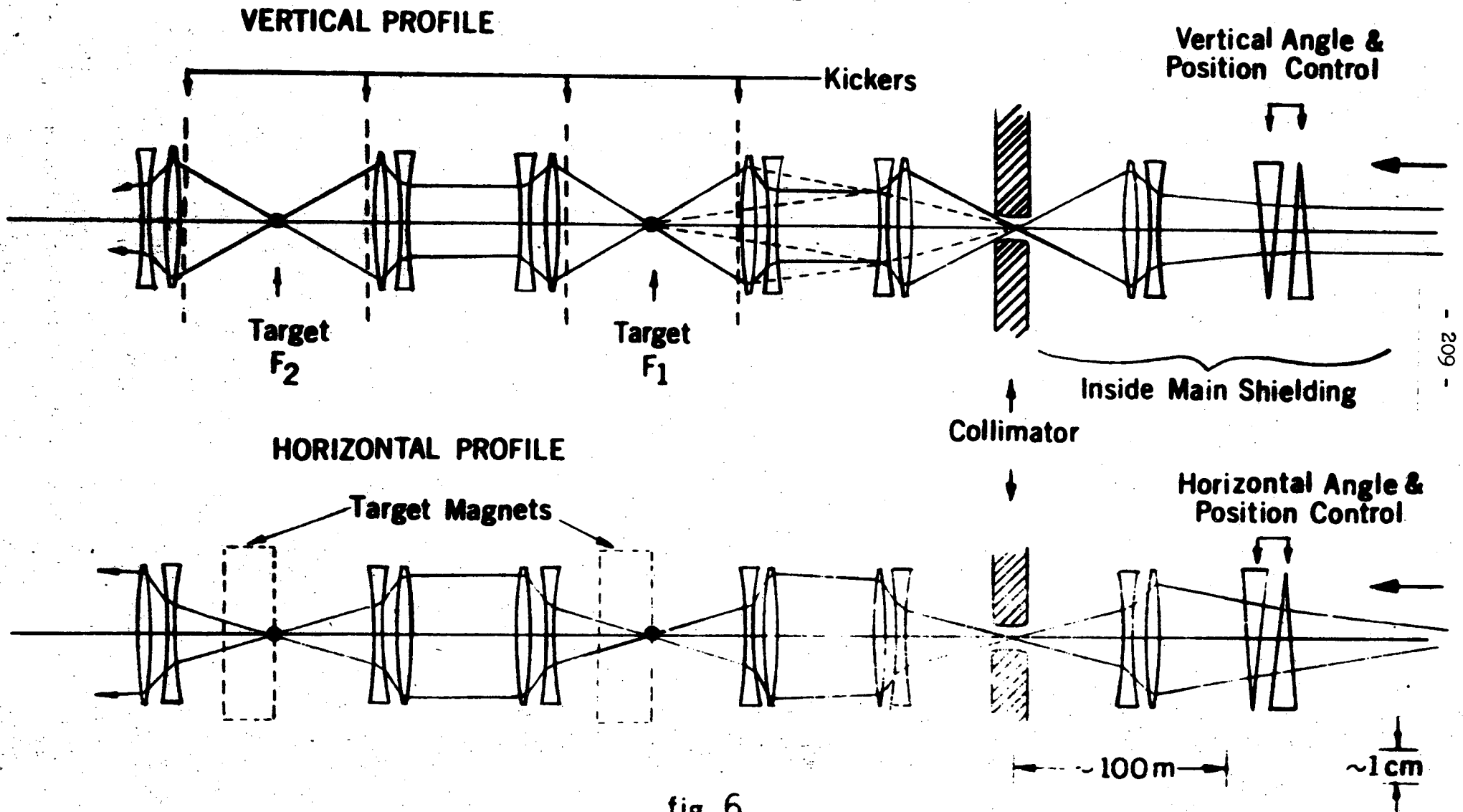

fig. 6

because of increased maintenance frequency, but in others, where a ribbon target may need elaborate cooling and still not have much mechanical rigidity, would be almost impossible. Further, a failure of the "flip" mechanism in the case of the mechanical solution, demands servicing at the point of maximum radioactivity, while in the case of the magnetic deflection solution, the servicing takes place at a much more remote location. Thus by suitable control over the kicker magnets, the "beam-shaving" operation can be carried out to any desired degree. Clearly other targets at the same target stations can be activated at different times and the kicker magnets used for rapid switching--the possibilities will not be pursued here since the main object at this juncture is to demonstrate the equivalence of the internal and external series target situations and also the relief possible in the lessened demand for high-speed mechanical flip mechanisms. A conventional method hitherto used with slow-spill internal targetting at the CPS and the AGS, has involved displacement of the closed orbit by mismatching the field and central momentum; the case envisaged here with the EPB kickers correspond to the more recently used techniques of local distortions of the orbit with the betatron periodicity) by means of kicker magnets.

Finally, it should be noted that where flip targets are used, their distance of travel need be only a few millimeters compared with centimeters in the case of internal targets--another advantage of having to deal with a small-emittance beam requiring little aperture in traversing the EPB system.

The really striking advantages of the external over the internal beam which underlie the present illustration, and cannot be overemphasized, are twofold. Firstly, the optics need to be designed only for one-shot operation, viz., misalignment, poor tracking, etc., of the various elements may result in small beam losses but they are not cumulative as in the case of the circulating beam. Secondly, quite drastic manipulations of the beam optics such as the creation of

sharp foci can easily be carried out externally but not internally. A third, less striking, but nonetheless relevant point is that the simultaneous requirement of high intensity and good optics poses a much more severe cooling problem with the internal target because of its smaller volume.

(c') Target Optics: We will rule out the importance of the operation of a rod target slanted at an angle θ to the beam on two grounds. Firstly, we wish to optimize the accelerator facilities for high energy secondary beams whereupon the angle θ becomes $\lesssim 1^{o}$, so that it is essentially parallel to the beam--thus the target holder is no longer far away from the beam and may be as efficient a source of particles as the target itself unless the latter is reasonably long. Secondly, this technique is most useful in optimizing the optics of a single experiment set up at angle θ to the beam--this requirement is almost trivial to attain in the external beam with a modest targetting magnet where in addition the production angle θ can be chosen to be 0-deg and so give an improvement in flux.

The argument that a very tiny target only a few millimeters long can provide point optics for several simultaneous experiments with independent secondary momentum control set up at non-zero production angles still remains valid. To match the appropriate fluxes in the EPB would need a longer target, and an experimenter at angle θ using a target of length L, would observe an increase in horizontal width of L Sin θ. This may, however, not be too serious a consideration in practice at high energies, because the assumed size of the internal target makes it impossible to contemplate, for cooling reasons, spilling more than a few percent of the beam on it--if it were 10% then an iron or copper external target with L $\approx$ 1 cm could match the flux conditions. Further, we must assume that secondary beams are predominantly of high energy, so that θ is on the average smaller than at present machines. With $\theta \sim 6^{o}$ and L = 1 cm, the extra breadth

is only 1 mm. It is hard to believe that this could be a critical consideration. In addition, some of the deterioration in quality in the horizontal plane can be offset through a gain in the vertical plane by the ability to achieve a small vertical spot size. Thus by suitable choice of his secondary beam characteristics, e.g., demagnification horizontally, the experimenter can escape at least some of the troubles of obliquity broadening.

An outstanding feature of the one-shot optics fo the EPB transport is the possibility of producing very small focal spots. Consider the case of striving for maximum production and minimum target size. Thus the length, L, of the target will be close to one m.f.p. If the emittance of the beam in one plane (πA) is represented by an ellipse (see Fig. 7), the acceptance of the target is a parallelogram of area 2 RL, and we can inquire the minimum value R_{min} needed to achieve matching. The answer is

$$R_{min} = \sqrt{AL}.$$

With A = 0.05 mm mr and L = 15 cm,

$$R_{min} = 0.09 \text{ mm} = 0.003 \text{ ins.}$$

Thus in the vertical plane a target 0.18 mm in total height could ensure a full traversal of all incident protons. If needed, the horizontal width could be made about the same. The assumption is that one could view the target at 0-deg. There would be some cooling problems with a target of this size if the full beam were to be used, however the desirability of good optics is separable from the need for maximum incident beam. Obviously, even thinner targets could be used, but only a fraction of the beam could traverse their entire length. Purely from the standpoint of optics, one wonders if there is a practical limit in size set by quadrupole aberrations, collimator slit sizes, etc; at the moment, a target $\approx$ 0.18 mm high seems considerably smaller than needed.

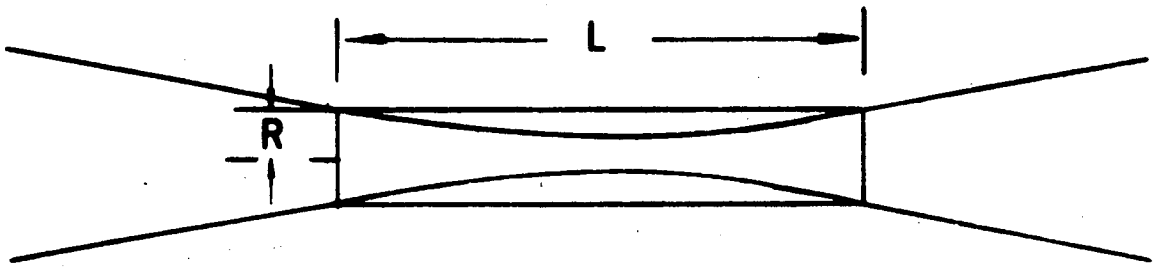

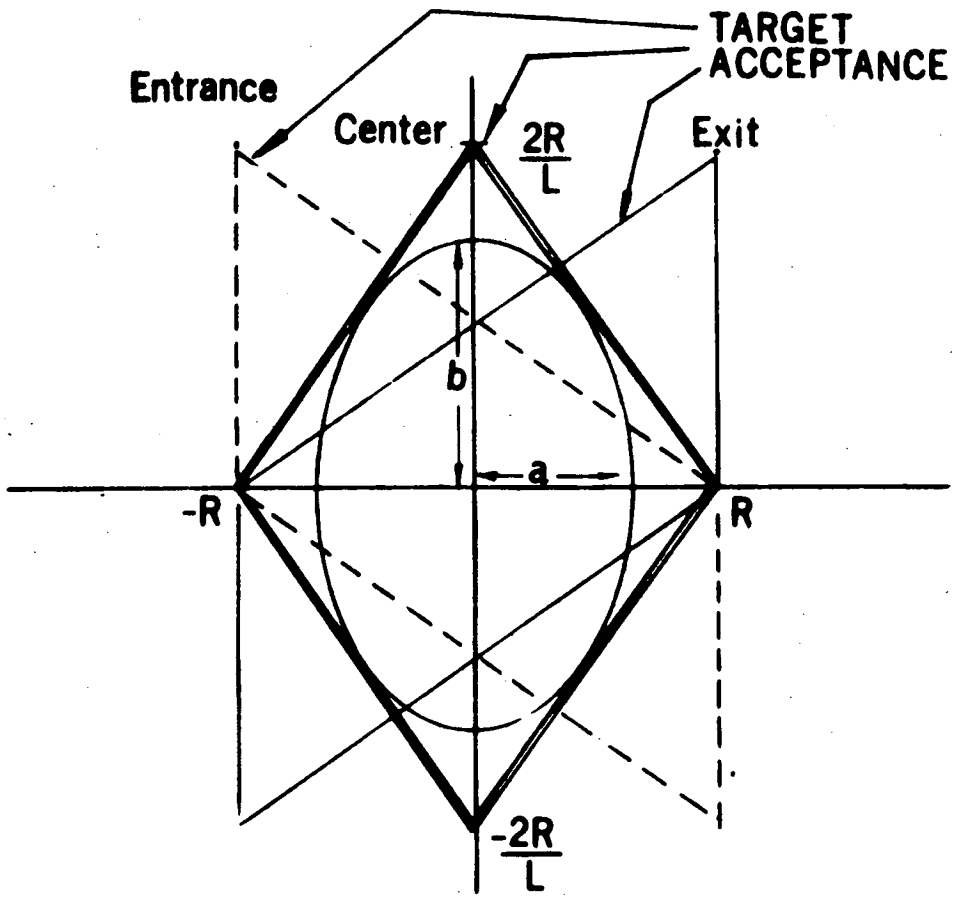

Beam Emittance = $\pi ab = \pi A$

Target Acceptance = $4R^2/L > \pi A$

R min = $\sqrt{AL}$

fig. 7

(iii) Preservation of the Accelerator: The discussions of the previous sections have shown that there are advantages in operating with external targets insofar as the experimenter's needs are concerned. There are also advantages from the point of view of the accelerator itself. The phrase "preservation of the accelerator" is intended to have the connotations of ease of maintenance, lifetime, minimum interferences with operation and running efficiency of the machine.

Several relevant reasons for developing external beams fairly extensively, even in the earliest phase, can be listed as follows:

(a) Internal target areas have 100% coupling with the main ring; the accelerator must be turned off to allow set up or repair of the front end of an experiment. The unstacking of the enormous mass of shielding and the handling and surveying of equipment in a radioactive environment involve times of several weeks, and not hours, of machine down time. Conversely, if troubles develop in the early transport sections of an experiment, then repairs will have to be delayed until a shutdown of substantial length can be negotiated. The more internal target areas there are, the more interference with continuous beam operation that will follow. Each of the two external beams, and, independently, certain of the target areas in each beam (see below) are easily decoupled without halting machine operation, and with minimum disturbance to the experimental program. A basic premise is that the maximum continuous operation of the accelerator is the most important thing to safeguard. Without the circulating beam, all experimental activities are at a standstill, whereas even if all experiments are for some reason incapable of running, accelerator study and development can proceed and possibly optimization of the beam may be made if needed. Another reason for minimizing interruptions to the operation of the main ring is to avoid the inevitable loss in time during start-up as the operators try to tune up

the machine again. The second objective to strive for is that set up or repair of an experiment should have the minimum interference with the rest of the experimental program. Given more than one experiment looking at the same target, it is inevitable that there has to be some interference, and the best that can be hoped for is to isolate individual target areas. Some schemes for allowing this without inordinate expense will be described later.

(b) Work in an internal target area must be started immediately after turn off because machine time is at a premium--this implies, however, the time of highest radioactivity. In an external area, a cool-down period of days is not difficult to arrange for.

(c) If the extraction efficiency is ~ 90% for slow beams and ~ 100% for fast beams, then the induced activity and the radiation damage in the machine are reduced by a factor in the neighborhood of 20.

(d) Movements and re-stacking of large amounts of shielding close to a target can result in misalignments of neighboring magnets. This may be annoying but tolerable in an external beam which the protons traverse only once, but intolerable in the main ring. An allied effect, resulting also in closed orbit deviations, arises from the proximity of pieces of experimenters' equipment to the target, such as separators or magnets with stray fields, and again the EPB is much less sensitive to this effect.

(e) Crane handling in the external beam target areas is removed from the constraint of the ring structure and tunnel and also from the maximum pressure of getting everything back together in the shortest possible time.

V. THE ROLE OF INTERNAL TARGET AREAS

Given the existence of external beams serving several target areas (c.f. VI, VII), then it is unreasonable to consider the inclusion of more than one internal area in the initial design.

After some years of operation, when expansion of the number of experimental areas is required, it would be possible to add a further experimental area utilitzing one of the other unused long straight sections. Whether this should be an internal area or external area could then be based on experience of operation with both systems. Not enough experience has been gained with external beams at AG machines to be certain that there are not unforeseen practical difficulties associated with running a large experimental program entirely externally. Both the Cosmotron and Bevatron programs rely heavily on the extracted beam--the superior quality and efficiency of the extraction system in an AG machine and the many arguments given earlier based on the differences at the high energy machine increase our confidence that there are no unforeseen major difficulties at the new machine. Apart from being extra insurance, other features which can be listed in favor of the retention of some internal target facilities are:

(i) Physics experiments utilizing an experimental target in the circulating beam: This is in contrast to the use of an internal metal target to produce secondary particles for experimental use. One good example is the use of a thin polyethylene foil target (c.f., Ref. 22), or, better, a gaseous hydrogen target, to study low-momentum-transfer p-p interactions. In this case, the thickness of the target is determined only by the need to allow low energy protons to escape from the target without too much scattering or energy loss. Thus, as lower momentum transfers are explored, the rate of events per traversal becomes smaller, and the experiment becomes very time-consuming in the EPB. (If the gas target length = 0.1 m, pressure = 0.1 atm, the target is 1×10^{-5} gm cm^{-2} thick. Thus only about 1 proton in 10^{8} will make an interaction of any kind, of which perhaps 10^{-4} are really low momentum transfer.) Internally, however, the protons can pass through the target some 10^{4} times, thus enhancing the rate without affecting the recoil escape conditions.

Here, then, is a case where there are great gains to be made by multiple traversals and, while one cannot be specific at this time, it is possible to imagine that other experiments with a similar requirement may be invented. To do such experiments requires a straight section free of extraction equipment to allow the secondary analysing and detection channel to be set up. In other words, these provisions consititute a rudimentary internal area of sorts, although the shielding need be far less than in a conventional internal area. For example, only a few percent of the beam need be utilized on the internal hydrogen area.

(ii) The tune-up period after turn-on: It is only realistic to assume that there is a period between one-half and one year when circulating protons of low intensity but in the new energy range are available inside the machine. During this time, tuning of the accelerator, and later, tuning of the extraction and external transport systems will take place. For several months, therefore, secondary beam survey work and certain experiments could usefully be operating from an internal target. This is the time when the beam is naturally low and when the damage and activation due to internal targetting are least serious. Much of this initial experimentation could be run parasitically to the accelerator development and as time went on, an increasing fraction of time could be made available purely for experimentation.

(iii) Decoupled "point" optics: Several experiments can obtain "point" optics with decoupled momentum requirements from a straight section target. The merits and demerits of this situation contrasted with what is obtainable in the external beam have already been discussed. The advantages for high energy beams have been shown to be negligible.

(iv) Indefinite small target emittance: In principle an extremely small target can be inserted in the internal beam and, provided a long enough flat-top is available, all particles (apart from

those lost to the walls) in the circulating beam will eventually interact in the target. Thus, in contrast to the external beam case, where the smallest transverse size consistent with high flux is determined by the matching condition, the time duration of the spill can be traded for an improved target emittance. This is a fundamental point of superiority of internal over external targets, but it is not clear whether the gain is nebulous in that it implies conditions that cannot be exploited. At such high energies the size of a matched external target is close to the limits set by component leveling tolerances and by the design of internal targets of any smaller dimensions is beset by the problems of finite target holder size and of cooling.

In conclusion, unless really fundamental disadvantages of external beams as maximum-utility areas emerge, it seems uneconomical to devote much money to the internal area in the initial phase, since the arguments for its existence are rather weak, and involve a short-term outlook. A rather modest building and crane with the minimum of de-mountable shielding would take care of requirements (i) and (ii), which are the most commanding, and would allow the exploitation of feature (iv)--with some inconvenience--if ever it became necessary. Money spent in too extensive a development of internal areas to the detriment of external areas would tend to steer part of the experimental program in a direction contrary to the basic philosophy of operation outlined earlier--the preservation of the machine as a unit and the decoupling of the experimental areas.

VI. EXTERNAL BEAM FACILITIES - STRATEGY

This section describes in broad outline a plan for the development of effective target facilities. Experience at past machines has shown that the initial planning of target facilities influences for many years the pattern of experimentation. It was only after several years of operation of internal targets that the Cosmotron and Bevatron were converted to external target operation; at the AGS and PS, although the prospects of more efficient beam extraction have been established, the mounting of an effective general purpose research effort based on external beams seems

several years in the future. At larger and more expensive machines the financial investment in and experimenters' commitment to the target facilities existing in the early years is expected to result in a considerable delay in changing the general approach to the experimental facilities. Thus it is important to avoid the attitude that external beam areas are an addendum which can be added later, because it would be very much later, if at all, and instead to recognize the clear advantages in their extensive development in the initial phase of operation. The separate features of the proposed development of target facilities in this direction may be itemized as follows:

Proposition 1: Heavy reliance for all phases of the experimental program will be placed on operating from external beam targets. At a minimum it is known that certain external beam facilities will be required--one obvious example is for neutrino experiments. Another is in the operation of a very large bubble chamber (which may be difficult to move) because an external beam allows the variation of target-to-detector distance by variation of the target location. Besides this, the success of the slow extraction system and the case of access to 0-deg production angle will increase the desirability of external beam targets for counter experiments. All the arguments in favor of making the transition from considering external target facilities merely as special-purpose or desirable facilities to treating them as general-purpose and major areas are strongly reinforced upon consideration of the new features to be met with at the 200 GeV accelerator (c.f., Sec. II) and of the diminished strength of the arguments for internal versus external targets (c.f., Sec. IV).

Proposition 2: More than one external beam is necessary. Even in the initial stages of operation at least two are required. This is a logical requirement once the major experimental program is oriented towards external targetting. The advantages of multiple external beams have been outlines in some detail in Sec. IV (iii).

Proposition 3: The magnet power supply and the extraction equipment will be designed for variable-energy operation, tentatively we assumed between E_o = 40 GeV and E_o = 200 GeV. Variable energy operation includes variable peak field, but also the ability to spill beam at an energy lower than the peak operation value. For fast spills the intermediate energy spill or spills could be delivered on the leading edge of the magnet cycle.

If the energy needed for a fast spill exceeds that for the slow spill it is preferable to deliver the fast spill earlier in the cycle and to deliver the slow spill later in the magnet cycle. If the slow spill were to occur during a "front porch" on the leading edge of the magnet cycle it would involve debunching and later rebunching the beam to carry it to higher energy. More beam is likely to be inadvertently lost in this operation than in negotiating inversion with the r-f phase-lock system in operation. Finally, in the interest of maximum overall efficiency it is always better to effect the more efficient extraction process first. The variable energy feature is important for four reasons: studying the interaction of primary protons; extra flexibility in serving experimenters with 0-deg beams (see VII); optimization of yield for low energy secondary beams (including neutrinos); and finally, the desire to run the machine at the minimum beam power acceptable to experimenters at any given time, to reduce activation and damage.

It may be worth having a target area to be used only for low primary energy, say in the neighborhood of E_o = 40 GeV. This could take the form of a separate extraction point in which all the septum extraction magnet apertures and peak fields were designed for best efficiency at E_o = 40 GeV or it could be an intermediate target station along a regular full-energy channel where one was allowed to place a target in the beam only at the low primary energy. There are two major advantages in such a scheme for feeding low energy experiments (say E ~ 5 GeV). Firstly, the flux of mesons will in general be higher even if the repetition rate is kept the same--this follows from the CKP formula

$$\frac{dN}{dE} = \frac{n\pi}{T} \; e^{-E/T} \qquad \text{where } n_\pi \propto E_o^{1/4}, \quad T \propto E_o^{3/4}$$

Hence $\frac{dN}{dE} \propto \frac{1}{E_o^{1/2}} \; e^{-E/T}$, which for small E increases as E_o is decreased. If the repetition rate is allowed to vary, the flux further increases since

$$\frac{dN}{dE} \alpha \left(\frac{1}{\tau + RE_o/100}\right) \frac{1}{E_o^{1/2}} e^{-E/T}$$

where τ = Dwell time + flat-top time

R = Regular rise time at 200 GeV

If we take τ = 0.3 sec and R = 0.7 sec, then dropping the primary energy from 200 GeV to 40 GeV gives a gain due to increased frequency of a factor of three, which is close to the ultimate gain 3.3 set by the irreducible time τ.

The second advantage is that the muon shielding can be drastically reduced at the low E_o target station (the shield for strongly interacting particles will change only slightly). This will allow experimenters to build shorter beams and reduce to a minimum the portion of their transport equipment inaccessibly buried in the shielding wall.

Proposition 4: The extraction system will be designed to allow comprehensive beam sharing. This includes being able to spill both fast and slow beams into a given channel and to spill beam into more than one external channel--in general at different energies--during a single beam pulse. A fast kicker close to the location of the perturbing magnet of the slow extraction system will be used to deflect the beam into the successive septum magnets and the fast beam will follow the same route as the slow beam. In principle, there need be no loss on the septum but this implies a kicker rise time $\leq$ 20 ns. If such a rise time cannot be achieved, the loss can be restricted either to the leading or the trailing edge of the kicker pulse by correct phasing with respect to a gap in the train of bunches in the main ring. Since a kicker pulse length ~ 50 ns can be attained, as few as 3 bunches or about 1/3% of the circulating beam intensity can be spilled at will. At least for bubble chamber use, therefore, very precise intensity partition will be possible.

Sharing of the slow beam in two or more separate channels will almost certainly have to be done sequentially (rather than simultaneously). Although it is possible to think of a scheme such that the particles growing in amplitude because of a perturbation at one place would be divided between the septum magnets at two extraction locations, it sounds difficult to achieve efficiently and we will assume that slow extraction will be completed at one channel and the perturbing magnet disabled before the

second channel is operated. Thus, there is time lost in sharing slow beams between alternative channels. The only possibility then of simultaneous slow spill sharing is by the use of series targets in one channel. Referring to Fig. 2, one sees that the beam is bumped into the perturbing magnets by means of two slow deflectors placed upstream and downstream. An intensity monitor in the external beam will be used to feed-back to these magnets to control the rate of spill-out. Thus, reasonably good intensity control for small fractions is possible for the slow beams though not as good as for the fast beams.

Proposition 5: It is desirable to develop the external beam with series targets. With reasonable transport equipment the external beam will emerge from a straight section at an angle of about 2° and will travel about 200 meters from the extraction point before it is clear of the shield and is useful for experimental purposes. In that distance, a number of vertical and horizontal steering magnets and quadrupoles are incorporated to allow for the adjustment of the position and size of the spot at the first focus, F_1 (Fig. 8). Successive target locations can be achieved by means of quadrupoles producing second, third, etc., foci downstream. Although the magnetic rigidity of the extracted beam is high, the quadrupoles are not unduly expensive because the small emittance allows the choice of small aperture (radius ~ 3 cm).

In principle, the external beam could be allowed to extend in a straight line and targets introduced as required at the foci. However, this forces one to use beams away from 0-deg production angles; it seems difficult to get closer than about 10 mr to the forward direction using such a "straight section" target. Furthermore, the first transport elements in the secondary beam are forced to be far away with consequent loss in solid angle. At low energies, the loss in flux is not very serious but for high energy beams it is catastrophic. For example, at 100 GeV secondary momentum the flux is two orders of magnitude less at 10 mr than at 0°. Therefore, we can be certain that for high energy beams a bending magnet of considerable size will be needed downstream of the target to deflect away the forward cone of secondary particles to bring it clear of the primary beam. We have assumed as typical a magnet with 20 Tesla-meters which would deflect the 200 GeV beam by 30 mr. In a high energy beam of energy E GeV, the angle of the bend of the 0-deg ray is

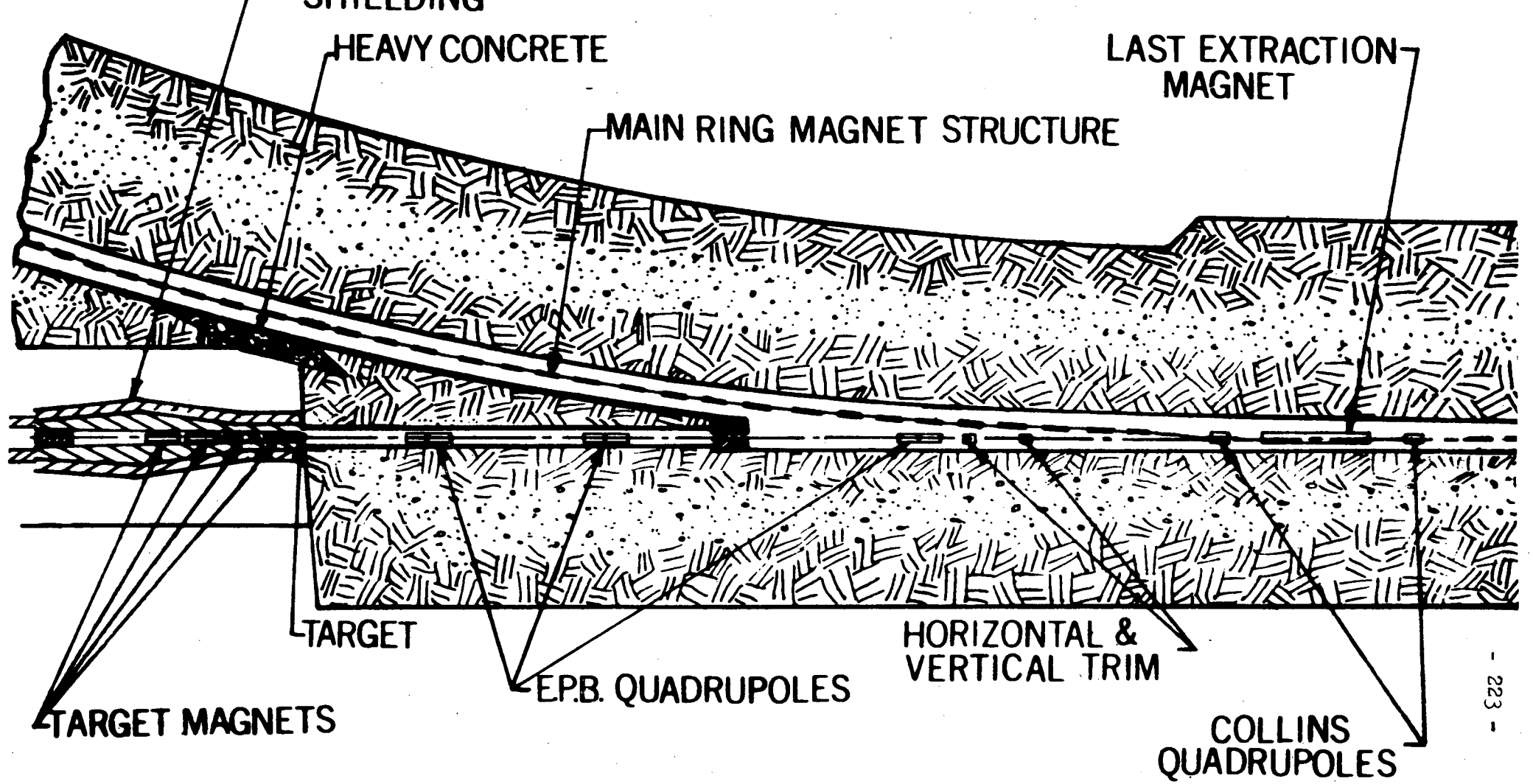

SCALE: 1cm-10M

fig. 8

$$\varphi = \left(\frac{3}{10E}\right) 20 = \frac{6}{E} \text{ radians}$$

which is to be compared with the rms production angle

$$\theta = \frac{0.54}{E} \text{ radians--using an average transverse momentum of 0.44 GeV/c.}$$

Thus, since $\varphi \approx 11\theta$, the entire cone can be deflected clear of the protons, and it can be easily shown that quadrupole lenses with elements about 2-3 m long are capable of capturing the major part of the produced flux into an experimenter's channel.

The methods of targetting will be considered later in more detail; at the moment we will confine ourselves to the gross features of the external beams. Firstly, it is attractive to try to set up several targets in series so that with a long spill time several experiments looking at different targets can be used. About three or four such series simultaneous targets seems a reasonable upper limit. Secondly, whether several experimenters chose to operate simultaneously or sequentially, a number of successive target stations in the same EPB channel would allow a variety of experiments to exploit the same EPB extraction and transport equipment and shielding and to utilize power and facilities in a more compact area. Thirdly, a very valuable feature for an experiment involving massive and immobile equipment (e.g., a neutrino experiment) is the ability to change the target-to-detector distance according as secondary beams involving different particle energies and lengths are required. With the choice of three or four target stations with intervals of 150-200 m between them, this creates a beam "trombone" of the order of one-half a kilometer. Another possible way which has been proposed for catering for this last requirement is to transport an external beam a very long distance without any permanent target areas in the direction of the remotely-sited equipment (say 2-3 km from the machine) and install a target wherever and whenever it is needed. Unfortunately, the shielding and transport equipment to carry the beam over great distances is never cheap and the special muon shielding required to be built around the chosen target location is so enormous that this concept of an indefinitely flexible "traveling" target does not seem practicalbe. After the machine

has been running for some years and an extension in the number of target areas is needed, the above are valid arguments why it might be preferable to extend serially one of the operating EPB channels rather than open up a new extraction point. There are, of course, arguments for the latter choice, the main one being the strategy of decoupling another batch of experiments so that if one EPB channel is turned off, only a small part of the experimental program is interrupted.

Proposition 6: It is desirable to incorporate switchyards in the external beam. Given the need for a large bending magnet just downstream of a target, an attractive possibility is the creation of an EPB switch-point simply by allowing for reversal of the field. The idea of using a bending magnet to switch an external beam between different areas is an old one, but there are some new features in the present case. Firstly, the switching magnets are free since they are needed for the target area--thus every target area is potentially a switch point. Secondly, in a scheme where each target is imaged onto the succeeding one by lenses, the magnets are very close to the foci and their field uniformity and tracking requirements are modest. Thirdly, a reversible field at the target is highly desirable for many high energy experiments--it enables one to have a beam of either sign particle of the same momentum down a fixed channel with all optical properties preserved. (An obvious example is the study of the small differences between the cross-sections of particles and antiparticles where it would be a great advantage to be able to alternate charges fairly frequently and still preserve the beam optics.)

Figure 9 shows a schematic layout of some possible combinations of series targets, some with switchyards. More details of the individual components are shown in Fig. 10. A more detailed layout is shown in Fig.11 for the arrangement of Fig. 9(e). A switchpoint for low energy (0-30 GeV) targetting in which the dispersion angle φ is chosen to be close to the RMS production angle θ (See Fig. 10(d)) has the advantage that the maximum transverse excursion of the EPB is only a few centimeters. Thus the various orbits of the EPB depending on the magnet setting can be recombined to the de-switching point 60 m downstream where another low energy target station is located. However, when the switchpoint is at a large bending magnet ($\varphi \simeq 30$ mr), this will be the natural choice for

SCHEMATIC LAYOUT OF SOME SERIES-TARGET ARRANGEMENTS

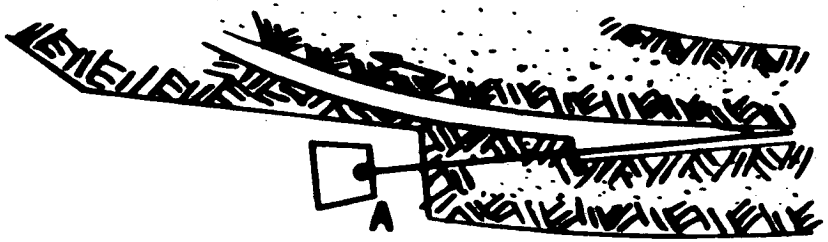

9 Single Backstop Area

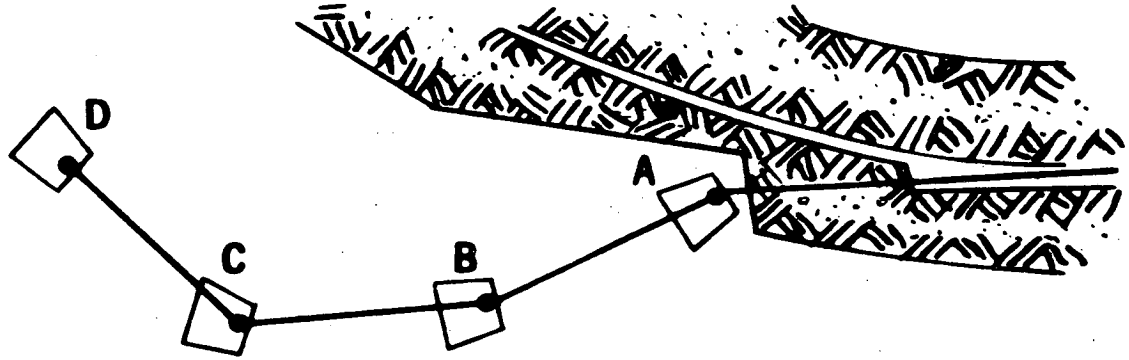

9d Series Targets No Switchyards

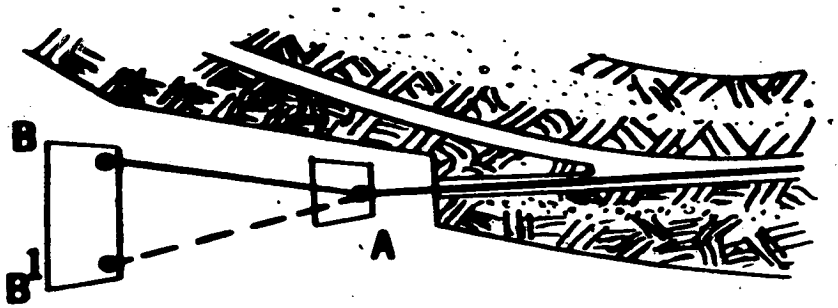

9b Switchyard With Two Alternative Backstop Areas

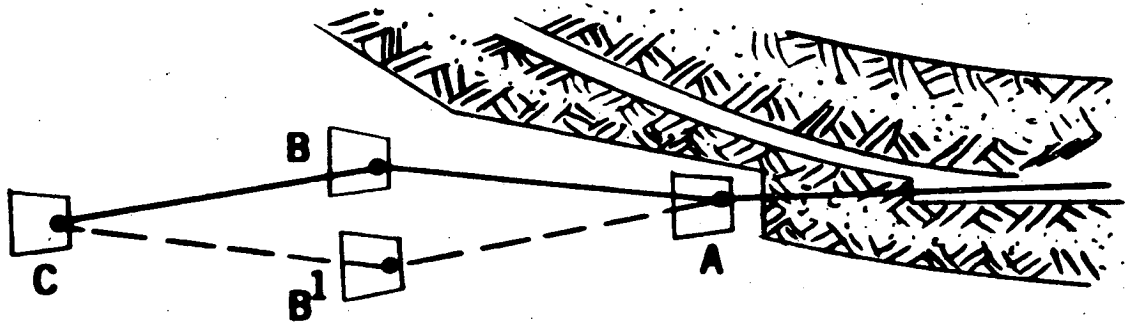

9e Series Targets With Switchyard and Recombination at Final Area

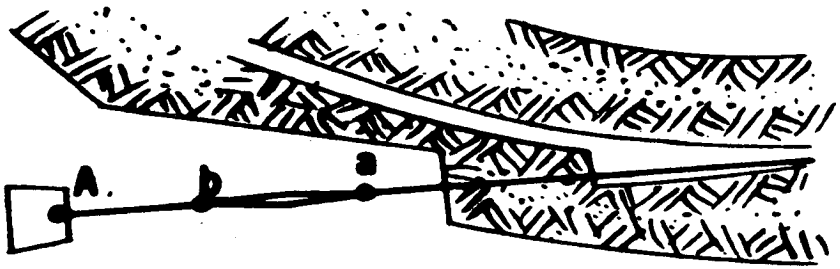

9c Low Energy Switchyard (-b) and Backstop Area

fig. 9

HIGH ENERGY TARGET STATIONS AND SWITCHYARDS

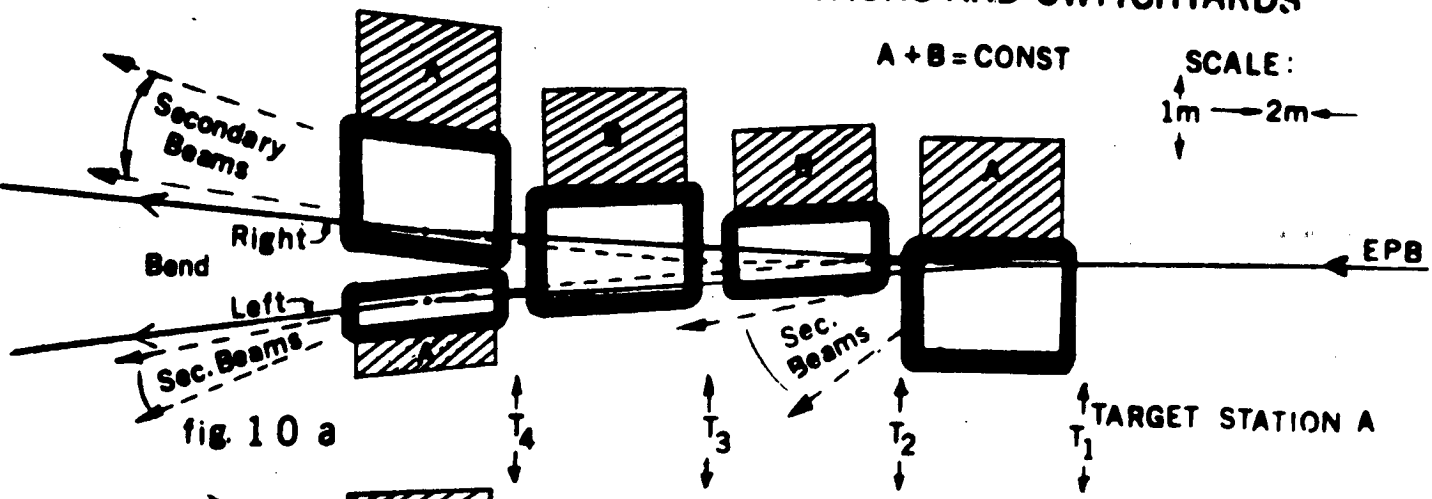

fig. 10 a

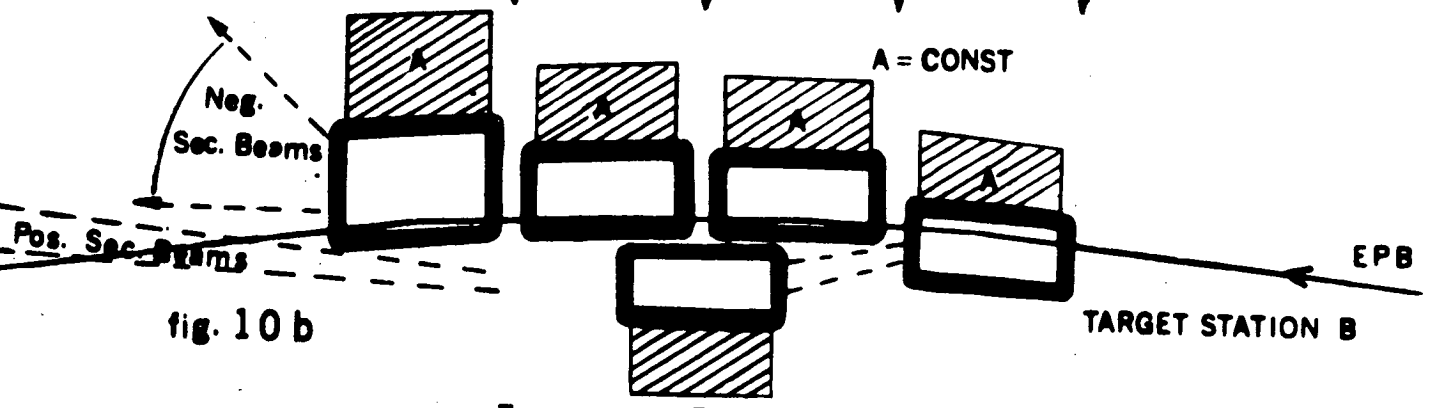

fig. 10 b

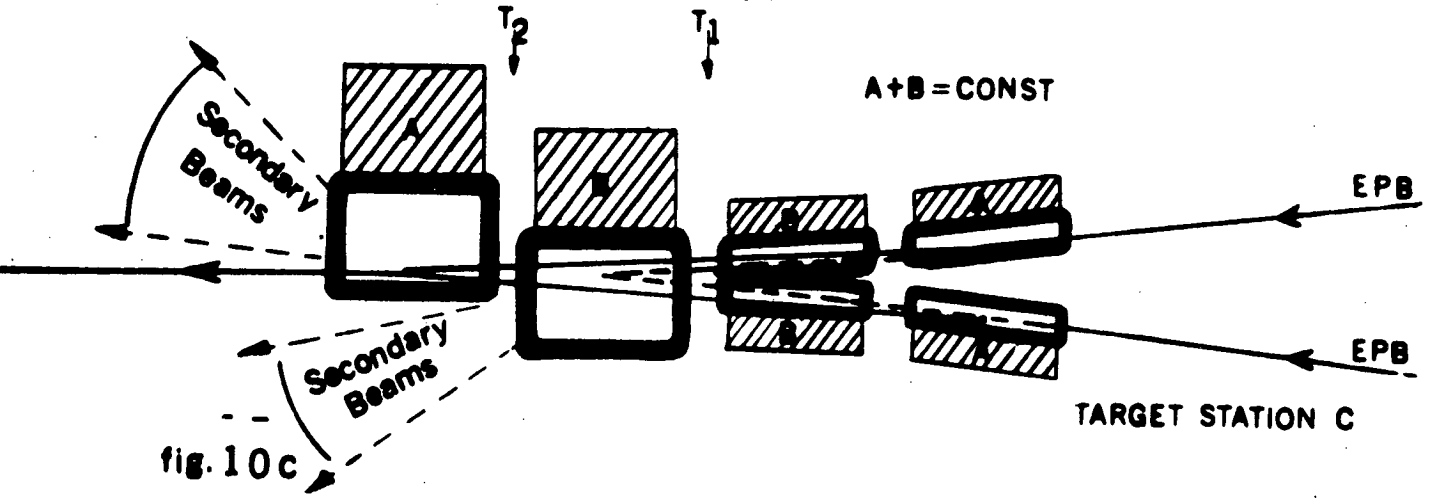

fig. 10 c

LOW - ENERGY TARGET STATIONS

SWITCHYARD WITH QUADRUPOLE RECOMBINATION

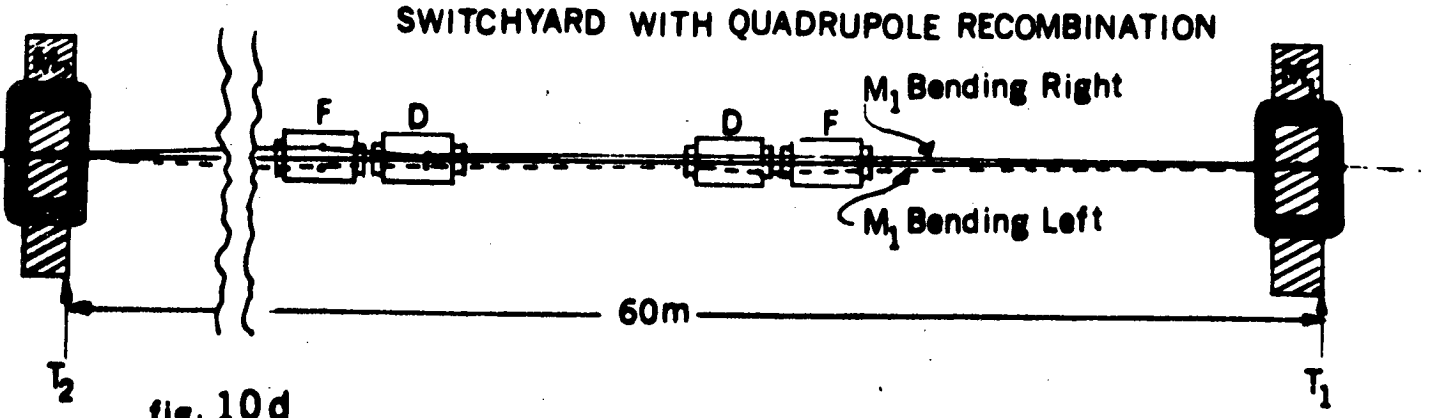

fig. 10 d

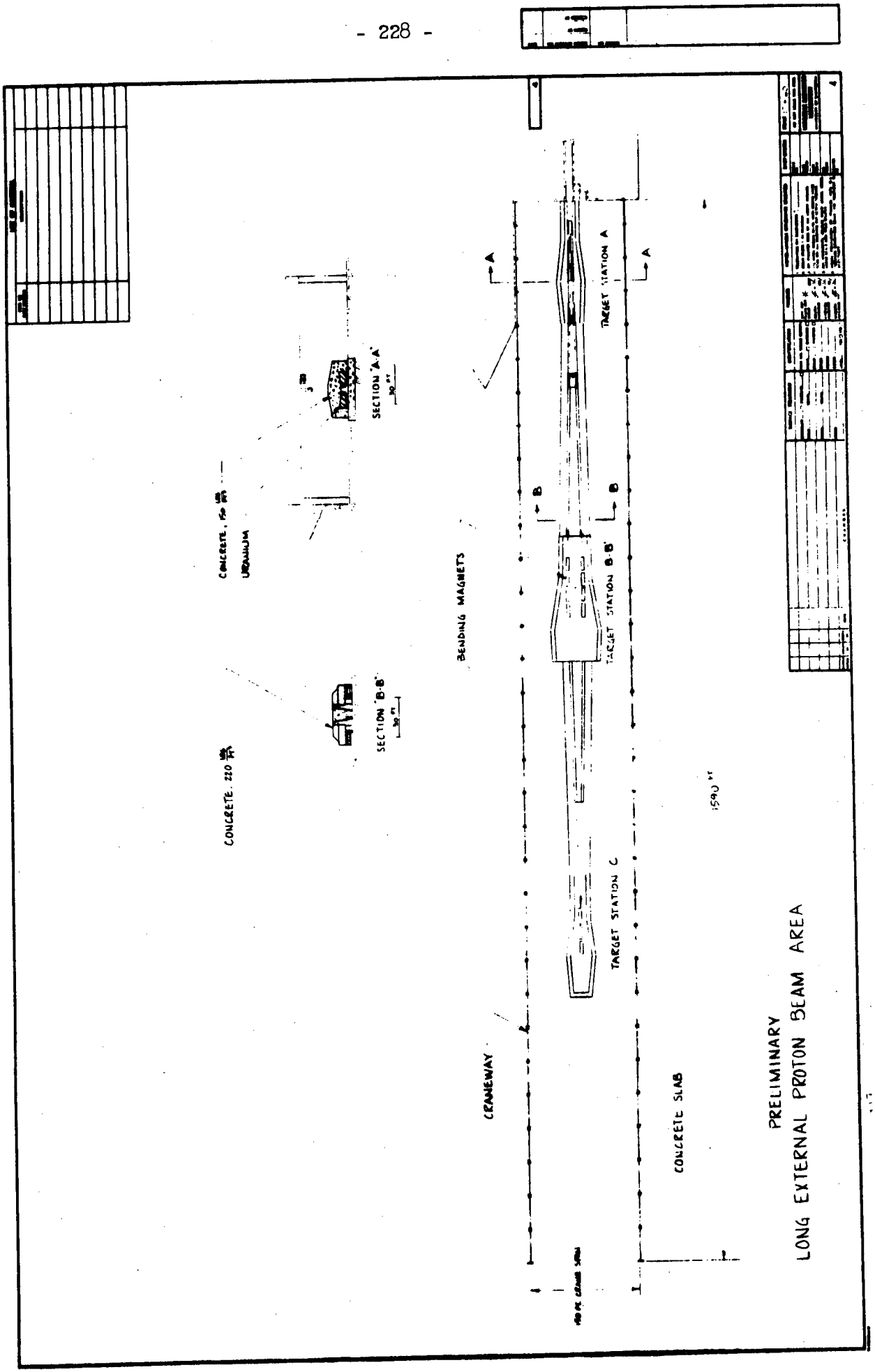
PRELIMINARY
LONG EXTERNAL PROTON BEAM AREA
TARGET STATION A
TARGET STATION B-B
TARGET STATION C
BENDING MAGNETS
CRANEWAY
CONCRETE SLAB
SECTION 'A-A'
SECTION 'B-B'
CONCRETE
URANIUM

Figure 11

a target to give high energy secondary beams, which in general require a long run-out distance within the transverse shielding wall for the EPB which such beams are bound to occupy. Therefore, it is advisable that the next target area downstream of the switchpoint should be no closer than about 150 m. However, the two forks of the EPB channel at this point (B, B' in Fig. 9(e)) have a separation of $\gtrsim 9$ m and thus essentially require two separate tunnels with a consequent extra cost in the shielding. The increase in cost is less than a factor of two, however, because the expensive modular shielding is needed only on the outside of each beam. The target magnets at this point are choen to bend both forks of the beam back to a common point some 150-200 m further downstream creating yet a further target area. (Location C in Fig. 9(e)). Since only one of the routes ABC of AB'C can operate at a given time, one of the target areas B or B' will be idle. One may question whether it would be better to pursue the alternative development shown in Fig. 9(d), abandoning any high energy switchyards, and simply spend the money on developing another series area, such as D, which has the additional advantage of being accessible from two sides. There are three arguments favoring the establishment of the choice B B'. Firstly, the shielding is less expensive, secondly, it enhances the flexibility of target location A by allowing charge reversal in existing beams, and thirdly, it allows the B or B' area to be decoupled from the A and C areas for set-up and maintenance. The weight of the third argument depends on the frequency and enormity of the set-up work; if we assume it to be a lengthy and tedious operation, then this higher-order decoupling may be very important, since experimenters could have most frequent access to the B or B' areas for the minimum interruption of the over-all schedule. There are other solutions, however: the extra area could be created by extracting another beam--this would be more costly and would not have the simultaneous series target feature. Alternatively, in the linear system without branchpoints a removable plug could be installed in the path of the beam at each target station which could be used to interrupt service to all points further down the line.

The choices mentioned do not exhaust the possibilities, but give an idea of the wide variety of plausible configurations and the possible directions of growth of the target areas.

Conclusions

The main advantages of using the external beams to decouple experimental areas and to provide series target operation in an extensively developed system can be summarized as follows:

(i) Access to 0-deg production angle for both positive and negative beams--a sine qua non for high energies--is easily achieved by means of a targetting magnet in the external beam.

(ii) Very good target optics (transverse target size ~ .005") are possible because the external beam has small emittance and can be focussed.

(iii) Target efficiencies very close to those obtainable with multiple-traversal internal targets can be obtained. In the worst case they are more than half the internal target efficiencies, in the best case they can be better, and, in general, the machine productivity integrated over all experiments is closely similar to the best achievable internally.

(iv) Operation of a "straight section" target in the external beam to feed low-energy (0-30 GeV) parasites who wish to have decoupled secondary momenta allows access to more forward angles of production because of the smaller size of vacuum chamber. The increased advantages of a "quasi-straight section", i.e., a weak target magnet, station have also been described.

(v) Rebuilding of the configuation of the target magnets to cater for special experimental set-ups is a very powerful aspect of the flexibility of external beam targetting. The EPB channel has boundary conditions, namely the input and output directions and turning point must be preserved, but these still allow considerable latitude in the positioning of the individual magnets making up the target magnet complex, e.g., they can be interchanged, or moved apart or, for special reasons, a very high-field short magnet substituted in their place.

(vi) Another form of rebuilding of the target station is possible when maximum flux is of utmost importance. The target can be moved upstream of the target-magnet and a quadrupole placed between target and magnet. Thus focussing of the secondary beam can begin before the dispersion; the other way around the quadrupole is constrained to be ~ 10 m away whereas in some cases it is necessary to have it only 2-3 m from the target.

(vii) Multiple secondary beam set-ups are easily achieved because the target magnet acts as a "fan-out" for beams of different momentum and charge. We envisage a clear distinction between the number of secondary beams installed at a given target location--probably between three and five--and the number which can actually use the same beam spill on the same target at that station--probably two. In general, several targets will be available at any target station, but perhaps only one operating at a given time for certain prime users--the other installed channels accepting particles of any momentum in order to time counters test spark chambers, etc.

In addition to the advantages for experimenters, there are distinct gains in the ease of targetting from the practical standpoint.

(i) The cooling problem is reduced in proportion to the single/multiple traversal ratio. Further, the freedom of access to the EPB vacuum chamber allows the use of a ribbon target cooled from the edges and through radiation by surfaces placed nearby above and below it.

(ii) For plunge or flip-targets the travel distance need be only a few millimeters.

(iii) A system using only modest kicker magnets and the long lever arms available in the EPB can be used to achieve rapid switching from target to target and minimize the need for mechanically moved targets.

The many details touched upon in this section all add up to a compelling argument in favor of the external areas being developed and encourage to the fullest. However, they do not constitute an argument for the complete abandonment of internal target areas unless one can prove that everything that can be done with an internal target can as well be done with an external target. Unforturately, no absolute proof can be given, although a detailed study of many different experimental situations shows that many experiments will be superior in the external beam and only in certain cases are there gains--even then only marginal--from operating internally. A reasonable scheduling rule based on the need to preserve the life, accessibility and efficiency of the accelerator would be "If an experiment can be done about as well internally or externally, then it is to be located externally." To enforce the rule, however, requires that the external areas are adequately equipped.

VII. EXTERNAL BEAM TACTICS AND DIFFICULTIES

Next we come to some serious problems associated with targetting at high energies. These difficulties are not so much pertinent to the debate over the relative advantages of internal and external targets but are a direct consequence of the physics of high energy particle production. The first problem of being able to look at 0-deg production angle is solved by the use of a target magnet which deflects the cone of secondary particles away from the primary proton direction so that it can be captured into a secondary beam transport system. The next problem which arises is how to achieve variation in this secondary momentum without interfering with the progress of the EPB. At a backstop the solution is simple. It is just a matter of changing the current in the target magnet and allowing the proton beam to be changed in position of impact into the beam dump. In an intermediate target location there are five possible solutions.

(a) Take the primary proton spill at a suitable energy such that the magnetic field, which is tracking the accelerator field, gives the correct $\int B d\ell$ to deflect the new momentum into the installed secondary channel.

(b) Move the target downstream in the magnet to establish the correct $\int Bd\ell$ in the remaining field for the new secondary momentum. The secondary channel now requires a steering magnet to correct for the change in angle of emergence from the target magnet.

(c) Construct the target magnet complex with magnets of different fields, the sum of which deflect the proton beam and only part of which deflects the secondary beam. Thus part of the field affecting the secondary beam can be adjusted to select the right momentum and the sum deflection of the EPB maintained simultaneously. A special case of such a system was proposed by Wenzel[23] several years ago for use in the external proton beam at the Bevatron; in this case the entrance and exit directions were the same (see Fig. 12(a)) and a kink could be inserted in the beam by means of a quartet of bending magnets operating such that $B_1 = -B_2 = -B_3 = +B_4$. If the secondary particles passed through only the B_1 (or B_2) field, then this was a freely variable parameter provided the boundary conditions were satisified, and control of B_1 could be used by an experimenter to vary the momentum of his secondary beam. A suggestion that this scheme could be incorporated in a $\pi/2$-type straight section for application in internal beam targetting was made by Kerth.[24] More general schemes involving the basic idea of a two component field, one of which is a free parameter can be drawn (Fig. 12) if the EPB is constrained only to have a fixed angle of bend and fixed turning point.[25] No particular advantage can be seen for the scheme of Fig. 12(b) and that of Fig. 12(c) is chosen to be representative of a usable target magnet configuration. It uses only half the electrical power of scheme (a) and allows for more flexibility in the layout of secondary beams.

(d) The arrangement converse to that described in (c) can be constructed, viz., to allow the proton beam to traverse a fixed field and to correct the secondary beam emerging from the target magnet by means of two further magnets to ensure

SOME TARGET MAGNET ARRANGEMENTS WITH TWO-COMPONENT FIELDS

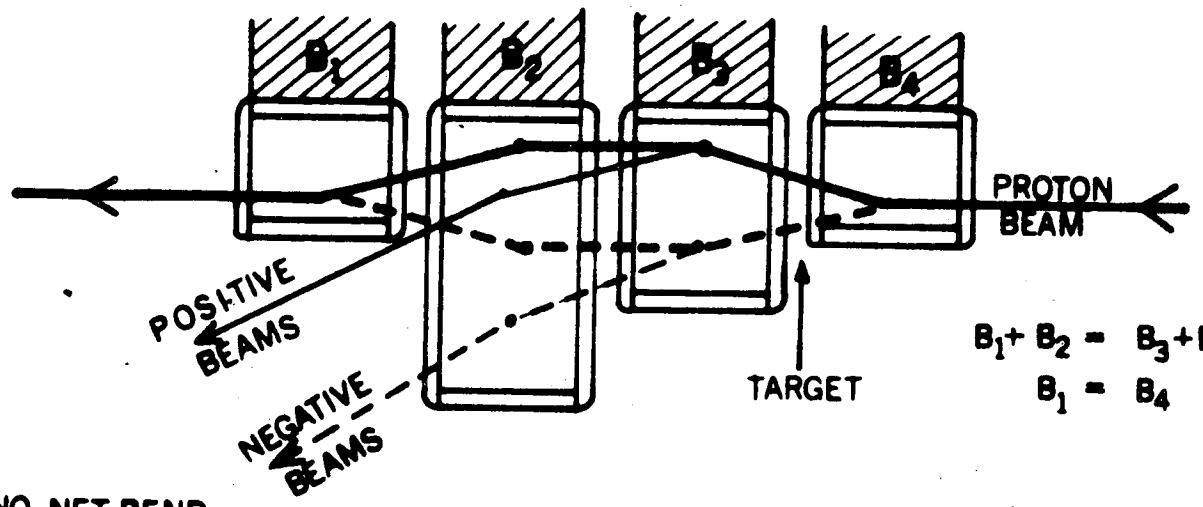

(12a) NO NET BEND

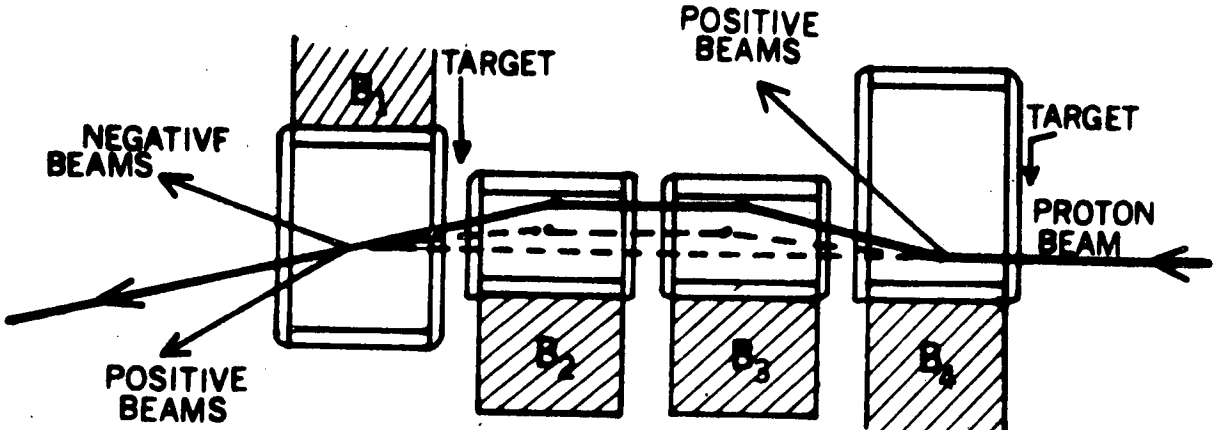

(12b) NET BEND

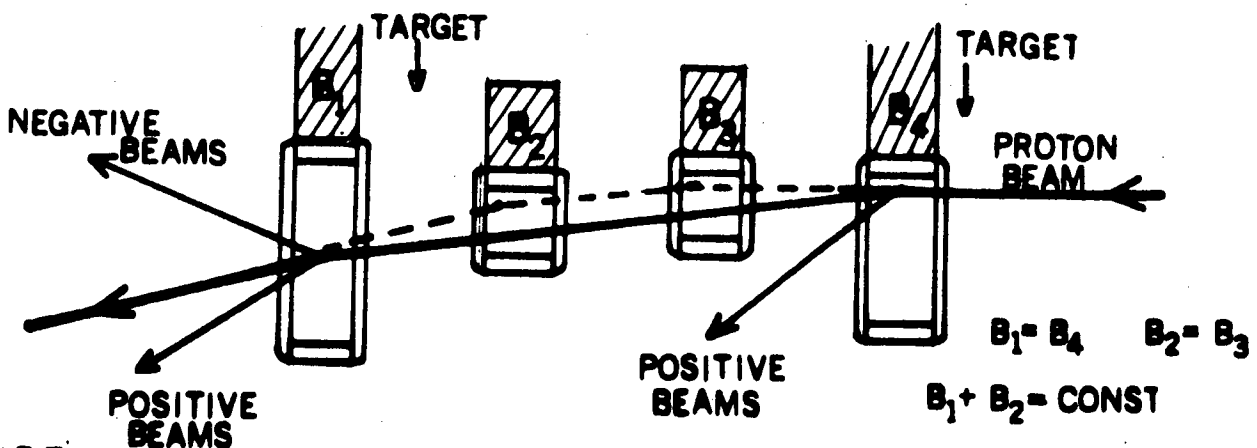

(12c) NET BEND

Fig. 12

the correct angle and position entering the secondary channel. This solution requires two rather large aperture magnets which physically interfere laterally with other possible beams and longitudinally postpone the placement of a quadrupole to capture maximum solid angle. In fact most secondary beams will have at least one steering magnet near the front end so that partial exploitation of this solution for modest changes in momentum can be assured.

(e) Accept beams at angles away from 0-deg. Examination of some typical cases indicates that changes in secondary momentum of ± 20% are reasonable. Only one steering magnet early in the secondary beam is needed and no change in either the target location or target magnet current. Changes in momentum much more than ± 20% result in serious loss in flux and broadening of the target by more than a factor of two.

Having achieved access to the forward direction and control over the selected secondary momentum, the major remaining problem is how to allow two experimenters using the same target station to have independent control over the momenta in their beams. If their beam spill requirements are incompatible, e.g., one requires a short spill for a bubble chamber, the other a long spill for a counter experiment, there is no problem. One can exploit solution (a) or (b) above, either delivering the two spills at different times or providing two targets at different times or providing two targets at different places flipped sequentially. When the two experiments are compatible in spill and intensity requirements and wish to share the same target and the same primary protons, then there is a serious problem in decoupling their individual variations in momentum. A classic example would be where each required the whole 600 ms flat-top, experimenter A needed to study all secondary momenta between (say) 25 GeV and 100 GeV and experimenter B needed momenta between (say) 50 GeV and 150 GeV. Alternatively, while A might need to span a wide range of momenta, B required all his running at a fixed momenta.

Unfortunately, there seems to be no general and practicalbe solution to this dilemma, although there are many partial solutions which would work in special cases. For example, the tactics described under (d) and (e) above, would allow A or B to vary momentum by about ± 20% independently of each other and, by negotiation, if one could accept a non-optimum situation the other could extend his range by changing the target magnet currents. Also by way of example in the second hypothesized situation, B could be set up so that his secondary beam passed through the whole bending field B_1 + B_2 + B_3 + B_4 and by definition remained unchanged in position and direction while A's beam emerged after the field B_1 and could therefore be varied freely in momentum. The possibility of using the two separate degrees of freedom momentum. The possibility of using the two separate degrees of freedom (b) and (c), viz., to move the target downstream and re-set the field B_1, immediately suggests itself. Unfortunately, in first order they are not independent degrees of freedom; when the target and field are changed to maintain the same momentum for A, it turns out that B is left with about the same momentum he had to start with. Likewise combining (a) and (c) or (a) and (b) still leaves the ratio of momenta in the two secondary channels almost the same. Finally, the ultimate solution lies in detailed scheduling. The very feature of wide changes in momentum which leads to the incompatibility between A and B could be turned to advantage by arranging the changes in momentum to occur approximately in step with each other. A final recourse in scheduling would be to re-locate A and B at separateseries target stations and in this way allow them to share the same spill--this is not really a solution but just defines the problem away. It is fruitless to pursue any further these hypothetical incompatibilities, but they do illustrate the nature of the coupling problem between experiments when a target magnet is used. Note that this problem arises only for medium and high energy beams for which there is no alternative to using a target magnet--a "straight section" target allows this de-coupling, but at the very high energies, this is the trivial solution corresponding to zero flux!

An interesting solution has been described by Williams.[26] If the target magnet is a C-magnet, then the profile of the open edge of the magnet can be shaped so as to create a momentum-focus several meters downstream. If a steering magnet is placed at this momentum focus then it can direct particles down a secondary channel despite the current

in the target magnet. In practice, this scheme seems most applicable in the range of secondary energies 10-30 GeV.

VIII. THE NUMBER AND CONFIGURATION OF THE LONG STRAIGHT SECTIONS

As pointed out in Section II(v), the invention of long straight sections since the last AG machines were constructed has provided us with exciting possibilities for the experimental exploitation of the machine. We are presented in fact with an embarras des richesses--an indefinite number of long access spaces, and--if we choose the π phase shift configuration--indefinite lengths are possible to incorporate in the design. The main worry is no longer how to obtain reasonably simple access to the machine; it is to decide on a reasonable upper limit to the possible uses and number of straight sections.

With the plan of experimental activity outlined in the previous sections, we are committed to a minimum of seven straight sections--one for injection, three for r-f acceleration stations, one for an internal area, and two for external areas. In deciding a reasonable number of spare straight sections, we note that the values for the number of straight sections preferred--for reasons of machine numerology--are 8, 9, 12, 16, with 10 and 14 as possible but less desirable choices. Experience has shown that a super-abundance of access space in the structure of the accelerator is always a desirable feature, partly because further expansion of experimental areas can be handled more flexibly. However, the greater the number of straight sections, the greater also are the tunnel cost and the radius of the machine. Thus, extremism in the pursuit of flexibility could indeed be vice.

In trying to imagine further development in the straight sections of the machine we arrive at the following list of examples:

(i) Increase in intensity of the machine would need the addition of more r-f cavities. Beam loading would then be clearly a dominating factor and the obvious solution would be to add more r-f cavities. One straight section might be absorbed in the process.

(ii) A scheme for the possible acceleration of anti-protons has been described elsewhere[27]--this in its most obvious form would require two straight sections, one for the extraction of the proton beam to create the anti-protons and one for the extraction of the anti-protons for use in an experimental area.

(iii) At some stage it could be desirable to add a storage ring tangential to the main ring. An energy of even a few GeV in the storage ring would increase greatly the energy available in the CM system for colliding beam experiments. The expression $E_{CM} = 2\sqrt{E_1 E_2}$ where E_1 and E_2 are the <u>total energies</u> of the colliding particles is a good approximation for $E_2 \geq 2$ GeV (while for $E_2 = 1$, $E_{CM} \approx \sqrt{2E_1}$) e.g., a 1 GeV ring would approximately double the energy in the CMS. There are many problems associated with colliding beam experimentation, but it is possible to imagine a situation wherein it became imperative to investigate a threshold beyond the capability of the 200 GeV machine used with a stationary proton target. Also the storage ring could be used to store particles other than protons.

(iv) Spatial deflection using r-f separators is well-known to be costly in real estate and to require small tolerances in the surveying and alignment of the transport elements. For example, a two-cavity system for 100 GeV/c operating at 9 kMc/s[15] would be 1.3 km in length. Another stage of separation would be a great help in purifying the beam and has been examined in detail for a proposed beam at the AGS.[28] A more economical way of obtaining an extra stage of separation without doubling the length of the beam could be to add a pre-bunching cavity within the accelerator to bunch the protons in the manner suggested by Veksler. The properties and dimensions of such a device operating at 3 kMc/s have been studied by Lamb;[17] it seems quite feasible to accommodate a plunged opensided cavity in a straight section space of not less than 10 m. This equipment would then occupy one long straight section.

(v) It is essential to ear-mark one or two straight sections for future expansion of target facilities. Presumably a decision on the necessity and the properties of these areas would only be appropriate several years after the machine has begun to operate. The installation of another internal area is one possibility although this would be a major reconstruction project. It is easier to visualize the extraction of further external beams for special purposes, e.g., exclusively for neutrino physics, or for low primary energy operation ($\leq$ 40 GeV, say) or simply because further parallel decoupling of areas is needed.

This list is intended to be illustrative and should be viewed with considerable reservations; it is probably not complete and almost certainly will become modified in time. We can surely presume that those items removed because of diminished importance are balanced by the introduction of new inventions, and thus arrive at a total of 6-7 for the number of desirable spare access points. However, not all of the applications outlined need have exclusive domination of a straight section; for example, the pre-buncher could be accommodated in one of the straight sections used in the anti-proton acceleration scheme. Furthermore, one should be optimistic that future ingenuity or invention will effect more compact solutions for some of these applications. Thus we will assume 6-7 spares to be an overestimate. Using this reasoning we arrive at a total of twelve straight sections as the most reasonable number, of which seven would be active from the moment of turn-on. A choice of ten would leave only three spares, which is too few, a choice of fourteen would leave 7 spares, which is too many, and neither of the periodicities 10 or 14 is as convenient as 12.

The next question to consider is the choice of length of the long straight sections. Many configurations of machines with $\pi/2$ straight sections only, π-straight sections only, compensated π-straight sections only and various mixtures of $\pi/2$ and π-straight sections (both compensated and uncompensated) have been explored by Garren.[29] One fact which quickly emerges is that the drift space between singlets in a $\pi/2$ straight section cannot be realistically made much more than 30 m.

(For certain purposes the presence of the two further drift spaces, each 8 m long between the quadrupole singlets and the main ring structure should not be ignored.) The quality and tracking precision of the quadrupole singlets in a $\pi/2$ straight section need not be very high. In the case of the π-straight sections, the quality and tracking precision of the quadrupole doublets, and the bending magnets in the compensated case turns out to account for 20-30% of the bending effect of the gradient magnets. If we ignore the cost factor which enters because of the changes in tunnel length, shielding, etc., arising from the different configurations for given prescribed boundary conditions and restrict ourselves only to the question of experimental usefulness, it is clear that for internal target purposes the longer the free drift space in the straight section, the better. Economically the choice would seem to be among machines with pure $\pi/2$ straight sections, pure π-type straight sections (compensated) and a mixed machine. The first is a machine with one type of precision component--gradient magnets--and less precise singlets, the second requires the design and operation of three types of precision components, while the third requires all kinds mentioned and in addition has a more undesirable periodicity and a much more complicated behavior of $\hat{\alpha}$ with azimuth (including negative values!). A strong conclusion from the arguments presented earlier in this report is the de-emphasis of internal target areas; if it was felt necessary to make the single target area in the initial proposal as long as possible, then at least two others ought to be inserted for numerological reasons and the disadvantage and extra cost of a mixed machine suffered. Alternatively some compromise could be sought whereby the internal target straight section length could be made, say 50 m (π-type), and all other straight section made the same to avoid the disadvantage of a mixed machine. Thus it becomes critical to construct criteria for the desirable length of straight sections and to establish whether there are really substantial gains in departing from the simplicity of an all $\pi/2$ straight section configuration with its upper limit of 30 m drift length. The criteria we can list as follows:

(a) The length should be comfortable for injection from the booster and for the possible inclusion of an anti-proton injection system. About 20 m seems adequate for both these requirements.

(b) The extraction of both fast and slow beams should be guaranteed. The necessary extraction equipment could be compressed into a straight section 20 m long.

(c) The length should be such that the r-f cavities do not occupy more than three long straight sections. If the acceleration of anti-protons is contemplated, the packing of the cavities is relatively inefficient since they should be spaced at intervals of 1/2 λ. In the $\pi/2$ straight section the available length is about one and one-half times the free drift length if we include the end spaces; in the compensated π-straight section, only the free drift space is available. A 31 m $\pi/2$ straight section, in this respect, is to be compared with a 49 m π-straight section. The total length of the drift occupied by r-f cavities needed to accelerate 3×10^{13} protons per pulse is about 140 m, which is easily accomplished within three $\pi/2$ straight sections. It could be accommodated in only two π-straight sections if they were each ~ 70 m long.

(d) At least one of the straight sections must be long enough for adequate internal targetting. Without knowing the nature of the experimental activity it is impossible to decide what may be needed, but the following examples illustrate how the difficulty of achieving high target efficiency diminishes with increasing length. The efficiency argument should not be pushed too far since an experiment requiring maximum flux is best located in the external beam where, for high energy beams, about half the total flux may be rather easily captured into a secondary beam channel. The object is instead to explore whether a variation in the length of the straight section produces any "break points" where the target efficiency changes drastically.

One example is illustrated in Fig. 13(a), where we consider a target in the upstream end of a straight section and rely only on the angle of production of the secondary particles to clear the obstruction of the quadrupole singlet at the downstream end of the straight section. The secondary particle

PRODUCTION OF PARTICLES FROM STRAIGHT SECTION TARGET

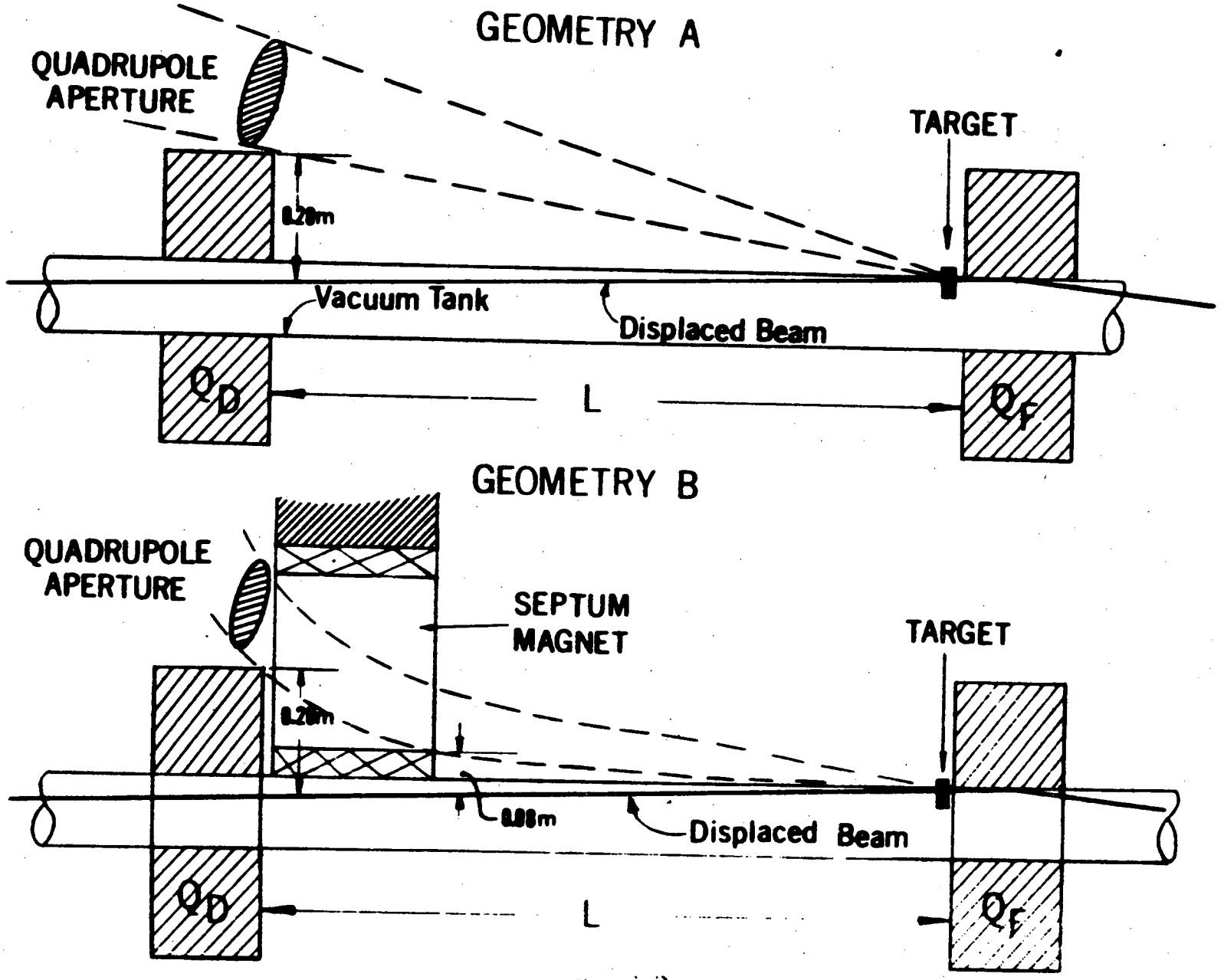

fig

flux is assumed to be captured into a secondary channel by means of a quadrupole with an entrance aperture with a 2:1 aspect ratio (horizontally focussing) located near the down-stream quadrupole. Aperture sizes chosen are 2" x 4", 4" x 8", 8" x 16", and "infinite"--the last indicating the upper limit to the flux; namely all that lies outside the transverse obstacle on one side. The secondary momentum considered is 100 GeV/c and the cross-section is assumed to have the CKP form

$$\frac{d\sigma}{d\Omega} = A\, e^{-p\theta/p_o} \quad \text{with } p_o = 0.22 \text{ GeV}$$

It is clear from Fig. 14(a) that the rate of improvement is small for lengths greater than ~ 40-50 m, whereas below 20 m the flux loss is considerable.

An important ingredient has yet to be included, viz., septum bending magnets (or combined-function bending quadrupoles). When one considers available lengths of many meters then the angular deviation produced by a bending field in only a small fraction of this space can far exceed the angle of production. For example:

$$\theta_{\text{production}} \approx \frac{.54}{\sqrt{2E}} \qquad \text{(projected)}$$

$$\phi_{\text{magnet}} = \frac{3\, B\ell}{10\, E}$$

and equating these we find

$$B\ell = \frac{10}{3}\left(\frac{.54}{\sqrt{2}}\right) = 1.3 \text{ Tesla-meters}$$

for the bending strength necessary to give an angle of bend equal to the rms projected production angle. With a 20 kG field the magnet need only be 0.65 meters long. Thus if for several meters of the straight section a magnetic field can be arranged (Fig. 13(b)) just outside the vacuum chamber (we assume B = 20 kG, septum thickness 5 cm) the main assistance in clearing the down-stream obstacle comes from the magnetic deflection, not the geometrical effect of finite production angle. With

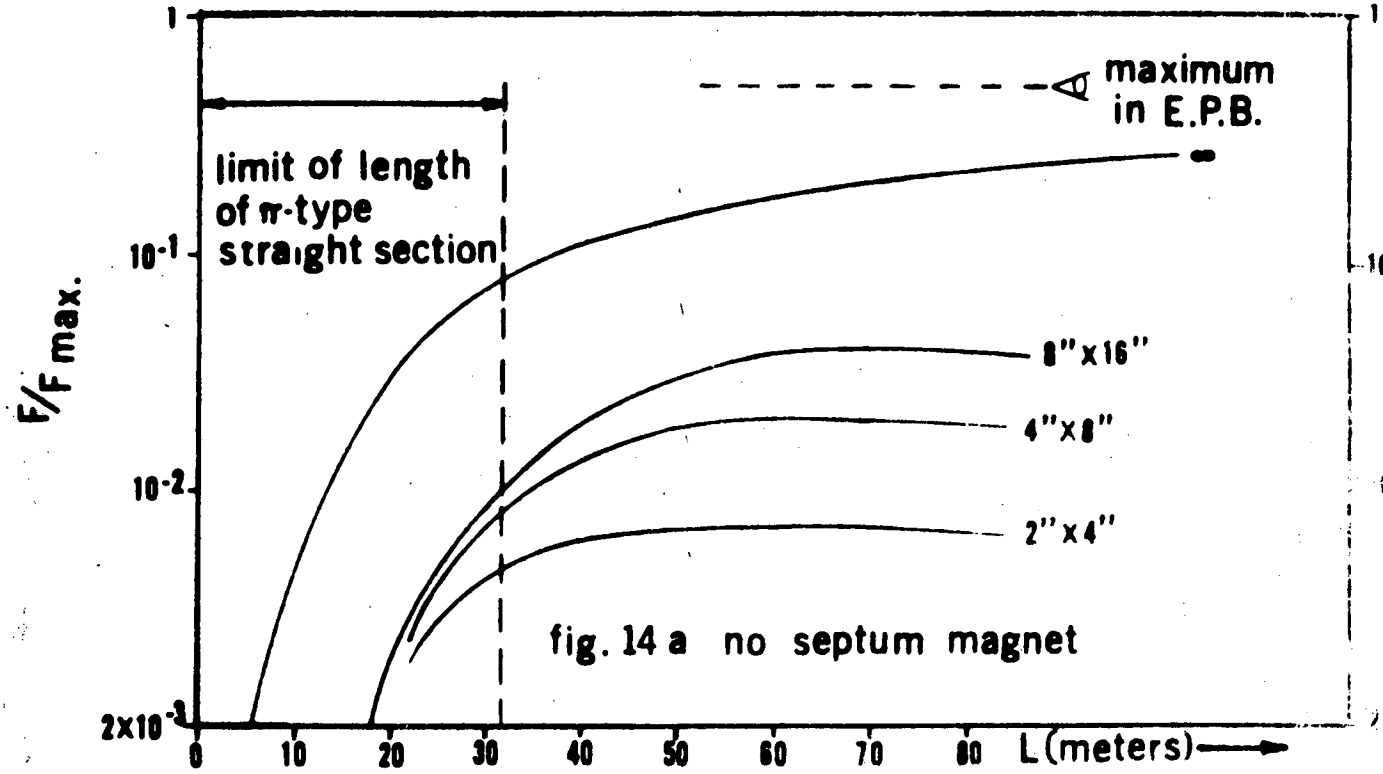

fig. 14 a no septum magnet

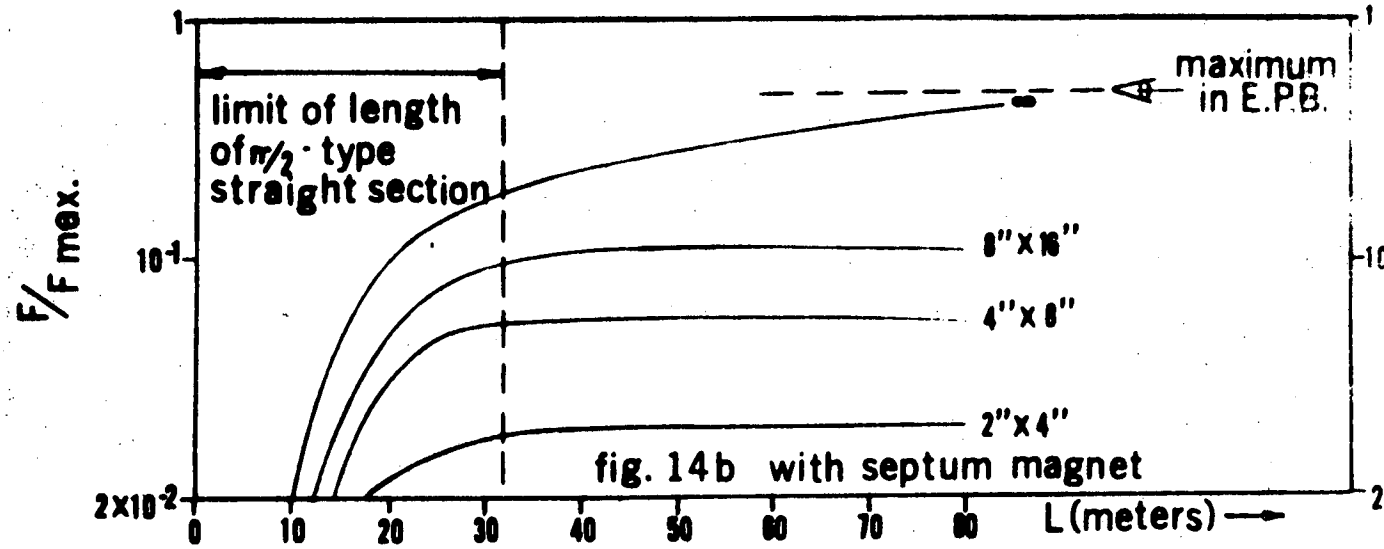

fig. 14b with septum magnet

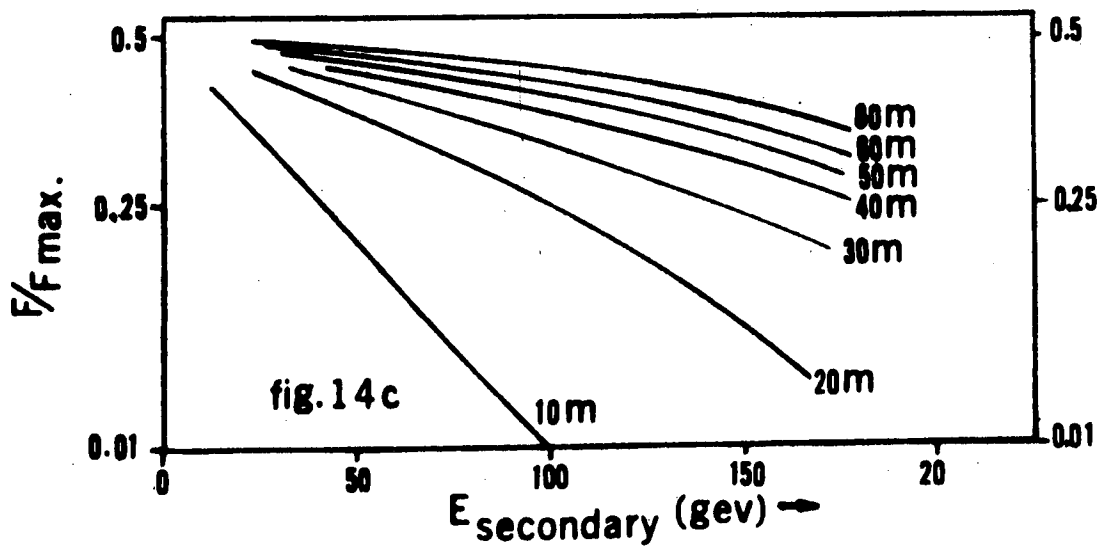

fig. 14 c

this effect included, the available (fractional) secondary flux curves are re-drawn in Fig. 14(b). They all lie higher than the corresponding curves in Fig. 14(a), and the "knee" in the curve at short lengths (20-30 m) is more abrupt and displaced to the left. There is a striking improvement in increasing the length from 10 m to 20 m and a rather slow rate of improvement beyond 30 m. Figure 14(c) illustrates the effect as a function of secondary momentum where again the slow rate of improvement for very long straight sections can be seen.

We therefore conclude that 30 m straight sections should be adequate for obtaining respectable fluxes up to very high energies. In fact, the major advantage of having a much longer straight section would more likely lie not in the slight improvement in secondary flux, but in the greater available uncluttered space in which to pack the rather long transport elements for several simultaneous experiments.

IX. ACKNOWLEDGMENTS

I have benefitted by and appreciated many stimulating discussions with G. R. Lambertson and W. A. Wenzel; in addition, I acknowledge an interesting discussion with M. G. Hine. I am grateful to F. T. Cole for his helpful suggestions.

sk

REFERENCES

[1] Keefe, D., "μ-Meson Shielding Problems at 200 GeV," UCID-10018, May 20, 1964.

[2] Gilbert, W. S., "Induced Activity and Radiation Damage," UCID-10014, April 17, 1964.

[3] Collins, T. L., "Long Straight Sections for AGS," CEA-86, July 10, 1961.

[4] Garren, A. A., Sessler, A. M., Smith, L., "Straight Sections of Arbitrary Length," LRL Internal Report, AS/Theoretical/02, August 16, 1964.

Garren, A. A., "Compensation of π-Straight Sections with Bending Magnets," UCID-10129, September 17, 1964.

[5] Hereward, H. G., "The Possibility of Resonant Extraction from the CPS," CERN AR/Int. GS/61-5.

[6] Bovet, C., Lambertson, G. R., Reich, K. H., "Measurements of Slow-Beam Ejection from the CPS," CERN 64-25, June 3, 1964.

[7] de Raad, B., "Matched Straight Sections, Secondary Beams and Ejection in a 300 GeV Proton Synchrotron," CERN AR/Int. SG/63-3, January 15, 1964.

[8] Murray, J. J., "Mass Analysis at High Energies," SLAC-5, p. 222, Summer 1962.

[9] Keefe, D., "Neutrino Beams at High Energy," UCID-10131, September 9, 1964.

[10] Longo, M. J., "150 GeV/c Beam for Spark Chamber Experiments," UCID-10124, August 21, 1964.

[11] Cocconi, G., Koester, B. J., Perkins, D. H., "Calculations of Particle Fluxes from Proton Synchrotrons of Energy 10 to 1000 GeV," Berkeley High Energy Physics Study (Summer 1961), UCRL 10022, p. 167.

[12] Citron, A., Galbraith, W., Kycia, T. F., Leontic, B. A., Phillips, R. H., Rousset, A., "Structure in the π-p Total Cross-Section Between 2.5 and 5.5 GeV/c," Phys. Rev. Letters 13, 205 (1964).

[13] Williams, R. W., "Choice of Parameters for Magnets and Bubble Chambers," UCID-10128, August 13, 1964.

Longo, M. J., "Note on Magnets for Use in High Energy Beams at the Proposed 200 GeV Accelerator," UCID-10123, July 23, 1964.

Keefe, D., "Notes on Scaling of Quadrupole Lenses for High Energy Beams," LRL Internal Report, July 1964 (unpublished).

[14] Dols, C., "Septum Quadrupole Suggestions," LRL Internal Report, AS/Experimental/03, August 11, 1964.

[15] Keil, E., "Parameters for R-F Separation of π and K at 100 GeV/c Design Momentum," CERN AR/Int. P Sep/62-3, October 8, 1964.

[16] Keefe, D., "Separation of Particle Beams at High Energies," Berkeley High Energy Physics Study, Summer 1961, UCRL-10020, p.52.

[17] Lamb, W. A. S., "R-F Separation Utilizing a Bunched Primary Proton Beam," UCID-10132, October 2, 1964.

[18] Gursey, F., Lee, T. D., Nauenberg, M., "Implications of Approximate SU3 Symmetry and Mass Formulae for the Mesons," in course of publication, 1964.

[19] Keefe, D., "Efficiency of a Multiple-Traversal Thin Target in a 200 GeV Machine," UCID-10105, March 9, 1964.

[20] Riddell, R., (private communication) to be published.

[21] Dekkers, D., Geibel, J. A., Mermod, R., Weber, G., Willits, T. R., Winter, K., "Experimental Study of Particle Production at Small Angles in Nucleon-Nucleon Collisions," CERN NP/Int/64-5, May 27, 1964.

[22] Baker, W. F., et al, "Large Angle p-p Elastic Scattering at 30 BeV," Phys. Rev. Letters 12, 132 (1964).

[23] Wenzel, W. A., (private communication).

[24] Kerth, L. T., "Some Considerations of Experimental Facilities for a 300 GeV Accelerator," Berkeley High Energy Physics Study, Summer 1961, p. 47, UCRL-10020.

[25] Keefe, D., "Experimental Areas and Facilities," LRL Internal Report, AS/Experimental/01, February 22, 1964.

[26] Williams, R. W., "Notes on Two Target Arrangements for the External Beam," LRL Internal Report, AS/Experimental/01, September 14, 1964.

[27] Keefe, D., "Acceleration of Anti-protons at the 200 GeV Machine," UCID-10020, June 16, 1964.

[28] Lach, J., "Use of a Third Cavity in an R-F Separated Beam, p. 102, Sandweiss, J., "Peak Energy R-F Separated Beam," p. 91, Possible Beams and Experiments for a High Intensity AGS, BNL, May 1964.

[29] Garren, A. A., and Eusebio, J. W., "SYNCH--An IBM 7094-44 Code for Analysis of Linear Orbit Properties in Synchrotrons," LRL Internal Report, AS/Theoretical/03, April 13, 1964.

UCID-10029
AS/Experimental/03
September 14, 1964
R. W. Williams

University of California
Lawrence Radiation Laboratory
Berkeley, California

NOTES ON TWO TARGET ARRANGEMENTS FOR THE EXTERNAL BEAM

A. The end station

Several characteristics distinguish the end station from target stations along the beam: shielding is easier; the target can be of arbitrary thickness; and the remainder of the external proton beam can be allowed to go off in any direction. These characteristics make the end station the natural choice for very high energy beams, since these require long targets to get intensity up, and since energy changes in such a beam will always re-steer the E.P.B. The setup illustrated in Dwg. 15A3936, "End Station with Tipped Beam" is intended to show how one might use these characteristics to advantage.

1) Shielding: the E.P.B. is tipped downward before a thick target is reached, so that muons from the target go under the experimental area and do not have to be stopped. The required angle of tip is approximately set by imagining the muon shield (e.g. Fig. 10 of the μ-shielding report by D. Keefe) tipped down until its top intersects the ground level at some suitable distance from the target, 80 meters in the drawing noted here. This seemed to require about 3°, or 18 meters of bending magnet. Further study of the effect of the neutron shielding may indicate that less tip will suffice.

The hope is that high energy beams will emerge from the shielding more quickly in such arrangement, thus justifying the extra trouble of having to level up the secondary beams.

Of course no additional muon shielding is required behind the beam stopper in this arrangement.

2) Beam stopper: the beam enters, at the earliest point consistent with clearance of high energy secondary beams, a re-entrant cavity with an energy absorber at the back. The slot and its back wall are wide enough to accept the remains of the E.P.B. regardless of the setting of the targeting magnet.

3) Parasite beams: the first tipping magnet can be an open C, facing up, which allows a thin target to be placed there for low-intensity beams of

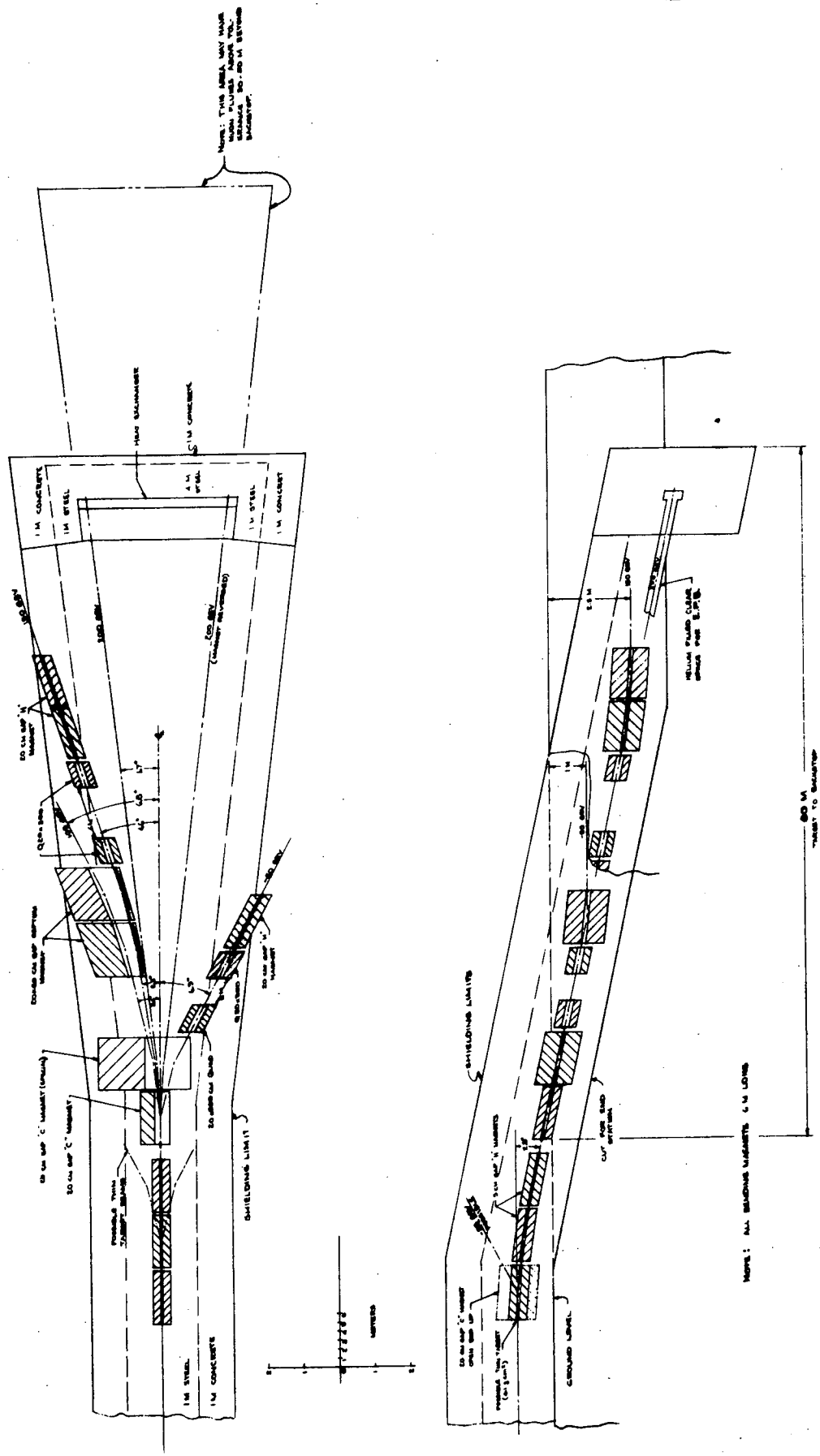

medium energy to be directed upward. These would be usable at the original ground level, B, momentum forms to permit the two independent users.

Drawing 15A3946 - "Target arrangement with momentum focus" - illustrates a method for permitting a second user to adjust his energy independent of the primary user when both are looking at 0^{o} at the same target. While one can in principle use two additional magnets to send a beam down a channel regardless of the bending it suffers in the targeting magnet, the required magnets become very wide if the momentum band in question is large - e.g., 3:1 in the case considered. We therefore attempt to send the beams out of the targeting magnet in the same direction, regardless of momentum.

Use the parabolic approximation to a circle. A particle suffers lateral deflection

$$y = \frac{1}{2}\frac{Z^2}{R} = \frac{0.15\ B\ Z^2}{P}$$

$$y' = \frac{0.3B\ Z}{P} = \frac{2y}{Z}$$

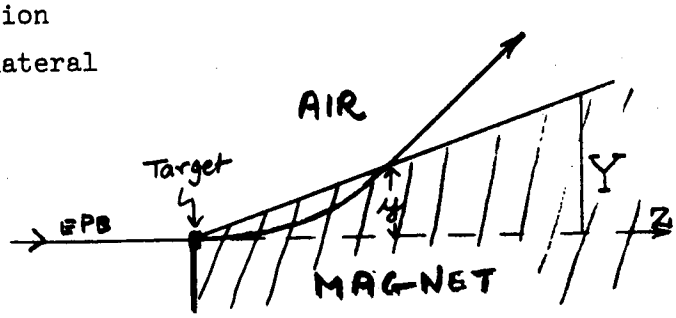

Neglecting fringing, a poor approximation here, we see that a magnet boundary which is a straight line, $Y = \frac{y'}{2} Z$ for y' a constant, will eject all 0^{o} beams at the same angle y'.

The drawing uses a C magnet, rotated slightly to eject low energy beams at a constant angle.

A refinement of this idea would shape the edge of the magnet so that all beams emerging from it would intersect as a point, thus eliminating one of the two subsequent magnets. The curve which concentrates all momenta less than

$$P_{max} = \frac{0.15\ B\ Z_o^{\ 2}}{Y_o}$$

at point (Y_o, Z_o) is

$$Y = \frac{Y_o\ Z}{2Z_o - Z}$$

which is a rectangular hyperbola with asymptotes $Y = -Y_o$ and $Z = 2Z_o$. The curve is in practice much too shallow to be of any use.

km

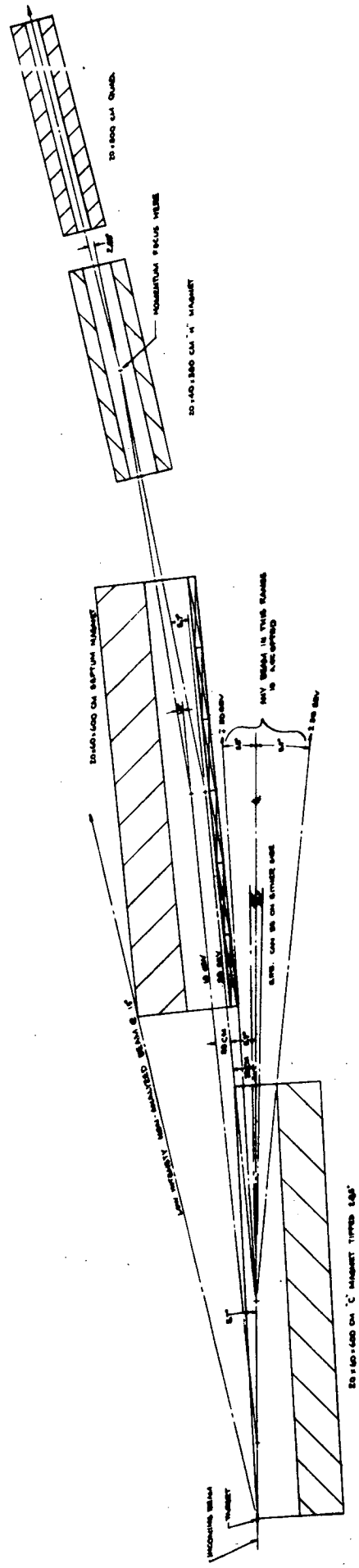

TARGET ARRANGEMENT WITH MOMENTUM FOCUS

UCID-10105
AS/Experimental/01
Denis Keefe
March 9, 1964

THE EFFICIENCY OF A MULTIPLE TRAVERSAL THIN TARGET IN A 200 GEV MACHINE

1. Introduction

Courant[1] has considered the relative fractions of protons traversing a thin target (i.e., $\ll 1$ m.f.p.) which undergo nuclear interactions or are lost by multiple Coulomb scattering. In the approximation used by him a nuclear interaction was considered to be measured by the total cross-section, σ_T ($=\sigma_a+\sigma_e$), and target efficiency was defined in terms of the probability of nuclear interaction versus the probability of loss by Coulomb scattering. However, a nuclear interaction may result in either a nuclear diffraction scattering (controlled by σ_e) or a nuclear absorption (controlled by σ_a). It is only the latter which are useful in producing secondary particles and therefore should be considered in estimating target efficiency. The diffraction scatterings may lead either to a large enough deviation to excite a betatron amplitude sufficient to cause loss of the proton at the wall of the vacuum vessel, or alternatively to a small enough amplitude to allow the particle to be retained in the accelerator and have another chance to interact. This report concerns the partition between these two circumstances arising from diffraction scattering. In later sections the numerical results will refer to the case of a 200 Gev machine run at three different primary energies, 200 Gev, 100 Gev and 30 Gev, in which the betatron wavelength is 240 meters, the vertical half-aperture 1.7 cm and the radial half-aperture 5.4 cm.

---

(1) E. D. Courant, BNL Accelerator Department Internal Report EDC-46, Feb 1962

2. Cross-Section Data

All the available high energy nucleon–nucleus absorption cross-section data are well represented by

$$\sigma_a = 43\ A^{0.69}\ \text{mb}$$

and what little information there is on nucleon–nucleus elastic scattering obeys

$$\sigma_e/\sigma_a = 0.57$$

independent of atomic number and energy, where σ_e = elastic cross-section σ_a = absorption cross-section. There is virtually no significant data on the shape of the angular distribution for elastic scattering at high energies. We here consider two models which have been successful in parameterizing nucleon–nucleon scattering — both of which assume the nucleus to be a grey disc with a certain "shape". If for unit incident amplitude the transmitted amplitude is a at an impact parameter r the two models are represented as follows:

Model 1: Uniform Grey Disc

$$1 - a = \text{Constant} \qquad o < r < R$$
$$= \quad 0 \qquad\qquad r > R$$

Model 2: Grey Gaussian

$$1 - a = \text{Constant}\ e^{-r^2/\rho^2}$$

Model (1) includes the idea of sharp edges and leads to zero-intensity diffraction minima which are unrealistic; Model (2) on the other hand has the correct "fuzzy-edge" property but may under-estimate the scattering at large angles. Defining ρ as the RMS radius of the disc which accords with the form given above for Model (2) we have the following results:

Model (1) $$\frac{d\sigma}{d\Omega} = \frac{\sigma_e}{\pi} \left[\frac{J_1(KR \sin\theta)}{\sin\theta} \right]^2$$

$$\frac{d\sigma}{dx} = 2\sigma_e \frac{\left[J_1(\sqrt{2}\,x)\right]^2}{x\sqrt{1-(x/K\rho)^2}}$$

where $\rho = R/\sqrt{2}$ and $x = K\rho \sin\theta$

Since the angles involved are of the order of 10^{-3} radians

$\sin\theta \approx \theta$ and $\cos\theta \approx 1$, hence

$$\frac{d\sigma}{dx} = 2\sigma_e \frac{\left[J_1(\sqrt{2}\,x)\right]^2}{x}$$

Model (2) $$\frac{d\sigma}{d\Omega} = \frac{\sigma_e}{\pi} K^2 \rho^2 e^{-K^2\rho^2\theta^2}$$

$$\frac{d\sigma}{dx} = \sigma_e \frac{x\, e^{-x^2/2}}{\sqrt{1-(x/K\rho)^2}}$$

$$\approx \sigma_e\, x\, e^{-x^2/2}$$

where $K = 4.8 \times 10^{13} \left(\frac{cP\ (Gev)}{938} \right)\ cm^{-1} = \begin{cases} 1.52 \times 10^{15} \text{ at } 30 \text{ Gev} \\ 5.1 \times 10^{15} \text{ at } 100 \text{ Gev} \\ 10.1 \times 10^{15} \text{ at } 200 \text{ Gev} \end{cases}$

$\rho = 0.71\ A^{1/3}$ Fermis corresponding to $R = 1.0\ A^{1/3}$ Fermis

3. Loss by Single Diffraction Scattering

Case (1a) Circular Aperture Radius A

For simplicity consider the target to be placed at a symmetry point in the machine where the acceptance is an upright ellipse. Assume in the

radial and vertical planes a limiting effective half aperture A and a transverse momentum limit $A/\lambda\!\!\!^{-}$ where $\lambda\!\!\!^{-}$ is the betatron wavelength divided by 2π. (See Figure 1(a)). The unperturbed beam near full energy will occupy only a small fraction of the available aperture and we assume that it has negligible extent. If a particle undergoes diffraction scattering it will be lost if the angle exceeds $A/\lambda\!\!\!^{-}$. Thus the probability of loss in the first scattering is

$$P_1 = \frac{1}{\sigma_e} \int_{x_c}^{K\rho} \frac{d\sigma}{dx} dx \approx \frac{1}{\sigma_e} \int_{x_c}^{\infty} \frac{d\sigma}{dx}$$

$$= \frac{1}{\sigma_e} \int_{x_c}^{\infty} \left[\frac{J_1(\sqrt{2}\, x)}{x} \right]^2 dx \qquad \text{Model (1)}$$

$$= \frac{1}{\sigma_e} \int_{x_c}^{\infty} x\, e^{-x^2/2}\, dx = \frac{1}{\sigma_e} \left(1 - e^{-x_c{}^2/2}\right) \qquad \text{Model (2)}$$

where $x_c = K \rho A/\lambda\!\!\!^{-} = \begin{cases} 0.52 \text{ mr for } A = 2 \text{ cm} \\ 1.05 \text{ mr for } A = 4 \text{ cm} \end{cases}$

Figure 2 shows P_1 for three different primary energies 30,100 and 200 Gev and two assumed values of A, 2 cm and 4 cm. The fraction of particles lost to the walls per nuclear scatter is simply $\frac{\sigma_e}{\sigma_e + \sigma_a} P_1 = 0.36\, P_1$. Thus for an internal thin target with the primary energy at 30 Gev, single nuclear scattering in almost every case will result in the loss of the proton to the walls. The difference between Models (1) and (2) is small when the loss is large but not so when the loss is small — unfortunately there is no evidence at present to suggest which may be closer to the truth. In what follows only Model (2) will be used; it is more convenient to handle analytically.

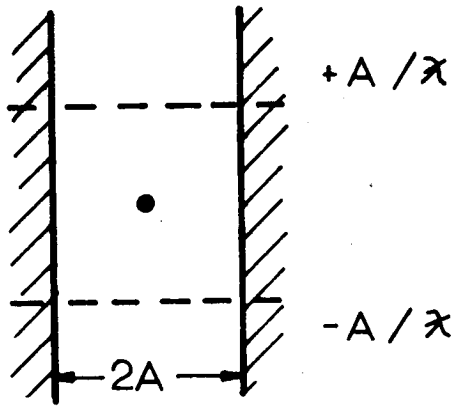

Radial (r, r^1) Plane

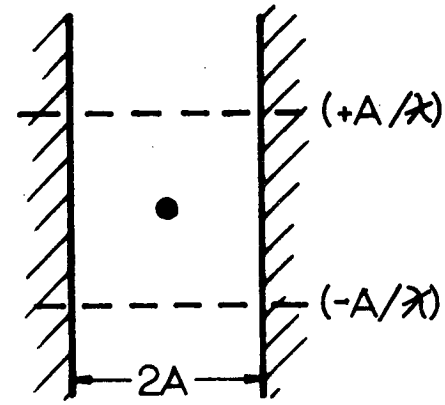

Vertical (v, v^1) Plane

Case 1 (a)

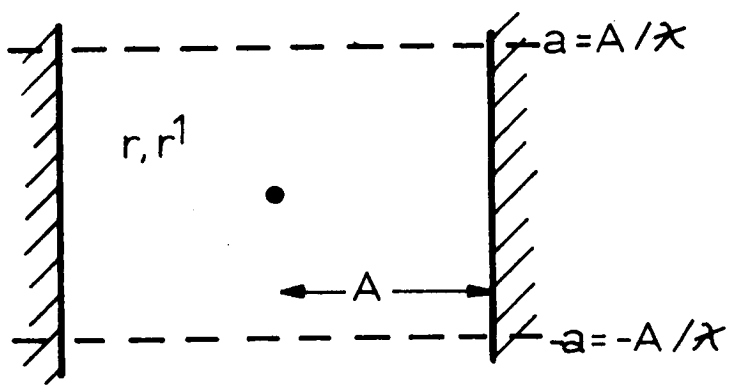

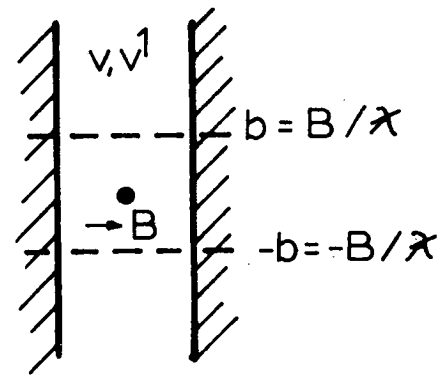

Case 1 (b)

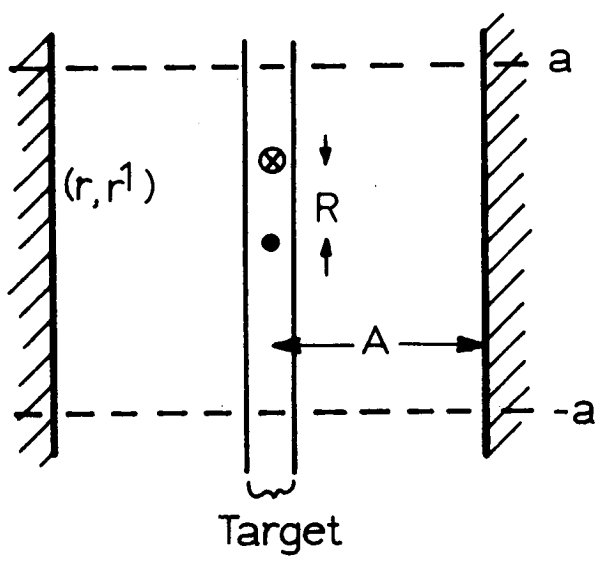

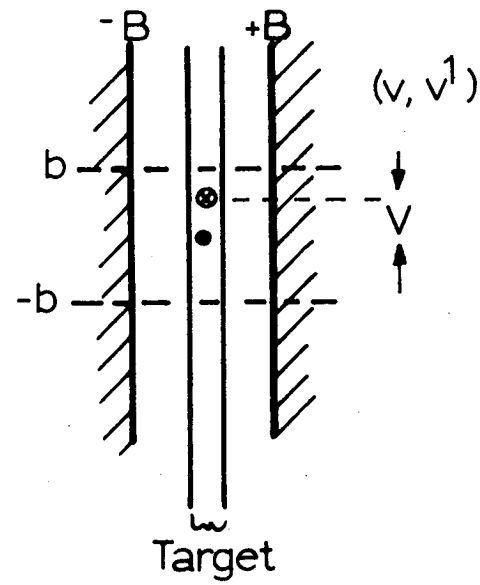

Case 2 Where first scatter has taken particle to (R,V) on next traversal

fig. 1

Circular Aperture {2cm Radius / 4cm "
Probability of Loss on First Scatter

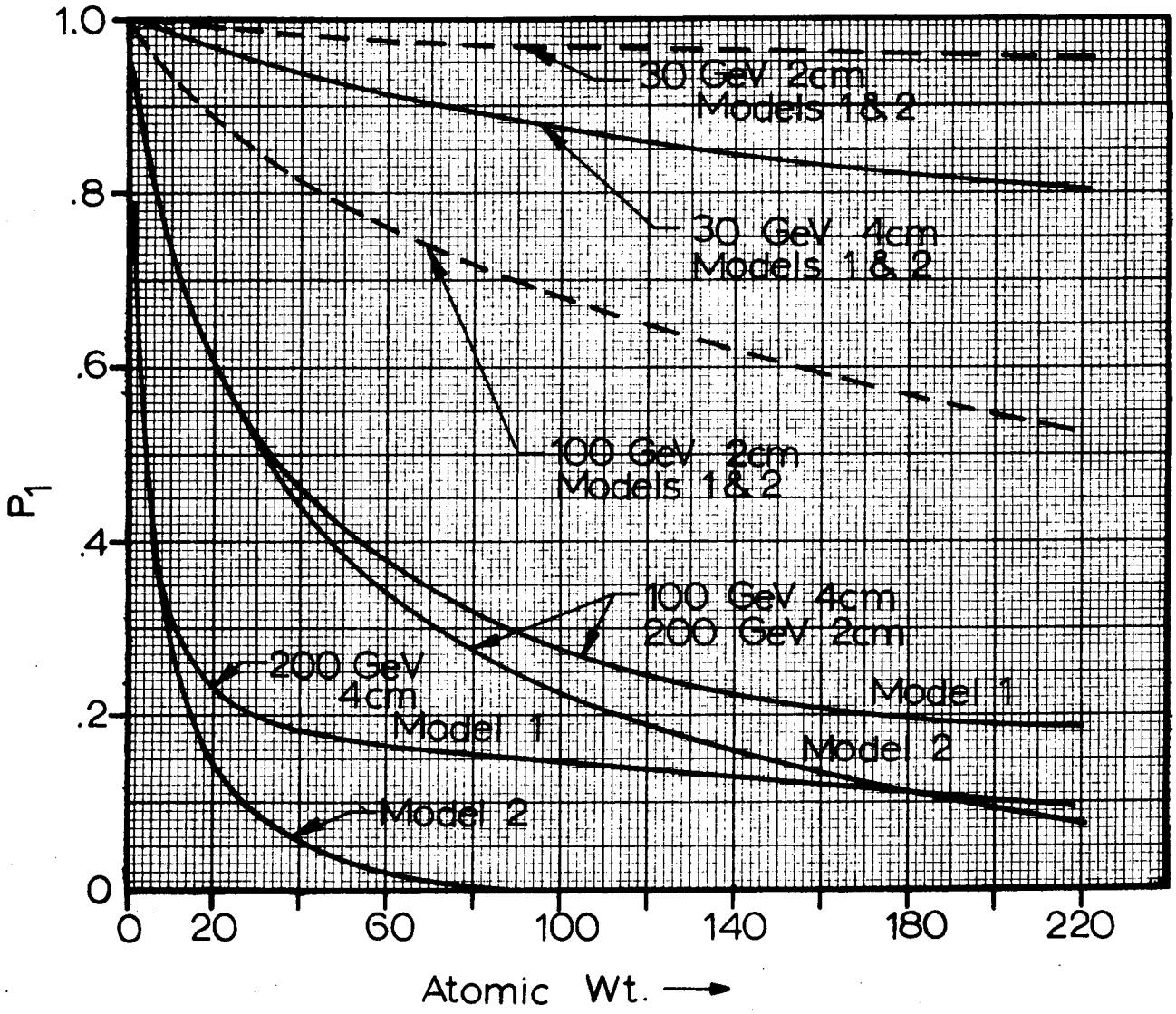

fig. 2

Case (1b) Rectangular Aperture, A by B

In the case of the Gaussian model it is easy to show that the probability of a projected scattering θ_r or θ_v is given by

$$P(z)\,dz = \frac{1}{\sqrt{2\pi}}\, e^{-z^2/2}\, dz$$

where $z = K \rho \theta_r$ or $K \rho \theta_v$

Denoting z by r for a radial scatter and v for a vertical scatter, the probability of a single scattering leading to a loss is (See Figure 1(b).) —

$$P_1 = \int_{-a}^{a} \frac{1}{\sqrt{2\pi}}\, e^{-r^2/2}\, dr \int_{b}^{\infty} \frac{2}{\sqrt{\pi}}\, e^{-v^2/2}\, dv + 2 \int_{a}^{\infty} \frac{1}{\sqrt{2\pi}}\, e^{-r^2/2}\, dr$$

$$= 1 - \frac{4}{\pi}\ \mathrm{Erf}\ \frac{a}{\sqrt{2}}\ \mathrm{Erf}\ \frac{b}{\sqrt{2}}$$

where $a = \frac{K \rho A}{\chi}$ and $b = \frac{K \rho B}{\chi}$

The fraction of nuclear interactions leading to a loss is then

$$\frac{\sigma_e}{\sigma_a + \sigma_e}\, P_1 = 0.36\, P_1$$

For the case of a radial half-aperture A = 5.4 cm and vertical half-aperture B = 1.7 cm, P_2 is shown in Figure 3. In this case $A/\chi = 0.45$ mr, $B/\chi = 1.42$ mr. Comparing Figures 2 and 3 indicates that this example lies roughly midway between the case for a circular aperture with radii 2 cm and 4 cm.

Rectangular Aperture
A x B

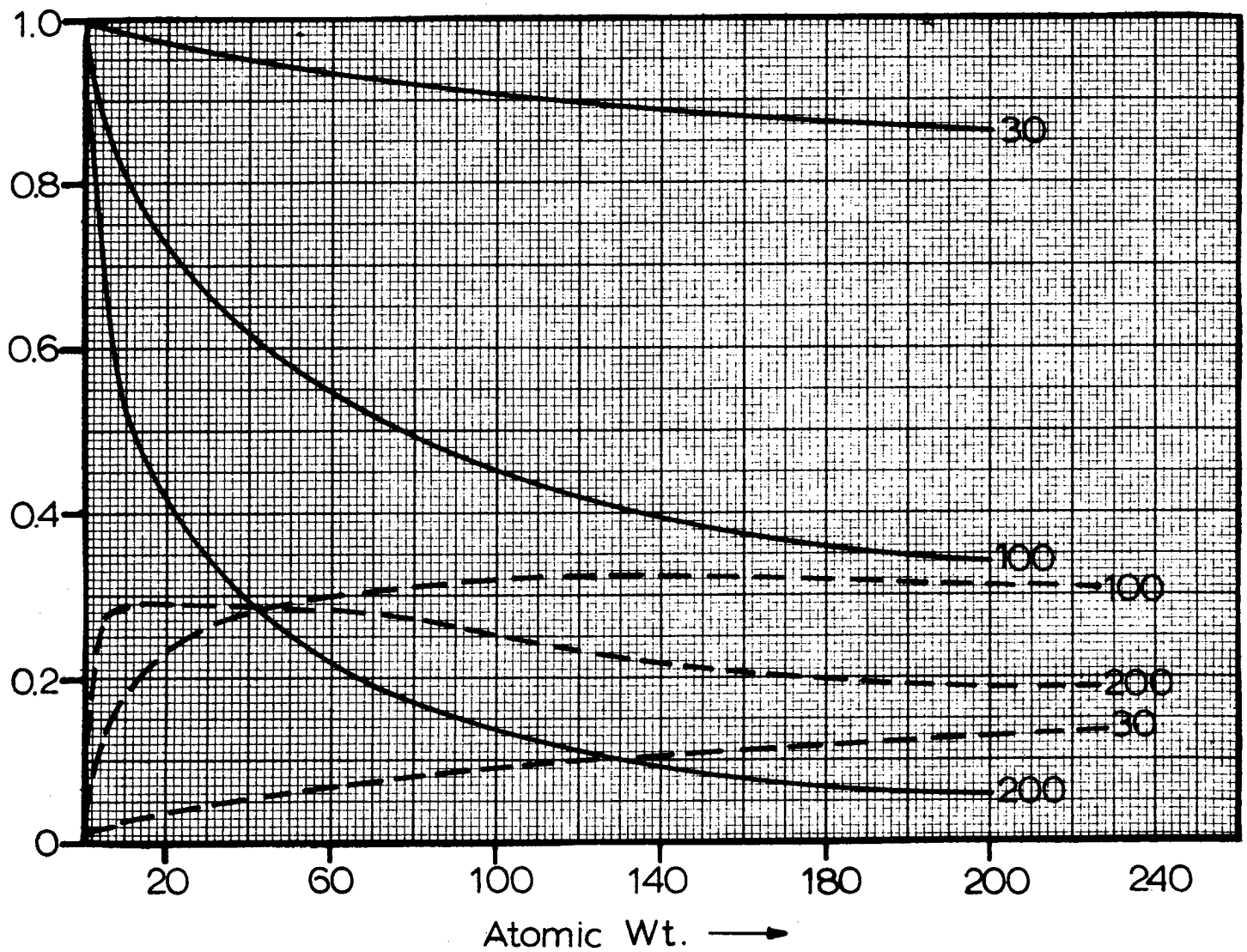

Full Curve: P_1, Probability of loss on first scattering.

Dashed Curve: P_2, Probability of loss on second scattering.

fig. 3

Case 2 Loss by Double Scattering: Rectangular Aperture

Before proceeding to the case of a second scattering it is interesting to note that from the single-scattering fractional loss one can already arrive at reasonably close limits for the ultimate target efficiency (ignoring Coulomb scattering for the moment). For example, on their first nuclear interaction the fraction of protons absorbed is 0.64. The fraction lost to the walls is $0.36\ P_1$ and the fraction surviving is $0.36\ (1 - P_1)$. On their second traversal the surviving fracti n will again have a further 0.64 probability of absorption, leading to the inequality for the fraction F_a of nuclear-interacting particles which are absorbed:

$$1.00 - 0.36\ P_1 > F_a > 0.64 + 0.64\ (0.36)\ (1 - P_1)$$
$$> 0.87 - 0.23\ P_1$$

It will be seen that a calculation of the probability of loss at the second diffraction scattering, P_2, establishes a tighter inequality which is sufficient to define F_a to about $1\frac{1}{2}\%$ at worst.

In general a target will be small in radial and vertical extent compared to the half-apertures A and B. If a particle on the first collision suffers projected angular deviations R and V (see Figure 1(c)) it is sufficient to consider the case where on its next collision the deviations are also (± R, ± V) since its radial and vertical displacements must be close to zero. The probability of the first scattering (R,V) is

$$p_1\ (R,V)\ dR\ dV = \left(\frac{1}{\sqrt{2\pi}}\right)^2 e^{-R^2/2}\ e^{-V^2/2}\ dR\ dV$$

Given such a scatter the probability of loss in the second diffraction scattering is

$$P_2 = \int_{a-R}^{a+R} \frac{1}{\sqrt{2\pi}} e^{-r^2/2}\, dr \left[\left\{ \int_{b-V}^{\infty} + \int_{b+V}^{\infty} \right\} \frac{1}{\sqrt{2\pi}} e^{-v^2/2}\, dv \right]$$

$$+ \left[\left\{ \int_{a-R}^{\infty} + \int_{a+R}^{\infty} \right\} \frac{1}{\sqrt{2\pi}} e^{-r^2/2}\, dr \right]$$

which after reduction gives

$$P_2 = 1 - \frac{1}{\pi} \left[\text{Erf} \frac{a+R}{\sqrt{2}} + \text{Erf} \frac{a-R}{\sqrt{2}} \right] \left[\text{Erf} \frac{b+V}{\sqrt{2}} + \text{Erf} \frac{b-V}{\sqrt{2}} \right]$$

Thus the total probability of loss in a second scattering is got by integrating over the allowed range of p_1 ——

$$P_2 = \int_{-a}^{a} \int_{-b}^{b} p_1\, p_2\, dR\, dV$$

which after reduction gives

$$P_2 = \frac{4}{\pi} \left\{ \text{Erf} \frac{a}{\sqrt{2}} \text{Erf} \frac{b}{\sqrt{2}} \right\} - \frac{2}{\pi^2} \int_0^a e^{-R^2/2} \left(\text{Erf} \frac{a+R}{\sqrt{2}} + \text{Erf} \frac{a-R}{\sqrt{2}} \right) dr$$

$$x \int_0^b e^{-V^2/2} \left(\text{Erf} \frac{b+R}{\sqrt{2}} + \text{Erf} \frac{b-R}{\sqrt{2}} \right) dV$$

The integral in the second term has been calculated numerically and the result for P_2 plotted in Figure 3.

To return to the inequality: the fraction of particles undergoing one nuclear collision and surviving around the machine is $0.36\ (1 - P_1)$, the fraction undergoing two collisions and still surviving is $(0.36)^2\ (1 - P_1 - P_2)$ and, of these survivors 64% will suffer absorption on the next collision. Thus by considering scattering up to the second generation and absorption up to the third generation, we have the following inequality for the absorption probability, F_a.

$$0.64 \left\{ 1 + 0.36\ (1 - P_1) + (0.36)^2\ (1 - P_1 - P_2) \right\} < F_a < \left\{ 1 - 0.36\ P_1 - (0.36)^2\ P_2 \right\}$$

Without having to consider the effects of third and higher-order scatterings this inequality defines F_a to about $1\frac{1}{2}\%$ in the worst case. The function F_a is plotted in Figure 4.

4. Multiple Coulomb Scattering

In the derivation by Blachman and Courant[2] of the loss by multiple Coulomb scattering the loss in the vertical direction only was assumed to dominate and the multiple scattering formula they used referred to projected angles. Here we assume also that the loss by vertical oscillation is the only important one and use the vertical half aperture B = 1.7 cm. Their result for the survival probability of a proton having traversed x gms of material is

---

(2) N. M. Blachman and E. D. Courant, Phys Rev 74, 140 (1948) and Phys Rev 75, 315 (1949)

Rectangular Aperture

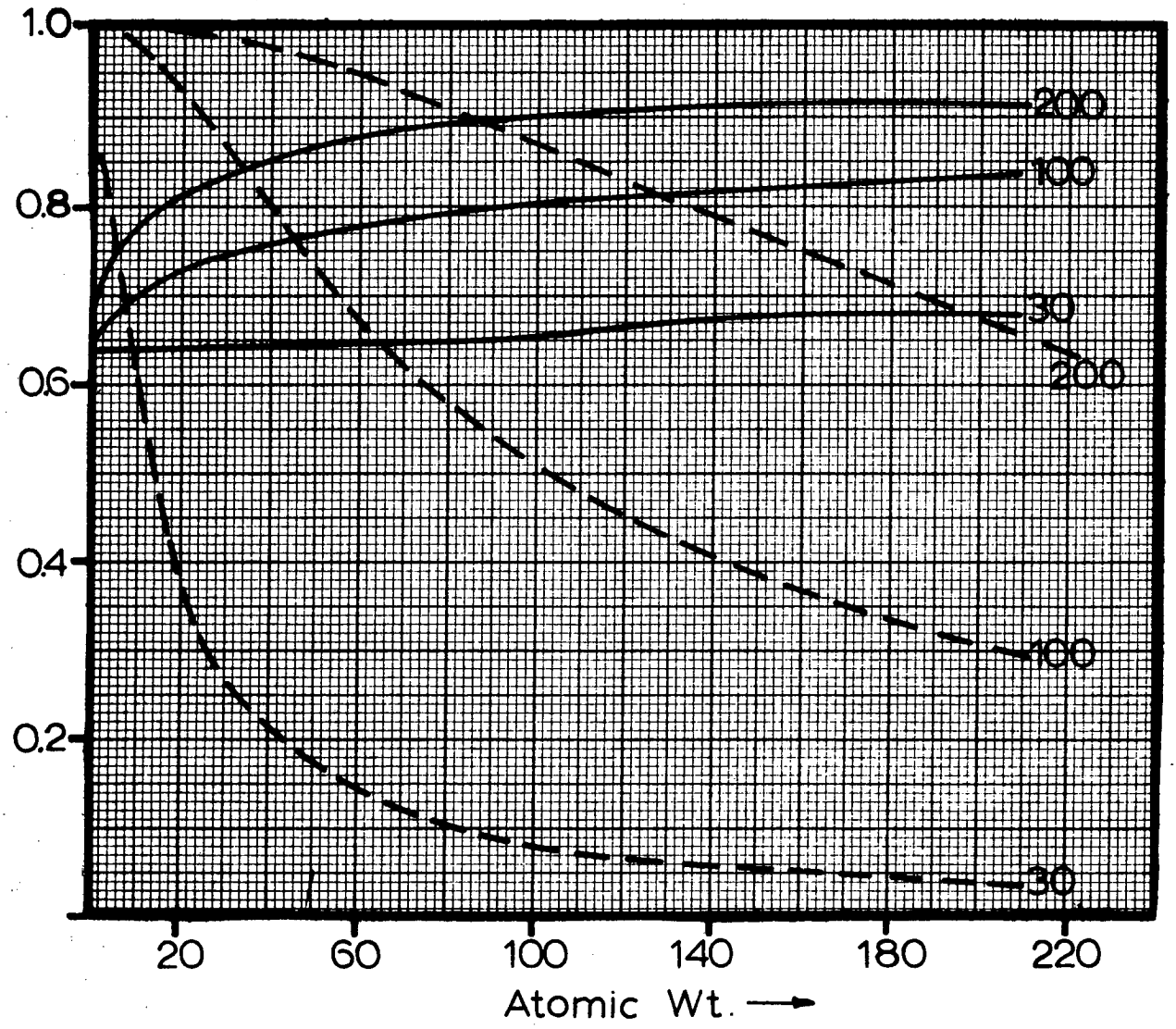

Full Curve: F_a, The fraction of nuclear-interacting particles which undergo absorption.

Dashed Curve: F_c, The fraction of protons which survive coulomb scattering.

fig. 4

$$P_C = 2 \sum_{s=1}^{\infty} \left[\frac{1}{\lambda_s J_1(\lambda_s)} \; e^{-\lambda_s^2 < \theta^2 > /4 \; \theta_o^2} \right]$$

where λ_s are the roots of $J_o(\lambda)$, $\theta_o = B/\mathcal{K}$.

Courant[1] then writes the fraction of particles that have undergone nuclear collision up to traversal x

$$F(x) = \frac{1}{L} \int_0^x P_C(x) \, e^{-x/L} \, dx$$

and integrating to infinity obtains

$$F_C = 2 \sum_s \frac{1}{\lambda_s J_1(\lambda_s)(1 + \lambda_s^2 \; Y)}$$

which depends only on Y, where

$$Y = \frac{225}{4} \; \frac{1}{E^2} \left(\frac{\mathcal{K}}{B}\right)^2 \frac{L}{L_R}$$

and L_R = Radiation length in the target material. Courant takes the nuclear removal length L to be L_T, that appropriate to the <u>total</u> nuclear cross-section assuming that all nuclear collisions resulted in loss. Since the parameter Y is a measure of the relative removal probabilities by nuclear events and multiple scattering, the spirit of the present calculation demands that the nuclear removal length L be taken as

$$L = F_a \, L_a = F_a \, L_T \left(\sigma_T/\sigma_a\right) = 1.57 \; F_a \, L_T$$

since the fraction of particles undergoing "useful" absorption is F_a, and also is the ratio (removal length)/(absorption length). The function F_C is shown in Figure 4 and the target efficiency $F = F_a F_C$ is shown in Figure 5.

5. Remarks

Certain effects have not been considered which will in general decrease the target efficiency. (i) Energy loss during multiple traversals will cause the orbit to move inwards and particles with small betatron amplitude will miss the target on every turn. (ii) The momentum compaction at 200 Gev ($\sim 10^{-3}$) means that particles can lose of the order of 200 Mev before they become unstable so this form of loss is probably small. (iii) The major effect which has been ignored is believed to be the loss due to a combination of multiple Coulomb scattering and diffraction scattering. This will be especially important in the 200 Gev case where both the diffraction scattering loss and Coulomb scattering loss are varying rather slowly with atomic number and where there is no sharp transition between one or the other effect dominating. Thus while the 200 Gev curve in Figure 5 is probably correct in indicating that there is no striking change in efficiency above $A \approx 12$ (even Lead is quite efficient), the maximum value of 84% is somewhat overestimated. (iv) No account has been taken here of the fact that for bubble chamber or r.f.-separator targets the spill-out time of 50-100 μsec does not correspond to the real "multiple traversal" situation since in a 200 Gev machine with a revolution time close to 20 μsec this corresponds to 3-6 traversals only. Particles suffering only a small deviation, much less than that needed to carry them to the walls, will require a number of revolutions depending on the tune of the machine before they strike the target again and have another chance to interact. A further

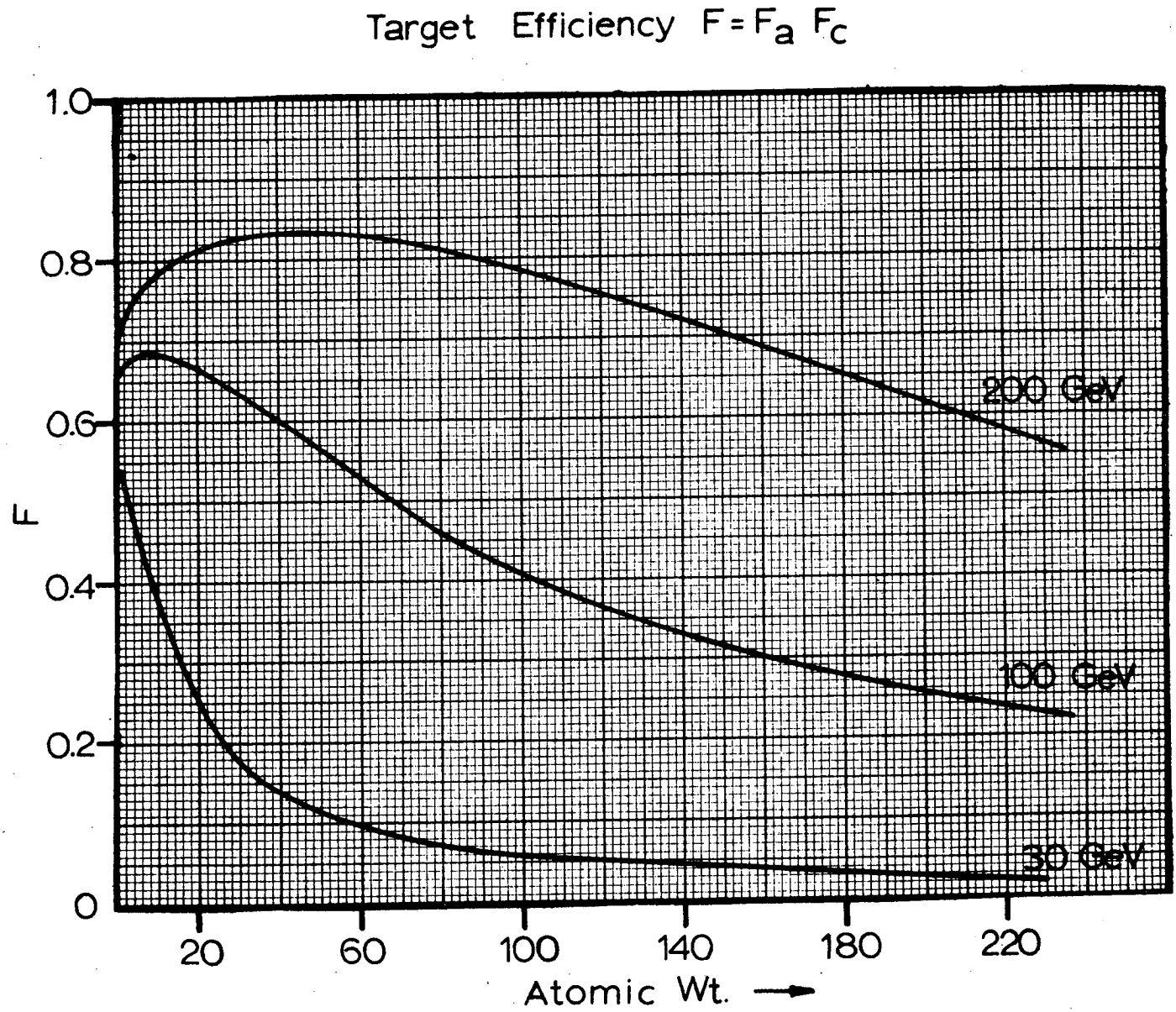

$1 - F_c$ = Fractional loss due to coulomb scattering.

F_a = Fraction going into production of secondaries.

$\lambda_{Betatron}$ = 240m.

B = Vertical Semi-Aperture = 1.7cm.

fig. 5

consequence of the small number of revolutions in the desired spill time is that the target should be close to one-half a mean free path in length. The inefficiency due to small angle scattering will be considerable and self-absorption of secondaries will no longer be negligible. Therefore, the curves of this report are not appropriate for spill times as short as 100 μsec.

(v) Finally, no account has been taken of the loss of particles on the target holder. Secondary particles produced in the target holder are undesired and presumably would be removed in a suitable collimator by the experimenter. The amount of this loss depends on the details of the target construction. The effect is impossible to avoid in the case of targets aligned parallel to the beam and production angles of 0°.

It can be seen from Figure 5 that (subject to the reservations above) target efficiencies of about 80% are predicted for operation at full energy. If, however, one desires to target at a lower energy in the machine the efficiency falls drastically and at 30 Gev even Beryllium or Carbon targets are only 30% - 40% efficient. Although both diffraction and Coulomb scattering losses decrease with increasing primary energy, the gain in multiple-traversal target efficiency in comparing the 30 Gev AGS and the 200 Gev accelerator are not as one might expect at first guess. In the higher energy design the vertical aperture is decreased and the betatron wavelength increased so that $\frac{1}{\lambda}$ (Aperture) is more than an order of magnitude smaller. Thus loss occurs for very much smaller angular deviations which offset the shrinkage of the angular distribution.

DK:amn

UCID-10170
AS/Experimental/01
February 15, 1965
D. Keefe

Efficiency of a Multiple Traversal Internal Target in the 200 GeV Proton Accelerator II

Targetting in a Collins Straight Section

I. Introduction

The efficiency of a thin internal target in a proton synchrotron has been studied by Courant[1] who calculated the effect of Coulomb scattering, and by Keefe[2] who added in the effect of nuclear diffraction scattering. These treatments of the problem assumed that loss of protons by Coulomb scattering occurred predominantly in one plane (vertical) and thus the calculation could be carried out with projected angles. In Reference 2 the formulae for loss in both planes due to diffraction scattering are given. It is the purpose of the present note to extend the Coulomb scattering calculation to the case where both radial and vertical loss are comparable and to give results for a specific design of a 200 GeV accelerator[3] under four specific conditions of operation.

The internal target is assumed to be placed close to the upstream quadrupole in a $\pi/2$-type (Collins) straight section. The multiple-traversal efficiency will depend on whether this lens is horizontally focussing (Case 1) or horizontally defocussing (Case 2). It is also of interest to examine how the target efficiency is diminished if the plunged septum magnets needed for the slow extraction system are allowed to remain in the plunged condition partially obstructing the aperture during the internal targetting operation. This would be the case if one desired to proceed without any loss of valuable flat-top time to internal target operation after the slow extraction was terminated.

The angular acceptance of the machine in both planes, at the location of the target is shown in Table I for the machine parameters described in Reference 3.

---

1 Courant, E. D., BNL Internal Report EDC-46 February 1962

2 Keefe, D., LRL Internal Report UCID-10105 March 1964

3 Garren, A., and Smith, L., Parameter List, AS/Theoretical/01 December 1964.

TABLE I

Case	Upstream Lens of Collins Straight Section	Septum Magnets	Full Angular Acceptance (mr)	
			$2\theta_V$	$2\theta_H$
1a	F (horizontally)	Retracted	1.25	1.11
1b	F (horizontally)	In aperture	0.78	1.11
2a	D horizontally	Retracted	0.55	2.50
2b	D horizontally	In aperture	0.34	2.50

If we assume either an effective good field aperture or a collimator aperture a_M somewhere in the machine structure at a maximum in the β-function, we can write the full angular acceptance (2θ) in one plane at the target

$$2\theta = \frac{a_c}{\beta_c} = \frac{a_M (\beta_c/\beta_M)^{1/2}}{\beta_c} = \frac{a_M}{(\beta_M \beta_c)^{1/2}}$$

where a_c and β_c refer to the aperture and β-function at the target location. At full field a_M was assumed to be 8 cm in all cases horizontally and 4 cm vertically in cases (1a) (2a) and 2.5 cm vertically in cases (1b) and (2b). These choices depend on the details of a slow extraction method developed for this machine by Lambertson[4]. In all cases β_M = 58.9 m and the values of β_c were 88 m and 17.3 m in the two planes respectively.

It is clear that at least in cases (1a, b) the loss due to scattering in the radial plane cannot be neglected.

II. Extension of Coulomb Scattering Calculations to include Both Planes

The probability that a proton survives without suffering a nuclear interaction (either elastic or absorptive) or being lost outside the horizontal aperture, after it has traversed a total thickness x gm cm^{-2} of the target material - in many revolutions - is[1]

---

[4] Lambertson, G. R., (unpublished) 1964.

$$P_c^H = 2 \sum_{i=1}^{\infty} \frac{1}{\lambda_i J_1(\lambda_i)} \exp\left(-\lambda_i^2 \langle\theta^2\rangle / 4\theta_H^2\right)$$

where λ_i are the roots of J_o and

$$\theta_H^2 = \frac{225}{4} \frac{1}{E^2} \frac{x}{X_o}$$

with E in MeV and X_o (the radiation length) in gm cm^{-2}.

A similar expression with θ_H replaced by θ_V will represent the probability P_c^V that a proton will not undergo projected angular deviations in the vertical plane which would carry it outside the aperture. Thus, the joint probability of survival is $P_c^H P_c^V$. The fraction undergoing nuclear collision before traversing a thickness x is

$$F(x) = \frac{1}{L} \int_o^x P_c^H P_c^V e^{-x/L} dx.$$

where L, which in Courant's paper was taken to be one nuclear mean free path, is a modified mean free path as discussed in Reference 2 to take account of the loss by diffraction scattering viz.

$$L = 1.57 F_a L_T$$

where L_T is a nuclear mean free path corresponding to the <u>total</u> cross-section (= elastic + absorption cross-sections) and F_a is the fraction of protons which <u>both</u> make a nuclear collision <u>and</u> are absorbed. [Note that some protons can make nuclear collisions, viz. elastic scatterings, and are <u>not</u> absorbed; whether they survive around the machine or are lost to the walls depends on the magnitude of the scattering angle.]

Integrating to $x = \infty$ we have the number undergoing nuclear collision

$$F_c = 4 \sum_i \sum_j \frac{1}{\lambda_i \lambda_j J_1(\lambda_i) J_1(\lambda_j)} \frac{1}{1 + \lambda_i^2 y_1 + \lambda_j^2 y_2}$$

where $y_1 = \frac{225}{4} \frac{1}{\theta_H^2} \frac{1}{E^2} \frac{L}{X_o}$

$$y_2 = \frac{225}{4} \frac{1}{\theta_V^2} \frac{1}{E^2} \frac{L}{X_o}$$

This expression for F_c is extremely tedious to compute by hand as a very large number of terms (which alternate in sign) has to be included. It is more convenient to consider approximations to P_c^H and P_c^V. If the losses are small these can be very well represented by error-functions. In the present instance the losses all turn out to be large (greater than a few percent) in which case a suitable approximation to P_c^H is just the leading term with a suitable cut-off to keep the probability correctly bounded, viz.

$$P_c^H = 1.6\, e^{-5.8\,\eta} \qquad \text{for } \eta = \frac{\langle\theta^2\rangle}{4\theta_H^2} = \gamma_1 x > 0.08$$

$$= 1 \qquad \text{for } \eta < 0.08$$

$$\gamma_1 = \frac{225}{4}\,\frac{1}{E^2}\,\frac{1}{\theta_H^2}\,\frac{1}{X_o}$$

See Fig. 1 for a comparison of the exact and approximate forms. A similar form holds for P_c^V with $\eta = \gamma_2 x$ where

$$\gamma_2 = \frac{225}{4}\,\frac{1}{E^2}\,\frac{1}{\theta_V^2}\,\frac{1}{X_o}$$

The integral for F_c is in three parts because of the dichotomies $\gamma_1 x \gtrless 0.08$, $\gamma_2 x \gtrless 0.08$ and the result is

$$F_c = 1 - e^{-\frac{0.08}{\gamma_1 L}} \left\{ \frac{5.8\,\gamma_1 L}{1 + 5.8\,\gamma_1 L} \right\} -$$

$$- 1.6\, e^{-\frac{0.08}{\gamma_1 L}} - \frac{0.47\gamma_1}{\gamma_2} \left\{ \frac{5.8\,\gamma_2 L}{(1 + 5.8\,\gamma_1 L)\,[1 + 5.8(\gamma_1+\gamma_2)L]} \right\}.$$

This function was computed for values of γ_1 and γ_2 appropriate to the four examples of machine operation quoted, and for a variety of elements between hydrogen and lead. The probability, F_a, of a particle making a nuclear interaction and ultimately being absorbed to produce useful secondaries was computed according to the method of Reference 2 which considers diffraction scattering up to and including the second generation and absorption up to and including the third generation. These values of F_a enter weakly into the computation of F_c because they occur in the definition of L. Finally, the product of

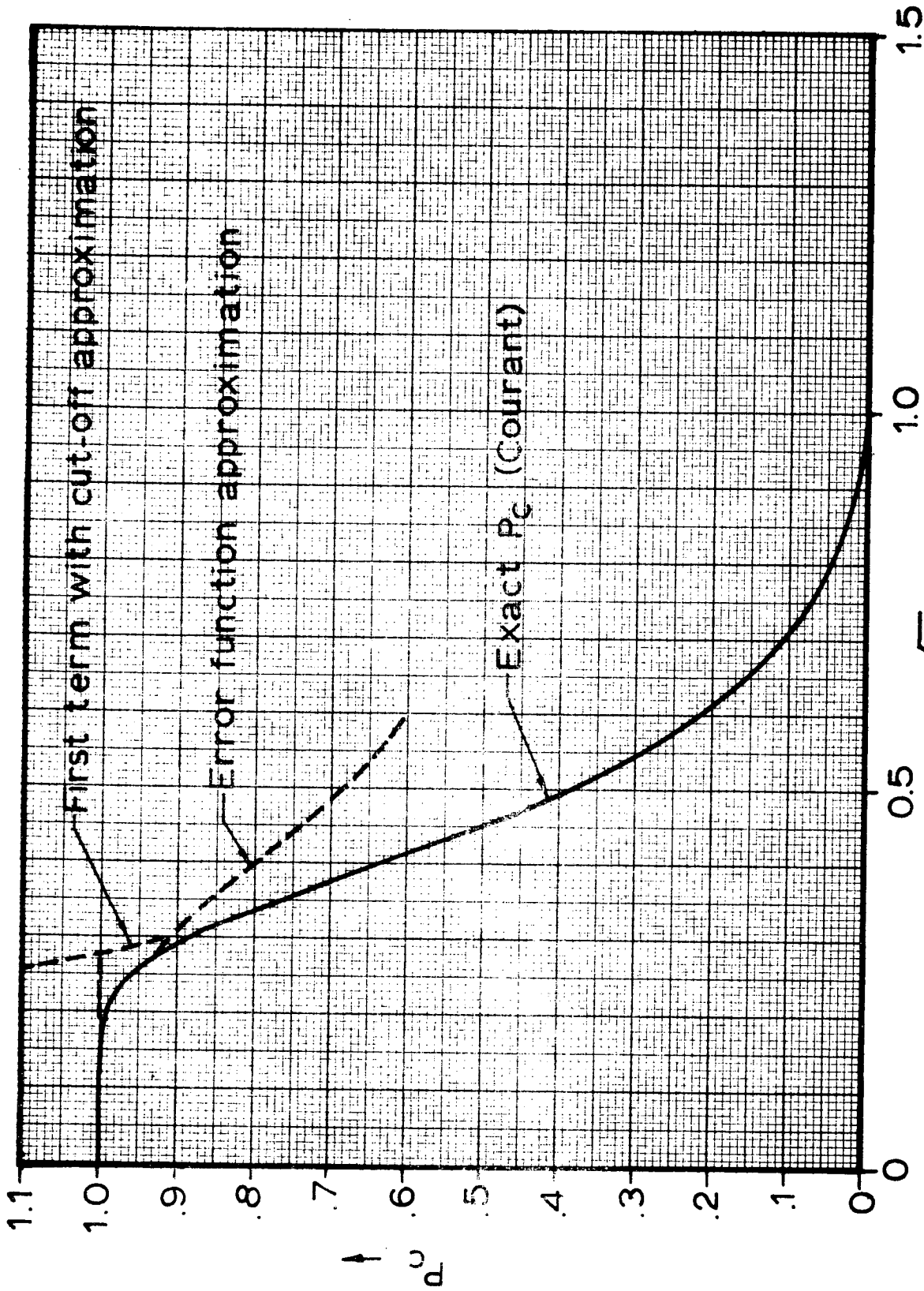
First term with cut-off approximation
Error function approximation
Exact P_c (Courant)
P_c →
$\sqrt{n}$ →
1.1
1.0
.9
.8
.7
.6
.5
.4
.3
.2
.1
0
0
0.5
1.0
1.5

fig.1

$F_a F_c$ for the different machine conditions and for various target elements is used to define the target efficiency viz. the fraction of protons which die in the target to produce secondary particles, and are not lost outside the aperture by multiple coulomb scattering or plural diffraction scattering. These efficiencies are plotted vs. atomic weight in Figs. 2,3,4 and 5.

III. Conclusions

To optimize internal target efficiencies it is clearly better to arrange for the horizontally focussing quadrupole to be at the upstream end of the Collins straight section (Cases 1a and 1b). Even here, however, we note again (cf Ref. 2) that the maximum efficiency falls drastically if the machine is operated at low energy. For other reasons, viz. ease of injection and especially of extraction, it is preferable to have the upstream quadrupole defocussing horizontally. If the major part of the experimental program is designed to be based on external proton beam operation, then this is a better choice. Comparison of Figs. 2 and 4 shows that the maximum efficiency drops from 85% to 74% if one makes this choice, which is not an excessive price to pay for the greater ease of extraction. In addition, targets of heavy elements would be very inefficient and should be used only at low primary intensity. The contrast between Figs. 4 and 5 shows that it would be advisable to arrange for the extraction magnets to be withdrawn from the aperture before beginning operation with the internal target.

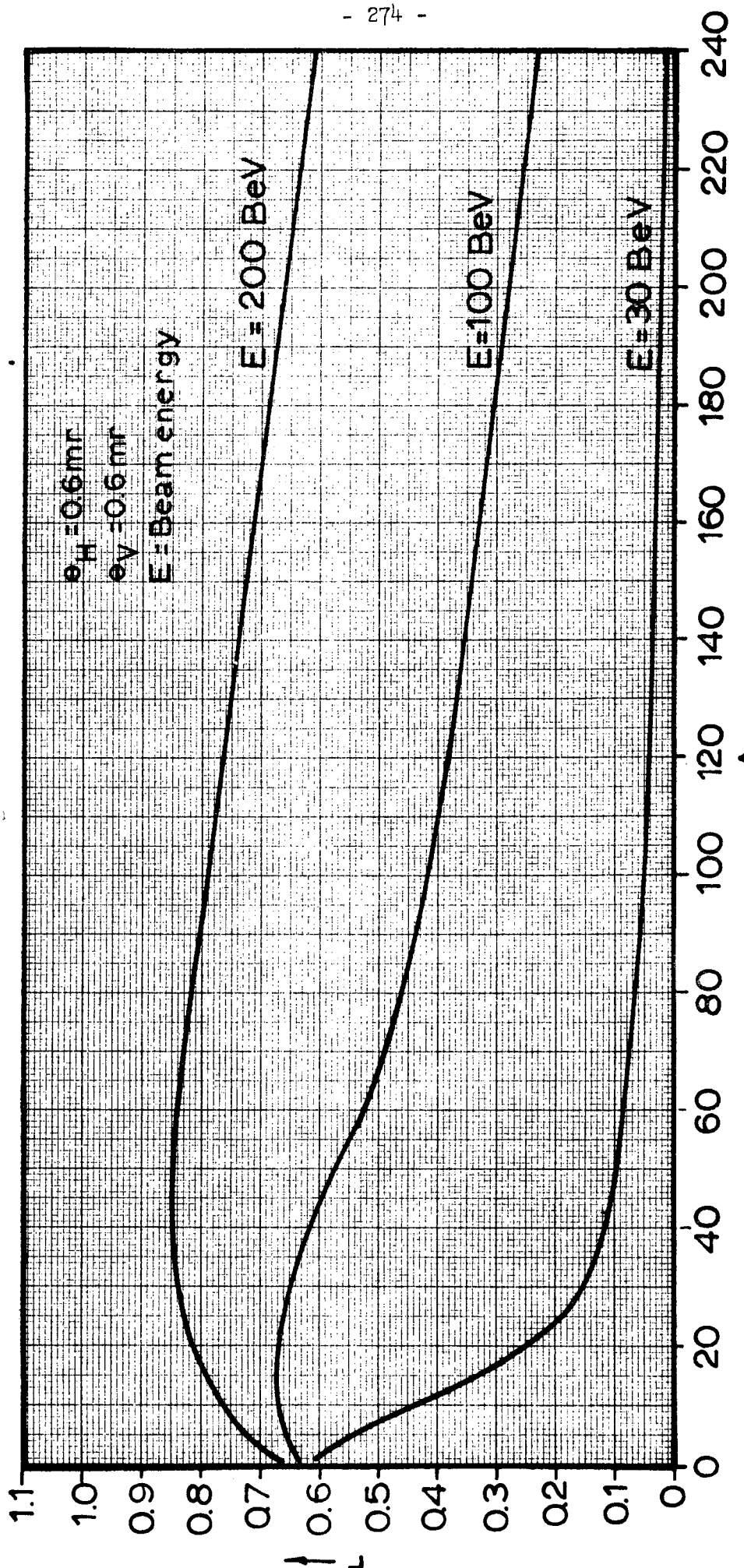

Case 1a

"Target Efficiency" F vs. Atomic Weight

fig. 2

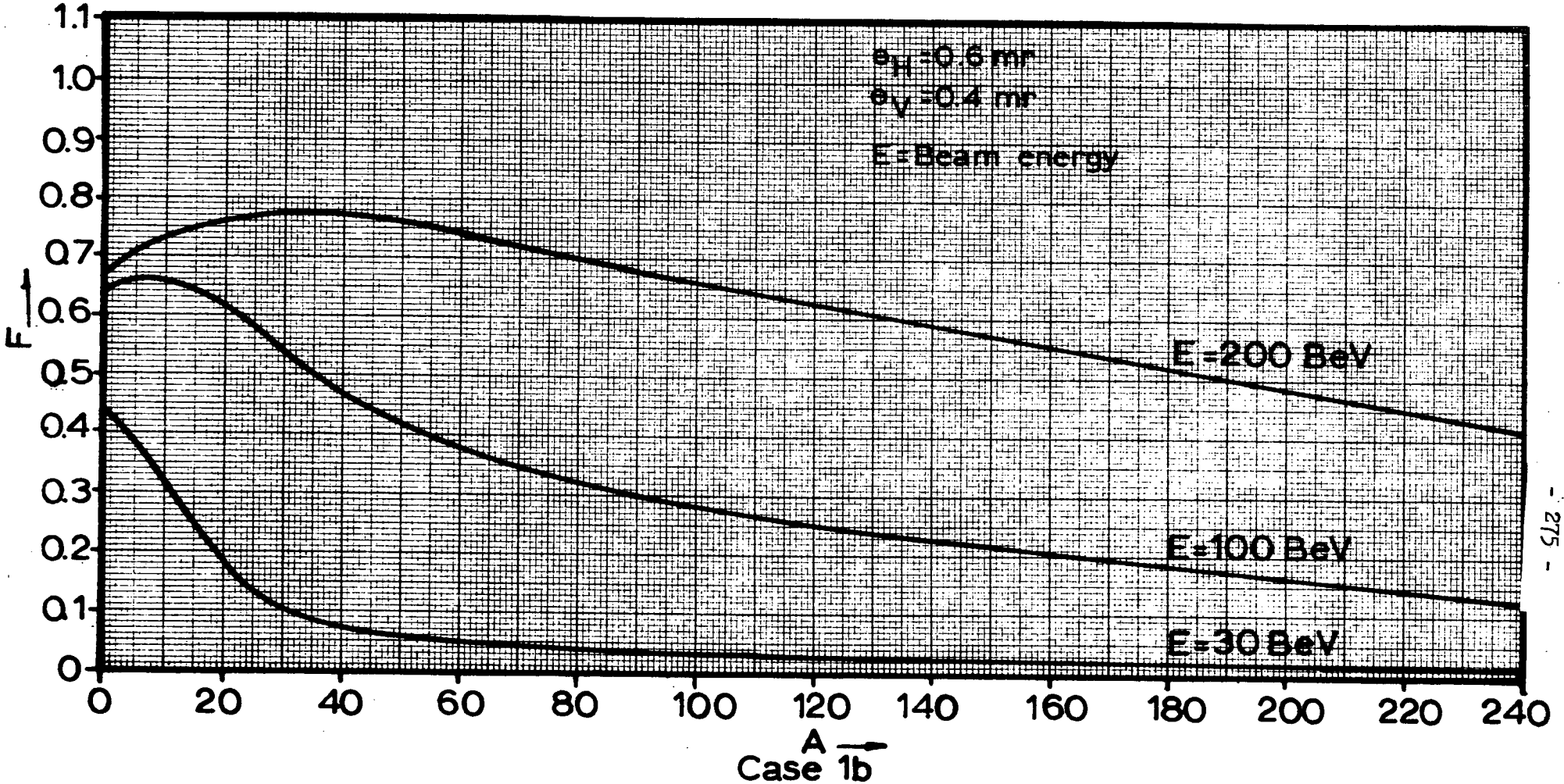

Case 1b

"Target Efficiency" F vs. Atomic Weight

fig. 3

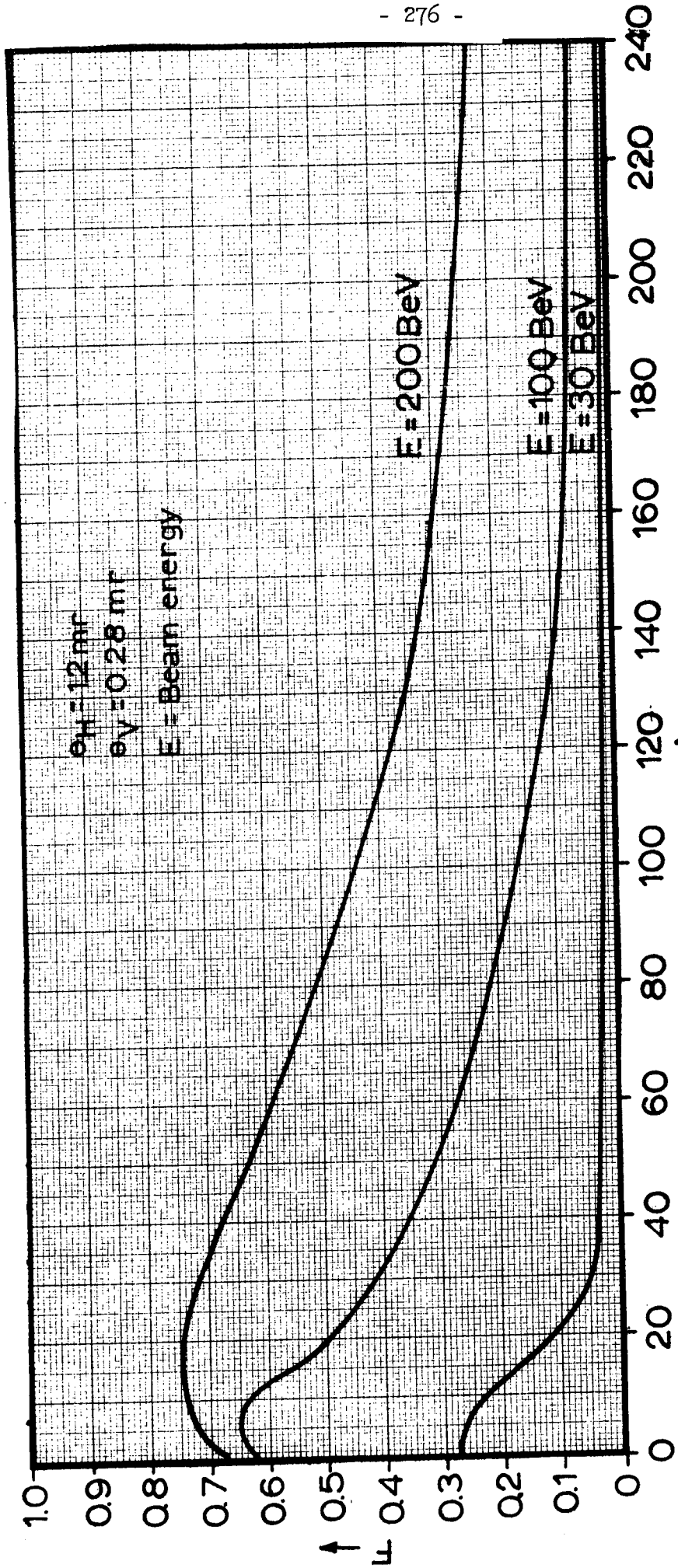

Case 2a
"Target Efficiency" F vs Atomic Weight
fig. 4

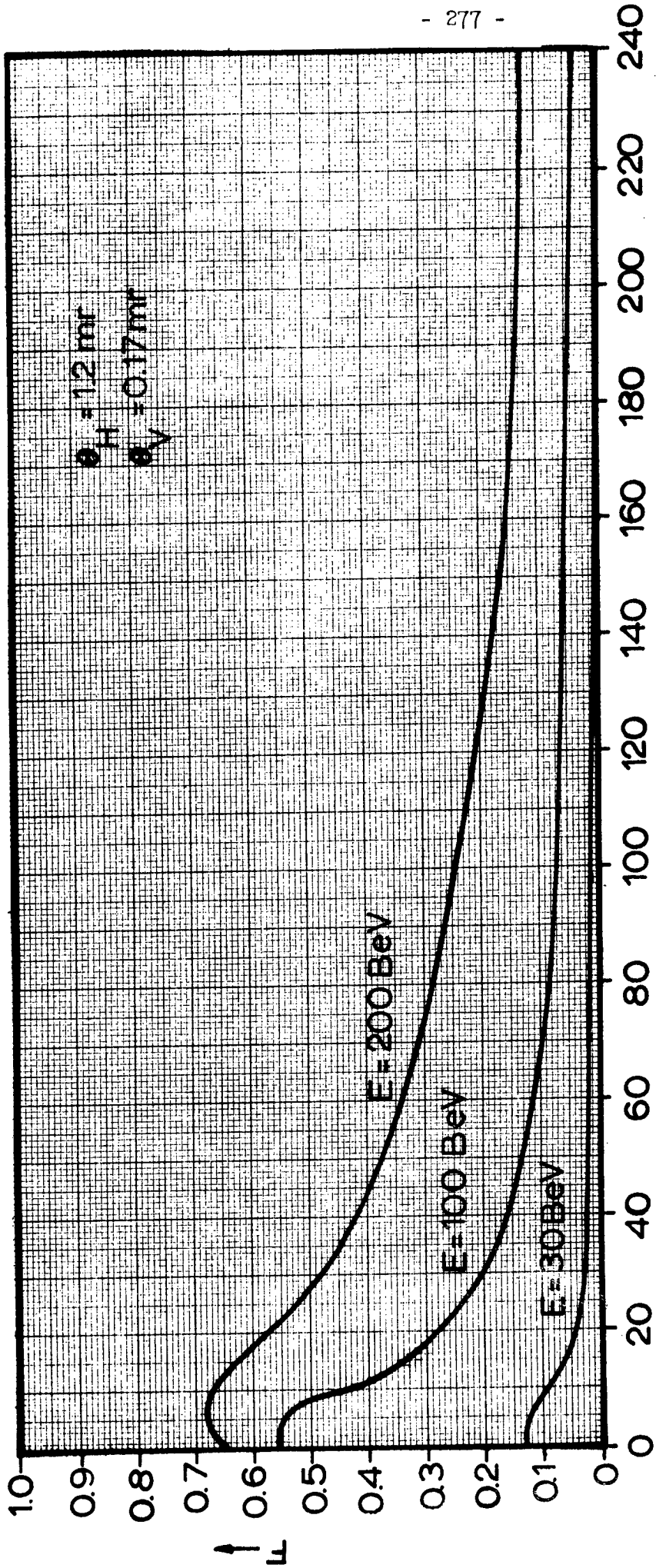

Case 2b

"Target Efficiency" F vs. Atomic Weight

fig. 5

UCID-10030

AS/Experimental/02
August 14, 1964
Timothy E. Toohig

A CONSIDERATION OF THE EFFECT OF FAST ELECTRON ESCAPE ON TARGET HEATING

An obvious bit of fallout from the study of the production of fast electrons by collision precesses[1] is the effect of such production on the heating of targets in the 200 GeV accelerator. A substantial portion of this heating is caused by the deposition of energy in the target by electrons produced in ionizing collisions by the beam particles. Keefe[2] has suggested that the high energy electrons which escape from the target might carry off enough energy to mitigate the problem of heating of targets in the 200 GeV AGS by beam particles traversing them.

At the energies of interest the fast electrons may be considered to be produced in proton-electron collisions with the target electrons at rest. From simple 2-body kinematics the kinetic energy of the secondary electron is expressible as:

$$T_{el} = T_{el}\ (\theta) \qquad (1)$$

where θ is the angle of the electron trajectory with respect to the primary beam direction. Assuming for simplicity a 0.05-inch diameter cylindrical target with the beam along the axis, the potential path in the target of a secondary electron, L, can be expressed as:

$$L_{el} = L_{el}\ (\theta) \qquad (2)$$

Equations (1) and (2) yield Fig. 1, the potential path of a scattered electron vs. its kinetic energy in an infinitely long target. Superimposed on Fig. 1 are the lines representing $1/2\ L_{int}$ for Al, Cu, U, representative of light, medium, and heavy target materials. These lines represent cutoffs on the potential path under the assumption that the ionizing collision takes place at the midpoint of the target.

---

1. T. E. Toohig. "An Experiment to Measure the Pion Form Factor at the 200 GeV Accelerator", AS/Experimental/02, July 15, 1964.

2. D. Keefe, (private communication).

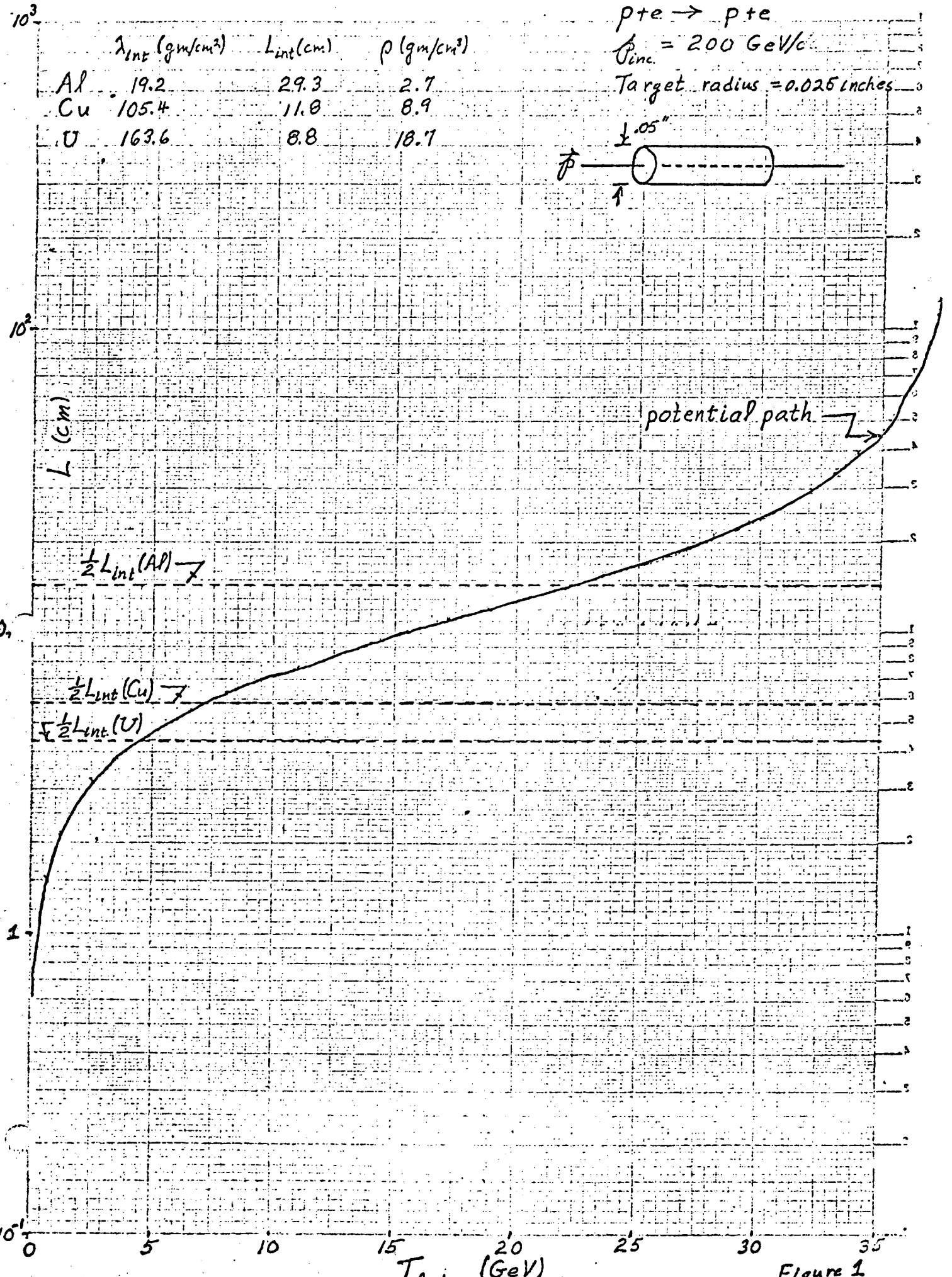
p+e → p+e
P_inc. = 200 GeV/c
Target radius = 0.025 inches
±.05"
λ_int (gm/cm²) L_int (cm) ρ (gm/cm³)
Al 19.2 29.3 2.7
Cu 105.4 11.8 8.9
U 163.6 8.8 18.7
potential path
L (cm)
½L_int (Al)
½L_int (Cu)
½L_int (U)
10³
10²
1
10⁻¹
0
5
10
15
20
25
30
35
T_electron (GeV)

Figure 1

In Fig. 2, we expand the low-energy end of the potential path curve and plot to the same scale the range-energy curves for electrons in Al, Cu, U. (Note the change in energy scale between Figs. 1 and 2 from GeV to MeV). The range-energy curves are calculated from the relation given by Evans.[3]

$$R\ (mg/cm^2) = 530\ E\ (MeV) - 106 \qquad (3)$$

Using a simple-minded approach, we assume that all those electrons whose potential path is less than their ranges escape from the target. From Fig. 2 $T_{escape}\ (Al) \tilde{} 1$ MeV, $T_{escape}\ (Cu) \tilde{} 2$ MeV, $T_{escape}\ (U) \tilde{} 5.5$ MeV.

We note that these escape energies all lie on the rising portion of the potential path curve before the $\frac{1}{2} L_{int}$ points. This indicates that the electrons escape through the sides of the targets so that the width, not the length, of the target is important in electron escape considerations.

Figure 3 gives the total energy loss of a 200 GeV/c proton as a function of the atomic number of the target from collision with atomic electrons.

Figure 4 divides the total energy loss of Fig. 3 into energy deposited in the target, $\frac{dT_s}{dx}$, by electrons having ranges shorter than their potential paths, and energy carried off from the target, $\frac{dT_h}{dx}$, by escaping electrons. Over the entire range of target materials, the fraction of energy deposited in the target relative to the total collision energy loss is ~ 75%.

The values of $\frac{dT_s}{dx}$ and $\frac{dT_h}{dx}$ are calculated by the program ELHEAT, by means of the relations,

$$\frac{dT_s}{dx} = \frac{2\pi\, m_e r_e^2}{\beta^2}\, nZ \left[\ell n \left(\frac{m_e T_i}{I^2}(\gamma^2 - 1)\right) - \beta^2\right] \text{ MeV/cm} \qquad (4)$$

and

$$\frac{dT_h}{dx} = nZ \int_{T_i}^{T_{max}} T\ \phi_h\ (T)\ dT \text{ MeV/cm} \qquad (5)$$

$$\phi_h\ (T)\ dT = \frac{2\pi\, m_e r_e^2}{\beta^2}\, nZ\, \frac{dT}{T^2} \left[1 - \beta^2 \frac{T}{T_{max}} + \frac{1}{2}\left(\frac{T}{E_o}\right)^2\right] \text{ cm}^2\text{/electron} \qquad (6)$$

Where nZ = electrons/cm^3 of target

m_e, r_e = mass and classical radius of the electron

3. R. D. Evans, The Atomic Nucleus, (McGraw-Hill Book Co., Inc., New York, 1955).

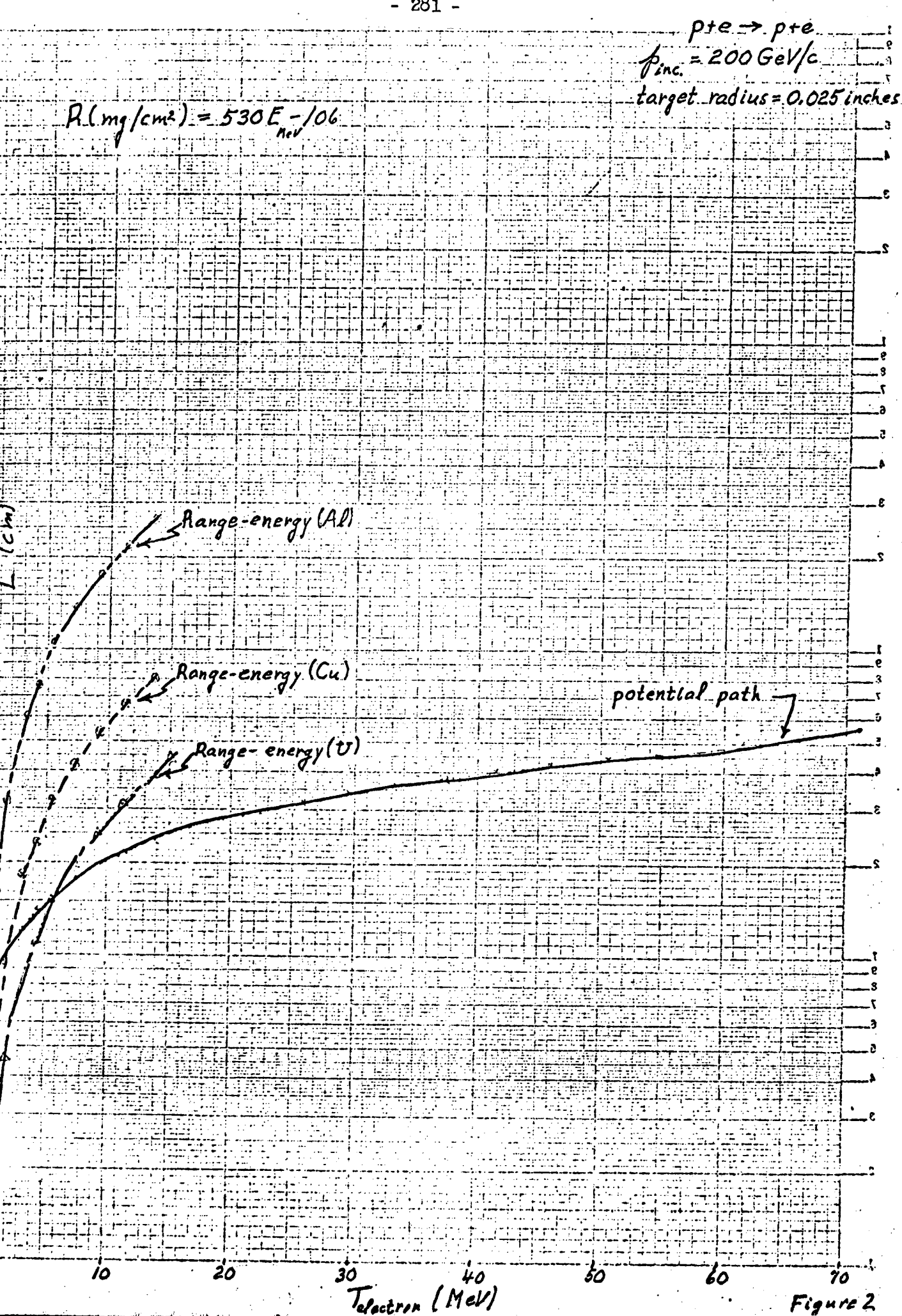
p+e → p+e
$p_{inc.}$ = 200 GeV/c
target radius = 0.025 inches
$R(mg/cm^2) = 530 E_{MeV}^{-106}$
Range-energy (Al)
Range-energy (Cu)
Range-energy (U)
potential path
10
20
30
40
50
60
70
$T_{electron}$ (MeV)

Figure 2

8/6/64

Energy loss in targets

.05 in cylindrical targets

$p_{beam} = 200$ GeV/c

$$\frac{dE}{dx} = \left(\frac{dE}{dx}\right)_{soft} + \left(\frac{dE}{dx}\right)_{hard}$$

(Program ELHEAT)

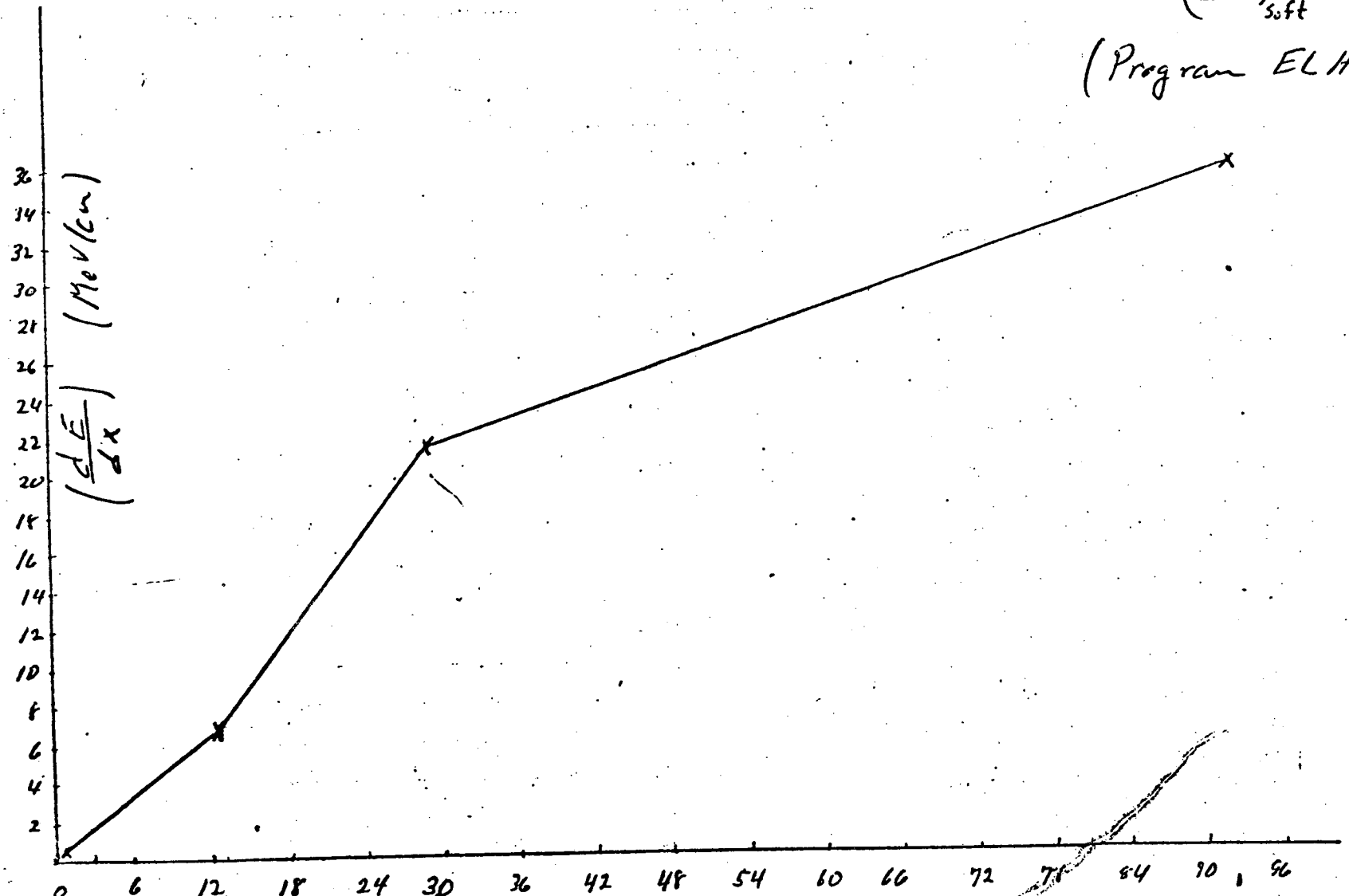

Figure (3)

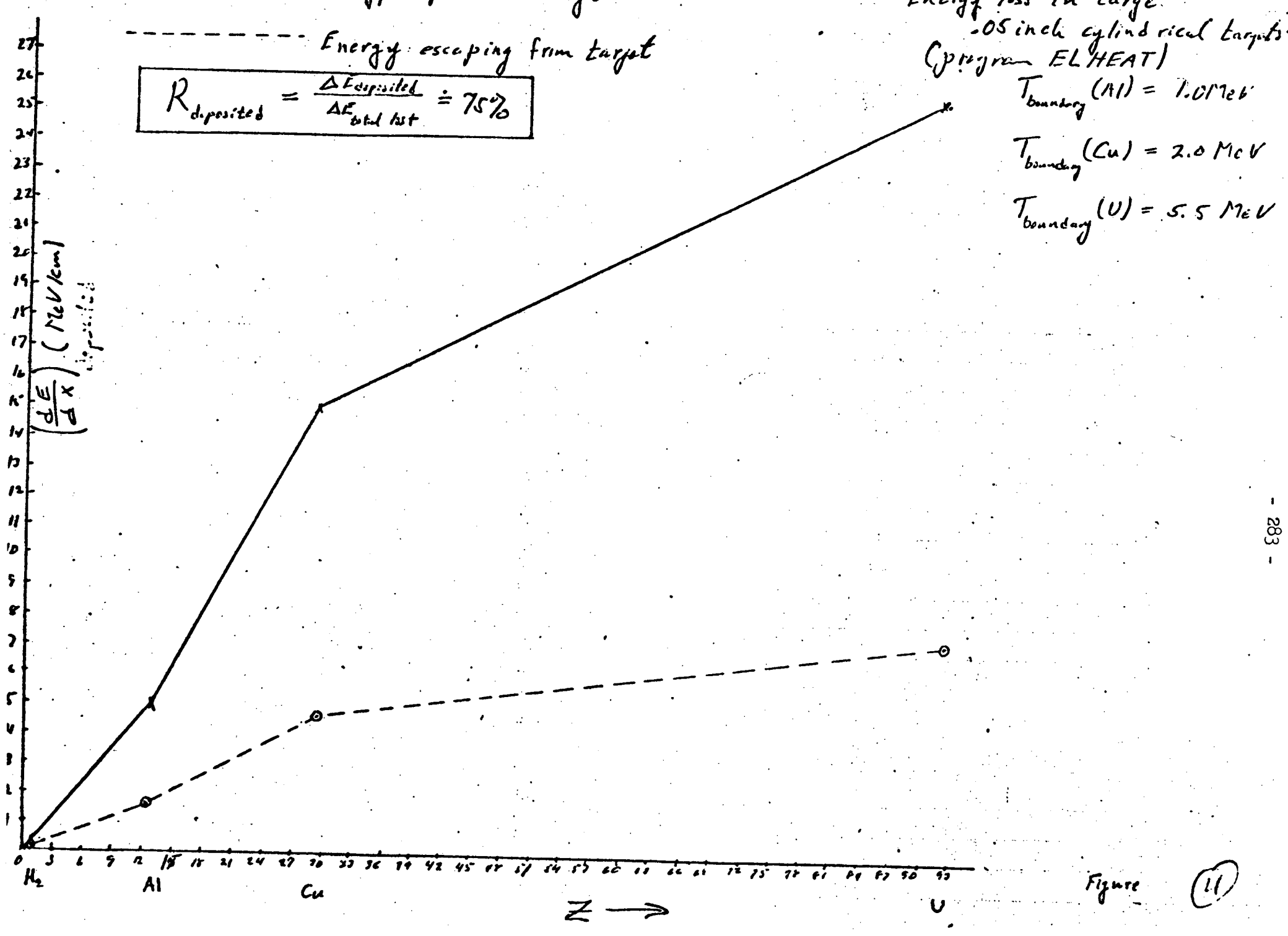
Energy escaping from target
$R_{deposited} = \frac{\Delta E_{deposited}}{\Delta E_{total\ lost}} \doteq 75\%$
Energy loss in large .05 inch cylindrical targets (program EL HEAT)
$T_{boundary}(Al) = 1.0 MeV$
$T_{boundary}(Cu) = 2.0 MeV$
$T_{boundary}(U) = 5.5 MeV$
$\left(\frac{dE}{dx}\right)_{deposited}$ (MeV/cm)
H2
Al
Cu
U
Z →

Figure 11

T = the kinetic energy of the scattered electron

T_i = the boundary between trapped and escaping electrons as determined from Fig. 2

T_{max} = maximum energy transfer to the electron

$$= T_o \left[\frac{1 + (2\,m/T)}{1 + (m + m_e)^2/2\,m_e T} \right]$$

T_O, E_o = incident particle kinetic and total energies

β, γ = β, γ of the incident particle

I = mean ionization potential of the target

$= 11.5\ Z$ (eV)

$\phi_h\,(T)\,dT$ is the cross-section for scattering of incident spin-1/2 particles by atomic electrons.

UCID-10174
AS/Experimental/02
September 28, 1965
Earl F. Hughes**

Lawrence Radiation Laboratory
University of California
Berkeley, California

A COMPUTER SOLUTION TO MAGNET ACTIVATION PROBLEMS

I. Introduction

The computer code described in this report is used to calculate the radiation dose received from a residual radiation field surrounding the main ring magnets of a proton AGS after shutdown. It is frequently desirable to have personnel in the vicinity of these magnets very soon after shutdown to make repairs or modifications; therefore, knowledge of the amount of dose received from this field is necessary. One of the first steps in the calculation of this shutdown gamma radiation field is to determine the activity of the magnet. By using the data gathered by CERN for a 20 GeV/c cascade, an activation model was devised that assumed a uniform beam loss around the vacuum chamber. It was further assumed that all the loss could be concentrated at the chamber center. The relative activation could then be traced out on a magnet cross section. The simplifying assumption was made that the radiation sources could be considered infinite line sources so that the radiation fields could be synthesized from these sources with a 1/R geometrical attenuation factor. This assumption makes the dose calculation a two-dimensional problem. (See UCID-10137, December 10, 1964 by W. S. Gilbert for detailed information.)

II. Description of Parameters

The mathematical form for the dose at a field point is given by

$$\iint \frac{\mathrm{Act}\ (I, J)\ \mathrm{Trn}\ (I, J)}{R(I, J)}\ \mathrm{d(Area)}$$

where Act(I, J) is the activity of the magnet at point (I, J), Trn (I, J) is the gamma transmission factor at point (I, J) for a given field point,

---

**National Science Foundation High School Teacher's Program

and R(I, J) is the distance from point (I, J) to the field point. The form that is used for computer computation is

$$\Sigma\Sigma \frac{Act(I, J) \cdot Trn (I, J) \Delta Area}{R(I, J)}$$

where one now calculates the activity, transmission factor, and distance from a point in the center of a finite area, then multiplies this by the area to get an incremental or Δ dose. One does this for all of the incremental areas in the magnet and sums them to get the number representing the dose at a field point. The activity factor is given by

$$Act (I, J) = Ce^{-c'\sqrt{x + R_o}}$$

where C, c', and R_o are constant determined by individual analysis and x is the distance in iron between the beam and source line. The transmission factor is given by

$$Trn (I, J) = Be^{-\mu t}$$

where B is the dose build-up factor of the form $1 + at + bt^2$; a and b are constants whose values are obtained from available build-up factor data by the methods of least squares, μ is the linear absorption constant of iron, and t is the thickness of iron between the source line and the field point. The distance R(I, J) is the total distance between the source line and the field point; this includes the distance in iron and the distance in air. An incremental magnet area of 1 cm^2 was chosen because it was the largest area that gave reasonable accuracy; this was determined by picking an arbitrary field point and calculating the dose with different grid sizes. At a point on the open side of the magnet the dose was .380 with an area of 4.0 cm^2, .322 with 2.25 cm^2, and .319 with 1 cm^2. Decreasing the area more would improve the accuracy an insignificant amount while computer running time would increase sharply.

III. Description of Computer Program

We need the distance in iron as well as the total distance between the source line and the field point, so it is necessary to inform the computer what is iron and what is air. This is done by superimposing a grid over a magnet profile and assigning a value of 1 to the grid point if it is in iron and a value of 0 if it is in air. The shape of the magnet was simplified to that shown on Fig. 1. The value of 1 or 0 is assigned by comparing the grid points with the magnet boundaries; if it exceeds the boundaries it is air, if not it is iron. A subroutine is used to calculate the distances in iron and the total distance. If (I, J) represents the source line on the grid, and (IO, JO) the field point, the total distance is calculated by $\sqrt{(IO-I)^2 + (JO-J)^2}$. The distance in iron is calculated by testing the points along the line connecting the source line and the field point to see if they are in iron or air. First the slope of the line segment is calculated, (JO-J)/(IO-I), then the actual scanning of the points is done by first testing point (I, J), moving to point (I+1, J+Slope · 1) and testing, then moving to (I+2, J+Slope · 2) and testing, etc. The number of positive tests for iron is designated as count so the distance in iron is given by $\sqrt{(Count)^2 + (Slope \cdot Count)^2}$. The problem of an infinite slope where IO - I = 0 is taken care of by moving along the J values and using the slope of the complementary angle to calculate the I movement when $|JO - J| > |IO - I|$. Now that we can calculate the necessary distances, the other factors can be calculated too. The activity factor should be calculated first and the values for each (I, J) stored in memory since the activity will remain the same for the magnet no matter how many field points we have or what their locations are. For calculating the Act (I, J) we call the position of the beam (IO, JO) so the subroutine will calculate the distance between the beam and each point (I, J). Act (I, J) then equals $Ce^{-c\sqrt{x}} + R_o$ where x is given by the subroutine. The transmission factor is a function of the distance in iron between the source line and the field point so it does not remain the same for all field points. The field points are read in from data cards, then two nested DO loops go through each value of (I, J) for which the subroutine is called, the transmission factor is calculated, the activity is brought in from memory, and the Δ dose is determined by

O = Proton beam

P = Source line

Q = Field point

R(I, J) = t + y

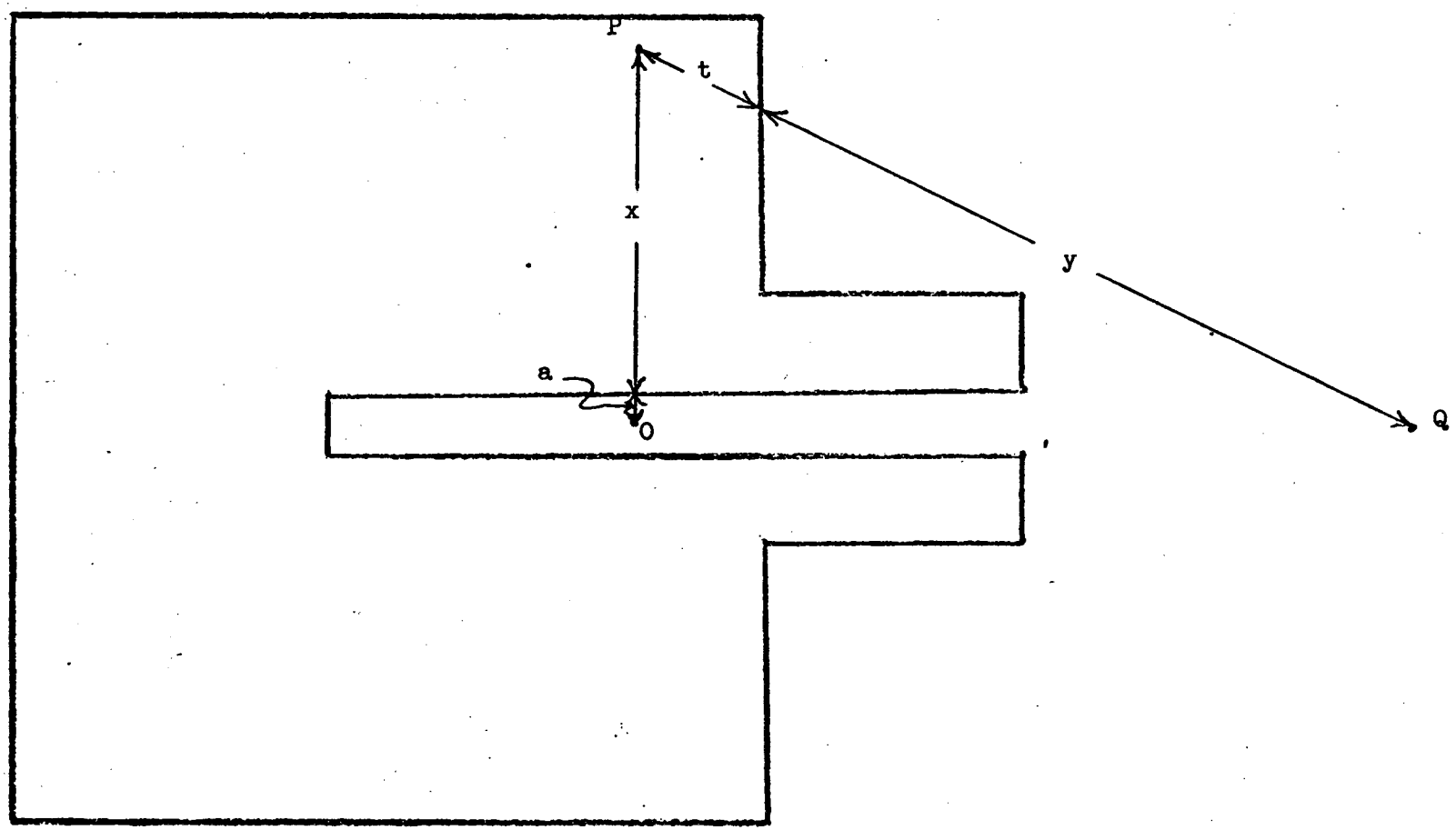

Figure 1

Magnet Approximation Used for Computer Solution

$$\frac{\text{Act (I, J) Trn (I, J)}}{\text{R(I, J)}}$$

and stored so the Δ dose from the next (I, J) can be added to it. There is no expression for area because the grid lines are 1 cm apart and the area is 1 cm^2 for each point. Also, all distances calculated by the subroutine are in cm. After all the Δ doses are accumulated to give the total dose at the field point, a new field point will be read in and the same operations done on it. The program ends when there are no more data cards available.

IV. Results of the Program

Before the computer program was available, some calculations for the dose were made by graphic numeric methods. These calculations were made for a point 30 cm from the yoke side at beam height and 30 cm from the coils on the open or C side at beam height. A gamma energy of .8 MeV from Mn^{56}, and an activity factor corresponding to the widest expected cascade were used on a full-sized drawing of the ring magnet for the proposed 200 GeV proton AGS when the calculation by hand was done. The computer program for the same energy and cascade was within 15% of the graphic numeric method on the yoke side and within 6% on the C side; this was considered good agreement. With this successful computer program it is now possible to compare doses at many field points with different activity factors and with different energies. A typical lower energy γ is the .8 MeV γ from Mn^{56} and the highest energy γ is the 2.75 MeV γ from Na^{24}; if these energies are combined with the activity factors representing the widest and narrowest cascade expected, the resulting doses will bracket the problem. These calculations were done for the proposed 200 GeV AGS ring magnet and for a BNL magnet. The results are given in Tables I and II. The doses are relative. Beam loss, cross sections, and decay schemes must be included to convert the doses to units of mR/hr.

TABLE I

200 GeV Proposed Magnet

	Narrow Cascade .8 MeV	Narrow Cascade 2.75 MeV	Wide Cascade .8 MeV	Wide Cascade 2.75 MeV
Yoke Side	.000086	.00015	.00200	.00310
C Side	.0147	.0173	.1237	.1364
$\frac{\text{C Side}}{\text{Yoke Side}}$	~ 171	~ 112	~ 62	~ 44

TABLE II

BNL AGS Magnet

	Narrow Cascade .8 MeV	Narrow Cascade 2.75 MeV	Wide Cascade .8 MeV	Wide Cascade 2.75 MeV
Yoke Side	.000723	.00138	.00810	.01268
C Side	.02635	.0349	.1462	.1761
$\frac{\text{C Side}}{\text{Yoke Side}}$	~ 36	~ 25	~ 18	~ 14

When comparing the lowest contribution to the dose (.8 MeV, Narrow Cascade) with the highest contribution (2.75 MeV, Wide Cascade) one finds they differ by a factor of 9.3 for the C side of the proposed magnet and by a factor of 6.2 for the C side of the BNL magnet. The numbers in the table were all done with the same magnet shape; therefore, they are comparable. Graphic numeric calculations for a 1 MeV gamma and narrow cascade have been done for both the proposed magnet and the BNL magnet. A value of .000055 was obtained for the yoke side of the proposed magnet and is lower than one would expect from observing the values given on the table, but it can be accounted for by the larger areas used in the hand calculation. On the same magnet the C side value was .0291; almost a factor of 2 larger than expected from the table. A program with a better approximation of the magnet geometry was then run and the value on the C side for the 2.75 MeV,

Narrow Cascade, went to .0408. This increase by a factor of 2.4 puts the computer results in good agreement with hand calculations again. The graphic numeric method for 1 MeV, narrow cascade gammas from the BNL magnet yields .0261 on the C side and .00036 on the yoke side. The C side value here is in the expected range because the geometry of the BNL magnet is better represented by the approximation. Better approximations of the magnet shape and methods of reducing computer running time are being worked on at the present time.

UCID-10020
AS/Experimental/01
June 16, 1964
Rev. September 28, 1964
D. Keefe

University of California
Lawrence Radiation Laboratory
Berkeley, California

ACCELERATION OF ANTI-PROTONS AT THE 200 GEV MACHINE*

I. Introduction

The previous references to the idea of accelerating anti-protons are Symon[1] and Symon and Tollestrup[2]. A major part of their argument, viz., the enhancement of momentum bite by choice of r-f of a low harmonic number is not really applicable since one runs first into a limit due to the physical aperture of the machine. Therefore, we are forced to consider a $\Delta p/p$ of the order of 2×10^{-3}. We will explore further the likely values of $d^2n/dp\, d\Omega$ in the forward direction in order to estimate the optimum primary energy; since the threshold is high (~ 6 BeV), the cross-section in the forward direction is strongly dependent on the Centre-of-Mass to Laboratory-System transformation. Since we can consider production by either the Booster (B) or the Main Ring (MR) protons, the differential cross-section will be examined from threshold up to 200 GeV.

To fix the topology, let us assume a booster external to the main ring and that protons are normally accelerated clockwise (C) in the booste anti-clockwise (AC) in the main ring. Then a logical division of the pla for accelerating anti-protons can be set up according to the following two-fold choices:

(i) Produce $\bar{p}$ by booster or by main ring,
(ii) Maintain field direction or reverse in booster,
(iii) Maintain field direction or reverse in main ring,
(iv) Accelerate protons simultaneously or not in main ring,

making sixteen choices in all.

---

*Memo to J. M. Peterson

Our philosophy at the moment (i.e., in the proposal stage) should, I believe, be to decide on an acceptable system without solving all the problems right now, but incorporating enough flexibility to allow it to be implemented in the future. As an example, if we decided that production of $\bar{p}$ by booster protons were the most desirable choice, then clearly an energy of 6 BeV would be unacceptable, and the frequency swing in the main ring would have to be more than necessary.

II. Experimental Importance

At this stage, let me make the case for the experimental importance of anti-proton acceleration. The object of the high energy accelerator, in the most simplistic terms, is to study the interaction of all known elementary particles with all other known particles. Restricting ourselves to stable or semi-stable secondary particles, we have the list of possible incident particles: nucleons, anti-protons, $\pi^{\pm}$ mesons, $K^{\pm}$ mesons, $\mu^{\pm}$ mesons, hyperons, gamma-rays, and electrons, and neutrinos. The last five (μ, Y, γ, e, ν) we can set aside as having particular properties allowing them to be separated (albeit with some difficulty) from all other particles, e.g., μ's and ν's are amenable to interaction separation and are individually distinguishable by virtue of collision loss in the one case and none in the other, hyperons are short-lived, γ-rays are neutral, electrons can be produced by neutral (γ-ray) intermediaries.

The main problem of isolating a reasonably pure beam of one type of particle arises when we consider charged, strongly interacting particles. If we select a beam emerging from a target, how can we select one of the components, proton (anti-proton), $\pi^{\pm}$ or $K^{\pm}$? It is our fervent hope that somebody in the next decade can dream up a way of separating these particles one from another, with a reasonably large momentum bandpass. At low energies electrostatic separators work, r-f separators at the cost of real estate and duty factor work up to the hundred GeV region, and Cerenkov counters (limited to ~1 Mc/s rates) may be extended indefinitely--again at the cost of real estate. However, protons enjoy a unique position in that the accelerator itself constitutes a mass-separator, with a high intensity and narrow momentum bite. It is a sine qua non of the 200 GeV machine that it should be capable of delivering protons of variable energy, for example, all the way from 30 GeV to 200 GeV. It can be readily shown that the

lifetimes of the π and K mesons are too short to allow their storage in a circular guide-field--although storage of μ-mesons seems (barely) justifiable--whereas anti-protons by virtue of the lifetime and their $|\ e/m\ |$ value are eminently suitable for storage and acceleration.

A critic may ask, "What's so good about having a beam of anti-protons?" In the spirit of the second sentence of this section, the answer is that we are further ahead in respect of having a particle beam facility of very sharp momentum resolution, good optics, variable and accurately known energy. The only other particle for which this is available is the proton. Admittedly, the $\bar{p}$ intensities we are discussing are of the order of 10^6 $\bar{p}$ pp as compared with 10^{13} - 10^{14} ppp. The same critic may ask, "What use has been made of the corresponding proton beam facilities at present accelerators?" If we ignore the work at low energies (< 1 GeV), where an immense amount of accurate nucleon-nucleon interaction information has been amassed illuminating strongly, as Chew has pointed out, not just the low, but also the high energy problems, then the answer turns out a little surprising, namely that the best work probably has yet to come in, say, the next four years. While external beam facilities have been available for some time at the Cosmotron, they have become so only recently at the Bevatron, and not yet at the PS or the AGS. These features of having large intensities, perfect mass separation and precisely known, and yet adjustable energy, have placed the study of p-p interactions, in my opinion, in a class apart from other elementary particle interactions, viz., they involve measurements intrinsically in the 1% ballpark, and are distinguished from the small sample, bump-hunting experiments fashionable more recently, while they also have the features of qualitative statements on the shrinking of diffraction peaks as in the recent PS and AGS experiments. The work at the PS and AGS machines has involved internal targets only and, to my mind, have provided only a fraction of the desired information in that they were constrained to work at fixed angles and were not free to vary the momentum transfer (t) and total energy (s) independent of each other. The external proton beam facility at the Bevatron has allowed the Lofgren Group recently to do a more complete type of experiment (no invidious comparisons of the data intended) although constrained to operate only at low energies (≤ 6 GeV) and has really served to whet our appetite to do more elaborate studies. Likewise, Cocconi and others have long pressed for external beam facilities to extend the scope of their measurements.

Without dwelling further on the history of p-p interaction studies exploiting the existence of a monochromatic, high-intensity beam of variable energy, I think that there is a lesson to be learned from this history. Namely, there is a research program, exciting to many of us, which involves several years of experimental endeavour. It is a little surprising to realize how long proton synchrotrons have been running and how much has still to be done with protons. With a similar anti-proton facility one can certainly predict a very large program along the same general lines, although the much-reduced intensity makes certain experiments tougher. An essential feature will be the possibility of using the anti-protons from very-low energies (a few GeV) all the way up to 200 GeV.

With only superficial thought about the uses of an anti-proton beam, several experiments spring to mind. (I do not claim they are easy to do! Neither is the list complete.)

(i) $\bar{p}$ - p Elastic Scattering: Rarita[3] has given a nice discussion of what we may expect on the basis of Regge pole theory. Basically the comparison of p-p and $\bar{p}$-p scattering should provide a clean isolation of the contribution from the vector meson trajectories. With 1% type experiments at $-t < 1(\text{BeV/c})^2$ a lot can be inferred to help sort out the Regge picture.

(ii) Pomerancuk Theorum: Classified by some as a "dull" experiment, it is nevertheless a certain one to be done and certainly needs a 1% or better precision. With a high optical quality $\bar{p}$ beam, it should be capable of its most accurate test for the p and $\bar{p}$ system.

(iii) Charge Conjugation Invariance: There are all sorts of experiments one can think of in the category. It is hard to get excited right now about these since everyone accepts C.C.I. Still, remember Parity and how she was violated!

(iv) πp, Kp, ep Scattering with Time-like Momentum Transfers: The first of such experiments will soon be tried at BNL. These involve the study of the two-body annihilation reactions:

$$\begin{aligned}\bar{p} + p &\rightarrow \pi^+ + \pi^- \\ &\rightarrow K^+ + K^- \\ &\rightarrow e^+ + e^-\end{aligned}$$

Other final states are possible--anti-baryon pairs of many kinds--which are easy to write down on paper, but probably more difficult to detect, though they could be done in a hydrogen bubble chamber.

(v) "Missing-Mass" Spectra: Again, there is a large number of experiments, the hottest of which will usually be dictated by the current fashions. An interesting feature of the $\bar{p}$-p system is that it has baryon number B = 0. (Compare this with the pp system which has baryon number B = 2.) For example, the reaction

$$\bar{p} + d \rightarrow p + (\text{Boson})^-$$

allows one, by studying the proton recoiling backwards in the CM (and therefore, of low energy in the laboratory system) to determine the mass spectrum of all bosons in the mass range 0 - 20 GeV with T = 1.

Other high mass strange and non-strange bosons can be studied by looking at the recoil momentum spectra in such reactions as

$$\begin{aligned}\bar{p} + p &\rightarrow \pi^\pm + (\text{Boson})^\pm \\ &\rightarrow K^\pm + (\text{Boson})^\pm\end{aligned}$$

while anti-baryon resonances (really connected with type (iii) experiments) can be found by investigating the proton recoil momentum in the reaction

$$\bar{p} + p \rightarrow p + (\overline{\text{Resonance}})$$

These experiments are only a short list based on current problems of interest and probably colored by our present tendency to consider only two-body or quasi-two-body final states. As a guess, at any stage in the development of the Elementary Particle Physics picture in the coming decade one could write down a different list of equal interest and urgency with similar facility and likewise imply an experimental program of several years with anti-protons alone.

In fact, a subsidiary implication is that every effort should be made to make the anti-proton facility symbiotic with the external proton beam facilities to avoid tying up the machine on a single class of experiments.

III. The Methods of Accelerating Anti-Protons

In order to avoid a large number of comparisons of the methods allowed by the choices mentioned in I, consider first the good and bad features associated with these choices.

(i) Field Directions in Main Ring and Booster: There appears to be very little problem or expense associated with being able to reverse the field in the Booster or Main Ring in a switching time of the order of 50 ms. While we can assume the technical feasibility of storing anti-protons traveling either direction in the Main Ring or Booster, there are, however, many effects contributing to closed orbit deviations (e.g., stray fields) will not respond to the reversing switch. In spite of the high injection field (~ 450 G), therefore, the closed orbit might not even lie wholly within the vacuum chamber. An additional consideration is that after a reversal in field the magnet would need at least one cycling to establish a repeatable cycle; in the case of the Main Ring, this would cost a factor of two in repetition rate.

(ii) Experimental Area for Anti-Protons: If the $\bar{p}$ are accelerated maintaining the normal field direction in the Main Ring, then a special $\bar{p}$ experimental area aimed in a reversed direction and special extraction magnets are needed. However, the $\bar{p}$ experimental area will be quite dissimilar to and much less costly than a regular proton area. The intensity will always be low and no elaborate backstop or transverse shield are needed; furthermore, no lengthy secondary transport and separating equipment is required, since the beam is ready for instant experimental use as soon as it emerges from the shielding wall.

(iii) Consequences of Making $\bar{p}$ by Booster: Two major and immediate decisions need to be made if the Booster manufactures the $\bar{p}$'s, viz., (a) the energy must be chosed substantially larger than 6 GeV, say for the purposes of numerical discussion, 10 GeV; (b) since the secondary anti-protons will mostly have energies much below 10 GeV--say, 5 GeV-- the frequency swing in the Main Ring has to be made large (say, four times.)

(iv) Control of R-F: It seems that it is unreasonable to have the r-f system programmed well enough from the $\int \dot{B}\, dt$ signal and it would be necessary to inject protons (counter to the anti-protons) of sufficient intensity, say $\sim 10^{10}$ ppp, to allow pick-up electrodes to sense their phase and control the r-f. G. Lambertson and J. Claus are calculating what fraction of the Main Ring periphery must contain protons to ensure adequate control. The requirement of injecting both protons and anti-protons imposes certain boundary conditions on the time-sequencing at injection and extraction.

In order to limit the discussion below to just a few likely cases, let us assume:

(a) Protons must be simultaneously accelerated to serve as a guide to the r-f. The guide protons are injected first and synchronize the r-f prior to $\bar{p}$ injection.

(b) The field in the Main Ring is never reversed.

(c) The field in the Booster is never reversed.

These choices are coupled: once the main ring polarization is chosen, there seems little advantage in ever reversing the booster. While the choice of the main ring field direction has the advantages of being able to use the accelerated protons, to bury them in an existing backstop and to maximize the repetition rate, it has the disadvantages of having to add a special area and extraction system.

Thus, we are down to the major choice of whether to manufacture the $\bar{p}$'s with the booster (Scheme 1) or main ring (Scheme 2). See Fig. 1. (With either scheme we can inject either the protons or anti-protons first in time; in the discussion below we will assume the protons are injected first).

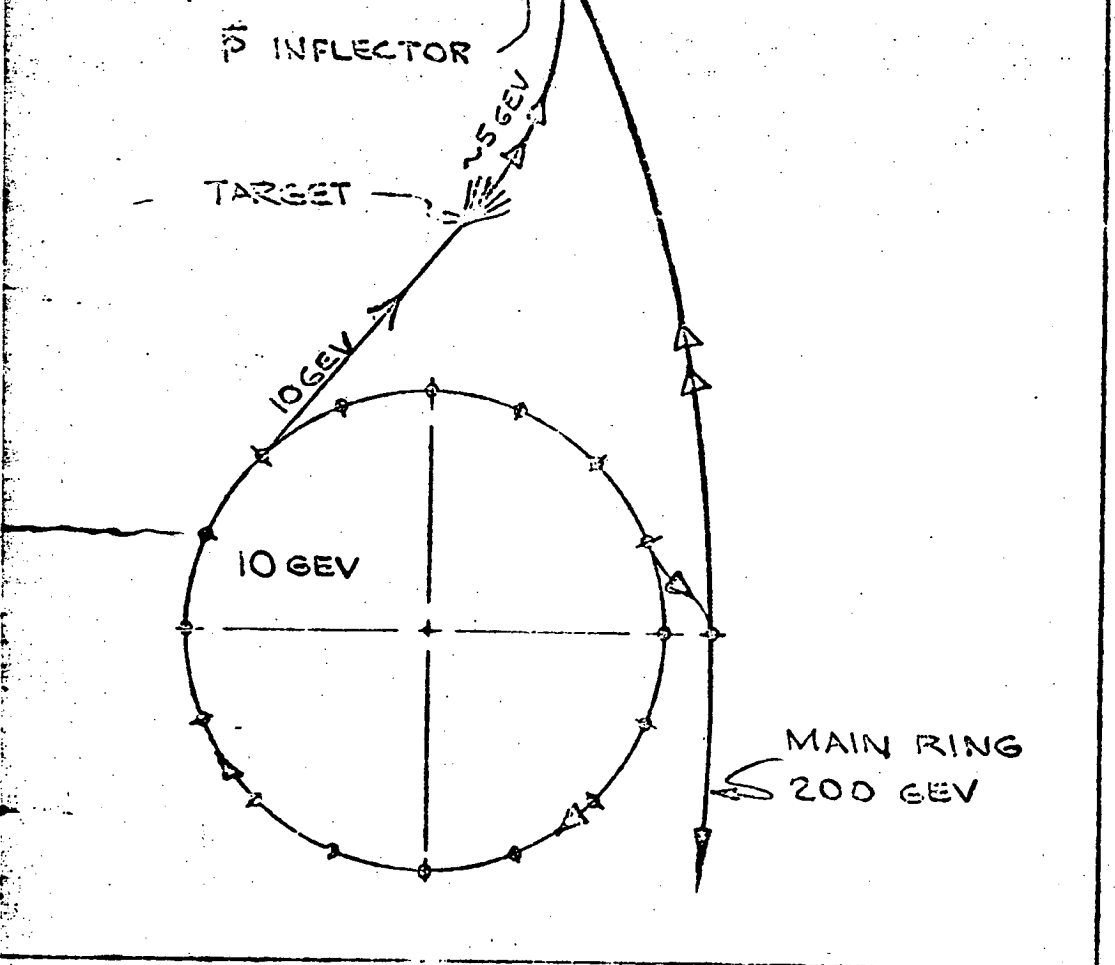

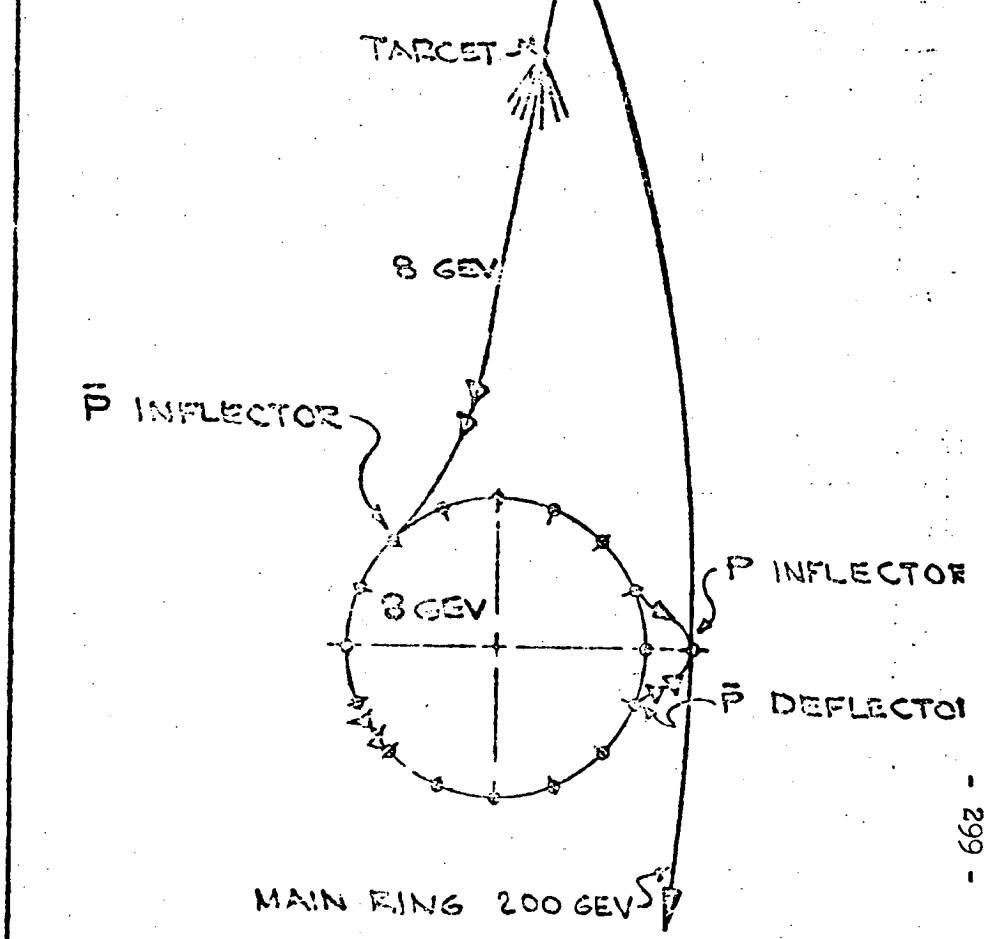

MAGNET CYCLES

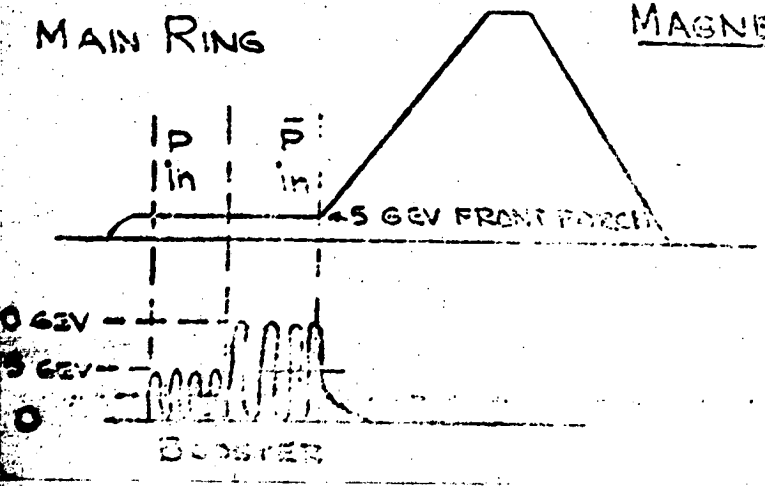

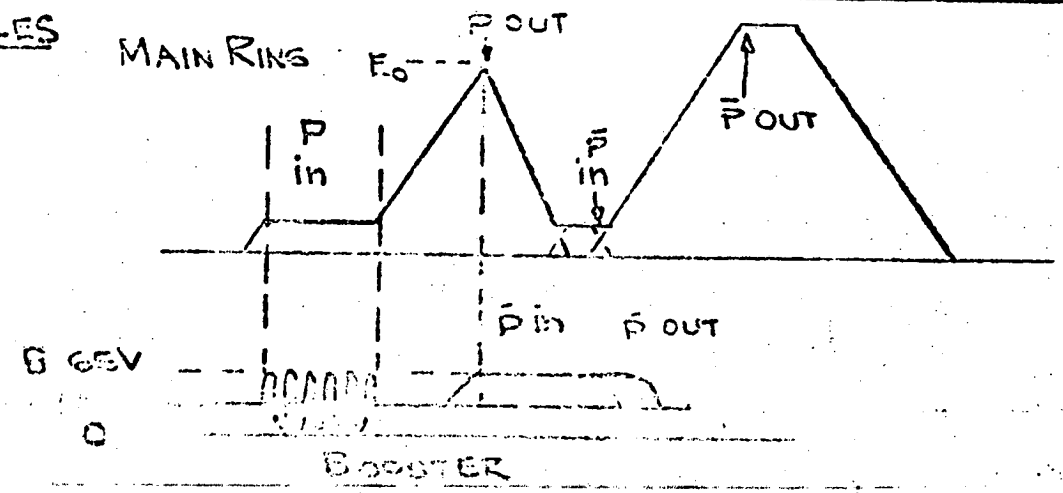

Scheme 1.

Suppose the energy of the Booster is 10 GeV and the flux of $\bar{p}$ at 5 GeV is satisfactory. (Actually the peak is at a somewhat lower secondary energy; 5 GeV is chosen to reduce the demands on the frequency swing in the main ring.) Assume the circumference ratio MR/B is 6. The sequence of operations is then: Flat top the MR at a field corresponding to 5 GeV. Inject $\underline{x}$ segments of protons at 5 GeV and catch them in the r-f system in the MR. A segment is defined as the length corresponding to the Booster circumference; $\underline{x}$ is the minimum number of segments required to keep the r-f control in good shape. Eject the next $(6 - x)$ booster segments at 10 GeV and focus them onto a target about 1 mfp long. The $\bar{p}$'s produced at 5 GeV in the forward direction must be injected into the main ring to fill the unoccupied $(6 - x)$ segment gap by correct phasing at the $\bar{p}$-inflector. Notice that in all schemes a kicker inflector for $\bar{p}$'s is an ejector for $\bar{p}$'s should they pass through the field at the same time. Note also that the timing of the ejection of the booster beam onto the target is very uncritical, viz., the tuned 5 GeV secondary $\bar{p}$ channel will still operate correctly irrespective of the primary energy at the target within broad limits. The $\underline{x}$ proton and $(6 - x)$ anti-proton segments may now be accelerated.

Denoting by $\underline{n}\ (E_o|E)$ the flux per steradian in the forward direction of $\bar{p}$ secondaries with energy E produced by a segment of primary protons with energy E_o from a one mfp target, we have the number captured into the MR:

$$N(\bar{p}) = n\ (E_o|E)\ \Delta\Omega\ (\Delta p)\ (6 - x) \quad x \geq 1$$

$$= n\ (10|5)\ \Delta\Omega\ (\Delta p)\ (6 - x)$$

where $\Delta\Omega = \left(\frac{A\nu}{R}\right)^2_{MR} \frac{1}{t_B}$, if the emittance of the target is matched to the acceptance of the main ring.

where A = effective cross-section of main ring vacuum chamber designed for 10 GeV injection and operated at 5 GeV.

Δp = effective momentum acceptance width of main ring designed for 10 GeV injection and operated at 5 GeV.

t_B = transverse cross-sectional area of target.

Scheme 2.

In this case with an 8 GeV Booster, the circumference ratio MR/B will be 7. Inject (x + 1) segments of protons (more if desired) in the normal way into the MR, accelerate to an energy E_o (between 8 GeV and 200 GeV) such that $\underline{n}\ (E_o|E)$ is a maximum when $E \sim 8$ GeV. (If the optimum yield is not very sensitive to the choice of E_o over a certain energy region, there are good reasons for trying to keep it small, viz., increase the repetition rate, weaker extraction magnets, etc.) Next, eject one segment at E_o onto a target and the $\bar{p}$ produced at $E \sim 8$ GeV can be stored in the booster. With r-f on, the main ring field is allowed to fall not to zero, but to B_{inj} (~ 500 G). A slowly-switched dc bias is needed for this, though the tolerances should not be as critical as for the main ring supply if the phase-lock system behaves as it should. When the regular injection front porch has been established--bias now off--the stored $\bar{p}$ are transferred from the booster to the main ring and acceleration proceeds. The number of $\bar{p}$ injected into the booster is

$$\begin{aligned} N(\bar{p}) &= n\ (E_o|E)\ \Delta\Omega\ (\Delta p)_B \\ &= n\ (E_o|8)\ \Delta\Omega\ (\Delta p)_B \qquad\qquad 200 > E_o > 8 \end{aligned}$$

and $\Delta\Omega = \left(\frac{A\nu}{R}\right)^2_B \frac{1}{t_{MR}}$, with A appropriate to 8 GeV injection.

Since the beam extracted at E_o is bunched when it strikes the production target, the anti-protons will be bunched entering the booster, thus one can turn on the r-f in the booster while it is flat topped.

However not all of this number is actually available for acceleration in the main ring, the limit being the acceptance of the main ring at 8 GeV. Thus, the number of $\bar{p}$ accelerated to high energy at

$$N(\bar{p}) = n\ (E_o|8)\ \left(\frac{A\nu}{R}\right)^2_{MR} \frac{1}{t_{MR}}\ (\Delta p)'$$

where A, $(\Delta p)'$ are the effective cross-section and momentum acceptance respectively of the MR both designed and operated at 8 GeV.

In this scheme the $\bar{p}$'s are stored at about 8 GeV for almost a second, so that even if they were fully debunched the r-f could be turned on slowly enough to allow them to be re-bunched without loss.

IV. Comparison of the Two Schemes

Certain costs are common to both schemes; for example, the transport and shielding of the extra $p \rightarrow \bar{p}$ channel between booster and main ring. The handling of the higher flux of 10 GeV protons in Scheme 1 largely offsets the handling of the higher energy (E_o) protons in Scheme 2.

Extra costs in Scheme 1 include the cost of making the higher energy booster and of making the MR frequency swing about 4 times larger than needed for protons. Less tangible is the loss of some safety factor in the main ring aperture when optimizing for the higher energy injector.

In Scheme 2 are involved kickers at E_o (say ~ 50 GeV), and two at 8 GeV, compared with kickers in Scheme 1 at 10 GeV and 5 GeV. The main extra cost probably lies in the more complicated manipulations with the main ring magnetic field (dc offset and added controls), although some manipulation of the booster cycle is needed in Scheme 1. The booster power supply has to be capable of flat-topping at 8 GeV.

A serious disadvantage of Scheme 1, to my mind though others may weight it less heavily, is the radically different operating condition at injection. It is true that any time the $\bar{p}$ facility is started up, a very large number of new elements will have to be made to work, but for the operators to have to contend with a radical change in the main ring r-f and perhaps an unknown and variable closed-orbit pattern at injection, seems a complication of a different order of magnitude. This is really the old argument that once the primary beam is circulating reproducibly, secondary systems can be tuned up and made to work, whereas if one cannot get beam around in the first place because of very unusual injection conditions life is much more complicated.

We do not have complete information to contrast the fluxes available by the two methods but we can consider the following comparison.

$$\frac{N(\text{Scheme 1})}{N(\text{Scheme 2})} = (6 - x) f \frac{r(10|5)}{r(E_o|6)} \left[\frac{A(\text{MR-10,5})}{A(\text{MR-6,6})}\right] \frac{t_{MR}}{t_B} \frac{(\Delta p)}{(\Delta p)'},$$

where the notation (MR-10, 5) means a main ring optimized for 10 GeV injection operating at 5 GeV injection. Let us consider these factors individually. Since x is unknown $(6 - x)$ lies between 1 and 5 and we will assume the higher value since a value of $x = 1$ seems likely to be adequate. The duty factor, f, arises from the difference between the magnet cycles in the two cases and depends on x and E_o and the desired experimental $\bar{p}$ energy--it is probably in the range 1 - 1.5. The aperture ratio is very close to unity. The Δp ratio depends on whether one is aperture-limited or bucket-limited--in the first case $\Delta p \propto p$ in the second $\Delta p \propto \gamma^{3/2}$. With the presently assumed parameters the limitation in both cases is bucket-size. Thus

$$\frac{\Delta p}{(\Delta p)'} = \left(\frac{5.9}{8.9}\right)^{3/2} = 0.54$$

The ratio of the target cross-sections is clearly in favor of Scheme 2 if we use a target 1 mfp (= L) long, matched to the appropriate extracted beam. For, assuming the fast extracted beam to have the same emittance as the internal beam, we have:

Target cross-sectional area, t, $\approx \frac{4 A\nu L}{\pi R}$ for a matched target.

Hence

$$\frac{t_{MR}(\text{matched})}{t_B(\text{matched})} = \frac{A(\text{MR at } E_o)}{A(\text{B at 10 GeV})} = \frac{A(\text{MR at } E_o)}{A(\text{MR at 10})} = \frac{10}{E_o} = \frac{1}{5}$$

for $E_o = 50$ GeV.

It is doubtful whether this factor could be exploited to its full extreme since it would imply the use of targets smaller than 1 mm^2 in cross-section. If not fully exploited, it nevertheless represents some sort of safety factor in the comparison.

Thus we have

$$\frac{N(\text{Scheme 1})}{N(\text{Scheme 2})} \leq 5(1.5)\left(\frac{1}{5}\right)(0.54)\frac{n(10|5)}{n(E_o|8)}$$

$$\leq 0.8\ \frac{n(10|5)}{n(E_o|8)}$$

The flux ratio is unknown; however a model has been recently developed[4] which accounts for the anti-proton fluxes at both 0^o and other angles observed at the CPS and the AGS, and can be extrapolated upwards in E_o. The model predicts a very rapid rise in the 0-deg production of secondary anti-protons in the 5 - 10 GeV region as E_o is increased up to ~ 40 GeV with a slow decrease at higher energies. With E_o = 50 GeV the flux ratio is 10^{-3} giving a factor of about one thousand advantage to Scheme 2. The flux expected using Scheme 2 is

$$N(\bar{p}) = \frac{N_o}{e}\ \frac{\sigma(\bar{p})}{\sigma_a}\ \left(\frac{A\nu}{R}\right)^2_{MR}\ \ \frac{1}{t_{MR}}\ \ (\Delta p)'$$

$$\approx \frac{3 \times 10^{13}}{7}\ \left(\frac{1}{2.7}\right)\ \frac{8}{180}\ \left(\frac{30x17}{70000}\right)^2\ \ \frac{1}{0.01}\ (5x10^{-3})\ \bar{p} \text{ per pulse}$$

$$= 2 \times 10^6\ \bar{p} \text{ per pulse from a target with } t_{MR} = 1\text{mm} \times 1\text{mm}$$

If a target much smaller than 0.01 cm^2 can be cooled about another order of magnitude in flux can be gained.

V. Extraction and Use of Anti-Protons

There is little difficulty in extracting either a slow or fast $\bar{p}$ beam. For slow extraction it is inevitable--since many traversals of the machine are involved--that the proton beam should be spilled simultaneously. It seems most convenient to spill the p and $\bar{p}$ beams in adjacent straight sections. If a non-linear perturbing magnet is placed mid-way between the straight sections (i.e., about 0.6 betatron wavelengths from either) then it takes probably two septum magnets along the structure and one at the straight section to extract either beam.

If fast extraction is desired, then a pulsed kicker placed at the location of the non-linear perturbation can accomplish the job. However,

an interesting possibility arises if the combined lengths of p and $\bar{p}$ segments are less than the main ring circumference. In this case it is possible to phase the relative positions of the anti-protons such that they can be kicked out without disturbing the protons. Thereafter the protons can be extracted either fast or slowly at any other desired location, or vice versa, the protons may be kicked out first into a pre-selected area and the anti-protons spilled at leisure later on.

VI. Conclusion

Scheme 2 looks preferable as a proposed anti-proton facility to be added at a later date, and should deliver 2×10^6 $\bar{p}$ per pulse independent of energy between 8 and 200 GeV.

sk

FOOTNOTE: The Booster as a μ-Meson Storage Ring

Using the preferred scheme (No. 2) for accelerating anti-protons we notice that in fact the transport system from the production target to the booster will transport all negative particles within the appropriate momentum bite. If the flight path between the target and the injection point is about 400 - 500 m, then over half the π-mesons will have decayed to μ-mesons and furthermore, the anti-proton bunches will be displaced about 10 ns from the π and μ meson bunches. In principle by turning on the r-f in the booster in the correct phase, the anti-protons could be lost, but this method of separation is probably only good for a factor of 10^{-2}, or so, rejection. A safer method would be to introduce a 50 Mc/s r-f transverse-field separator cavity close to the injector into the booster and to use the 50 Mc/s bunch structure of the anti-protons to knock them out. The μ-mesons will make about 76 traversals. The momentum acceptance of the booster at flat-top is 1% and if a matched achromatic channel with $\Delta p/p \sim 2\%$ can be achieved between production target and booster, then about 10^8 μ-mesons can be injected. This is a very respectable intensity for experimentation--the major disadvantage of the scheme would be the interference between the experimental equipment such as targets and the operation of the booster in its prime function as an injector. A less conflicting solution would be the construction of a small μ-storage ring with high field and lower energy close by the injector at the termination of the transport channel.

FOOTNOTES

[1]K. R. Symon, BNL IA-10 (1961).

[2]K. R. Symon and A. V. Tollestrup, BNL IA KRS~AVT-1 (1961).

[3]W. Rarita, UCID-10111 (1964).

[4]D. Keefe, G. Mealy and G. H. Trilling, AS/Experimental/01, (Sept. 1964).

AS/Experimental/01
December 10, 1964
D. Keefe; M. Scolnick

TABLE OF MEAN FREE PATH AND RADIATION LENGTH FOR VARIOUS MATERIALS

The cross-section for interaction of strongly interacting particles with nuclei is relatively insensitive to the value of the cross-section on individual nucleons for particles with energies in the GeV range. In other words, whether the cross-section on a nucleon is 20 mb or 30 mb or 40 mb becomes unimportant when the number of nucleons in the nucleus is large, since the probability of penetration of the nucleus without interaction is in any case small. The results of several measurements[1] of the absorption cross-section of high energy particles (protons, neutrons and π-mesons) with a variety of nuclei are shown in Fig. 1 and are well represented by the formula

$$\sigma_a = 43\ A^{0.69}\ \text{mb} \qquad (1)$$

where A is the atomic weight.[2] This formula is not valid for hydrogen, and the work of Rarita[3] should be consulted for the expected behavior of the individual particle cross-sections on hydrogen as a function of energy. Results from nuclear emulsions for very high energy particles indicate that there are not drastic changes in the cross-sections of nucleons and mesons on nuclei even in the TeV region, so that Eq. (1) is expected to hold in the energy range at least up to 200 GeV.

The absorption mean free path measured in gm cm^{-2} is

$$\lambda_a = \rho/n\sigma_a$$

where ρ = density in gm cm^{-3}, and $n = \rho N_o/A$ is the number of nuclei per cm^3. λ is a monotonic function of atomic weight as shown in Fig. 1:

$$\lambda_a = 38.5\ A^{0.31}\ \text{gm cm}^{-2}$$

In units of centimeters it is far from monotonic and this fact is very important in connection with targetting where it is frequently important to have a target

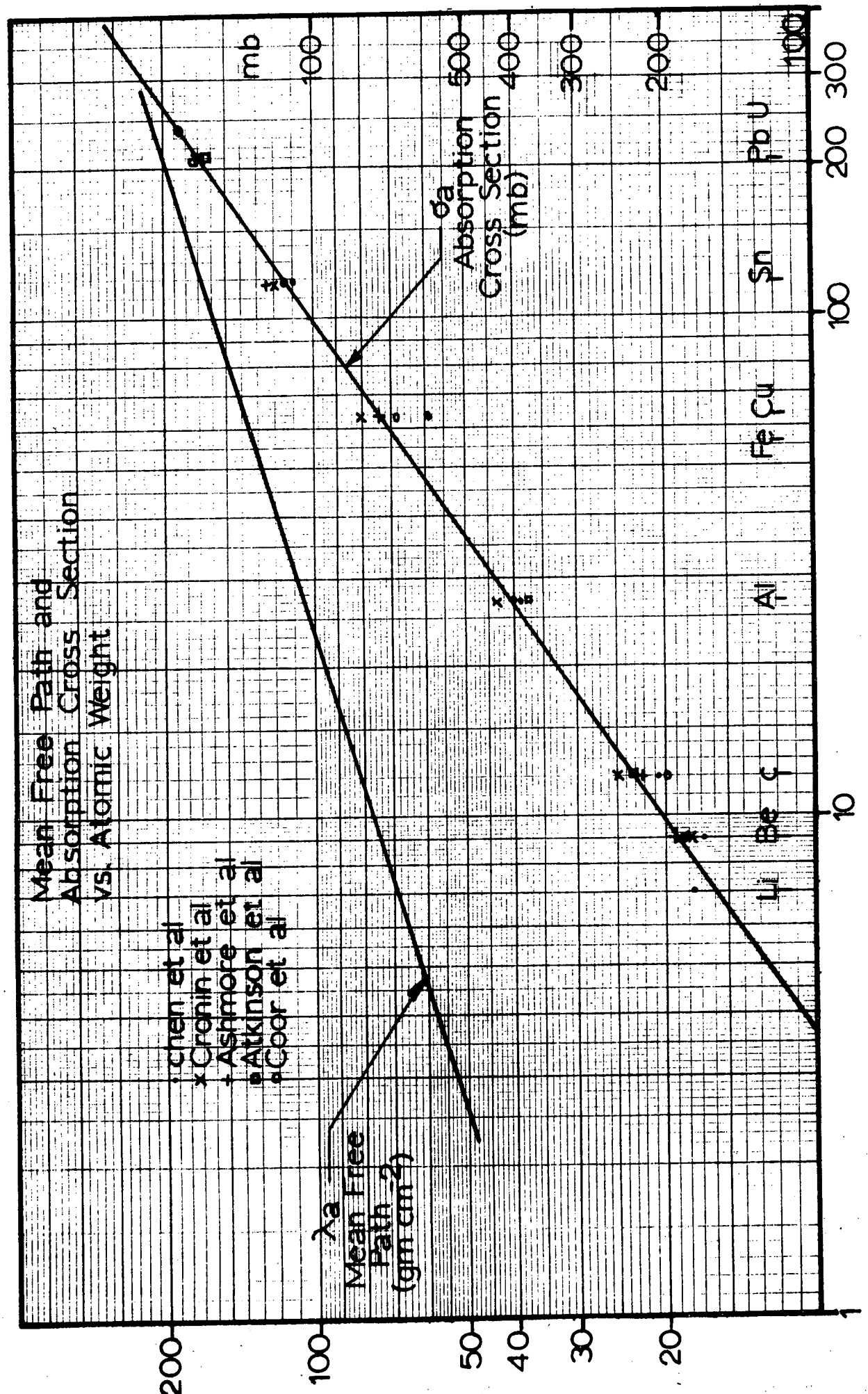
Mean Free Path and
Absorption Cross Section
vs. Atomic Weight
: Chen et al
x Cronin et al
+ Ashmore et al
• Atkinson et al
° Coor et al
λa
Mean Free
Path
(gm cm⁻²)
σa
Absorption
Cross Section
(mb)
mb
Li Be C Al Fe Cu Sn Pb U
A

fig. 1

close to a mean free path in thickness but as short as possible when measured in centimeters. Table I shows the values of λ_a in both sets of units for a variety of materials which are suitable for targets.

An examination of the data[1] indicates that there is no strong dependence of the ratio of the elastic cross-section (σ_e) to the absorption cross-section σ_a on either energy or atomic weight. The data may be fitted by a formula

$$\frac{\sigma_e}{\sigma_a} = 0.57$$

Thus the mean free path appropriate to the total cross-section, $\sigma_T = \sigma_a + \sigma_e$, can be obtained from the value of λ_a tabulated in Table I by dividing by 1.57.

The final column of Table I gives the radiation length in gm cm^{-2}, and these are plotted in Fig. 2.

REFERENCES

1. Ashmore et al, Phys Rev Letters 5 576 (1960).
Atkinson, Phys Rev 123 1850 (1961).
Chen et al, Phys Rev 99 857 (1955).
Coor et al, Phys Rev 98 1369 (1955).
Cronin et al, Phys Rev 107 1121 (1957).

2. Williams, R. W., Preprint on "Empirical Formula for Absorption Cross Sections on Nuclei," 1964.

3. Rarita, W., UCID 10111 April 9, 1964.

TABLE I

Element	A	ρ gm cm^{-3}	σ_a mb	absorption mean free path gm cm^{-2}	cm	radiation length gm cm^{-2}
Li	6.94	0.534	164	70	131.0	77.5
Be	9.01	1.84	196	76	41.4	62.2
B	10.82	2.5	222	80.5	32.2	52
C	12.01	2.25	240	83.2	37.2	42.5
Mg	24.32	1.74	389	99.5	57	24.6
Al	26.98	2.7	417	107	39.7	23.9
Cr	52.01	7.0	655	131	18.7	14.9
Mn	54.94	7.42	680	133	18.4	14.6
Fe	55.85	7.7	688	134	17.4	13.8
Co	58.94	8.7	718	136	15.7	13.55
Ni	58.71	8.7	714	136	15.7	12.6
Cu	63.54	8.9	752	139	15.6	12.8
Zn	65.37	7.0	770	140	20	12.35
Ag	107.87	10.5	1085	164	15.6	8.6
Sn	118.69	7.0	1160	168	24	8.54
Ba	137.34	3.78	1285	177	47	7.85
Ta	180.95	16.6	1555	192	11.6	6.35
W	183.85	18.8	1565	193	10.2	6.28
Ir	192.2	22.42	1610	196	8.8	6.15
Pt	195.1	21.37	1638	197	9.25	6.05
Au	196.96	19.0	1640	198	10.4	6.0
Hg	200.59	13.5	1655	198	14.6	6.10
Pb	207.19	11.0	1710	202	18.4	5.8
U	238.03	18.7	1870	210	11.2	5.5

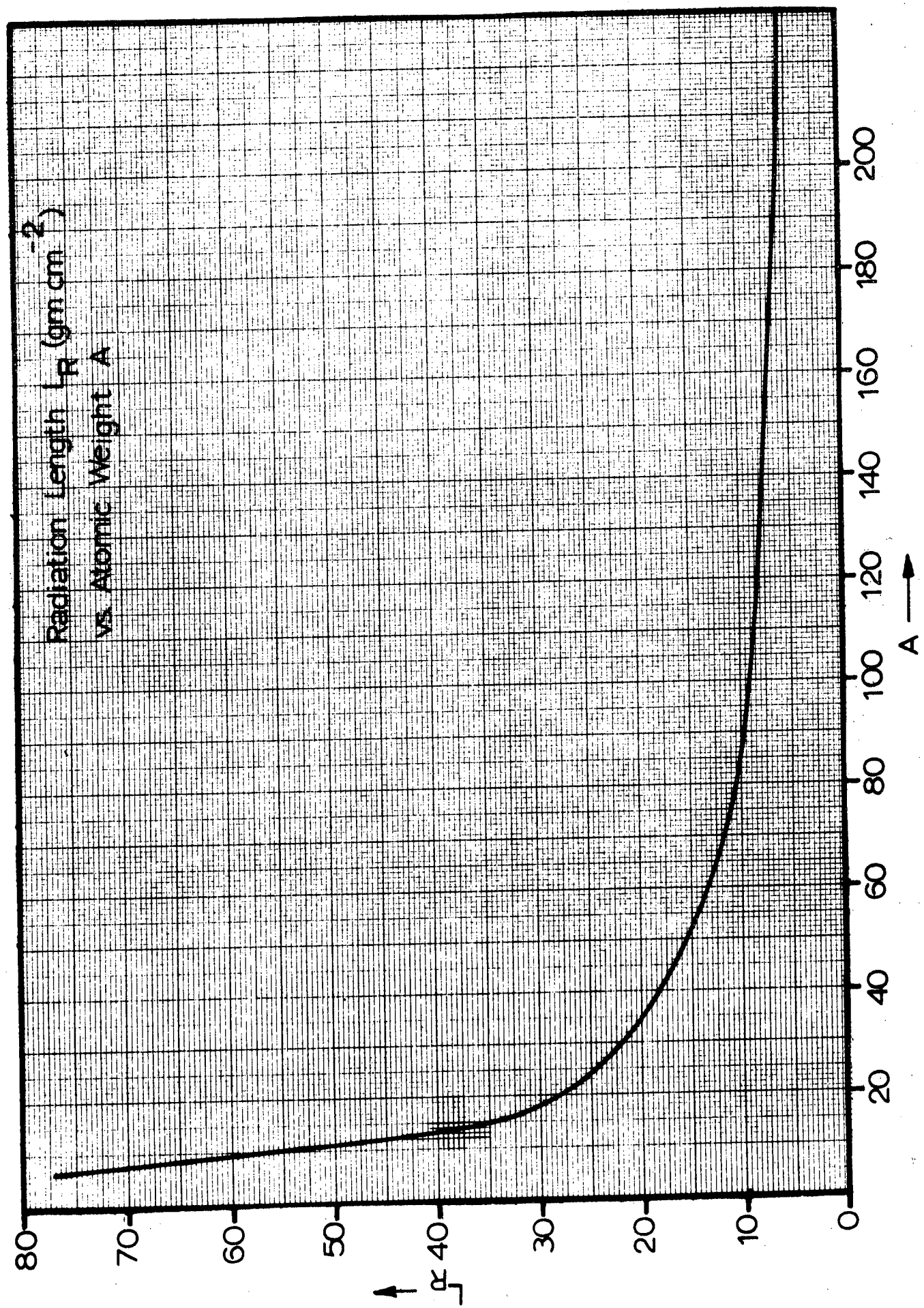
Radiation Length L_R (gm cm^{-2})
vs. Atomic Weight A
L_R
A
0
10
20
30
40
50
60
70
80
20
40
60
80
100
120
140
160
180
200